

The background of the cover is a black and white electron micrograph of Neisseria meningitidis bacteria. The bacteria appear as numerous spherical cells, some in pairs (diplococci) and others in small clusters. They have a distinct outer capsule and a rougher inner surface. The lighting creates highlights and shadows, giving the cells a three-dimensional appearance.

Towards a *Neisseria meningitidis* B vaccine

Introducing systems biology in process development

Gino J.E. Baart

Stellingen

1. Realistische modellen van celmetabolisme bevatten altijd onderbepaaldheden (dit proefschrift).
2. Het berekenen van numerieke waarden voor onderbepaalde fluxen is een wiskundige oefening (dit proefschrift).
3. *In vitro* celkweek is een typisch voorbeeld van de tragedie van de meent [1,2].
[1] MacLean RC, Gudelj I. 2006. Resource competition and social conflict in experimental populations of yeast. *Nature* 441:498–501
[2] Hardin G. 1968. The Tragedy of the Commons. *Science* 162:1243–1248.
4. Biotechnologie is een trukendoos.
Variant op de stellingname: De truc van ruimtevaart is vallen (André Kuipers, 2005).
5. Het zou de groenste universiteit van Nederland sieren als eerste het drukken van proefschriften af te schaffen.
6. De slogan "leuker kunnen we het niet maken, wel makkelijker" kan de belastingdienst beter vervangen door "leuker kunnen we het nooit maken, ook niet makkelijker".

Stellingen behorende bij het proefschrift:

Towards a *Neisseria meningitidis* B vaccine
Introducing systems biology in process development

Gino J.E. Baart

17 oktober 2008

Towards a *Neisseria meningitidis* B vaccine

Introducing systems biology in process development

Gino J.E. Baart

Promotor

Prof. dr. ir. J. Tramper

Hoogleraar in de bioprocestechnologie, Wageningen Universiteit, Nederland

Co-promotoren

Dr. ir. D.E. Martens

Universitair docent sectie proceskunde, Wageningen Universiteit, Nederland

Dr. E.C. Beuvery

Bionnovations, Nederland

Promotiecommissie

Prof. dr. ir. J.J. Heijnen

Technische Universiteit Delft, Nederland

Prof. dr. ir. J. van der Oost

Wageningen Universiteit, Nederland

Prof. dr. ir. E. Vandamme

Universiteit Gent, België

Prof. dr. B.A.M. van der Zeijst

Nederlands Vaccin Instituut; Universiteit Leiden, Nederland

Dit onderzoek werd uitgevoerd op het Nederlands Vaccin Instituut te Bilthoven, Nederland, binnen de onderzoekschool VLAG.

Gino Johannes Elisabeth Baart

Towards a *Neisseria meningitidis* B vaccine

Introducing systems biology in process development

Proefschrift

Ter verkrijging van de graad van doctor
op gezag van de Rector Magnificus
van Wageningen Universiteit,
Prof. dr. M.J. Kropff
in het openbaar te verdedigen
op vrijdag 17 oktober 2008
des namiddags te half twee in de Aula

Baart GJE. 2008.

Towards a *Neisseria meningitidis* B vaccine - Introducing systems biology in process development
Ph.D. thesis, Wageningen University, Wageningen, The Netherlands – With summary in Dutch

ISBN 978-90-8504-997-5

*Aan mijn geliefden
voor mezelf*

Life comes down to a few moments. This is one of them.

Oliver Stone

CONTENTS

Chapter 1	General introduction	1
Chapter 2	Modeling <i>Neisseria meningitidis</i> metabolism: from genome to metabolic fluxes	35
Chapter 3	Modeling <i>Neisseria meningitidis</i> B metabolism at different specific growth rates	107
Chapter 4	Heterologous expression of phosphofructokinase in <i>Neisseria meningitidis</i>	153
Chapter 5	Scale-up for bulk production of vaccine against meningococcal disease	199
Chapter 6	General discussion	227
Summary		241
Samenvatting		249
Glossary		257
Dankwoord		265
About the author		273

Chapter 1

General introduction

NEISSERIA MENINGITIDIS

Meningococcal disease

The genus *Neisseria* belongs to the family *Neisseriaceae* of the β -proteobacteria [1] and is named after Albert Neisser who discovered the gonococcus in 1879 [2]. The genus includes a group of closely related cocci that are primarily commensal organisms of mucosal surfaces of mammals [3]. Two species: *Neisseria gonorrhoeae* (the gonococcus) and *Neisseria meningitidis* (the meningococcus), are important human pathogens [4]. Anton Weichselbaum first identified *N. meningitidis* as the causative agent of bacterial meningitis in 1887 [5]. *N. gonorrhoeae* is considered to be always pathogenic and causes the sexually transmitted disease gonorrhea, while *N. meningitidis* colonizes oro- and nasopharyngeal mucosa, its sole ecological niche, asymptotically, which means that not all people who harbor the meningococcus develop disease [6, 7]. Transfer of meningococci from one person to another can occur via direct contact with nasal or oral secretions or through inhalation of droplets [8]. Acquisition of meningococci may result in invasive disease, which normally occurs 1-14 days after acquisition or lead to colonization (carriage) [8]. Carriage leads to the induction of ‘natural acquired’ immunity against the organisms [9]. In non-epidemic situations approximately 10% of the adult population is colonized by meningococci [10-13], but increased carriage rates have been observed during epidemics and close contacts [12, 14]. The highest incidence of meningococcal disease occurs in young children under the age of four. In addition, an incidence peak is observed among teenagers, most likely as a result of increased exposure to environmental risk factors, such as the number and closeness of contacts (e.g. intimate kissing) [15] and (passive) smoking [16]. By a mechanism that remains unknown, some *N. meningitidis* strains are able to cross the mucosa into the bloodstream from where they can cause invasive meningococcal disease with severe clinical syndromes [17]. Understanding how the meningococcus can both be a harmless commensal and a devastating human pathogen has been a major quest in the biology and in the design of prevention strategies for *N. meningitidis*.

Meningococcal disease is a life-threatening illness with annual incidence rates varying from 1 to 1000 per 100 000 persons in different parts of the world [8, 12]. The disease is characterized by a variety of clinical symptoms [17] and in the early phase mild symptoms like chills, fever and muscle aches can change rapidly (within hours) into bacterial meningitis or septicaemia, potentially leading to shock and death [17]. Despite antibiotic treatment, the mortality rate is about 10 to 30% in the case of meningitis and sepsis, respectively [18]. Early antibiotic treatment should be applied as soon as possible when clinical diagnosis confirms meningococcal meningitis since effective antibiotics immediately stop proliferation of *N. meningitidis* [19]. Without antibiotic treatment, death rates can increase up to 80% [20]. About 5-20% of the surviving patients suffer from permanent damage, such as amputation of limbs, mental retardation, and deafness [20]. The rapid onset of invasive meningococcal disease [17], the high incidence in young children [19], the high mortality rate [18] and the severe permanent damage in patients recovering from disease [20] indicate the importance of vaccine development against this devastating pathogen.

Microbiology

N. meningitidis is a heterotrophic, aerobic Gram-negative coccus, occurring as single coccus but often as diplococcus with adjacent sides flattened and ranging from 0.6–1.9 μm in diameter [1]. Meningococci are obligate human pathogens that have an optimal growth temperature of 35-37 °C. The cell envelope of *N. meningitidis* is typical for a Gram-negative bacterium and composed of an outer membrane and an inner membrane, separated by the periplasmic space that contains a peptidoglycan layer and proteins (Figure 1.1). The inner membrane is a phospholipid bilayer containing mainly proteins involved in transport of proteins and nutrients across the inner membrane, while the outer membrane is asymmetrical containing mainly lipopolysaccharide (LPS) on the outer leaflet and phospholipids on the inner leaflet [21]. The outer membrane contains various outer membrane proteins (OMPs) of which the major ones are: Porin A (PorA), Porin B (PorB), reduction-modifiable protein M (RmpM),

opacity proteins (Opa, Opc) and the lactoferrin receptor proteins. Virulent bacteria are covered by a capsule [11] composed of polysaccharides. Through this capsule fimbriae (type IV pili) protrude. These pili are filamentous proteins and are found to play an important role in a number of processes such as: the initial attachment of meningococci to host cells [22], natural transformation [23], twitching motility (movement) [24] and biofilm formation [25]. Although type IV pili are immunogenic,

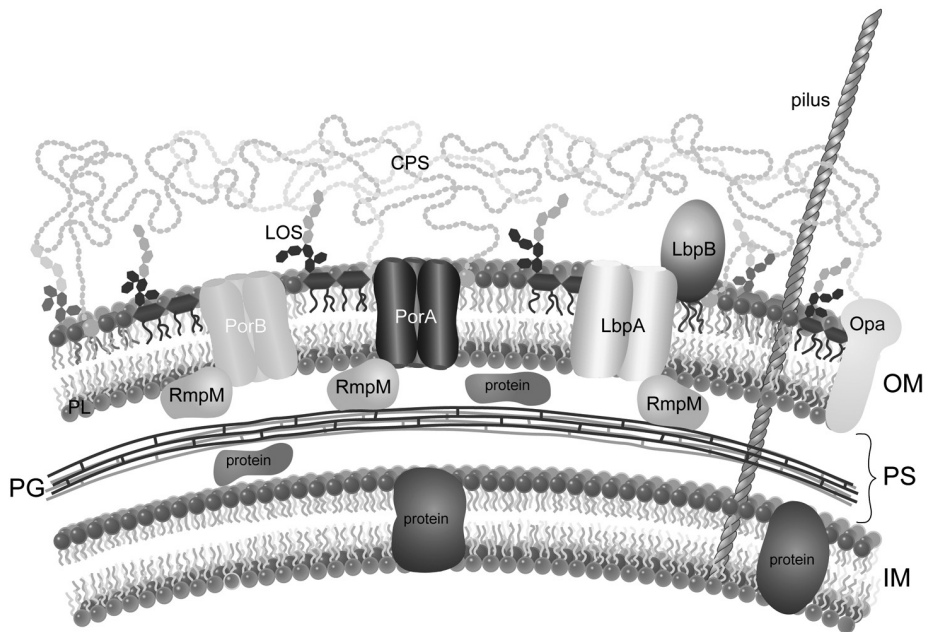


Figure 1.1 Cross-sectional view of the *N. meningitidis* cell surface.

The cell envelope is composed of an outer membrane (OM) and an inner membrane (IM), separated by the periplasmic space (PS) that contains a peptidoglycan layer (PG). The cell surface is surrounded by capsular polysaccharide (CPS) that is anchored in the OM via a phosphatidyl glycerol moiety. Type IV pili (pilus) protrude through the entire envelope and extend several thousand nm from the surface [19]. The IM is a phospholipid (PL) bilayer containing mainly proteins involved in transport of proteins and nutrients across the inner membrane. The OM is asymmetrical containing mainly phospholipids on the inner leaflet and lipopolysaccharide (LPS) on the outer leaflet. Furthermore, it harbors integral and surface exposed outer membrane proteins (OMPs). LbpA and LbpB are integral and cell-surface exposed OMPs respectively, which together constitute the lactoferrin receptor that is involved in the acquirement of iron from the environment. Opa: Opacity protein (class 5 OMP), PorA: protein Porin A (class 1 OMP), RmpM: reduction-modifiable protein M (class 4 OMP). Courtesy Wilma Witkamp, Netherlands Vaccine Institute.

they are not suitable as vaccine candidates, because of the high degree of antigenic variability [20] and the phase variation of expression [23]. Flagella are absent in *Neisseriaceae* [1]. In addition, CPS, LPS (endotoxin) and OMPs present in the outer membrane are linked to meningococcal virulence [26] and protection against meningococcal disease, and are discussed in more detail below and in Chapter 2.

N. meningitidis strains can be classified into thirteen serogroups based on differences in the structure of their CPS, but only six serogroups (A, B, C, W-135, Y, and X [19]) cause most of the disease [10]. Further classification into serotypes and serosubtypes is based on the outer membrane porin proteins PorB and PorA, respectively, while the immunotype is determined by the LPS structure [19]. The different serogroups show a regional distribution: group B and C meningococci dominate in western countries while group A and C dominate in less developed countries [19]. The highest burden of meningococcal disease, predominantly caused by group A organisms, occurs in sub-Saharan Africa, which is known as the “Meningitis Belt” [27] (Figure 1.2).

The genome sequences of *N. meningitidis* strains MC58 (serogroup B), strain Z2491 (serogroup A) and strain FAM18 (serogroup C) have been published [28-30]. Meningococcal genomes possess several important characteristics that differ from other Gram-negative bacteria like *Escherichia coli*. Next to differences in genome sizes (i.e. 2.2 MB vs 4.6 MB for *N. meningitidis* and *E. coli*, respectively), and the number of different genes (i.e. ~ 2065 genes vs 4288 genes for *N. meningitidis* and *E. coli*, respectively), the genomes of meningococci are highly instable as a result of different mutational events. These events originate from either local genomic changes caused by repeat sequences, phase and antigenic variation, recombination and horizontal gene transfer, or globally from mutator alleles [23, 30]. All contribute to the highly variable dynamics of meningococcal genomes. For example, phase and antigenic variation alone involve approximately 100 genes [31], whereas, in *E. coli*, less than 10 genes are subject to phase variation [23]. These differences are likely to be caused by the differences

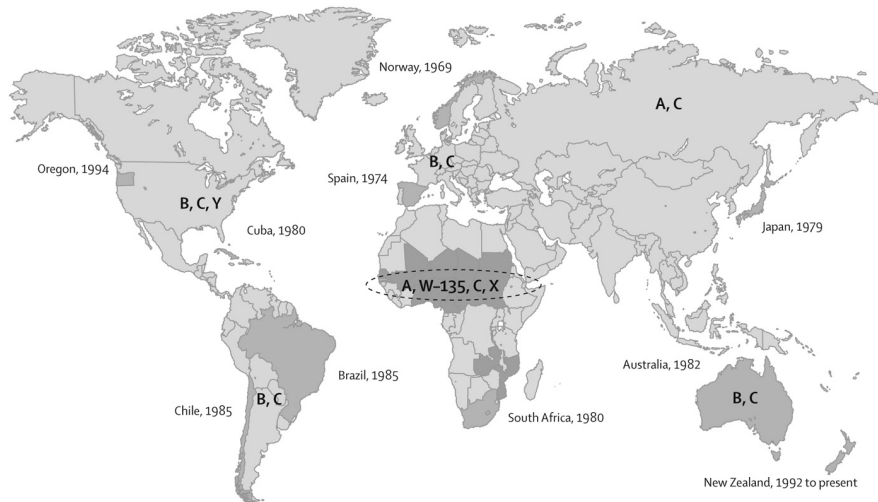


Figure 1.2 Global distribution of major meningococcal serogroups and of serogroup B outbreaks (shaded in dark grey). The meningitis belt (dotted line) of sub-Saharan Africa and other areas of substantial meningococcal disease in Africa are shown. Adapted from [19].

between the habitats of both bacteria. The sole natural habitat of *N. meningitidis* is mucus layer that covers the oro- and nasopharynx, whereas *E. coli* shuttles between different habitats in the human body. The latter explains the battery of sophisticated regulatory systems in *E. coli* [32], to sense and respond to different environmental conditions, which enables adaption to, and survival in, these different environments. Along with a small genome size, the meningococcal survival strategy involves a reduced DNA-repair capacity [33] in combination with events that promote genome plasticity, mentioned above. Instead of sensing and responding to the environment, meningococci generate a surplus of genetic variants that are subjected to natural selection [34]. The strains that evade recognition by the host immune system, and consequently innate immune killing, survive. In addition, *N. meningitidis* is equipped with secretory proteins that are involved in the adherence to host cells or required to suppress the host's defence mechanisms [35], of which the site-specific proteases to cleave human immunoglobulin A1 (IgA1), the first line of defense at mucosal membranes [36] and PorB [37], are an example.

The central metabolism of *N. meningitidis* (Figure 1.3) is similar to the central metabolism of other aerobic Gram-negative organisms with some particular differences. Glucose, an important substrate for growth, is processed via the Entner-Doudoroff (ED) pathway and the pentose phosphate (PP) pathway. The glycolytic Embden-Meyerhof-Parnas (EMP) pathway, the main glucose processing pathway in many other organisms, does not contribute to pyruvate synthesis [38-43] because the gene encoding the enzyme phosphofructokinase (PFK) is not present in the *N. meningitidis* genome [29]. The tricarboxylic acid cycle (citric acid cycle) is operational but to establish oxidation of malate to oxaloacetate, FAD-dependent malate:quinone oxidoreductase is used instead of malate dehydrogenase. Lactate is an important carbon source for the bacterium during colonization and is necessary for growth of the bacterium in nasopharyngeal tissue [44], however *in vivo* studies indicate a lower biomass yield when grown on lactate [45]. The amino-acid biosynthetic pathways are present, however for some *N. meningitidis* strains the additional need for glutamate, arginine, glycine, serine, and cysteine has been indicated [46]. A detailed review of the primary metabolism of *N. meningitidis* is given in Chapter 2.

Vaccines and vaccine candidates

For more than a century, vaccine development has followed the principle of Louis Pasteur: “isolate, inactivate and inject” the causative microorganism [47]. Vaccines that have been produced based on this principle consist of whole killed pathogens (e.g. the whole cell *Bordetella pertussis* vaccine) or live attenuated pathogens (e.g. oral polio vaccine). Technological breakthroughs during the past three decades have extended the power of the vaccines produced according to Pasteur’s principles considerably. Especially subunit vaccines, composed of purified protective components, cause less adverse reactions upon administering in comparison with a whole cell vaccine [48]. The subsequent development of polysaccharide-protein conjugate vaccines has been another important breakthrough. In this case, the polysaccharide vaccines that were known to be able to induce protective immunity, but they could not engage lasting

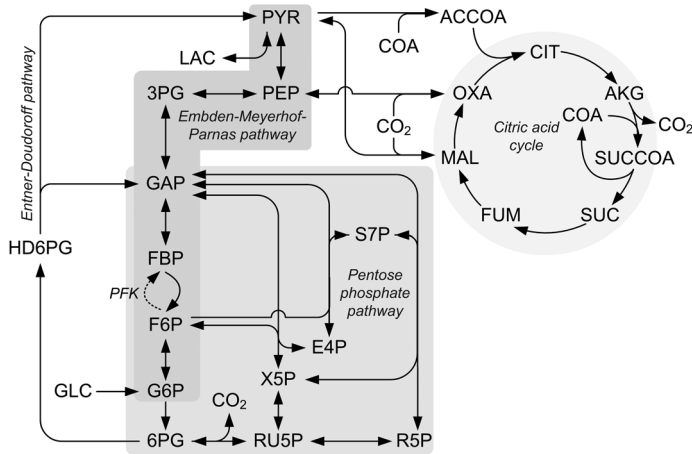


Figure 1.3 Central metabolism of *N. meningitidis* (simplified). The dashed arrow indicates phosphofructokinase (PFK), which is not present in *N. meningitidis*. Abbreviations are listed in Appendix 2.2.

immunological memory and failed to work in infants, were conjugated to a carrier protein. This made these vaccines very effective in infants, opening the way to the development of several safe and effective vaccines [48]. In addition, the application of adjuvants enhances the immune responses against antigens of several vaccines [49, 50]. Effective polysaccharide and polysaccharide-protein conjugate vaccines that offer protection against infection with meningococcal serogroups A, C, Y and W-135 are being developed or have been licenced and are available worldwide [51, 52]. Efforts to use the capsular polysaccharide of serogroup B meningococci as vaccine have been hampered by its poor immunogenicity [53], even when conjugated to a carrier protein [54, 55]. However, recent studies suggest the capsular polysaccharide can be engineered to express unique epitopes suitable as vaccine candidates [56, 57]. In addition, a recent study demonstrates evidence towards the proof-in-principle that by using specific LPS

conjugates, coupled via the lipid A region of LPS, it is possible to elicit functional and protective antibodies against meningococcal infection [58]. Since serogroup B meningococci contribute significantly to the burden of meningococcal disease in many industrialized countries where both epidemic and endemic infections occur [59], different approaches to the development of vaccines are followed. Current vaccine development against serogroup B strains has mainly focussed on major subcapsular protein antigens, that are contained in outer membrane vesicles [51] produced from noncapsular recombinant strains, or other antigen delivery systems, like liposomes [60, 61]. The availability of genome sequences dramatically changed the scope for developing improved or novel vaccines by increasing the speed of target identification in comparison with conventional approaches [62-66]. This systematic search to identify novel protein antigens from genomic information has been termed 'reverse vaccinology' [65] and has been successful, in particular for identification of novel serogroup B antigens [63].

Different OMP antigens are being investigated as vaccine candidates (e.g. PorA, PorB, Opa/Opc, NspA, NadA) but PorA is the most highly expressed OMP by almost all meningococci and induces strong protective serum bactericidal antibodies (SBA), pinpointing PorA as a promising vaccine candidate [67]. Unfortunately, these bactericidal antibodies are usually directed against the two highly variable regions (VRs) of PorA [68]. PorA contains eight exposed surface loops (loops I to VIII) and most variability between PorA proteins resides in VR1 and VR2, which correspond to loops I and IV, respectively [68]. According to the PorA sequence database [69], a total of 177 variants of VR1 and 482 of VR2 are identified to date. Because of the high level of heterogeneity found in these regions, a vaccine based on a single PorA (i.e. isolated from one strain) shows only a narrow range of specificity. Therefore, the development of vaccines containing different PorA serosubtypes (i.e. a multivalent vaccine) is an absolute requirement to provide cross-protection against a variety of heterologous meningococcal isolates. Notably, significant differences in SBA titers between different PorAs have been observed [70], which means that the human immune response is PorA-

specific. However, the problem of weakly immunogenic PorAs can be overcome by using a different immunization schedule [71].

The Netherlands Vaccine Institute has produced an outer membrane vesicle vaccine (OMV vaccine), containing multiple PorAs, which has been through Phase II clinical trials. This hexavalent OMV vaccine (HexaMen), containing OMVs that were produced from two recombinant *N. meningitidis* strains that each express three PorA serosubtypes, has been studied in infants, toddlers and children [72, 73]. Potential efficacy, based on the induction of SBA, has been promising with this vaccine however cross-protection to PorA serosubtypes not contained in the vaccine has been a limitation. To overcome the limitations of the hexavalent vaccine, three additional PorAs have been added to a new nonavalent formulation (i.e. nine PorA serosubtypes). This NonaMen vaccine stimulates high SBA responses in mice [74], and further preclinical trials are underway. An important aspect of the further development trajectory of this promising vaccine is the development of a production process that is capable of producing sufficient amounts of vaccine in order to have a meaningful impact on public health.

VACCINE PROCESS DEVELOPMENT

Background

The development of a vaccine is not limited to identification of protective components, adjuvants, formulation and delivery systems, but also includes technical, manufacturing, analytical and regulatory skills that are important determinants for successful translation of a vaccine candidate to a licensed vaccine. On average, the total development time from vaccine candidate to a vaccine is 15-20 years. The central issue related to technology skills is the translation of a laboratory scale vaccine production process to a process that can be scaled-up and run reproducibly in the ultimate manufacturing environment to make a sufficient amount of vaccine. Notably, for a vaccine with a wide utility, the manufacture of tens of millions of doses per year is required [75]. From an economical point of view, rapid early phase process development is required, but also processes capable of delivering high yields of product of the desired quality are important. The broad quality goal is that each and every dose is equivalent, safe and effective. The central issue related to manufacturing is the requirement of validated process equipment and procedures meeting the requirements of good manufacturing practices (GMP) [76], including the control of the starting materials (e.g. growth media, inoculum), design and layout of the manufacturing facility, dedicated training of personnel, cleaning, maintenance, etc. The central issue related to regulation is the level of proof and documentation necessary to provide guarantees that consistent product quality is realized after each production run.

Because it is more difficult to characterize a whole cell vaccine or a vaccine in a complicated formulation, in comparison with small-molecule pharmaceuticals and with well-defined biopharmaceuticals like monoclonal antibodies, the regulatory oversight for the production and release of a ‘classical’ vaccine is more stringent. In addition, the stringent regulatory oversight in vaccine production and release is also a result of the historic tendency of vaccine manufacturers to state that the production process of

the vaccine itself defines the product, which is in principle correct, but paved the way for regulatory interference in all aspects of the production process. Any change in either scale or process, requires comparability (i.e. reassurance that the product will remain unchanged in terms of quality, efficacy, and safety) and satisfactory proof is demanded by the regulatory authorities [77, 78]. As a result, many vaccine production processes are outdated and stay outdated. This illustrates the importance of process development in the development of a new vaccine.

Production process

The production process of a vaccine (and all biopharmaceuticals derived from pro- and eukaryotic cells) can be divided into two major steps: upstream processing (USP), where the product is made, and downstream processing (DSP), where the product is purified and formulated to its final presentation. USP involves media preparation and a number of successive cultivation steps. The upstream process starts with thawing of a single cryovial with bacteria (or another microorganism) from a cell-bank followed by inoculation of liquid medium in a small flask. Once the culture reaches a certain density, subsequent transfer of the culture to systems of increasing volumes is carried out. In each passage the culture is diluted approximately 20 times (inoculum ~5%). These successive cultivation steps are required to start-up the final large-scale bioreactor with a sufficient amount of growing cells in order to avoid a lag phase and promote reproducibility.

When the final cultivation step is finished the DSP starts. In general, the DSP is much more diverse and strongly depends on the type of product [79] and its quality requirements. For example for the manufacture of whole cell vaccines, two DSP steps are executed; 1) harvesting the culture and 2) inactivation of the bacterial suspension by heat or a chemical compound. However, most times DSP involves other and/or more steps like concentration, extraction, detoxification, purification, blending, adjuvation and freeze drying before the final product is obtained. During both USP and DSP

samples are taken, measured and compared to set specifications. These samples, or in-process controls, are important determinants for the release of a product. In particular, the quality controls of the final product determine whether safety and potency testing in animals will be carried out and may include identity, sterility, opacity, pH, protein content, LPS content and specific toxicity [76]. The research described in this thesis, was mainly focused on the USP part of the process development of a vaccine against *N. meningitidis* based upon components derived from the outer membrane of the bacterium and incorporated in vesicles.

Upstream development and scale-up

Upstream processing or cultivation is, as mentioned before, an integral part of vaccine development. Regulatory requirements must be taken into consideration in the development of the cultivation step. Another important, economically driven, requirement is to maximize the product yield, which is in the case of *N. meningitidis* primarily the maximization of biomass formation. The development of a cultivation process involves equipment like shake flasks, small-scale bioreactors, medium-scale bioreactors (pilot-scale), and large-scale bioreactors, of which the medium-scale and large-scale systems are used for scale-up research, whereas small-scale systems are used to establish the basis of the cultivation process. On the basis of mode of operation, a bioreactor may be classified as batch, fed-batch, chemostat or perfusion system (Figure 1.4).

Since final product quality and quantity are primarily determined in the cultivation process [80], gaining knowledge about the organisms' metabolism is crucial. The information provided by the *N. meningitidis* genome [29] can be used to obtain information on the metabolic capabilities of the organism. As described in Chapter 2, this is done by screening the genome for genes that code for enzymes present in the primary metabolism yielding a genome-scale metabolic model. This process of network reconstruction, followed by the synthesis of *in silico* models describing their functionalities, is the essence of systems biology [81]. Genome-scale metabolic models have been built

for several organisms [82, 83] and were used to analyze cultivation data, to get a better understanding of cellular metabolism, to develop metabolic engineering strategies [84-86], to design media and processes [86-88] and even for on-line control of the process [89], which illustrates their usefulness for the development of an efficient cultivation step. Especially, the development of defined synthetic media is important in biopharmaceutical production processes to ensure reproducible growth and prevent regulatory difficulties. In particular, the use of raw materials of animal origin must be avoided to prevent possible introduction of prion diseases [90] and because the quality of animal originating materials is hard to control and could easily have impact on process performance.

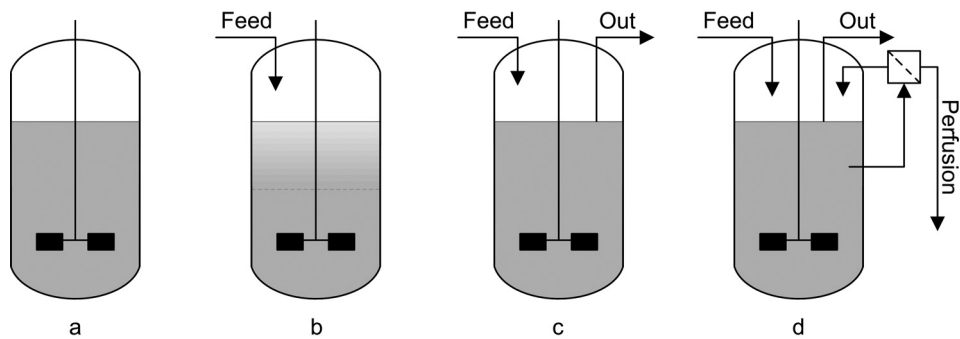


Figure 1.4 Schematic overview of bioreactors with different modes of operation. In a batch process (a) medium and microorganisms are added at the start. When an essential nutrient becomes limiting, growth will stop and the culture can be harvested. The batch process can be prolonged by addition of (limiting) nutrients (fed-batch) leading to a higher biomass density and higher product yield (b). A fed-batch process starts with a low volume batch process (dashed line) and at the end of the batch phase feed medium is added until the maximum volume is reached. Notably, different feed rate profiles (e.g. linear, exponential) can be applied. In a chemostat (c), or continuous stirred tank reactor (CSTR), medium is added constantly and culture is removed constantly at the same speed, which allows the control of the growth rate of the microorganism and consequently its physiology and metabolism. In a perfusion system (d) nutrients are refreshed continuously, while the microorganisms are retained in the bioreactor. The perfusion system is commonly used for cultivation of animal cells.

Once a small-scale cultivation process with defined culture conditions has been established, the process can be scaled-up. Notably, it is essential that the quality of the starting material (the strain) has been established. The quality of the inoculum can

have a substantial impact on process consistency and performance in terms of productivity, product quality and process control [91]. Therefore, in practice, the development of a chemically defined medium often occurs in parallel with the development of the first representative cell bank (or seedlot) for the vaccine, in which the organism has been adapted to the culture conditions, resulting in a reproducible and robust inoculation train. Its worth noting, that a cell bank is, like all other steps in vaccine development, subject to stringent regulation and needs to last until the life-cycle of the vaccine is completed (i.e. when no vaccine is required anymore because of eradication).

Scale-up can be defined as a procedure for the design and construction of a large-scale system on the basis of the results of experiments with small-scale equipment. It is an important step in process development that leads to the production of sufficient amounts of vaccine and thus has a meaningful impact on public health. Factors affected by scale are, for instance, the number of generations (i.e. population doublings), medium preparation, temperature, pH and DO control, agitation, aeration and pressure. As described in Chapter 5, transport phenomena are the most important phenomena that are dependent on scale [92] and therefore become the basis of every bioreactor scale-up procedure. Method-based procedures for scale-up and optimization of cultivation (and fermentation) processes in large-scale stirred-tank reactors include: fundamental methods, semifundamental methods (computational fluid dynamics), dimensional analysis and scale-down, regime analysis and scale-down, rules of thumb and finally trial and error [93]. No scale-up strategy as such is generally established, so for each product, process and facility a suitable scale-up strategy needs to be determined [94]. Many factors like overall production yields, costs, efficiency, time, knowledge, knowhow, and GMP compliance of process equipment play an important role in scale-up. Furthermore, the downstream process must be taken into account and preferably scaled-up interactively with the up-stream process, since enlarged volumes and/or higher product concentrations may affect the DSP and vice-versa. From a research point of view, defining the process attributes that affect the productivity or the product quality

during scale-up is very important, to ensure the control of the relevant process variables in order to obtain a bacterial suspension with defined characteristics. Optimization of the vaccine production process can be done until clinical phase III production (market scale), given that no changes will be implemented with respect to bacterial strains and starting materials that might change the characteristics of the vaccine product. Demonstration that the process at phase III/market scale is comparable to the medium-scale phase I/II process, and meets the pre-set criteria for process and product is always demanded by the regulatory authorities.

MATHEMATICAL TOOLS FOR THE STUDY OF METABOLISM

Metabolism and metabolic models

Metabolism can be defined as the complete set of chemical reactions that occur in living organisms in order to maintain life. Enzymes are the main players in this process as they are responsible for catalyzing the chemical reactions. The enzyme-reaction relationships can be used for the reconstruction of a network of chemical reactions, which leads to a metabolic model of metabolism. Similarly, annotation of genes (present in the genome of an organism) leads to gene-enzyme relationships, as explained in Chapter 2. A genome-scale metabolic network of chemical reactions that take place inside a living organism is reconstructed from the information that is present in its genome. Metabolism is divided into catabolism and anabolism and a simplified repre-

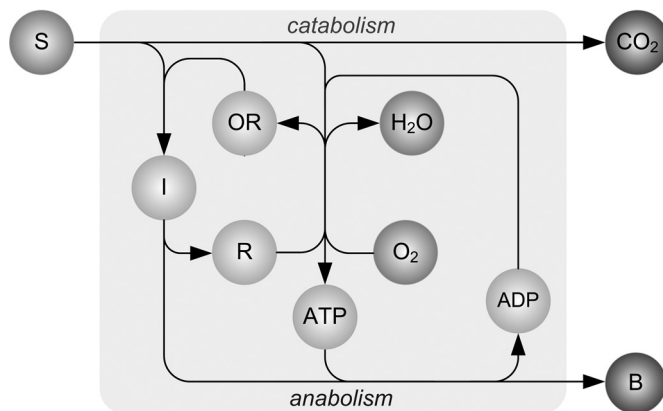


Figure 1.5 Simplified representation of aerobic metabolism. In catabolism substrate (S) is oxidized to metabolic intermediates (I) and CO₂, delivering reducing equivalents (R) and energy (ATP) for biomass formation (B). In aerobic respiration, the reducing equivalents are converted back to their oxidized form (OR) using the electron acceptor oxygen (O₂) which is converted to water (H₂O). This process is called oxidative phosphorylation. In anaerobic metabolism (not shown in the figure) ATP is generated using a process called substrate level phosphorylation, which occurs in glycolysis and is far less efficient than oxidative phosphorylation. The reducing equivalents in anaerobic metabolism are converted back to their oxidized form by using intermediate metabolites as electron acceptors and the reaction products are excreted by the organism (e.g. ethanol, lactic acid).

sentation of aerobic metabolism is shown in Figure 1.5. Catabolism is the part of metabolism that delivers metabolic intermediates, reducing equivalents (e.g. NADH, NADPH, FADH₂) and energy carriers (ATP) to anabolism, leading to the formation of biomass (for growth and maintenance) and the production of CO₂.

A stoichiometric metabolic network describes the way in which the different metabolites, substrates and products present inside and outside the organism are connected with each other through the different enzymatic reactions. There are three types of metabolic models: (1) steady state models, which only take into account the flow of metabolites through the system in steady state; (2) steady state kinetic models, which take into account the flow of metabolites through the system in steady state and contains at least one kinetic equation that relates the concentration of a metabolite to a reaction rate; and (3) dynamic kinetic models, which take into account the kinetics of all different enzymes involved in the reaction network that are valid under dynamic conditions. All metabolic models contain stoichiometric information, which means that for each reaction in the network the number of moles of each substrate and product taking part in the reaction is specified. Methods to solve a steady state model of metabolism are discussed in literature [95-100] and a brief summary is given below.

Metabolic modeling

A simplified metabolic network in which a substrate (S) can be converted into biomass (B) and a by-product (P) through several chemical conversions with a stoichiometry of 1, and which involves five intracellular metabolites (Mi) is shown in Figure 1.6.

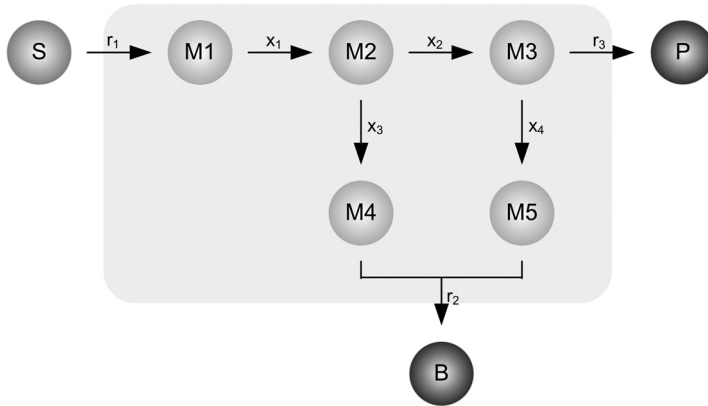


Figure 1.6 Simplified metabolic network. Substrate (S) can be converted into biomass (B) and product (P) through several chemical conversions involving intracellular (light grey area) metabolites (Mi).

The mass balance equations over the intracellular metabolites of the metabolic network in matrix notation are:

$$\frac{d}{dt} \begin{bmatrix} M1 \\ M2 \\ M3 \\ M4 \\ M5 \end{bmatrix} = \begin{bmatrix} -1 & 0 & 0 & 0 & 1 & 0 & 0 \\ 1 & 1 & 1 & 0 & 0 & 0 & 0 \\ 0 & 1 & 0 & 1 & 0 & 0 & -1 \\ 0 & 0 & 1 & 0 & 0 & -1 & 0 \\ 0 & 0 & 0 & 1 & 0 & 0 & -1 \end{bmatrix} \cdot \begin{bmatrix} x1 \\ x2 \\ x3 \\ x4 \\ r1 \\ r2 \\ r3 \end{bmatrix} = A \cdot \begin{bmatrix} x \\ r \end{bmatrix} \quad (1.1)$$

The stoichiometric matrix A ($m \times n$) is the matrix in which m (rows) corresponds to the number of intracellular metabolites and n (columns) is the number of fluxes (x)

and exchange rates (r). In (pseudo) steady state it is assumed that there is no accumulation of the intracellular metabolites (law of conservation of mass). Hence, their net conversion rate is zero:

$$A \cdot \begin{bmatrix} x \\ r \end{bmatrix} = 0 \quad (1.2)$$

This results in a set of linear equations and the set of all possible solutions for the fluxes to this set of linear equations (under the steady-state assumption) is called the null space or solution space of A . The dimension of the null space will be determined by the number of free variables (the degree of freedom) in the set of linear equations, which is equal to the number of unknowns minus the number of independent relations. The number of independent relations is equal to the rank of the stoichiometric matrix (i.e. $\text{rank}(A)$). In the network in Figure 1.6, there are 5 intracellular metabolites and 7 reactions (5 equations and 7 unknowns). Therefore, the null space is two-dimensional (Figure 1.7a).

In general, stoichiometric matrices have more reactions than metabolites, which is caused by branching in the metabolic network. In addition, some combinations of metabolites might be conserved. For example, reducing equivalents like FADH_2 and NAD(P)H are coupled to their oxidized forms (i.e. FAD and NAD(P)): If in a reaction FADH_2 is converted to FAD , there is always a coupled reaction that regenerates FADH_2 and therefore the FAD and FADH_2 amounts in the cell form a pool of constant size (i.e. $\text{FAD} + \text{FADH}_2 = \text{constant}$) and the sum of their production rates is zero (i.e. $r_{\text{FAD}} + r_{\text{FADH}_2} = 0$). These compounds are called conserved moieties and introduce linear dependencies in the set of linear equations. The set of equations in 1.2 is usually underdetermined. The null space can be used to determine underdeterminacies in the metabolic network like for instance the detection of parallel pathways. This check for network sensitivity problems can be done by doing singular value decomposition (SVD) [101], as explained in Chapter 2. Notably, for a realistic metabolic network,

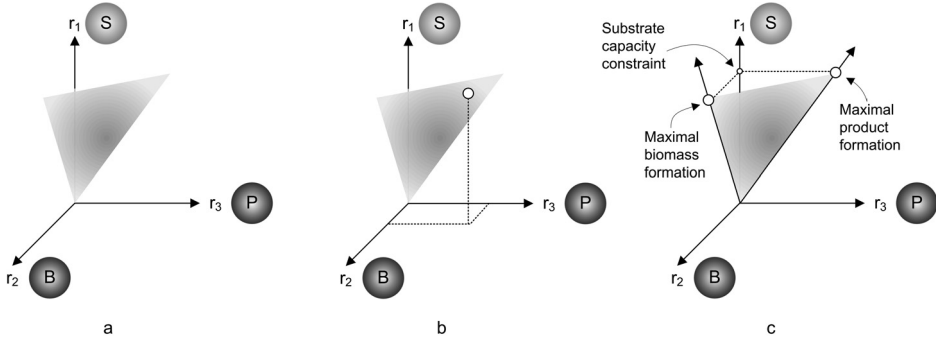


Figure 1.7 The null space of the example network is two-dimensional (a). Metabolic flux analysis (MFA): if consumption and production rates are measured a unique solution can be calculated (b). Flux balance analysis (FBA): If only the substrate conversion rate (S) is known from measurement, a solution that optimizes a particular objective, like maximize biomass formation or maximize product formation, can be calculated using linear programming (c). Adapted from [102].

that contains far more reactions, the null space is n -dimensional and mathematical computer software (e.g. Matlab) is required to calculate the null space. Since a part of the exchange rates might be unknown, Equation 1.2 can be rearranged to:

$$A \cdot \begin{bmatrix} x \\ r \end{bmatrix} = [A_c \ A_m] \cdot \begin{bmatrix} r_c \\ r_m \end{bmatrix} = 0 \quad (1.3)$$

or

$$A_c \cdot r_c + A_m \cdot r_m = 0 \quad (1.4)$$

Where submatrix (A_c) is linked to the fluxes and exchange rates that need to be calculated (r_c) and submatrix (A_m) is linked to the measured exchange rates (r_m). The solution now becomes:

$$r_c = -A_c^\# \cdot A_m \cdot r_m + \text{null space}(A_c) \cdot \lambda \quad (1.5)$$

Where $-A_c^\#$ is the pseudo inverse of matrix A_c and λ is a vector with as many elements as there are columns in the nullspace of A_c . Again, the number of independent linear equations in the A_c matrix is equal to the rank of the matrix (i.e. $\text{rank}(A_c)$). Notably, for all possible values of λ the solution remains valid. The degree of freedom of the system is given by:

$$df = n_c - n_m - \text{rank}(A_c) \quad (1.6)$$

Where n_c is the number of unknowns (fluxes and unknown exchange rates), and n_m is the number of known measured exchange rates. Metabolic networks can be classified based on determinancy and redundancy.

Determinancy

1. Underdetermined: The $\text{rank}(A_c)$ is smaller than the number of unknowns ($df > 0$). There are not enough linear independent relations to calculate all the unknowns, r_c , from the measured rates r_m . Notably, some of the unknowns may be calculable.
2. Determined: The $\text{rank}(A_c)$ equals the number of unknowns ($df = 0$). All unknown rates can be calculated from the measured rates.

Redundancy

1. Redundant: There is at least one linear relation between two or more measured rates and these rates can be balanced. This means that the measurements can be inconsistent, or in other words there is no r_c for the given r_m that exactly matches Equation 1.5. For instance, in the example network the biomass production rate should always be twice the substrate consumption rate ($r_1 = r_3 + 2 \cdot r_2$). Notably, the term overdetermined, which is often encountered, is, in principle, not correct, since a system that is redundant can at the same time be underdetermined.
2. Non-redundant: There is no relation between measured rates and the system is always consistent.

In line with the above classification for networks also rates and fluxes can be classified. Non-measured rates can be classified according to whether they can be calculated from Equation 1.5 or not:

Calculable: The rate can be uniquely calculated from Equation 1.5. Only when all rates are calculable the system is determined.

Non-calculable: The rate cannot be uniquely calculated from Equation 1.5. If one of the rates is non-calculable the system is underdetermined.

Measured rates can be classified according to whether they are balanceable or not:

Balanceable: There is a linear relation between the rate and at least one other rate. If the linear relation does not hold, the measurements are inconsistent. If two or more rates are balanceable the system is redundant.

Non-balanceable: There is no relation between the rate and any of the other measured rates. If all rates are non-balanceable the system is non-redundant.

If values for the substrate consumption rate (r_1) and the biomass formation rate (r_2) are known from measurements, the degree of freedom of the network shown in Figure 1.4 is zero, which means that the system is determined and a single unique solution for all fluxes and the product formation rate (r_3) can be calculated using linear-algebra techniques. This unique solution is shown in Figure 1.7b. If, in addition, a value for the product formation rate (r_3) is also known from measurements, the system is redundant. In this case the measurement errors can be used to balance the measured rates (see Chapter 2), which yields a unique and more reliable solution. Solving determined and redundant metabolic networks is mostly referred to as metabolic flux analysis (MFA). In the case where only a value for the substrate consumption rate (r_1) is known from measurement, the system is underdetermined ($df=1$). A solution to Equation 1.5 can be calculated (i.e. estimated) by assuming that the system fulfills an

optimality condition. By using a particular objective function, like for instance maximize the biomass formation rate (r_2), the optimal solution (i.e. optimal flux distribution) that optimizes this object function can be found using linear programming (Figure 1.7c), as explained in Chapter 3. To find a particular maximum, one or more constraints are required, otherwise the solution to the optimization will be unbounded (the vector goes to infinity). At the given substrate consumption rate (indicated as substrate capacity constraint in Figure 1.6c), the corresponding optimal solutions for biomass and product formation can be calculated (indicated as dots in Figure 1.7c). The technique for solving an underdetermined metabolic model is commonly referred to as flux balance analysis (FBA) and is often used in genome-scale models, in which the number of unknown fluxes is too large to calculate from measurements [102]. It is worth noting that in the case where the metabolic model is both redundant and underdetermined, the techniques for solving the determined part including balancing and the underdetermined part (optimization) can both be applied. In this case a solution that optimizes a particular objective function is calculated for the underdetermined parts, whereas a unique solution is calculated for the determined parts of the model.

AIM AND THESIS OUTLINE

The aim of this thesis research was to develop the upstream part of the production process of a vaccine based upon PorA entrapped in outer membrane vesicles directed against *N. meningitidis* serogroup B organisms. For this, an extensive study on the primary metabolism of *N. meningitidis* serogroup B was used as a starting point, which led to the design of a chemically defined minimal synthetic medium for growth. A recombinant *N. meningitidis* strain that expresses a heterologous phosphofructokinase was genetically engineered to illustrate the potential of genetic engineering from a manufacturing point of view and gather more insight into the evolution of part of the primary metabolism of *N. meningitidis*. Besides covering the *N. meningitidis* primary metabolism in detail, the cultivation process was further optimized and scaled-up, including bioreactor design and bioreactor operation strategy. The upstream production process, including the realized manufacturing bioreactor configuration is compliant with cGMP and can be used for bulk production of the vaccine against meningococcal disease at the ultimate production scale.

Chapter 2 describes the construction of a genome-scale flux model for the primary metabolism of *N. meningitidis* using the genomic database of *N. meningitidis* serogroup B together with biochemical and physiological information from the literature. Hence, this chapter contains a detailed review on the *N. meningitidis* primary metabolism. The validity of a simplified metabolic network derived from the genome-scale metabolic network was verified using flux-balance analysis. In addition, several useful predictions were obtained from *in silico* experiments, including substrate preference, which led to the design of a minimal medium for growth of *N. meningitidis*.

Chapter 3 describes the influence of the growth rate of *N. meningitidis* on its macromolecular composition and its metabolic activity. Besides the determination of yield and energy parameters, the reliability of the calculated flux distribution was indicated

using Monte Carlo simulation, which has not been done previously for this type of analysis. Furthermore, a mathematical split ratio analysis between the Entner-Doudoroff and the pentose phosphate pathway indicated a required minimal flux through the Entner-Doudoroff pathway and a minor effect on ATP formation rate. This approach led to a range of possible flux solutions as a function of the split ratio. Therefore, flux ranges are presented for underdetermined parts of metabolic network rather than single flux values, which is more commonly done in literature. The metabolic model for *N. meningitidis* serogroup B presented in Chapter 2 and 3 is the first available metabolic model, offering a framework to study *N. meningitidis* metabolism as a whole or certain aspects of it. For example, the knowledge gathered in Chapter 2 and 3 was used for *in silico* FBA prediction of the impact of heterologous expression of phosphofructokinase in *N. meningitidis* on biomass yield as described in Chapter 4.

Chapter 4 describes the genetic engineering of a recombinant *N. meningitidis* strain that expresses a heterologous phosphofructokinase from *E. coli* to address the questions why the *N. meningitidis* genome lacks the gene encoding this enzyme from an evolutionary point of view, and to possibly improve the production strain in terms of biomass yield on substrate. In particular since expression of phosphofructokinase enables a functional glycolysis in *N. meningitidis* and *in silico* FBA predictions indicated a higher biomass yield on substrate which might lead to process improvement. Genetic engineering in vaccine development against *N. meningitidis* is, in general, focused on the identification of vaccine candidates by expressing these potential candidates in *E. coli* (reverse vaccinology), whereas improvement of *N. meningitidis* from a manufacturing point of view is hardly investigated. Genetic engineering has been applied in *N. meningitidis* in order to express different porA serosubtypes in one strain [103] or to detoxify LPS [104], but it has not been applied to possibly improve production strains from a manufacturing point of view (e.g. increase the yield of biomass on substrate or reduce by-product formation). The research described in Chapter 4 is a

first step in this direction.

Chapter 5 describes the scale-up approach for the upstream process at 1,2 m³ scale and the resulting bioreactor design and operation strategy that led to a feasible solution for the production of a vaccine against meningococcal disease based upon OMVs. The bioreactor was technically realized following cGMP guidelines and is appropriate for bulk production of the vaccine for phase III clinical trials and for the vaccine after licensing of the product. In addition, the design of the bioreactor allows production of other bacterial vaccines (e.g. diphtheria) without the need for fundamental changes (i.e. multi-purpose).

Chapter 6 places this work in a broader context and highlights some of the results described in this thesis. Furthermore, suggestions for the further improvement and optimization of vaccine process development against *N. meningitidis* serogroup B organisms are given.

REFERENCES

1. Tønnum T. Genus I. *Neisseria*. In: Bergey's Manual of Systematic Bacteriology. Edited by Brenner DJ, Krieg NR, Staley JT, vol. 2, 2 edn. New York: Springer; 2005.
2. Neisser ALS. 1879. Über eine der Gonorrhoe eigentümliche Microccenform. *Centralblatt für die medicinischen Wissenschaften* 17:497-500.
3. Knapp JS. 1988. Historical perspectives and identification of *Neisseria* and related species. *Clin Microbiol Rev* 1:415-431.
4. Stein D. The *Neisseria*. In: The Prokaryotes. 2006: 602-647.
5. Weichselbaum A. 1887. Ueber die Aetologie der akuten meningitis cerebrospinalis. *Fortschr Med* 5:573.
6. Broome CV. 1986. The carrier state: *Neisseria meningitidis*. *J Antimicrob Chemother* 18 Suppl A:25-34.
7. Hart CA, Rogers TRF. 1993. Meningococcal disease. *J Med Microbiol* 39:23-25.
8. Stephens DS. 2007. Conquering the Meningococcus. *FEMS Microbiology Reviews* 31:3-14.
9. Goldschneider I, Gotschlich EC, Artenstein MS. 1969. Human immunity to the meningococcus. II. Development of natural immunity. *J Exp Med* 129:1327-1348.
10. Rosenstein NE, Perkins BA, Stephens DS, Popovic T, Hughes JM. 2001. Meningococcal disease. *N Engl J Med* 344:1378-1388.
11. Caugant DA, Hoiby EA, Magnus P, Scheel O, Hoel T, Bjune G, Wedege E, Eng J, Froholm LO. 1994. Asymptomatic carriage of *Neisseria meningitidis* in a randomly sampled population. *J Clin Microbiol* 32:323-330.
12. Caugant DA, Tzanakaki G, Kriz P. 2007. Lessons from meningococcal carriage studies. *FEMS Microbiol Rev* 31:52-63.
13. Yazdankhah SP, Caugant DA. 2004. *Neisseria meningitidis*: an overview of the carriage state. *J Med Microbiol* 53:821-832.
14. MacLennan J, Kafatos G, Neal K, Andrews N, Cameron JC, Roberts R, Evans MR, Cann K, Baxter DN, Maiden MC et al. 2006. Social behavior and meningococcal carriage in British teenagers. *Emerg Infect Dis* 12:950-957.
15. Cookson ST, Corrales JL, Lotero JO, Regueira M, Binsztein N, Reeves MW, Ajello G, Jarvis WR. 1998. Disco fever: epidemic meningococcal disease in northeastern Argentina associated with disco patronage. *J Infect Dis* 178:266-269.
16. Stuart JM, Cartwright KA, Robinson PM, Noah ND. 1989. Effect of smoking on meningococcal carriage. *Lancet* 2:723-725.
17. van Deuren M, Brandtzaeg P, van der Meer JW. 2000. Update on meningococcal disease with emphasis on pathogenesis and clinical management. *Clin Microbiol Rev* 13:144-166.
18. Peltola H. 1983. Meningococcal disease: still with us. *Rev Infect Dis* 5:71-91.
19. Stephens DS, Greenwood B, Brandtzaeg P. 2007. Epidemic meningitis, meningococcaemia, and *Neisseria meningitidis*. *Lancet* 369:2196-2210.
20. Poolman JT. 1995. Development of a meningococcal vaccine. *Infect Agents Dis* 4:13-28.
21. Bos MP, Tommassen J. 2004. Biogenesis of the Gram-negative bacterial outer membrane. *Curr Opin Microbiol* 7:610-616.
22. Nassif X. 1999. Interaction mechanisms of encapsulated meningococci with eucaryotic cells: what does this tell us about the crossing of the blood-brain barrier by *Neisseria meningitidis*? *Curr Opin Microbiol* 2:71-77.
23. Davidsen T, Tønnum T. 2006. Meningococcal genome dynamics. *Nat Rev Microbiol* 4:11-22.
24. Wolfgang M, Park HS, Hayes SF, van Putten JP, Koomey M. 1998. Suppression of an absolute defect in type IV pilus biogenesis by loss-of-function mutations in pilT, a twitching motility gene in *Neisseria gonorrhoeae*. *Proc Natl Acad Sci U S A* 95:14973-14978.
25. Yi K, Rasmussen AW, Gudlavalleti SK, Stephens DS, Stojiljkovic I. 2004. Biofilm formation by *Neisseria meningitidis*. *Infect Immun* 72:6132-6138.
26. Tzeng YL, Stephens DS. 2000. Epidemiology and pathogenesis of *Neisseria meningitidis*. *Microbes Infect* 2:687-700.
27. World Health Organization (<http://www.who.int/en/>).
28. Parkhill J, Achtman M, James KD, Bentley SD, Churcher C, Klee SR, Morelli G, Basham D, Brown D, Chillingworth T et al. 2000. Complete DNA sequence of a serogroup A strain of *Neisseria meningitidis* Z2491. *Nature* 404:502-506.
29. Tettelin H, Saunders NJ, Heidelberg J, Jeffries AC, Nelson KE, Eisen JA, Ketchum KA, Hood DW,

- Peden JF, Dodson RJ et al. 2000. Complete genome sequence of *Neisseria meningitidis* serogroup B strain MC58. *Science* 287:1809-1815.
30. Bentley SD, Vernikos GS, Snyder LA, Churcher C, Arrowsmith C, Chillingworth T, Cronin A, Davis PH, Holroyd NE, Jagels K et al. 2007. Meningococcal genetic variation mechanisms viewed through comparative analysis of serogroup C strain FAM18. *PLoS Genet* 3:e23.
 31. Snyder LA, Butcher SA, Saunders NJ. 2001. Comparative whole-genome analyses reveal over 100 putative phase-variable genes in the pathogenic *Neisseria* spp. *Microbiology* 147:2321-2332.
 32. The BioCyc collection of Pathway/Genome Databases (<http://www.biocyc.org/>).
 33. Richardson AR, Stojiljkovic I. 2001. Mismatch repair and the regulation of phase variation in *Neisseria meningitidis*. *Mol Microbiol* 40:645-655.
 34. Feil EJ, Spratt BG. 2001. Recombination and the population structures of bacterial pathogens. *Annu Rev Microbiol* 55:561-590.
 35. van Ulsen P, Tommassen J. 2006. Protein secretion and secreted proteins in pathogenic *Neisseriaceae*. *FEMS Microbiol Rev* 30:292-319.
 36. Vitovski S, Sayers JR. 2007. Relaxed cleavage specificity of an immunoglobulin A1 protease from *Neisseria meningitidis*. *Infect Immun* 75:2875-2885.
 37. Massari P, King CA, Ho AY, Wetzler LM. 2003. *Neisserial* PorB is translocated to the mitochondria of HeLa cells infected with *Neisseria meningitidis* and protects cells from apoptosis. *Cell Microbiol* 5:99-109.
 38. Holten E. 1974. 6-Phosphogluconate dehydrogenase and enzymes of the Entner-Doudoroff pathway in *Neisseria*. *Acta Pathol Microbiol Scand [B] Microbiol Immunol* 82:207-213.
 39. Holten E. 1975. Radiorespirometric studies in genus *Neisseria*. I. The catabolism of glucose. *Acta Pathol Microbiol Scand [B]* 83:353-366.
 40. Jyssum K. 1962. Dissimilation of C14 labelled glucose by *Neisseria meningitidis* 1. The formation of CO₂ and acetate from glucose carbon. *Acta Pathol Microbiol Immunol Scand [B]* 55:319-324.
 41. Jyssum K. 1962. Dissimilation of C14 labelled glucose by *Neisseria meningitidis* 2. The incorporation of 1-C14 and 6-C14 into cellular components in short time experiments. *Acta Pathol Microbiol Immunol Scand [B]* 55:325-334.
 42. Jyssum K. 1962. Dissimilation of C14 labelled glucose by *Neisseria meningitidis* 2. The incorporation of 1-C14 and 6-C14 into pyruvate. *Acta Pathol Microbiol Immunol Scand [B]* 55:335-341.
 43. Jyssum K, Borchgrevink B, Jyssum S. 1961. Glucose catabolism in *Neisseria meningitidis*. 1. Glucose oxidation and intermediate reactions of the Embden-Meyerhof pathway. *Acta Pathol Microbiol Scand* 53:71-83.
 44. Exley RM, Shaw J, Mowe E, Sun YH, West NP, Williamson M, Botto M, Smith H, Tang CM. 2005. Available carbon source influences the resistance of *Neisseria meningitidis* against complement. *J Exp Med* 201:1637-1645.
 45. Leighton MP, Kelly DJ, Williamson MP, Shaw JG. 2001. An NMR and enzyme study of the carbon metabolism of *Neisseria meningitidis*. *Microbiology* 147:1473-1482.
 46. Catlin BW. 1973. Nutritional profiles of *Neisseria gonorrhoeae*, *Neisseria meningitidis*, and *Neisseria lactamica* in chemically defined media and the use of growth requirements for gonococcal typing. *J Infect Dis* 128:178-194.
 47. Robbins JB, Schneerson R, Trollfors B, Sato H, Sato Y, Rappuoli R, Keith JM. 2005. The diphtheria and pertussis components of diphtheria-tetanus toxoids-pertussis vaccine should be genetically inactivated mutant toxins. *J Infect Dis* 191:81-88.
 48. Rappuoli R. 2007. Bridging the knowledge gaps in vaccine design. *Nat Biotechnol* 25:1361-1366.
 49. Singh M, O'Hagan D. 1999. Advances in vaccine adjuvants. *Nat Biotechnol* 17:1075-1081.
 50. Fransen F, Boog CJ, van Putten JP, van der Ley P. 2007. Agonists of Toll-like receptors 3, 4, 7, and 9 are candidates for use as adjuvants in an outer membrane vaccine against *Neisseria meningitidis* serogroup B. *Infect Immun* 75:5939-5946.
 51. Girard MP, Preziosi MP, Aguado MT, Kiény MP. 2006. A review of vaccine research and development: meningococcal disease. *Vaccine* 24:4692-4700.
 52. Trotter CL, Ramsay ME. 2007. Vaccination against meningococcal disease in Europe: review and recommendations for the use of conjugate vaccines. *FEMS Microbiology Reviews* 31:101-107.
 53. Finne J, Bitter-Suermann D, Goridis C, Finne U. 1987. An IgG monoclonal antibody to group B meningococci cross-reacts with developmentally regulated polysialic acid units of glycoproteins in neural and extraneural tissues. *J Immunol* 138:4402-4407.
 54. Zollinger WD, Moran EE, Devi SJ, Frasch CE. 1997. Bactericidal antibody responses of juvenile

- rhesus monkeys immunized with group B *Neisseria meningitidis* capsular polysaccharide-protein conjugate vaccines. *Infect Immun* 65:1053-1060.
55. Devi SJ, Zollinger WD, Snoy PJ, Tai JY, Costantini P, Norelli F, Rappuoli R, Frasch CE. 1997. Preclinical evaluation of group B *Neisseria meningitidis* and *Escherichia coli* K92 capsular polysaccharide-protein conjugate vaccines in juvenile rhesus monkeys. *Infect Immun* 65:1045-1052.
 56. Moe GR, Dave A, Granoff DM. 2005. Epitopes recognized by a nonautoreactive murine anti-N-propionyl meningococcal group B polysaccharide monoclonal antibody. *Infect Immun* 73:2123-2128.
 57. Moe GR, Dave A, Granoff DM. 2006. Molecular analysis of anti-N-propionyl *Neisseria meningitidis* group B polysaccharide monoclonal antibodies. *Mol Immunol* 43:1424-1431.
 58. Cox AD, Zou W, Gidney MA, Lacelle S, Pledet JS, Makepeace K, Wright JC, Coull PA, Moxon ER, Richards JC. 2005. Candidacy of LPS-based glycoconjugates to prevent invasive meningococcal disease: developmental chemistry and investigation of immunological responses following immunization of mice and rabbits. *Vaccine* 23:5045-5054.
 59. Zimmer SM, Stephens DS. 2006. Serogroup B meningococcal vaccines. *Curr Opin Investig Drugs* 7:733-739.
 60. Humphries HE, Williams JN, Blackstone R, Jolley KA, Yuen HM, Christodoulides M, Heckels JE. 2006. Multivalent liposome-based vaccines containing different serosubtypes of PorA protein induce cross-protective bactericidal immune responses against *Neisseria meningitidis*. *Vaccine* 24:36-44.
 61. Arigita C, Luijckx T, Jiskoot W, Poelen M, Hennink WE, Crommelin DJ, Ley P, Els C, Kersten GF. 2005. Well-defined and potent liposomal meningococcal B vaccines adjuvated with LPS derivatives. *Vaccine* 23:5091-5098.
 62. Meinke A, Henics T, Nagy E. 2004. Bacterial genomes pave the way to novel vaccines. *Curr Opin Microbiol* 7:314-320.
 63. Pizza M, Scarlato V, Masignani V, Giuliani MM, Arico B, Comanducci M, Jennings GT, Baldi L, Bartolini E, Capecchi B et al. 2000. Identification of vaccine candidates against serogroup B meningococcus by whole-genome sequencing. *Science* 287:1816-1820.
 64. Poolman J, Berthet FX. 2001. Alternative vaccine strategies to prevent serogroup B meningococcal diseases. *Vaccine* 20 Suppl 1:S24-26.
 65. Rappuoli R. 2001. Reverse vaccinology, a genome-based approach to vaccine development. *Vaccine* 19:2688-2691.
 66. Rappuoli R. 2001. Conjugates and reverse vaccinology to eliminate bacterial meningitis. *Vaccine* 19:2319-2322.
 67. Vermont CL, van Dijken HH, Kuipers AJ, van Limpt CJ, Keijzers WC, van der Ende A, de Groot R, van Alphen L, van den Dobbelaars GP. 2003. Cross-reactivity of antibodies against PorA after vaccination with a meningococcal B outer membrane vesicle vaccine. *Infect Immun* 71:1650-1655.
 68. van der Ley P, Heckels JE, Virji M, Hoogerhout P, Poolman JT. 1991. Topology of outer membrane porins in pathogenic *Neisseria* spp. *Infect Immun* 59:2963-2971.
 69. <http://neisseria.org/nml/>. PorA sequence database.
 70. Luijckx TA, van Dijken H, Hamstra HJ, Kuipers B, van der Ley P, van Alphen L, van den Dobbelaars G. 2003. Relative immunogenicity of PorA subtypes in a multivalent *Neisseria meningitidis* vaccine is not dependent on presentation form. *Infect Immun* 71:6367-6371.
 71. Luijckx T, van Dijken H, van Els C, van den Dobbelaars G. 2006. Heterologous prime-boost strategy to overcome weak immunogenicity of two serosubtypes in hexavalent *Neisseria meningitidis* outer membrane vesicle vaccine. *Vaccine* 24:1569-1577.
 72. de Kleijn ED, de Groot R, Labadie J, Lefeber AB, van den Dobbelaars G, van Alphen L, van Dijken H, Kuipers B, van Omme GW, Wala M et al. 2000. Immunogenicity and safety of a hexavalent meningococcal outer-membrane-vesicle vaccine in children of 2-3 and 7-8 years of age. *Vaccine* 18:1456-1466.
 73. de Kleijn E, van Eijndhoven L, Vermont C, Kuipers B, van Dijken H, Rumke H, de Groot R, van Alphen L, van den Dobbelaars G. 2001. Serum bactericidal activity and isotype distribution of antibodies in toddlers and schoolchildren after vaccination with RIVM hexavalent PorA vesicle vaccine. *Vaccine* 20:352-358.
 74. van den Dobbelaars GP, van Dijken HH, Pillai S, van Alphen L. 2007. Immunogenicity of a combination vaccine containing pneumococcal conjugates and meningococcal PorA OMVs. *Vaccine* 25:2491-2496.
 75. Buckland BC. 2005. The process development challenge for a new vaccine. *Nat Med* 11:S16-19.
 76. Müller KM, Gempeler MR, Scheiwe M-W, Zeugin BT. 1996. Quality assurance for biopharmaceuticals:

- An overview of regulations, methods and problems. *Pharmaceutica Acta Helvetiae* 71:421-438.
77. European Medicines Agency (<http://emea.europa.eu/>).
 78. U.S. Food and Drug Administration (<http://www.fda.gov/>).
 79. Ulmer JB, Valley U, Rappuoli R. 2006. Vaccine manufacturing: challenges and solutions. *Nat Biotechnol* 24:1377-1383.
 80. Streefland M, van de Waterbeemd B, Happe H, van der Pol LA, Beuvery EC, Tramper J, Martens DE. 2007. PAT for vaccines: the first stage of PAT implementation for development of a well-defined whole-cell vaccine against whooping cough disease. *Vaccine* 25:2994-3000.
 81. Palsson BO. *Systems Biology: Properties of Reconstructed Networks*. New York: Cambridge University Press; 2006.
 82. Price ND, Papin JA, Schilling CH, Palsson BO. 2003. Genome-scale microbial *in silico* models: the constraints-based approach. *Trends Biotechnol* 21:162-169.
 83. Kim HU, Kim TY, Lee SY. 2007. Metabolic flux analysis and metabolic engineering of microorganisms. *Mol BioSyst* 4:113-120.
 84. Hua Q, Joyce AR, Fong SS, Palsson BO. 2006. Metabolic analysis of adaptive evolution for *in silico*-designed lactate-producing strains. *Biotechnol Bioeng* 95:992-1002.
 85. Fong SS, Burgard AP, Herring CD, Knight EM, Blattner FR, Maranas CD, Palsson BO. 2005. *In silico* design and adaptive evolution of *Escherichia coli* for production of lactic acid. *Biotechnol Bioeng* 91:643-648.
 86. Smid EJ, Molenaar D, Hugenholtz J, de Vos WM, Teusink B. 2005. Functional ingredient production: application of global metabolic models. *Curr Opin Biotechnol* 16:190-197.
 87. Teusink B, van Enkevort FH, Francke C, Wiersma A, Wegkamp A, Smid EJ, Siezen RJ. 2005. *In silico* reconstruction of the metabolic pathways of *Lactobacillus plantarum*: comparing predictions of nutrient requirements with those from growth experiments. *Appl Environ Microbiol* 71:7253-7262.
 88. Xie L, Wang DIC. 1994. Stoichiometric analysis of animal cell growth and its application in medium design. *Biotechnol Bioeng* 43:1164-1174.
 89. Provost A, Bastin G. 2004. Dynamic metabolic modelling under the balanced growth condition. *J Proc Control* 14:717-728.
 90. Thiry M, Cingolani D. 2002. Optimizing scale-up fermentation processes. *Trends Biotechnol* 20:103-105.
 91. Okonkowski J, Kizer Bentley L, Listner K, Robinson D, Chartrain M. 2005. Development of a robust, versatile, and scalable inoculum train for the production of a DNA vaccine. *Biotechnol Prog* 21:1038-1047.
 92. Mavituna F. Strategies for Bioreactor scale-up. In: *Computer and Information Science Application in Bioprocess Engineering*. Edited by Moreira AR, Wallace KK. Dordrecht, The Netherlands: Kluwer Academic Publishers; 1996.
 93. Sweere APJ, Luyben KCAM, Kossen NWF. 1987. Regime analysis and scale-down: Tools to investigate the performance of bioreactors. *Enzyme Microb Tech* 9:386-398.
 94. Schmidt FR. 2005. Optimization and scale up of industrial fermentation processes. *Appl Microbiol Biotechnol* 68:425-435.
 95. Edwards JS, Ibarra RU, Palsson BO. 2001. *In silico* predictions of *Escherichia coli* metabolic capabilities are consistent with experimental data. *Nat Biotechnol* 19:125-130.
 96. Edwards JS, Ramakrishna R, Schilling CH, Palsson BO. Metabolic flux balance analysis. In: *Metabolic Engineering*. Edited by Lee SY, Papoutsakis ET. New York: Marcel Dekker Inc.; 1999: 13-57.
 97. Forster J, Gombert AK, Nielsen J. 2002. A functional genomics approach using metabolomics and *in silico* pathway analysis. *Biotechnol Bioeng* 79:703-712.
 98. van Gulik WM, Heijnen JJ. 1995. A metabolic network stoichiometry analysis of microbial growth and product formation. *Biotechnol Bioeng* 48:681-698.
 99. Vallino JJ, Stephanopoulos G. Flux determination in cellular bioreaction networks: applications to lysine fermentations. In: *Frontiers in bioprocessing*. Edited by Sikdar SK, Bier M, Todd P. Boca Raton, Fla: CRC press; 1990: 205-219.
 100. Baart GJ, Zomer B, de Haan A, van der Pol LA, Beuvery EC, Tramper J, Martens DE. 2007. Modeling *Neisseria meningitidis* metabolism: from genome to metabolic fluxes. *Genome Biol* 8:R136.
 101. van der Heijden RTJM, Romein B, Heijnen JJ, Hellinga C, Luyben KCAM. 1994. Linear constraint relations in biochemical reaction systems: I. Classification of the calculability and the balanceability of conversion rates. *Biotechnol Bioeng* 43:3-10.

102. Teusink B, Smid EJ. 2006. Modelling strategies for the industrial exploitation of lactic acid bacteria. *Nat Rev Microbiol* 4:46-56.
103. van der Ley P, van der Biezen J, Poolman JT. 1995. Construction of *Neisseria meningitidis* strains carrying multiple chromosomal copies of the *porA* gene for use in the production of a multivalent outer membrane vesicle vaccine. *Vaccine* 13:401-407.
104. Ley Pvd, Steeghs L, Hamstra HJ, Hove Jt, Zomer B, Alphen Lv. 2005. Modification of lipid A biosynthesis in *Neisseria meningitidis lpxL1* mutants: influence on lipopolysaccharide structure, toxicity, and adjuvant activity. *Infect Immun* 69:5981-5990.

Chapter 2

Modeling *Neisseria meningitidis* metabolism: from genome to metabolic fluxes

This chapter has been published as: Baart GJ, Zomer B, de Haan A, van der Pol LA, Beuvery EC, Tramper J, Martens DE. 2007. Modeling *Neisseria meningitidis* metabolism: from genome to metabolic fluxes. *Genome Biology* 8(7):R136.

ABSTRACT

Neisseria meningitidis is a human pathogen that can infect diverse sites within the human host. The major diseases caused by *N. meningitidis* are responsible for death and disability especially in young infants. In general, most of the recent work on *N. meningitidis*, focuses on potential antigens and their functions, immunogenicity, and pathogenicity mechanisms. Very little work has been carried out into *Neisseria* primary metabolism over the past 25 years. Using the genomic database of *N. meningitidis* serogroup B together with biochemical and physiological information provided in the literature we constructed a genome-scale flux model for primary metabolism of *N. meningitidis*. The validity of a simplified metabolic network derived from the genome-scale metabolic network was checked using flux balance analysis in chemostat cultures. Several useful predictions have been obtained from *in silico* experiments, including substrate preference. A minimal medium for growth of *N. meningitidis* was designed and tested successfully in batch and chemostat cultures. The verified metabolic model describes the primary metabolism of *N. meningitidis* in a chemostat in steady state. The genome-scale model is valuable because it offers a framework to study *N. meningitidis* metabolism as a whole, or certain aspects of it, and can also be used for vaccine process development purposes (for example the design of growth media). The flux distribution of the main metabolic pathways (that is, the pentose phosphate pathway and the Entner-Doudoroff pathway) indicates that the major part of pyruvate ($69\pm6\%$) is synthesized through the ED-cleavage, a finding that is in good agreement with literature.

INTRODUCTION

Neisseria meningitidis is a human pathogen that can infect diverse sites within the human host. The major diseases caused by *N. meningitidis* - meningitis and meningococcal septicemia - are responsible for death and disability, especially in young infants. There are different pathogenic *N. meningitidis* isolates of which serogroups B and C cause the majority of infections in industrialized countries, whereas strains of group A and C dominate in less developed countries [1]. Some disease control has been achieved by vaccination with polysaccharide vaccines. Effective conjugate vaccines against group C organisms have been licenced in the United Kingdom and other countries [2]. At present there is no vaccine available against group B organisms, which are the predominant cause of meningococcal disease in developed countries [3]. Development of a safe and effective vaccine based on the serogroup B capsular polysaccharide is complicated because of the existence of identical structures in the human host [4]. This results in poor immunogenicity and the risk of inducing autoimmunity [5].

Current strategies for developing a vaccine to prevent disease caused by serogroup B meningococci include outer membrane protein- and lipopolysaccharide- based approaches [3]. In addition, the systematic search of genomic information, termed 'reverse vaccinology', has been used to identify novel protein antigens [6-10]. Genomic-information-based analysis of pathogens has dramatically changed the scope for developing improved and novel vaccines by increasing the speed of target identification in comparison with conventional approaches [11].

The outer membrane protein PorA has been identified as a major inducer of, and target for, serum bactericidal antibodies and is expressed by almost all meningococci, which pinpoints PorA as a promising vaccine candidate [12]. However, PorA appears to be heterogeneous, requiring the development of a multivalent vaccine in which various PorA subtypes are present in order to induce sufficient protection. Although

various approaches can be used in the development of a multivalent vaccine, the use of genetically-engineered strains expressing more than one *porA* subtype to overcome the problem of heterogeneity seems promising [13]. At the Netherlands Vaccine Institute (NVI), a vaccine against serogroup B meningococci is currently being developed. It is based on different PorA subtypes contained in outer membrane vesicles (OMVs). An important aspect of this development trajectory is the process development of the cultivation step, which includes, for example, the design of a culture medium. Genome-scale constraints-based metabolic models are a useful tool for this.

In general, most of the recent work on *N. meningitidis*, whether based on genomic information or not, focuses on potential antigens and their functions, on immunogenicity, and on pathogenicity mechanisms. Very little work has been carried out on *Neisseria* primary metabolism over the past 25 years. However, the information provided by the genome can also be used to obtain information on the metabolic capabilities of the organism. This is done by screening the genome for open reading frames (ORFs) that code for enzymes present in the primary metabolism yielding a genome-scale metabolic network. Such a network may still contain gaps due to the incomplete or incorrect annotation of the genome. Using biochemical literature, transcriptome data or by direct measurements, the presence of missing enzymatic reactions may be proved and the network can be completed. Often, such a complete model contains underdetermined parts due to the presence of parallel or cyclic pathways. This means that for certain parts of the network the flux values cannot be determined. In order to narrow down the number of possible solutions for these parts, constraints can be set on certain enzymatic reactions based on biochemical and thermodynamic information found in the literature or determined experimentally. A schematic diagram of how the genome-scale flux model was constructed and verified using flux balance analysis (FBA) is shown in Figure 2.1.

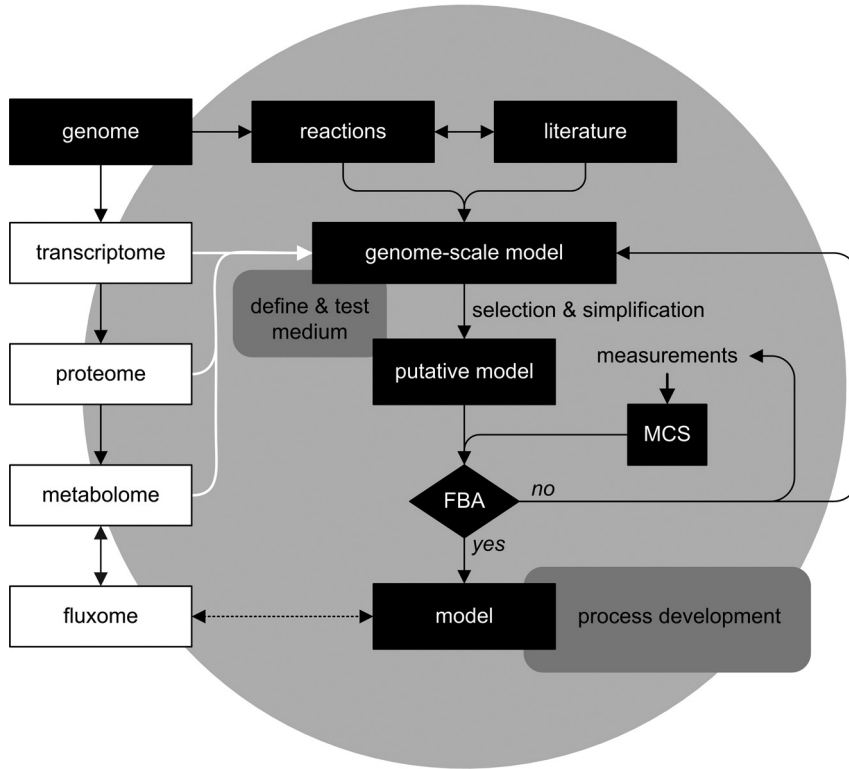


Figure 2.1 Schematic representation of model construction. The genome can be classified as the first-level database holding the potential functions of an organism. The transcriptome can be classified as the second-level database of functions describing the actual expression of genes, and the proteome can be classified as the third-level database of functions describing the actual expressed proteins. The metabolome (and fluxome) can be classified as the fourth-level database holding the complete collection of metabolites and reactions in which the metabolites participate. The metabolome, and to a lesser extent the proteome, determine the functionality of the cell [146]. In principle, all databases can be used as source of input for construction (or extension) of a genome-scale model (white arrows). In our study, information provided by the genome and the literature was used for model construction (black boxes). A minimal medium for growth was derived from the genome-scale model (upper gray box). The genome-scale model was simplified as described in the text, resulting in the 'putative model'. The measured specific metabolic rates and the corresponding measurement variances used in flux balance analysis (FBA) were calculated using Monte Carlo simulation (MCS) with the measured experimental data and their standard deviation as input. The final model, verified by FBA, can be used for process development purposes (for example, optimization of growth medium, lower gray box). Subsequently, the model can be extended to the desired informative level using all available sources of information (light gray circle).

Genome-scale constraints-based metabolic models have been built for several organisms as summarized by Palsson and colleagues [14]. They can be used to analyze cultivation data, to get a better understanding of cellular metabolism, to develop metabolic engineering strategies [15-17], design of media and processes [17-19] and even for on-line control of the process [20]. Knowledge about metabolism, as contained in these models, is very useful for the development of an efficient cultivation process. Notably, product quality and quantity are primarily determined in the cultivation process.

The aim of this study was to construct a metabolic model of serogroup B *N. meningitidis* (MenB) based on genome annotation and biochemical literature for effective process development purposes. The model was verified experimentally using flux balance analysis (FBA) for steady state chemostat data.

MATERIALS AND METHODS

Strain.

N. meningitidis strain HB-1, a nonencapsulated, nonpiliated variant of the group B isolate H44/76 [100], was used throughout this study. Stock cultures of strain HB-1 were stored at $-135\text{ }^{\circ}\text{C}$ and when required, a 500 mL shake flask, containing 150 mL of the chemically defined medium described below, was inoculated. After approximately 8 hours of incubation at $35\text{ }^{\circ}\text{C}$ with shaking at 200 rpm in an aerobic humid atmosphere, the culture was used to inoculate the medium in the bioreactor.

Medium.

The composition of the chemically defined medium described in this study are based on the information provided by the genome and available literature as described in the text. The composition of the minimal medium is given in Table 2.1. The trace-element solution contained (values in mM) $\text{CaCl}_2 \cdot 2\text{H}_2\text{O}$, 68; $\text{ZnSO}_4 \cdot 7\text{H}_2\text{O}$, 0.17; $\text{Na}_2\text{MoO}_4 \cdot 2\text{H}_2\text{O}$, 0.08; $\text{MnCl}_2 \cdot 4\text{H}_2\text{O}$, 0.4; $\text{CoCl}_2 \cdot 6\text{H}_2\text{O}$, 0.04 and $\text{CuSO}_4 \cdot 5\text{H}_2\text{O}$, 0.04. The medium was sterilized by filtration (0.22 μm). To prevent precipitation, the minimal medium and a sterile solution containing $\text{FeCl}_3 \cdot 6\text{H}_2\text{O}$ in 0.6 M HCl were added separately to the reactor by using two pumps (Watson Marlow).

Chemostat cultures.

Bacteria were grown in a 3-L autoclavable ADI bioreactor (Applikon, Schiedam, The Netherlands), operated in chemostat mode, with a working volume of 1.4 L. Temperature, pH, dissolved oxygen (DO) concentration, and stirrer speed were controlled at $37\text{ }^{\circ}\text{C}$, 7.0, 30% and 600 rpm, respectively. The total gas flow rate was kept constant at $1.0\text{ L}\cdot\text{min}^{-1}$. The oxygen concentration was controlled by changing the oxygen fraction in the gasflow using headspace aeration only. The growth rate was controlled at 0.04 h^{-1} . After at least three residence times, physiological steady state was assumed based on online measurements (constant DO signal, O_2 and CO_2 -concentration

in the off-gas) and offline measurements (constant optical density, zero glucose concentration). In steady state a 1.0 L sample was taken and divided into portions. After centrifugation of the portions (3000g, 1 h at 4 °C) cells were washed once with saline solution (0.85 w/v % NaCl) and centrifuged again. After centrifugation the saline solution was discarded and the pellet was freeze-dried without additives (Leybold, Cologne, Germany). The freeze-dried pellet was stored at -80 °C until further analysis. The chemostat cultures were performed in duplicate.

Table 2.1 Medium composition. All values in mM unless stated otherwise.

Component	Concentration
NH ₄ Cl	23.5
NaCl	102
MgSO ₄ ·7H ₂ O	2.43
K ₂ HPO ₄	12.5
KH ₂ PO ₄	4.58
FeCl ₃ ·6H ₂ O	0.30
Trace-element solution (mL.L ⁻¹)	2.0
D-Glucose Monohydrate	31.1
Na ₂ S ₂ O ₃ ·5H ₂ O	0.38

Analytical Procedures

Biomass concentration

Dry biomass concentration was determined in fourfold for each sample by centrifugation (8000 g) of 50.0 mL of culture broth in preweighed tubes. The cell material was dried at 80 °C for at least 24 h. Before weighing, the tubes were cooled in a dessicator for at least 1 h. Dry cell weight was corrected for salts present in the medium.

Off-Gas analysis

The oxygen and carbon dioxide concentrations in the exhaust gas from the chemostat cultures were measured with a mass spectrometer (Prima White Box 600, Thermo Electron, Winsford, United Kingdom).

k_La determination

The volumetric oxygen transfer coefficient, k_La , in the bioreactor was determined accurately at 37 °C using a steady state set-up and a phosphate buffered saline solution (NVI, Z3000) as reference liquid. The steady-state determination method makes use of the global balance of oxygen over the bioreactor in the gas phase and liquid phase. The calculated values were confirmed using the dynamic method with correction of electrode response time [126].

Metabolite concentrations

Glucose and lactate were determined with a YSI 2700 glucose/lactate analyser (Yellow Springs Instruments, Yellow Springs, USA). Ammonium was determined with an enzymatic kit (Boehinger Mannheim). Acetate, ethanol and other possible metabolites present in the culture supernatant were determined by ^1H -NMR using a Jeol JNM ECP 400 spectrometer operating at 400 MHz (JEOL, Tokyo, Japan) equipped with a JEOL stacman autosampler for 16 samples. Culture supernatant was analyzed by adding 0.1 mL of D_2O containing 3-(trimethylsilyl)[D_4]propionic acid sodium salt (TMSP, 0.167 mM) to 0.9 mL sample. The water signal was suppressed by irradiating the signal with standard NMR software. The spectra were referenced using the TMSP signal at 0 ppm. Metabolite concentrations were quantified by integration of the relevant signals.

Protein

The amino acid composition of biomass protein was determined after hydrolysis (6 M HCl, 24 h, 110 °C) and subsequent amino acid analysis using an HPLC method

as described before [127]. Free amino acids in the culture supernatant were determined using the same method. Cysteine and tryptophan, which were destructed during acid hydrolysis, were calculated based on the predicted amino acid composition in the genome by using a ratios as described in Appendix 2.1. Glutamine and asparagine were converted to glutamate and aspartate, respectively, during acid hydrolysis were calculated based on the predicted amino acid composition in the genome using ratios as described in Appendix 2.1. Total biomass protein was calculated by summation of the measured amino acid concentrations and corrected for salt present in the freeze-dried biomass. No correction was done for amino acids present in peptidoglycan. The methods recovery was determined as $0.85 \pm 4\%$ based on measurements of pure Bovine Serum Albumin and corrections were made accordingly. The measured amino acid composition and the assembly into protein can be found in Appendix 2.1.

Fatty acids

The amount of total fatty acids and the fatty acid composition was analyzed using a modified gaschromatography method [128]. Saponification reagent (1.2 ml of 3.75 M NaOH in 50/50 v/v methanol/water) was added to 12 mg freeze dried biomass to liberate the fatty acid from cellular lipid. After vortex mixing for 10 seconds the samples were placed at 100 °C for 30 min. After cooling for 15 minutes to room temperature, 2.4 ml of methylation reagent (3.25 M HCl in methanol) was added and after vortex mixing for 10 seconds the samples were placed at 80 °C for 20 min. After cooling down to room temperature, the fatty acid methyl esters were extracted by adding 1.5 ml hexane reagent (50/50 v/v hexane/methyl tertiary butyl ether). Samples were mixed for 15 minutes and centrifuged (3 min, 1834 g). The aqueous layer was removed and the organic phase was washed by adding 3.0 ml of washing agent (0.3 M NaOH). The samples were mixed for 5 minutes and centrifuged again (3 min, 1834 g). The organic phase was finally transferred to a GC-vial and analyzed using a 6890 Agilent gaschromatograph [129]. The standards and samples were injected into the GC equipped with a flame ionization detector via an automated sequence run.

An Agilent 19091B-102 capillary column (Ultra 2; 5% Phe-Methylsiloxane; 25 m * 0.200 mm; film thickness: 0.33 µm) was employed. Oven temperature was programmed as follows: 60 °C: hold 3 min - 280 °C at 25 °C/min: hold 4 min - 320 °C at 15 °C/min: hold 2 min - 340 °C at 20 °C/min: hold 0 min). The injector temperature was set at 275 °C and detector temperature was set at 375 °C. Helium was used as carrier gas at a constant flow-application of 2.0 ml/min. Fatty acid methyl-esters were identified by their retention times in comparison to those of a commercial standard (Microbial USA). Calibration curves of pure fatty acids present in *N. meningitidis* were made based on the identified fatty acids [128] and confirmed in literature [130]. The pure fatty acids used as calibration standards were dissolved in dichloromethane (Sigma). All fatty acids were purchased from Sigma, except for palmitelaidic acid (C16:1-trans 9) which was purchased from ICN Biomedicals. Quantification of hydroxy-fatty acids has been done using C12:0-2OH as an internal standard whereas non-hydroxy-fatty acids have been quantified using C15:0 as an internal standard. The measured fatty acid concentrations were corrected for salt present in the freeze dried biomass. The measured fatty acid composition and the assembly into lipid can be found in Appendix 2.1.

Lipopolysaccharide

LPS was isolated by hot phenol-water extraction as described before [131]. Isolation and structural analysis of lipid A was performed by nanoelectrospray tandem MS on a Finnigan LCQ in the positive ion mode as described previously [132]. LPS was quantified based on the measured amount of C12:0-3OH (see Fatty acids).

RNA and DNA

The biomass RNA content was determined as described previously [133] and the biomass DNA content was determined colorimetrically as described previously [134]. The DNA composition was derived from the complete nucleotide composition in the genome sequence. For RNA the uridine content was based on the thymine content in

the genome sequence [23]. The measured concentrations were corrected for salt present in the freeze dried biomass. The calculated RNA and DNA composition and their assembly can be found in Appendix 2.1.

Biomass composition

Biomass biosynthesis was set as a linear combination of the macromolecules: protein, DNA, RNA, lipid, peptidoglycan and LPS, which were considered to account for the overall biomass composition. The energy requirement for biomass assembly was also considered and estimated to be 13.27 mol ATP / mol biomass. This value was calculated using linear regression of available $1/Y_{x/ATP}$ vs. growth rate data from *E. coli* [122]. The accuracy of the estimation is, however, quite low. A detailed calculation of the biomass composition and its assembly, next to an overview of the metabolites measured in the culture supernatant and off-gas can be found in Appendix 2.1.

Modeling aspects

Mathematical formulation

First the genome-scale metabolic network was simplified as described in the text. Next, the stoichiometric matrix was constructed from the set of reactions using a self-made computer program running in Visual Basic (Microsoft, Seattle, USA). Both MCS and FBA were performed in self-made computer programs running in Matlab (Matlab, version 6.5 r13; The Mathworks Inc, USA). Methods for solving a metabolic network or set of linear equations are discussed extensively elsewhere [135-138]. A brief summary is given below. In steady-state growth, the reactions of the considered metabolites form a set of linear equations which can be expressed in matrix notation as:

$$A \cdot v = A \cdot \begin{bmatrix} x \\ r \end{bmatrix} = 0 \quad (2.1)$$

where A ($m \times n$) is the stoichiometric matrix which contains m metabolites and n

reactions, including measured exchange reactions, and v is the flux vector that contains the unknown fluxes x and measured exchange rates r . A solution to the metabolic network will exist provided that A is nonsingular. Singularities in A may arise due to reaction dependence or network observability problems. Equation (2.1) states a compound balance for each of the metabolites in the system. If measurements are performed on substrate and product concentrations, and the conversion rates of these metabolites are calculated, such a set of measured rates should match equation (2.1).

Error diagnosis and balancing

Methods for error diagnosis and balancing are discussed extensively elsewhere [117, 118]. A brief summary is given here. In order to be able to do error diagnosis the measurement set should contain balanceable rates. Balanceable rates can be found by calculating the redundancy matrix [117], which contains linear relations between measured rates that are thus balanceable. Parts of the relations are usually formed by a carbon, nitrogen and redox balance. In practice all measurements suffer from measurement noise, and sometimes process noise, which lead to unavoidable inaccuracies in the measured conversion rates. Consequently, the product of the redundancy matrix and the measured rates is not zero, but yields a vector of residuals, ε :

$$R \cdot r_m = \varepsilon \quad (2.2)$$

where R is the redundancy matrix and r_m the measured conversion rate vector. To test whether ε can be explained from random measurement errors the following test function was developed [139]:

$$h_\varepsilon = \varepsilon^T \cdot \psi_\varepsilon^{-1} \cdot \varepsilon \quad (2.3)$$

where h_ε is the test function and ψ_ε is the variance-covariance matrix of the residual vector ε , which is calculated from the variance-covariance matrix ψ_δ of the measurements

according to:

$$\psi_\varepsilon = R \cdot \psi_\delta \cdot R^T \quad (2.4)$$

When ε is due to random measurements only, h_e follows a χ^2 -distribution with the number of degrees of freedom equal to the rank of ψ_e [118]. When no gross errors are detected the measured rates should be balanced to obtain more reliable intracellular fluxes:

$$r_t = r_m - \delta \quad (2.5)$$

where r_t is the vector containing the balanced specific production rates ($\text{mol.g}^{-1}.\text{h}^{-1}$) and δ is the vector containing the deviations between measured and balanced rates, which can be calculated using a weighed minimum last square approach according to the following equation:

$$\delta = \psi_\delta \cdot R^T \cdot \psi_\varepsilon^{-1} \cdot \varepsilon \quad (2.6)$$

The resulting balanced measurement rate vector can be used to calculate the unknown fluxes and production rates. As described in more detail below, Monte Carlo simulation can be used to determine the variance of a measured conversion rate.

Network sensitivity analysis

The matrix containing the mass balances over the intracellular compounds can be checked for network sensitivity problems by performing singular value decomposition (SVD). SVD is a mathematical technique that decomposes matrix A into three matrices as follows:

$$A = U \cdot W \cdot V^T \quad (2.7)$$

The matrix W is an orthogonal matrix containing the eigenvalues of the matrix. The columns of U , whose corresponding elements of W are non-zero, form an orthonormal basis that span the range of A . The columns of V , whose corresponding values of W are zero, are an orthonormal basis for the nullspace of A . In other words these columns of V contain the combination of fluxes and rates that cannot be uniquely identified. Here we use SVD to identify and isolate the combinations of fluxes and unknown exchange rates that cannot be uniquely identified (i.e. calculated from the measurements) [138]. It is worth noting that no measurements are needed to perform this check. If underdetermined parts are present the number of solutions for the flux vector is infinite.

To reduce the number of allowable solutions for these underdetermined parts of the metabolic network, limits on the range of individual flux values can be set based on available biochemical and thermodynamic literature of the enzymatic reactions. These constraints have the form:

$$\alpha \leq v \leq \beta \tag{2.8}$$

where α and β are the lower and upper limits, respectively. Thermodynamic constraints, regarding the reversibility or irreversibility of a reaction can be applied by setting α for the corresponding flux to zero. To further shrink the original solution space to a single solution, linear optimisation can be used to find the solution that optimizes a particular objective function. Some examples of objective functions are maximize biomass formation or minimize the production of ATP, NADH, NADPH or a particular metabolite [135, 140]. An alternative objective function is to minimize the sum of the squares of the fluxes also called the minimum-norm constraint. The minimum-norm constraint minimises the length of the solution vector without any further restrictions using the Moore-Penrose-pseudo-inverse of A [141]. The Moore-Penrose-pseudo-inverse gives the one solution vector that has the smallest Euclidian norm (e.g. the smallest square of its length). Like Bonarius [119], we hypothesize that the minimum-

norm constraint correctly assumes that the total flux activity is minimized in order to fulfill the efforts of the bacteria to achieve an efficient flux distribution.

Monte Carlo simulation

Error diagnosis and balancing are important aspects of flux balance analysis. Before error diagnosis can be done, errors in the primary measurements need to be translated to errors (i.e. variances) in measured conversion rates. This can be done using a Monte Carlo approach [115, 116] as follows: The various measured values and their standard deviations were used as input to calculate the measured conversion rate of a specific metabolite numerous times. The value of each measured variable in the mass balance equation of this specific metabolite was simulated randomly within the allowed standard deviation interval of each variable. For example, the mass balance describing the conversion rate of glucose contained four measured variables being the glucose concentration in the incoming and outgoing medium, the medium flow and the biomass concentration. In each Monte Carlo run a random value was assigned to each measured variable within the allowed standard deviation interval of that variable. This was done separately for all of the four measured variables. The resulting four random values were used to calculate the conversion rate of glucose. After numerous simulation runs, the average glucose conversion rate and the corresponding variance was calculated from all the simulated conversion rates. As stated in the text, accurate results were obtained after 10000 simulations, resulting in an average measured conversion rate with a normal error distribution (a prerequisite for part of the flux balance analysis procedure). All other measured conversion rates were calculated similarly, resulting in a set of measured conversion rates and corresponding variances that were subjected to error diagnosis.

In silico modeling

All *in silico* experiments were done using the simplified metabolic model. All simulations were performed in a self-made computer programs running in Matlab (version 6.5 r13;

The Mathworks Inc, USA). The flux through the non-growth associated ATP maintenance reaction was fixed to $2.8 \text{ mmol.g}_{\text{dw}}^{-1}.\text{h}^{-1}$ [122]. The lower limit of irreversible reactions was set to zero and fluxes through all other intracellular reactions had no upper or lower limit. In addition, the production rate of all amino acids and extracellular protein was set to zero. The following external metabolites were allowed to freely enter and leave the system: ammonia, water, phosphate, thiosulfate, sulfate, carbon dioxide, oxygen and protons. In addition, acetate, hydrogen sulfide and ethanol were only allowed to leave the system. Growth on different carbon sources was simulated by allowing the carbon source under study to enter the system. The consumption rate of all carbon sources was fixed to $4.23 \text{ mmol.g}_{\text{dw}}^{-1}.\text{h}^{-1}$. In all simulations, maximization of biomass formation was used as objective function.

RESULTS AND DISCUSSION

Construction of the genome-scale metabolic model

The available genome sequence of *N. meningitidis* serogroup B [21] and its annotation in the Kyoto Encyclopedia of Genes and Genomes (KEGG) database [22] was taken as starting point for model construction. As described by Heinemann and co-workers [23], the KEGG database was corrected for obvious errors [24] and complemented using the database of the Institute for Genome Research (TIGR) [25], which is based on the same sequence data, but runs a different annotation methodology, and the BioCyc database [26]. These databases, along with biochemical information found in the literature provided the information needed to construct the genome-scale metabolic model. The genome-scale model was next simplified by lumping successive reactions and removing dead ends. This led to the simplified model shown in Figure 2.2. The complete reaction database along with the genes involved, enzyme numbers and metabolites can be consulted in the Additional data. From this reaction database, parts that describe the main primary pathways were selected and cross-checked with the literature.

Glucose metabolism

According to the genomic information for MenB, glucose can be completely catabolized through the Entner Doudoroff pathway (ED) and the pentose phosphate pathway (PP). The Embden-Meyerhof-Parnas pathway (EMP, glycolysis) is not functional, because the gene for phosphofructokinase (EC 2.7.1.11) is not present. Studies on the utilization of glucose in *N. meningitidis* [27-33] confirm the presence of enzymes related to EMP, ED and PP pathway. However, it was found that the EMP pathway does not contribute to pyruvate synthesis, indicating that, in accordance with the missing phosphofructokinase gene, this pathway is not functional. On the basis of genomic information, glyceraldehyde phosphate and fructose-6-phosphate, which are formed in the PP pathway, can be recycled to glucose-6-phosphate. This indicates that

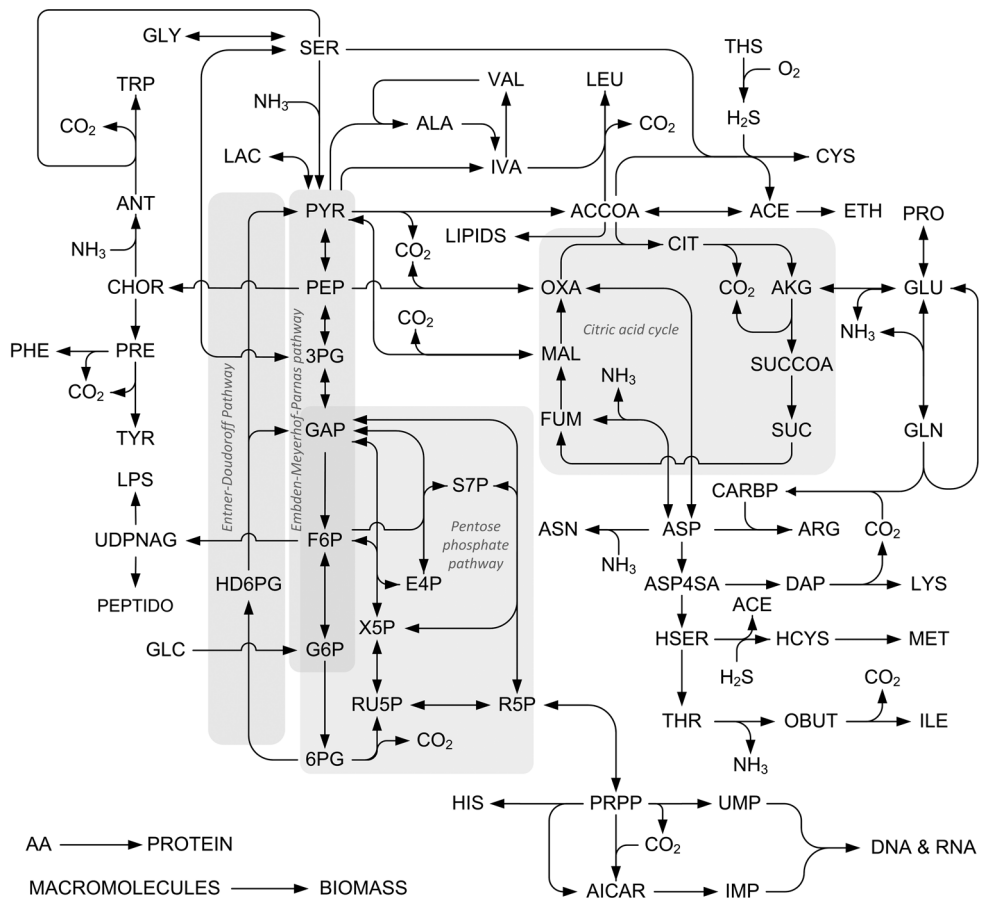


Figure 2.2 Simplified metabolic model of *N. meningitidis*. As described in the text, the simplified model was obtained by simplification of the genome-scale model. For ease of understanding, only the main pathways were admitted into the diagram illustrated here. A complete overview of the model including a list of all abbreviations used is in Appendix 2.2.

in theory glucose can be completely oxidized in the PP pathway to CO_2 forming six NADPH. In practice it was found that glucose is mainly catabolized by the ED pathway and to a lesser extent by the PP pathway [32]. On the basis of ^{14}C studies, Jyssum [32] roughly calculated that the ED cleavage always synthesizes the major part

of pyruvate (67-87%) and the PP pathway accounts for the remaining part. Morse and co-workers [34] found similar results for *Neisseria gonorrhoeae*, which is biochemically similar to *N. meningitidis* [35].

The tricarboxylic acid cycle

All the genes for the tricarboxylic acid cycle (TCA cycle) enzymes are present in the MenB genome, except the gene for malate dehydrogenase. To establish oxidation of malate to oxaloacetate, the MenB genome suggests the FAD-dependent malate:quinone oxidoreductase (NMB2069). Studies of the citric-acid cycle and related reactions [35-42] in *N. meningitidis* and *N. gonorrhoeae* indeed confirm the presence of all citric-acid-cycle enzymes except malate dehydrogenase. Although activity of the FAD-dependent malate:quinone oxidoreductase has not been measured, its presence is plausible as indicated by an operational TCA cycle. The TCA cycle, ED pathway, PP pathway and the disfunctional EMP pathway are shown schematically in Figure 2.2.

Anaplerotic reactions

In the MenB genome a gene for phosphoenolpyruvate carboxylase (NMB2061) is present. Studies on phosphoenolpyruvate carboxylase activity [35, 43, 44] confirm the presence of a specific irreversible phosphoenolpyruvate carboxylating activity, EC 4.1.1.31. Other phosphoenolpyruvate carboxylating enzymes have not been annotated in the MenB genome. In addition, the gene for malic enzyme, EC 1.1.1.38 (NMB0671) is present in the genome. Based on genomic information, *N. meningitidis* does not possess a functional glyoxylic acid cycle, since the genes for isocitrate lyase (EC 4.1.3.1) and malate synthase (EC 2.3.3.9) are not present. This was confirmed by Holten [45] and Leighton [35], who both did not detect these enzymes in cell-free extracts.

Metabolism of lactate, acetate, glutamate and CO₂

The first work on growth requirements of *Neisseria* in a chemically defined environment was published in 1942 [46] and provided the basis for many later metabolic studies.

Growth of *N. meningitidis* requires glucose, pyruvate or lactate as sole carbon source, and during cultivation on any of these carbon sources, secretion of acetate into the medium occurs [47, 48]. In addition, a certain environmental CO₂ tension was required to initiate growth [49]. *In silico* simulation of biomass growth using the metabolic model showed that when bacteria are grown on glucose and the oxidation capacity is limiting, acetate secretion occurs. Limitations in oxidation capacity may be due to limitations in metabolism or limitations in oxygen supply to the culture. *In silico* simulation of limited oxygen supply was added as an example to the Additional data.

Studies on lactate utilization [50] demonstrated that L-lactate can be utilized by different meningococcal lactate dehydrogenases (LDH). In the MenB genome a LDH gene (NMB1377) specific for L-lactate (EC1.1.2.3, EC 1.1.1.27) has been annotated. The predicted amino acid sequence of this gene, *lldA*, is homologous to that of the *Escherichia coli lldD* gene (43% similarity) and to other prokaryotic and eukaryotic flavin mononucleotide-containing enzymes that catalyze the oxidation of L-lactate. However, in *E. coli* the corresponding *lldD* gene is part of an L-lactate regulated operon also containing genes for *lldP* (permease) and *lldR* (regulatory), whereas the meningococcal L-LDH gene does not appear to be part of an operon [50]. A meningococcal *lld* mutant had reduced L-LDH activity, but was still able to grow on L-lactate indicating that a second L-LDH must exist [50]. At this moment, no additional genes have been annotated. Two LDH genes specific for D-lactate (EC 1.1.1.28) have been annotated in the MenB genome. These genes, NMB0997 and NMB1685, are homologous to the *E. coli dld* and *ldhA* genes, respectively (71% and 66% similarity). In agreement with this, an NAD-dependent D-LDH activity was identified by Erwin and Gotschlich [51]. *ldhA* is associated with fermentative processes [52]. L-lactate is an established and important intermediate in mammalian metabolism. It is less clear whether D-lactate also originates from mammalian metabolism. D-lactate can be produced as a byproduct of glucose metabolism by some lactic acid bacteria as well as by *E. coli*, so it may be available on the mucosal surfaces that pathogenic *Neisseria* colonize.

De Vrese and co-workers [53] showed that after human consumption of food containing DL-lactic acid (such as yogurt), significant levels of both L- and D-lactic acid were present in blood. Although both L- and D-lactic acids were metabolized rapidly, the availability of D-lactate in humans might explain the presence of specific D-lactate dehydrogenases in *N. meningitidis*. Erwin & Gotschlich [51] showed that *N. meningitidis* was able to grow on L-lactate at least as well as on glucose, but more recent work of Leighton [35] contradicts this work. He found that growth on L-lactate gave a lower biomass yield and suggested that the additional ATPs produced during glucose catabolism to pyruvate, which are not formed when growing on lactate, accounted for this observation. In addition, the C₅ and C₆ carbohydrates required for bioynthesis of macromolecules, are synthesized using the gluconeogenesis pathway when grown on lactate, which also requires additional ATPs. *In silico* simulation of biomass growth using the metabolic model confirmed the observation of Leighton [35] and predicted a 10% higher yield of biomass on glucose (see Table 2.2).

Table 2.2 *In silico* yield, $Y_{x/s}$ of biomass on substrate for growth on different carbon sources

Substrate	$Y_{x/s}$ <i>in silico</i> (g.Cmol ⁻¹)
Glucose (GLC)	10.7
Lactate (LAC)	9.6
Glutamate (GLU)	8.2
Acetate (ACE)	0.0 (not possible)
GLC + LAC (50/50 Cmol/Cmol)	10.4
GLC + GLU (50/50 Cmol/Cmol)	9.7
LAC + GLU (50/50 Cmol/Cmol)	9.0
ACE + GLU (50/50 Cmol/Cmol)	6.3

According to genomic information, acetate is synthesized via phosphate acetyltransferase, EC 2.3.1.8 (NMB0631) and acetate kinase, EC 2.7.2.1 (NMB0435,

NMB1518) or acetate-CoA ligase, EC 6.2.1.1 (NMB1555). The presence of phosphate acetyltransferase and acetate kinase was confirmed by activity measurements [35]. The hypothesis that acetate is synthesized from pyruvate [38] via cytochrome-linked pyruvate dehydrogenase (EC 1.2.2.2) might be incorrect, as the required gene is not annotated. Studies on the catabolism of pyruvate and acetate [38] showed that acetate can be oxidized, but only when glutamate is present, indicating that acetate can be oxidized under specific growth conditions. Because the glyoxylate cycle is not present, C₂ compounds cannot be converted to C₄ compounds, which explains the requirement for glutamate in this case. *In silico* simulation of biomass growth using the metabolic model, confirm that acetate can be oxidized in the presence of glutamate. The result of this *in silico* experiment can be found in the Additional data. Ethanol is synthesized from acetaldehyde using alcohol dehydrogenase, EC 1.1.1.1 (NMB0546). Remarkably, no gene(s) involved in the biosynthesis of acetaldehyde are found in the MenB genome. Because ethanol was measured in the culture supernatant, a biosynthetic pathway to ethanol must be present. Hence, aldehyde dehydrogenase (EC 1.2.1.3) was assumed to be present in the metabolic model to complete the biosynthetic pathway to ethanol.

Both Frantz [46] and Grossowics [48] described glutamate as requirement in their growth media for meningococci, but Jyssum [54] showed that ammonium can serve as sole nitrogen source after adaption to glutamate-free medium. The genes encoding NAD-specific glutamate dehydrogenase (NMB1476) and NADP-specific glutamate dehydrogenase (NMB1710) are present in the MenB-genome as well as genes for several aminotransferases. The presence of NAD-dependent glutamate dehydrogenase was demonstrated [54] and additional studies of meningococcal transaminase activity also revealed the presence of transamination to 2-oxoglutarate from a number of amino acid donors. Holten & Jyssum [55] also found NADP-linked glutamate dehydrogenase activity. They found that NAD-linked glutamate dehydrogenase was most active in glutamate-containing media, while the NADP-linked enzyme dominated in absence

of glutamate [55]. They observed that the NAD-linked enzyme mainly converts glutamate to 2-oxoglutarate and ammonia (catabolism), whereas the NADP-linked enzyme is responsible for the reverse reaction (anabolism). Because in our present study glutamate-free medium was used, only the NADP-linked glutamate dehydrogenase was admitted in the metabolic model.

To initiate growth, a certain environmental CO₂ tension is required [49]. This finding is most probably associated with the high CO₂ concentration present in the nasopharynx. In more recent studies, additional CO₂ tension is only used when bacteria are grown on solid media and is omitted in liquid cultures. It seems plausible that the CO₂ tension is only important in glutamate-free media, where phosphoenolpyruvate carboxylase (NMB2061) must be an important link to the citric acid cycle, whereas this is normally fed by glutamate. This hypothesis is supported by results obtained by Holten [38] and in an earlier study by Jyssum and Jyssum [56], who studied the effect of KHCO₃ on endogenous phosphorylation [56].

Amino acid metabolism

All genes involved in amino-acid biosynthesis are present in the MenB genome except the genes coding for alanine transaminase, alanine dehydrogenase, and phosphoglycerate dehydrogenase, which is part of the biosynthetic pathway to serine. For the synthesis of alanine the MenB-genome suggests the gene (NMB1823) encoding valine-pyruvate aminotransferase (EC 2.6.1.66). To complete the biosynthesis of serine, phosphoglycerate dehydrogenase was assumed to be present. In 1989 the physiology and metabolism of *N. gonorrhoea* and *N. meningitidis* was reviewed by Chen and co-workers [57], with emphasis on selected areas that have implications for the pathogenesis. The main focus of this work was iron metabolism, and amino acid metabolism was touched briefly for *N. gonorrhoea*. Catlin [58] investigated growth requirements for various *Neisseria* species pointing out the additional need for glutamate, arginine, glycine, serine and cysteine for some *N. meningitidis* strains. However, amino-acid-free

growth medium was used earlier [54], indicating that all biochemical pathways for amino-acid synthesis in *N. meningitidis* are available, as supported by the genome. This is confirmed by Leighton [35] who measured enrichments of all individual amino-acid carbon after growth on 2-¹³C and 3-¹³C labeled pyruvate.

Oxidative phosphorylation

MenB genome sequence information indicates the presence of respiratory complexes I, II and III, suggesting that electrons enter the respiratory chain through NADH dehydrogenase (EC 1.6.5.3) or succinate dehydrogenase (EC 1.3.99.1) and are transferred to the cytochrome *bc*₁ complex through ubiquinone (EC 1.10.2.2). Oxygen is utilized by cytochrome *cbb*₃ oxidase (EC 1.9.3.1), which is the only respiratory oxidase encoded by the MenB-genome. The *cbb*₃ type oxidases are usually found in proteobacteria that express these oxidases in response to micro-aerobic conditions to permit the colonisation of oxygen-limited environments. Thus *cbb*₃ type oxidases may be an important determinant of pathogenicity for MenB [59]. *N. meningitidis* fails to grow under strictly anaerobic conditions. Under oxygen limitation the bacterium expresses a denitrification pathway. This reduction of nitrite to nitric oxide, via nitrite reductase, EC 1.7.2.1 (NMB1623), is regulated by oxygen depletion and nitrite availability [60, 61]. Thus, under microaerobic conditions nitrite can replace oxygen as an alternative respiratory substrate in *N. meningitidis*. Because our experiments were not carried out under microaerobic conditions, nitrite was not added to the growth medium, and subsequently the denitrification pathway was omitted from the simplified model.

Sulfur metabolism

Frantz [46] and Grossowicz [48] described that reduced sulfur in the form of cysteine, cystine, or thiosulfate was required for growth. Catlin [58] showed that some strains of meningococci have an absolute requirement for cysteine (or cystine). Jyssum [54] showed that after adaption these sulfur sources could be replaced by sulfate. This was confirmed by Port and co-workers [62], who demonstrated that numerous sulfur sources

could be used as alternative for cysteine. DeVoe and co-workers [63] identified thiosulfate reductase activity in *N. meningitidis* serogroup B, but no gene specifically encoding thiosulfate reductase has been annotated in the genome. A wide range of sulfur-acquisition routes is available in *N. meningitidis*. Genes encoding sulfate adenylyltransferase (EC 2.7.7.4), phosphoadenosine phosphosulfate reductase (EC 1.8.4.8), and sulfite reductase (EC 1.8.1.2) are present in the MenB genome. On the basis of this information, both thiosulfate and sulfate were selected as sulfur sources in the growth medium for the production of cysteine and other sulfur containing compounds.

Cysteine can be converted to the thiol glutathione (GSH) via glutamate-cysteine ligase, EC 6.3.2.2 (NMB1037), and glutathione synthetase, EC 6.3.2.3 (NMB1559). In turn, GSH can be converted to cysteine via gamma-glutamyltranspeptidase, EC 2.3.2.2 (NMB1057) and aminopeptidase N, EC 3.4.11.2 (NMB1416) yielding a functional γ -glutamyl cycle (see Figure 2.3). This cycle helps to maintain the redox balance [64]. GSH can be oxidized to glutathione disulfide (GSSG) by glutathione peroxidase, EC 1.11.1.9 (NMB1621), thereby controlling the cellular hydrogen peroxide level [65].

In solution, cysteine can be converted chemically to cystine. Yu and DeVoe [66, 67] corrected for this so-called auto-oxidation and suggested that electrons from cysteine enter the electron transport chain at the flavoprotein level in a manner similar to those from succinate and NADH. They even suggested the presence of a specific cysteine oxidase, but no gene encoding this enzyme has been annotated in the MenB genome and no additional evidence supporting this hypothesis was found in literature. It seems plausible that cysteine can increase the protonmotive force to drive oxidative phosphorylation. During oxidation of cysteine to cystine, electrons from cysteine are transferred to oxygen, yielding reactive oxygen, O_2^- , as shown in Figure 2.3. This reactive oxygen can reduce cytochrome c, which in turn can provide a source of electrons for cytochrome *cbb*₃, which reduces oxygen to water, causing the concomitant generation of a proton motive

force, $\Delta\mu^{H^+}$, and ATP [68]. In addition, cysteine might be used directly as electron donor by cytochrome *cbb*₃ but no evidence supporting this hypothesis was found in the literature.

Oxidative stress

The reactive oxygen can also be processed by the superoxide dismutases, *SodC* present in the periplasm or *SodB* present in the cytosol, EC 1.15.1.11 (NMB0884, NMB1398) followed by catalase, EC 6.3.5.5 (NMB1849, NMB1855) to regenerate oxygen, or by glutathione peroxidase as described above (see Figure 2.3). This protection mechanism

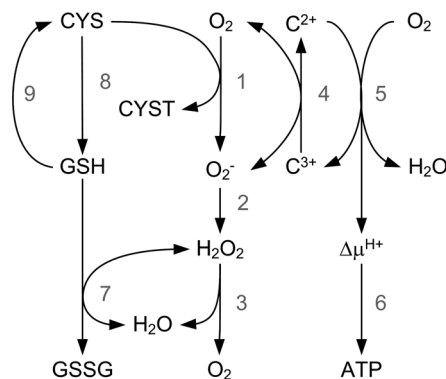


Figure 2.3 Oxidation of cysteine to cystine. Cysteine (CYS) is oxidized to cystine (CYST), forming reactive oxygen O_2^- (step 1), which can reduce cytochrome *c* (step 4). The electron is used by cytochrome *cbb*₃, which reduces oxygen to water and causes the concomitant generation of a protonmotive force, $\Delta\mu^{H^+}$ (step 5). The protonmotive force is in turn used to form ATP (step 6). Step 2 involves the formation of hydrogen peroxide (H_2O_2) from O_2^- by superoxide dismutase followed by catalase to regenerate oxygen (step 3). Cysteine can be converted to glutathione (GSH), via glutamate-cysteine ligase and glutathione synthetase (step 8). In turn, GSH can be converted to cysteine via gamma-glutamyltranspeptidase and aminopeptidase N (step 9), yielding a functional γ -glutamyl cycle. GSH can be oxidized to glutathione disulfide (GSSG), by glutathione peroxidase (step 7).

against oxidative stress has been studied extensively [65]. Seib and co-workers concluded that *N. meningitidis* SodB plays a key role in protection against oxidative killing. The *sodC* mutant of *N. meningitidis* used in their study was no more sensitive to oxidative killing than the wild type. Paradoxically, Wilks and co-workers [69] found that a *sodC* mutant is significantly less virulent indicating that SodC contributes to the virulence of *Neisseria meningitidis*, most probably by reducing the effectiveness of toxic oxygen host defenses. This was confirmed by Dunn and co-workers [70], who showed that SodC contributes to the protection of serogroup B *Neisseria meningitidis* from phagocytosis by human monocytes/macrophages, with SodC mutant organisms being endocytosed in significantly higher numbers than wild-type organisms. *In vitro*, oxidative stress might be induced by a high dissolved oxygen concentration possibly resulting in oxidative killing. Therefore, the dissolved oxygen concentration in the chemostat experiments was controlled at a low level of 30%.

Metabolism of macromolecules

The metabolism of pyrimidine bases and nucleosides in *N. meningitidis* has been reviewed and studied extensively [71]. Although some of the early work contradicts the current information from the MenB genome in terms of pathway description, the results indicate that the required routes for pyrimidine biosynthesis are available in the genome. Furthermore, the MenB genome contains all the genes encoding the enzymes for the biosynthesis of UMP. Activities of the enzymes for this biosynthetic pathway were found previously in cell-free extracts [72].

In Gram-negative bacteria, such as *N. meningitidis* and *E. coli*, the cell envelope consists of an outer membrane, a dense peptidoglycan layer and a cytoplasmic or inner membrane. The outer membrane has an asymmetrical organization in which the outside layer is primarily composed of lipopolysaccharide (LPS) and proteins and the inside layer contains phospholipids [73]. The inner membrane has a symmetrical phospholipid bilayer structure, holding proteins primarily responsible for regulating

the flow of nutrients and metabolic products in and out of the bacterium [74].

Membrane phospholipids form a major constituent of the cell envelope of *N. meningitidis* and maintain the integrity of the outer membrane. Rahman and co-workers [75] summarized early studies conducted in the 1960s and 1970s that indicated that the major phospholipid component of membranes isolated from *N. gonorrhoeae* consisted largely of phosphatidylethanolamine (PE) with varying amounts of phosphatidylglycerol (PG), cardiolipin (CL) and lysophosphatidylethanolamine (LPE). Subsequently, the total cellular fatty acids and extractable cellular lipids of *N. meningitidis* isolates were found to be similar to those of gonococci. The precise structures of *N. meningitidis* phospholipids, including their fatty acylation patterns, have been elucidated quite recently [75]. Interestingly, the latter study shows that a major fraction (about 11%) of the total phospholipids appears to be phosphatidate (PA).

Lipid biosynthesis can be divided into two parts: (i) biosynthesis of the fatty acids that are responsible for the characteristic hydrophobicity of lipids and (ii) attachment of the completed fatty acids to *sn*-glycerol-3-phosphate (GL3P) followed by the addition and modification of the polar head groups to yield phospholipids [76].

The fatty acid biosynthetic pathway in *N. meningitidis* is similar to that in *E. coli*. All genes, except a homologue to the β -hydroxyacyl-ACP dehydrase, *FabA*, are present in the MenB genome. The absence of a *fabA* homologue in the MenB genome is not unique as summarized by Rahman and co-workers [75], who state that the production of unsaturated fatty acids in *N. meningitidis* and other species, may proceed via different biochemical pathways to that of *E. coli*. Homologs to glycerol-3-phosphate acyltransferase (PlsB) and cardiolipin synthase (YbhO) from *E. coli* were not found in the MenB genome. The reported phospholipid compositions in *Neisseria* species [75, 77-79] in which no, or only trace quantities of CL were found can be explained by the absence of a homolog for *ybhO*, but the absence of a homolog for *plsB* is striking. Apparently the gene(s) encoding the enzyme responsible for the formation of 1-acyl-

sn-glycerol-3-phosphate has not been found in *N. meningitidis*. In fact, only 38 of the 125 prokaryotic genomes reported [22] annotated *plsB* or *plsB* homologues, all classified as γ -proteobacteria. Although it is possible that the reaction proceeds via a different biochemical pathway to that of *E. coli*, it is incorporated in the present metabolic model to complete the biosynthetic pathway to phospholipids.

The overall phospholipid composition used in our study was based on the information provided by Rahman and co-workers [75], including 11 % PA, 71 % PE and 18% PG. In their study no evidence supporting the presence of LPE was found. Bos and co-workers [80] reported a neisserial *pldA* gene (NMB0464), encoding a phospholipase, and characterized it as a neisserial autolysin that acts after bacteria have stopped dividing. This is consistent with LPE only being measurable when cells are harvested in the late exponential growth phase or stationary growth phase.

LPS, a second major constituent of the cell-envelope of *N. meningitidis*, is often referred to as endotoxin and plays an important role in virulence. It is held responsible for the severe pathological effects during invasive meningococcal disease [81]. LPS consists of three parts: a lipid A part containing unique hydroxy-fatty-acid chains, a core oligosaccharide containing 3-deoxy-D-manno-octulosonate (KDO) and heptoses, and a highly variable sugar backbone. In *E. coli* lipid A is essential for cell viability [82, 83], whereas an LPS deficient meningococcal strain remains viable [84]. All genes involved in the lipid A biosynthesis of LPS are present in the MenB genome. Unlike the LpxA acyltransferase, present in the biosynthetic pathway of *E. coli*, the MenB LpxA acyltransferase (NMB0178) favors the substrate 3-OH C12 acyl-ACP [85], yielding a lipopolysaccharide structure as described before [86]. The HB-1 strain used in this study lacks expression of *galE* as a result of the deletion made into the capsule (*cps*) locus [87] leading to the synthesis of galactose-deficient LPS [88].

Heterogeneity in the LPS sugar backbone can be caused by phase variation of the genes involved [89], but phase variable genes have not been found in the lipid A biosynthetic

pathway. Kulshin and co-workers [90] found minor fractions of penta- and tetra-acylated lipid A structures in *N. meningitis*, but the hexa-acylated structure predominated. Heterogeneity in lipid A has been found before in other species. Rebeil and co-workers [91] found that a shift in growth temperature of the genus *Yersinia* induced changes in the number and the type of acyl groups on the lipid A, suggesting that the production of a less immunostimulatory form of LPS upon entry into the mammalian host is a conserved pathogenesis mechanism and that species-specific lipid A forms may be important for life cycle and pathogenicity differences. Other bacterial species, such as *Salmonella typhimurium* and *Pseudomonas aeruginosa* are able to covalently modify their lipid A through the enzymes PagL and PagP [92, 93], but homologs to PagP and PagL have not been found in meningococcal genomes [94]. Structural analysis by mass spectroscopy of lipid A from strain HB-1 (results not shown) revealed that a monophosphorylated form of the above described hexa-acylated lipid A was present.

The capsular polysaccharide (whose synthesis is directed by the *cps* locus) is an important virulence factor in meningococcal pathogenesis and contributes to the survival of *N. meningitidis* in the bloodstream [95, 96]. The biosynthesis of capsular polysaccharide in *N. meningitidis* was first described by Blacklow and Warren [97]. They found that, unlike mammalian cells, N-acetylneuraminic acid (Neu5Ac) is synthesized from N-acetylmannosamine (ManNAc) and phosphoenol-pyruvate without phosphorylated intermediates. Neu5Ac is the most common form of sialic acid found in humans and plays an important role in intercellular and/or intermolecular recognition [98], explaining the difficulty of developing a safe and effective polysaccharide-based vaccine. Gotschlich and co-workers [99] determined the composition and structure of meningococcal group B capsular polysaccharide and found that it is composed of α -2,8-poly-sialic acid polymer chains, which are integrated in the outer membrane by a phospholipid anchor that is attached to the reducing end of the carbohydrate chain. This phospholipid anchor of capsular polysaccharide polymers may help stabilize the outer membrane of the meningococcal mutant without endotoxin [84]. As mentioned above, the

strain used in this study lacks the *cps* locus, as confirmed by Bos and Tommassen [100]. We therefore removed genes involved in sialic acid biosynthesis and polysaccharide transport, as well as the *galE* gene. Subsequently, the *rfbB*, *rfbA* and *rfbC* genes located downstream of *galE*, which code for enzymes involved in the biosynthesis of dTDP-rhamnose were also removed yielding a disfunctional biosynthetic pathway. Hence, these pathways were not included in the simplified model.

Peptidoglycan forms the third major constituent of the cell envelope of *N. meningitidis*. Antignac and co-workers [101] determined the biochemical structure of peptidoglycan in various *N. meningitidis* strains in detail and found that it consists of a maximum of two layers. Variations in the degree of cross-linking and O-acetylation appeared to be associated with the genetic background of the strains. The percentage of crosslinking of the peptidoglycan was around 40%, which is consistent with that determined for other gram-negative bacteria [102-105], whereas the percentage of O-acetylation per disaccharide was on average 36%. O-acetylation of peptidoglycan results in resistance to lysozyme and to other muramidases [106], suggesting that non-specific lysis of the bacteria in the host environment by lysozyme can be prevented. Other studies show that peptidoglycan structures are recognized by the innate immune system [107, 108]. Consequently, O-acetylation might contribute to affect the proper response to infection. Most of the strains analysed by Antignac and co-workers [101] predominantly contained muropeptides carrying a tetrapeptide chain, but di-, tri- and pentapeptide chains were also found. Their analysis also showed that none of the muropeptides carried glycine residues on the peptide backbone, as has been observed in gonococci [109, 110]. Hence, meningococci only synthesize D-alanyl-meso-deaminopimelate cross-bridges. However, the gene involved in alanyl-meso-deaminopimelate cross-bridging, for biosynthesis of the peptidoglycan polymer structure, has not been annotated. The enzyme involved in glycine cross-bridging of peptidoglycan (EC 2.3.2.10) is not present in the MenB genome, thus confirming the observations by Antignac and co-workers [101]. The biosynthetic pathway for peptidoglycan bio-synthesis in the metabolic

model includes the information provided by Antignac and co-workers [101], using 36% O-acetylation per disaccharide and 40% cross-linking, whereas the model muropeptide only contains the predominantly present tetra-peptide backbone.

Main characteristics of the genome-scale model

The main characteristics of the genome-scale metabolic network are summarized in Table 2.3. The MenB genome contains 2226 ORFs of which 2155 are protein encoding genes, 59 are tRNA encoding genes and 12 are rRNA encoding genes [111]. At present, 1307 genes from the total of 2155 protein encoding genes have an annotated function (60.6 %), of which 146 genes encode transporter functions [112].

Table 2.3 Main characteristics of the genome-scale metabolic network of *N. meningitidis*

ORFs	555
Annotated functions	509
Annotated putative functions	46
Unannotated functions	38
Metabolites	
Unique intracellular metabolites	471
Extracellular metabolites (minimum, based on measurements)	33
Reactions	496
Intracellular reactions	451
Transport fluxes	74
Biosynthesis of macromolecules and biomass assembly	5

For construction of the genome-scale model, a total of 555 ORFs were considered corresponding to at least 496 associated reactions (including membrane transport reactions) and at least 471 unique metabolites. The exact number of metabolites can-

not be determined accurately because of the presence of polymerisation reactions in which numerous intermediate compounds can be synthesized. In cases where numerous ORFs accounted for a single reaction (e.g. the various subunits in ATPase), the reaction was counted once, which explains the lower reaction count compared to other genome-scale networks [14]. To complete the metabolic network, two chemical oxidation reactions were added based on literature, four reactions were added to account for biosynthesis of the macromolecules DNA, RNA, Protein and Lipid, one reaction was added for biomass assembly and 38 reactions were added to account for pathway gaps (unannotated functions in Table 2.3). For these unannotated functions a corresponding gene has not been found in *N. meningitidis*. Furthermore, for nine of these functions a corresponding gene has never been found in any organism. The complete reaction database along with involved genes, enzyme numbers and metabolites can be consulted in the Additional data. A detailed description of the biomass composition and its biosynthesis can be found in Appendix 2.1.

Construction of a simplified metabolic model

The genome-scale model was simplified to the model shown in Figure 2.2. Simplification was carried out purely for ease of understanding and was done as follows: First, successive reactions in a linear pathway were lumped up to the first branch point. Second, some reactions were neglected (e.g. biosynthesis of amines, co-factors and vitamins) because the production rate of these metabolites is very small in comparison with the production rate of macromolecules required for biomass assembly. Third, reactions were omitted to prevent dead ends. A ‘dead end’ exists in a metabolic network if a metabolite is at the end of a metabolic pathway and, based on literature and our own measurements, the metabolite does not accumulate in biomass nor is it excreted to or taken up from the medium. Examples in our case are hydroxy-pyruvate and lactaldehyde. In reactions that can use NADH or NADPH as co-factor, the NADH co-factor was used in the model unless stated otherwise in the Additional data. In the approach used, a distinction between NADH and NADPH preference can-

not be made. Additional enzymatic analysis to distinguish between NADH or NADPH preference, is complicated because of the presence of transhydrogenase. The final simplified model used for flux balance analysis included 161 reactions (129 intracellular reactions, 33 transport fluxes) and 131 intracellular metabolites and can be consulted in the Appendix 2.2.

Modeling of the metabolic network

In metabolism, substrates are converted into the different macromolecules that together make up biomass. Thus, the macromolecular composition of biomass determines the flux distribution, and a shift in the macromolecular composition of biomass will result in a shift in the flux distribution. Consequently, experimental determination of the biomass composition is very important in mathematical modeling of cellular metabolism, as described in detail elsewhere [113, 114]. The measured concentrations of substrates, biomass and products, which can be found in Appendix 2.1, were converted to measured conversion rates using mass balances.

Monte Carlo simulation

Before error diagnosis was performed, errors in the primary measurements were translated to errors in measured conversion rates using a Monte Carlo approach [115, 116]. In complex mass balance equations (for example CO₂ production rate) in which various measured values with various standard deviations are included, determination of the total variance is quite laborious using standard error propagation. Therefore variances of the measured conversion rates of the various substrates and products were calculated using Monte Carlo simulation. The exact procedure involved mass balances that were formulated for the reactor configuration and is described in detail in the Materials and methods section. Accurate results were obtained after 10000 simulations as shown in Figure 2.4. The resulting average measured conversion rates and their corresponding variances were then used as input for flux balance analysis. In addition (results not shown), all separate simulated measured conversion rates were also used directly as

input for flux balance analysis, resulting in 10000 flux distributions. The final average flux distribution, calculated from these 10000 distributions, was identical to the one obtained using the average measured conversion rates as input. All calculated conversion rates as well as the fluxes appeared to be normally distributed.

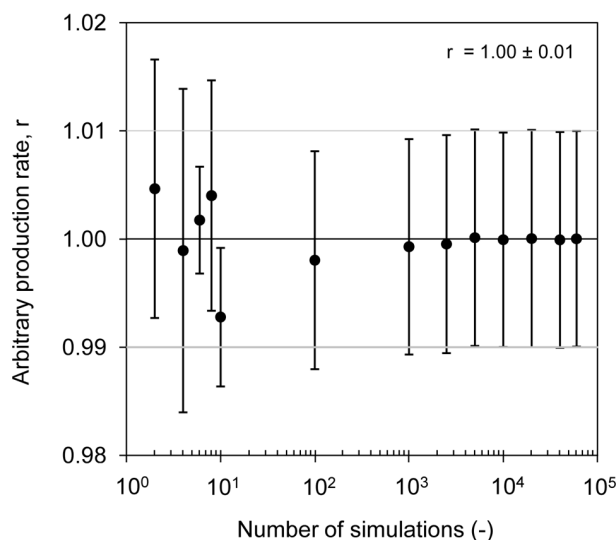


Figure 2.4 Determination of measurement variance using Monte Carlo simulation. When an arbitrary value (r) for the production rate of a hypothetical product of 1.00 with standard deviation of 0.01 was used as input for Monte Carlo simulation, 104 simulations were required to obtain the original input value (1.00 ± 0.01), showing that accurate results for the actual measured input values can be expected after 10^4 simulations.

Error diagnosis and balancing

Laws of conservation result in a number of linear constraints on the measured conversion rates of the various compounds. The measured conversion rates and their corresponding variances, that were calculated using Monte Carlo simulation, were subjected to gross error diagnosis. First the redundancy matrix, R , was calculated as described previously [117]. Matrix R , expressing the conservation relations between

the measured conversion rates only, contained two independent equations. Inspection of these equations indicated a carbon and a nitrogen balance. The residuals obtained after multiplication of the redundancy matrix with the measured conversion rates could be explained on the basis of random measurement variances [118] with test values of $h_e = 1.598$ and $h_e = 1.391$ for the first and second experimental set of measured rates, respectively, where the 95% chi-square critical value is 5.992. Also the individual carbon and nitrogen balance could be closed for both datasets. Thus, the measurements contained no gross errors and the model is also valid with respect to the measurements. The results of the statistical test are shown in Appendix 2.2. Hence, the measured rates were balanced by minimising the square of the distance between the actual measurement and the adjusted measurement with the measurement variance as a weighing factor as described previously [117]. The resulting balanced measurement rate vector, which is more accurate than the primary measurement rate vector, was used to calculate the unknown fluxes and conversion rates (see Appendix 2.2). The combinations of fluxes and unknown exchange rates that cannot be uniquely identified (that is, calculated from the measurements) were isolated using singular value decomposition. These underdetermined parts of the simplified network are listed in Appendix 2.2.

Flux distribution

As stated, the network contains underdetermined parts, for which the flux values cannot be calculated from the measured rates. To calculate a solution for these fluxes constraints can be set on certain enzymatic reactions based on available biochemical and thermodynamic literature. In addition, objective functions and linear optimisation can be used in order to calculate fluxes and unknown rates in the underdetermined part(s) of the network, as explained in the Materials and methods. The main objection against the technique of linear programming to find a solution for an underdetermined part of the network is that the objective function may not be valid for the biological system. The minimum norm constraint is an optimisation function that minimises the

length of the solution vector without any further restrictions, as explained in more detail in the Materials and methods, and was used to calculate fluxes and unknown rates in the underdetermined part(s) of the network. Like Bonarius[119], we hypothesize that the minimum-norm constraint correctly assumes that the total flux activity is minimized in order to fulfil the efforts of the bacteria to attain an efficient flux distribution. The flux values are given in Appendix 2.2. For most of the underdetermined fluxes realistic values are obtained using the minimum norm solution. For instance, the calculated fluxratio between the ED cleavage and the PP pathway shows that the major part of pyruvate ($69\pm6\%$) is synthesized through the ED cleavage, which is in agreement with literature [32]. Furthermore, we calculated that $91\pm7\%$ of the NADPH that is produced in both the PP-pathway (flux 17 and 18) and the TCA cycle (flux 2) is used for biosynthesis while $9\pm7\%$ is converted to NADH using transhydrogenase (flux 74). Some of the flux values obtained for underdetermined fluxes using the minimum-norm constraint are unlikely and are clearly an artefact of the minimum-norm solution. These are the positive sulfate production rate and the negative flux from pyrophosphate to phosphate (flux 71). By measuring thiosulfate, sulfate and H_2S , these underdetermined fluxes become determined and this problem can be solved. It must be emphasized that the actual flux distribution through the underdetermined parts may very well be different from the minimum-norm solution. Only isotopic tracer experiments can deliver true flux values for some underdetermined parts, like, for example, the ED and PP pathway. Nevertheless, the calculated flux distribution in the present study also shows that it is in agreement with literature for specific underdetermined parts of the network.

Application of the model for process development purposes

The metabolic model presented in this paper offers a framework to study *N. meningitidis* metabolism as a whole or certain aspects of it. For example, gene deletion analysis could be done to study, which genes are essential for growth in the host environment, which in turn could serve to identify possible targets for new antibiotics. In the present

study, apart from the data analysis discussed above, the model was developed for process development purposes. In particular, the model was used for the design of minimal medium for growth of *N. meningitidis* as discussed in more detail below.

Design of minimal medium

The amount of available literature describing the requirements for growth of *N. meningitidis* is tremendous, which provided an easy starting point for designing a minimal growth medium. The MenB genome was next checked for the presence of the membrane-transport functions that are required for utilization of substrates. In the case of carbon, nitrogen and sulfur substrates the genome was also checked for the presence of subsequent processing pathways.

The membrane-transport functions for utilization of the inorganic ions Na^+ , K^+ , Mg^{2+} , Cl^- and PO_4^{3-} are annotated in the MenB genome. Furthermore, genes for membrane transport of the trace elements Fe^{3+} , Cu^{2+} , Zn^{2+} , Co^{2+} , Ca^{2+} and Mn^{2+} are also annotated. These ions often function as cofactors for metal-activated enzymes or metalloenzymes. For instance, copper-zinc superoxide dismutase is a metalloenzyme that uses copper and zinc to help catalyze the conversion of superoxide anion to molecular oxygen and hydrogen peroxide. Furthermore, aconitase (a TCA enzyme) contains several iron atoms bound in the form of iron-sulfur clusters, which participate directly in the isomerization of citrate to isocitrate. The only trace element added as a supplement to the medium that could not be related to an annotated function in the genome was molybdenum. In general, molybdenum is necessary for the activity of several enzymes [120] and is added as trace element in media for growth of various bacteria like *E. coli* [121]. For this reason MoO_4^{2-} was added to complement the minimal medium. However, it remains unclear whether molybdenum is an essential requirement for growth of *N. meningitidis*.

N. meningitidis is able to metabolize a variety of sugars and amino acids for biosyn-

thesis of macromolecules and their precursors as indicated by the presence of the relevant transporter genes and the available processing pathways (ED-pathway, PP-pathway, amino-acid biosynthesis). The main utilizable carbon sources include glucose, sucrose, lactose, fructose, maltose, gluconate, lactate and pyruvate. An amino acid like glutamate can serve as both a carbon- and a nitrogen source, as the glutamate deamination product (α -ketoglutarate) can be metabolized via the citric acid cycle. However, in the literature no media were found in which glutamate was used as sole carbon and nitrogen source for growth of *N. meningitidis*. A possible disadvantage of using other amino acids as carbon and/or nitrogen source is that the deamination might result in acid products that cannot be processed in metabolism and therefore will accumulate. To select the best carbon source, the metabolic model was used to simulate growth on different carbon sources *in silico*. In all *in silico* experiments, ammonium was selected as sole nitrogen source based on the presence of the ammonium transporter, Amtb (NMB0615) and the NADP specific glutamate dehydrogenase processing pathway (NMB1710). For the *in silico* simulations, the uptake of the carbon source was fixed at a certain value and biomass formation was optimized. Furthermore a maintenance requirement of $2.81 \cdot 10^{-3} \text{ mol.g}^{-1}.\text{h}^{-1}$ was set, which was obtained from literature [122]. The predicted yields of biomass on various carbon substrates are given in Table 2.2. The metabolic model predicted that glucose is the preferred carbon substrate for growth of *N. meningitidis* in terms of biomass yield. Accordingly, glucose was selected as sole carbon source for growth. When growth was simulated using glucose as carbon source, the predicted C:N consumption ratio was 9:1 indicating the minimal amount of ammonium that is required in the growth medium. A wide range of sulfur-acquisition routes is available in *N. meningitidis*. Both thio-sulfate [63] and sulfate [54] were selected as sulfur sources in the growth medium.

In silico predictions showed that thiosulfate is the preferred sulphur source for growth, which can be explained from the fact that less energy is required for utilization of thio-sulfate in comparison with sulfate. The results of these *in silico* experiments are listed

in the Additional data. Constraint-based models give information on which substrates to use and, for some substrates, in which ratio they should be used. However, they give no information on the actual concentrations that should be used. For this work the required concentrations (by order of magnitude) of the various compounds in the minimal medium were derived from the relevant literature referred to earlier. The resulting minimal medium (see Table 2.1) is suitable for growth of *N. meningitidis* (Figure 2.5). To obtain higher biomass concentrations at the end of a batch culture further optimization of the concentrations is needed.

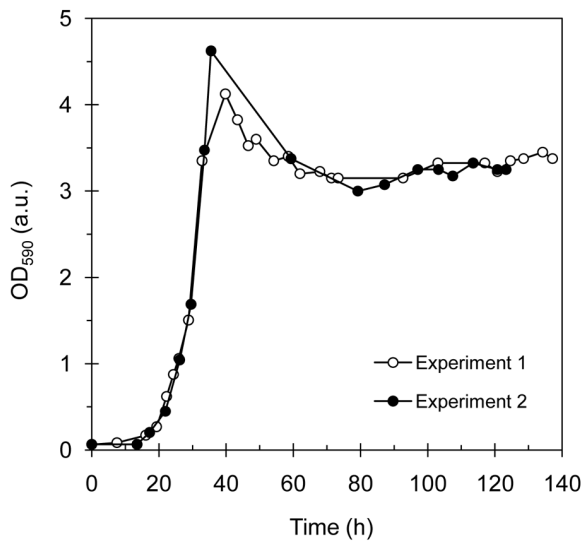


Figure 2.5 Growth of *N. meningitidis* in a minimal medium designed from the model. Growth of *N. meningitidis* strain HB-1 in minimal medium in a bioreactor operated in chemostat mode after an initial batch phase of approximately 36 h were assessed by optical density. Two experiments in identical medium and growth conditions are shown here. Conditions were as described in Materials and methods.

CONCLUSIONS

In silico genome-scale flux models have been proven to provide insight into the complexity of metabolism and can be used successfully as tools for medium design and metabolic engineering strategies. Many studies lack sufficient experimental data sets to check the consistency of the measurements and the validity of the metabolic network model. In the present study, the experimental data sets used in flux balance analysis proved to be sufficient to check for the presence of gross measurement errors or errors in the model, neither of which was found to be present.

Working from the genomic database of MenB together with biochemical and physiological information provided in literature, a genome-scale flux model for vaccine process development purposes was constructed. From these information sources a minimal medium for growth was designed and tested successfully in batch and chemostat cultures. The simplified metabolic network that was derived from the genome-scale metabolic network was verified using FBA in two duplo chemostat cultures. The specific rates, being the input of the model, were generated from the measured concentrations using Monte Carlo simulation. The model contains underdetermined parts, for which fluxes were calculated using the minimum norm constraint, providing a possible solution for these underdetermined parts. Despite the unlikely positive sulfate production rate and the negative flux from pyrophosphate to phosphate, which are both underdetermined parts of the network, the flux distribution for the remaining underdetermined parts seems plausible. This is strengthened by the observation that the major part of pyruvate ($69\pm 6\%$) is synthesized through the ED cleavage, which is in good agreement with the literature [32].

Methods for integration of metabolic network information with gene expression profiles (transcriptomics) were described recently [123-125]. Such studies bridge the gap between the putative, homology-based, information provided by the genomes and the actual situation, and greatly contribute to further improvement of our understanding of cellular processes and function.

ADDITIONAL DATA

The following additional data are available on CD-rom. The file named Additional data Chapter 2.xlsx is an excel file that includes 7 worksheets. The first worksheet named 'genome-scale model' includes the complete reaction database along with involved genes, enzyme numbers and metabolites. The second worksheet named 'simplified model' contains the simplified metabolic model. The third worksheet named 'abbreviations' contains a list of abbreviations of the metabolites. The fourth worksheet named 'redundancy matrix' contains the redundancy matrices of the experimental data sets. The fifth worksheet named 'measured rates, balanced rates' contains a table in which the experimental set of measured rates and balanced rates is given. In addition, the results of the statistical acceptance test are given in this table. The sixth worksheet named 'calculated fluxes' contains the calculated flux distributions of both experimental data sets using the minimum norm constraint. The seventh worksheet named '*in silico*' contains the flux distributions of the *in silico* experiments.

ACKNOWLEDGEMENTS

We thank Peter van der Ley for sharing his extensive knowledge on various *Neisseria*-related fields, Marieke Willemsen for practical assistance, Cor van Ingen for the freeze-drying work, Elnaz Khatami for k_{La} measurements, Jan ten Hove and Tom Ploeger for LPS structural analysis, and Peter Teunis and Gerda Doornbos for answers to statistical questions.

REFERENCES

1. Morley SL, Pollard AJ. 2001. Vaccine prevention of meningococcal disease, coming soon? *Vaccine* 20:666-687.
2. Jodar L, Feavers IM, Salisbury D, Granoff DM. 2002. Development of vaccines against meningococcal disease. *Lancet* 359:1499-1508.
3. Girard MP, Preziosi MP, Aguado MT, Kieny MP. 2006. A review of vaccine research and development: meningococcal disease. *Vaccine* 24:4692-4700.
4. Finne J, Bitter-Suermann D, Goridis C, Finne U. 1987. An IgG monoclonal antibody to group B *Neisseria meningitidis* cross-reacts with developmentally regulated polysialic acid units of glycoproteins in neural and extraneural tissues. *J Immunol* 138:4402-4407.
5. Frasch CE. 1989. Vaccines for prevention of meningococcal disease. *Clin Microbiol Rev* 2:134-138.
6. Pizzo M, Scarlato V, Masignani V, Giuliani MM, Arico B, Comanducci M, Jennings GT, Baldi L, Bartolini E, Capecci B et al. 2000. Identification of vaccine candidates against serogroup B *Neisseria meningitidis* by whole-genome sequencing. *Science* 287:1816-1820.
7. Poolman J, Berthet FX. 2001. Alternative vaccine strategies to prevent serogroup B meningococcal diseases. *Vaccine* 20 Suppl 1:S24-26.
8. Rappuoli R. 2001. Reverse vaccinology, a genome-based approach to vaccine development. *Vaccine* 19:2688-2691.
9. Rappuoli R. 2001. Conjugates and reverse vaccinology to eliminate bacterial meningitis. *Vaccine* 19:2319-2322.
10. Rodriguez-Ortega MJ, Norais N, Bensi G, Liberatori S, Capo S, Mora M, Scarselli M, Doro F, Ferrari G, Garaguso I et al. 2006. Characterization and identification of vaccine candidate proteins through analysis of the group A *Streptococcus* surface proteome. *Nat Biotechnol* 24:191-197.
11. Meinke A, Henics T, Nagy E. 2004. Bacterial genomes pave the way to novel vaccines. *Curr Opin Microbiol* 7:314-320.
12. Vermont CL, van Dijken HH, Kuipers AJ, van Limpt CJ, Keijzers WC, van der Ende A, de Groot R, van Alphen L, van den Dobbelsteen GP. 2003. Cross-reactivity of antibodies against PorA after vaccination with a meningococcal B outer membrane vesicle vaccine. *Infect Immun* 71:1650-1655.
13. de Kleijn E, van Eijndhoven L, Vermont C, Kuipers B, van Dijken H, Rumke H, de Groot R, van Alphen L, van den Dobbelsteen G. 2001. Serum bactericidal activity and isotype distribution of antibodies in toddlers and schoolchildren after vaccination with RIVM hexavalent PorA vesicle vaccine. *Vaccine* 20:352-358.
14. Price ND, Papin JA, Schilling CH, Palsson BO. 2003. Genome-scale microbial *in silico* models: the constraints-based approach. *Trends Biotechnol* 21:162-169.
15. Hua Q, Joyce AR, Fong SS, Palsson BO. 2006. Metabolic analysis of adaptive evolution for *in silico*-designed lactate-producing strains. *Biotechnol Bioeng* 95:992-1002.
16. Fong SS, Burgard AP, Herring CD, Knight EM, Blattner FR, Maranas CD, Palsson BO. 2005. *In silico* design and adaptive evolution of *Escherichia coli* for production of lactic acid. *Biotechnol Bioeng* 91:643-648.
17. Smid EJ, Molenaar D, Hugenholtz J, de Vos WM, Teusink B. 2005. Functional ingredient production: application of global metabolic models. *Curr Opin Biotechnol* 16:190-197.
18. Teusink B, van Enkevort FH, Francke C, Wiersma A, Wegkamp A, Smid EJ, Siezen RJ. 2005. *In silico* reconstruction of the metabolic pathways of *Lactobacillus plantarum*: comparing predictions of nutrient requirements with those from growth experiments. *Appl Environ Microbiol* 2005, 71:7253-7262.
19. Xie L, Wang DIC. 1994. Stoichiometric analysis of animal cell growth and its application in medium design. *Biotechnol Bioeng* 43:1164-1174.
20. Provost A, Bastin G. 2004. Dynamic metabolic modelling under the balanced growth condition. *J Proc Control* 14:717-728.
21. Tettelin H, Saunders NJ, Heidelberg J, Jeffries AC, Nelson KE, Eisen JA, Ketchum KA, Hood DW, Peden JF, Dodson RJ et al. 2000. Complete genome sequence of *Neisseria meningitidis* serogroup B strain MC58. *Science* 287:1809-1815.
22. KEGG: Kyoto Encyclopedia of Genes and Genomes (<http://www.genome.ad.jp/kegg/>)
23. Heinemann M, Kummel A, Ruinatscha R, Panke S. 2005. *In silico* genome-scale reconstruction and validation of the *Staphylococcus aureus* metabolic network. *Biotechnol Bioeng* 92:850-864.

24. Green ML, Karp PD. 2005. Genome annotation errors in pathway databases due to semantic ambiguity in partial EC numbers. *Nucleic Acids Res* 33:4035-4039.
25. The Institute for Genomic Research (<http://www.tigr.org/>)
26. The BioCyc collection of Pathway/Genome Databases (<http://www.biocyc.org/>)
27. Holten E. 1974. Glucokinase and glucose 6-phosphate dehydrogenase in *Neisseria*. *Acta Pathol Microbiol Scand [B] Microbiol Immunol* 82:201-206.
28. Holten E. 1974. 6-Phosphogluconate dehydrogenase and enzymes of the Entner-Doudoroff pathway in *Neisseria*. *Acta Pathol Microbiol Scand [B] Microbiol Immunol* 82:207-213.
29. Holten E. 1975. Radiorespirometric studies in genus *Neisseria*. I. The catabolism of glucose. *Acta Pathol Microbiol Scand [B]* 83:353-366.
30. Jysum K. 1962. Dissimilation of C14 labelled glucose by *Neisseria meningitidis* 1. The formation of CO₂ and acetate from glucose carbon. *Acta Pathol Microbiol Immunol Scand [B]* 55:319-324.
31. Jysum K. 1962. Dissimilation of C14 labelled glucose by *Neisseria meningitidis* 2. The incorporation of 1-C14 and 6-C14 into cellular components in short time experiments. *Acta Pathol Microbiol Immunol Scand [B]* 55:325-334.
32. Jysum K. 1962. Dissimilation of C14 labelled glucose by *Neisseria meningitidis* 2. The incorporation of 1-C14 and 6-C14 into pyruvate. *Acta Pathol Microbiol Immunol Scand [B]* 55:335-341.
33. Jysum K, Borchgrevink B, Jysum S. 1961. Glucose catabolism in *Neisseria meningitidis*. 1. Glucose oxidation and intermediate reactions of the Embden-Meyerhof pathway. *Acta Pathol Microbiol Scand* 53:71-83.
34. Morse SA, Stein S, Hines J. 1974. Glucose metabolism in *Neisseria gonorrhoeae*. *J Bacteriol* 120:702-714.
35. Leighton MP, Kelly DJ, Williamson MP, Shaw JG. 2001. An NMR and enzyme study of the carbon metabolism of *Neisseria meningitidis*. *Microbiol* 147:1473-1482.
36. Hebelers BH, Morse SA. 1976. Physiology and metabolism of pathogenic *neisseria*: tricarboxylic acid cycle activity in *Neisseria gonorrhoeae*. *J Bacteriol* 128:192-201.
37. Hill JC. 1971. Effect of glutamate on exogenous citrate catabolism of *Neisseria meningitidis* and of other species of *Neisseria*. *J Bacteriol* 106:819-823.
38. Holten E. 1976. Radiorespirometric studies in genus *Neisseria*. 3. The catabolism of pyruvate and acetate. *Acta Pathol Microbiol Scand [B]* 84:9-16.
39. Holten E. 1976. Radiorespirometric studies in genus *Neisseria*. 2. The catabolism of glutamate and fumarate. *Acta Pathol Microbiol Scand [B]* 84:1-8.
40. Jysum K. 1960. Intermediate reactions of the tricarboxylic acid cycle in meningococci. *Acta Pathol Microbiol Scand* 48:121-132.
41. Tonhazy NE, Pelczar MJ, Jr. 1953. Oxidation of amino acids and compounds associated with the tricarboxylic acid cycle by *Neisseria gonorrhoeae*. *J Bacteriol* 65:368-377.
42. Weiss E. 1970. Catabolic Activities of *Neisseria meningitidis*: Utilization of Succinate. *J Bacteriol* 101:133-137.
43. Holten E, Jysum K. 1974. Activities of some enzymes concerning pyruvate metabolism in *Neisseria*. *Acta Pathol Microbiol Immunol Scand [B]* 82:843-848.
44. Jysum K, Jysum S. 1962. Phosphoenolpyruvic carboxylase activity in extracts from *Neisseria meningitidis*. *Acta Pathol Microbiol Immunol Scand [B]* 54:412-424.
45. Holten E. 1976. Pyridine nucleotide independent oxidation of L-malate in genus *Neisseria*. *Acta Pathol Microbiol Scand [B]* 84:17-21.
46. Frantz ID. 1942. Growth Requirements of the Meningococcus. *J Bacteriol* 43:757-761.
47. Fitting C, Scherp HW. 1950. Observations on the metabolism of a strain of *Neisseria catarrhalis*. *J Bacteriol* 59:277-286.
48. Grossowicz N. 1945. Growth Requirements and Metabolism of *Neisseria intracellularis*. *J Bacteriol* 50:109-115.
49. Chapin CW. 1918. Carbon dioxide in the primary cultivation of the gonococcus. *J Infect Dis* 19:558-561.
50. Erwin AL, Gotschlich EC. 1996. Cloning of a *Neisseria meningitidis* gene for L-lactate dehydrogenase (L-LDH): evidence for a second meningococcal L-LDH with different regulation. *J Bacteriol* 178:4807-4813.
51. Erwin AL, Gotschlich EC. 1993. Oxidation of D-lactate and L-lactate by *Neisseria meningitidis*: purification and cloning of meningococcal D-lactate dehydrogenase. *J Bacteriol* 175:6382-6391.
52. Jiang GR, Nikolova S, Clark DP. 2001. Regulation of the *ldhA* gene, encoding the fermentative

- lactate dehydrogenase of *Escherichia coli*. Microbiology 147:2437-2446.
53. de Vrese M, Koppenhoefer B, Barth CA. 1990. D-lactic acid metabolism after an oral load of dl-lactate. Clinical Nutrition 9:23-28.
54. Jysum K. 1959. Assimilation of nitrogen in meningococci grown with the ammonium ion as sole nitrogen source. Acta Pathol Microbiol Scand 46:320-332.
55. Holtén E, Jysum K. 1973. Glutamate dehydrogenases in *Neisseria meningitidis*. Acta Pathol Microbiol Scand [B] Microbiol Immunol 81:43-48.
56. Jysum S, Jysum K. 1970. Endogenous incorporation of ^{32}P in *Neisseria meningitidis*. I. The effects of CO_2 and electron flux. Acta Pathol Microbiol Scand [B] Microbiol Immunol 78:337-342.
57. Chen CY, Genco CA, Rock JP, Morse SA. 1989. Physiology and metabolism of *Neisseria gonorrhoeae* and *Neisseria meningitidis*: implications for pathogenesis. Clin Microbiol Rev 2 Suppl:S35-40.
58. Catlin BW. 1973. Nutritional profiles of *Neisseria gonorrhoeae*, *Neisseria meningitidis*, and *Neisseria lactamica* in chemically defined media and the use of growth requirements for gonococcal typing. J Infect Dis 128:178-194.
59. Pitcher RS, Watmough NJ. 2004. The bacterial cytochrome cbb3 oxidases. Biochim Biophys Acta 1655:388-399.
60. Rock JD, Mahnane MR, Anjum MF, Shaw JG, Read RC, Moir JW. 2005. The pathogen *Neisseria meningitidis* requires oxygen, but supplements growth by denitrification. Nitrite, nitric oxide and oxygen control respiratory flux at genetic and metabolic levels. Mol Microbiol 58:800-809.
61. Rock JD, Moir JW. 2005. Microaerobic denitrification in *Neisseria meningitidis*. Biochem Soc Trans 33:134-136.
62. Port JL, DeVoe IW, Archibald FS. 1984. Sulphur acquisition by *Neisseria meningitidis*. Can J Microbiol 30:1453-1457.
63. DeVoe IW, Port J, Holbein BE, Ingram JM. 1982. Thiosulfate reductase activity in *Neisseria meningitidis*. FEMS Microbiol Lett 14:267-270.
64. Ritz D, Beckwith J. 2001. Roles of thiol-redox pathways in bacteria. Annu Rev Microbiol 55:21-48.
65. Seib KL, Tseng HJ, McEwan AG, Apicella MA, Jennings MP. 2004. Defenses against oxidative stress in *Neisseria gonorrhoeae* and *Neisseria meningitidis*: distinctive systems for different lifestyles. J Infect Dis 190:136-147.
66. Yu EK, DeVoe IW. 1980. Terminal branching of the respiratory electron transport chain in *Neisseria meningitidis*. J Bacteriol 142:879-887.
67. Yu EK, DeVoe IW. 1981. L-cysteine oxidase activity in the membrane of *Neisseria meningitidis*. J Bacteriol 145:280-287.
68. Pereverzev MO, Vygodina TV, Konstantinov AA, Skulachev VP. 2003. Cytochrome c, an ideal anti-oxidant. Biochem Soc Trans 31:1312-1315.
69. Wilks KE, Dunn KL, Farrant JL, Reddin KM, Gorringer AR, Langford PR, Kroll JS. 1998. Periplasmic superoxide dismutase in meningococcal pathogenicity. Infect Immun 66:213-217.
70. Dunn KL, Farrant JL, Langford PR, Kroll JS. 2003. Bacterial [Cu,Zn]-cofactored superoxide dismutase protects opsonized, encapsulated *Neisseria meningitidis* from phagocytosis by human monocytes/macrophages. Infect Immun 71:1604-1607.
71. Jysum S, Jysum K. 1979. Metabolism of pyrimidine bases and nucleosides in *Neisseria meningitidis*. J Bacteriol 138:320-323.
72. Jysum S. 1983. Pyrimidine biosynthesis in *Neisseria meningitidis*. 1. Demonstration of enzyme activities. Acta Pathol Microbiol Immunol Scand [B] 91:251-255.
73. Nikaido H. 1999. Microdermatology: cell surface in the interaction of microbes with the external world. J Bacteriol 181:4-8.
74. Kadner RJ. Cytoplasmic membrane. In: *Escherichia coli* and *Salmonella typhimurium*: Cellular and Molecular Biology. Edited by Neidhardt FC, Curtiss R, Ingraham JL, Brooks Low K, Magasanik B, Reznikoff WS, Riley M, Schaechter M, Umberger HE, vol. 1, 2 edn. Washington D.C.: American Society for Microbiology; 1996: 59-87.
75. Rahman MM, Kolli VS, Kahler CM, Shih G, Stephens DS, Carlson RW. 2000. The membrane phospholipids of *Neisseria meningitidis* and *Neisseria gonorrhoeae* as characterized by fast atom bombardment mass spectrometry. Microbiol 146 (Pt 8):1901-1911.
76. Cronan JE, Rock CO. Biosynthesis of membrane lipids. In: *Escherichia coli* and *Salmonella typhimurium*: Cellular and Molecular Biology. Edited by Neidhardt FC, Curtiss R, Ingraham JL, Brooks Low K, Magasanik B, Reznikoff WS, Riley M, Schaechter M, Umberger HE, vol. 1, 2 edn. Washington D.C.: American Society for Microbiology; 1996: 613-636.

77. Guymon LF, Walstad DL, Sparling PF. 1978. Cell envelope alterations in antibiotic-sensitive and-resistant strains of *Neisseria gonorrhoeae*. J Bacteriol 136:391-401.
78. Senff LM, Wegener WS, Brooks GF, Finnerty WR, Makula RA. 1976. Phospholipid composition and phospholipase A activity of *Neisseria gonorrhoeae*. J Bacteriol 127:874-880.
79. Sud IJ, Feingold DS. 1975. Phospholipids and fatty acids of *Neisseria gonorrhoeae*. J Bacteriol 124:713-717.
80. Bos MP, Tefsen B, Voet P, Weynants V, van Putten JP, Tommassen J. 2005. Function of neisserial outer membrane phospholipase a in autolysis and assessment of its vaccine potential. Infect Immun 73:2222-2231.
81. van Deuren M, Brandtzaeg P, van der Meer JW. 2000. Update on meningococcal disease with emphasis on pathogenesis and clinical management. Clin Microbiol Rev 13:144-166.
82. Nikaido H: Outer membrane. In: *Escherichia coli* and *Salmonella typhimurium*: Cellular and Molecular Biology. Edited by Neidhardt FC, Curtiss R, Ingraham JL, Brooks Low K, Magasanik B, Reznikoff WS, Riley M, Schaechter M, Umberger HE, vol. 1, 2 edn. Washington D.C.: American Society for Microbiology; 1996: 29-47.
83. Raetz RH: Bacterial lipopolysaccharides: a remarkable family of bioactive macroamphiphiles. In: *Escherichia coli* and *Salmonella typhimurium*: Cellular and Molecular Biology. Edited by Neidhardt FC, Curtiss R, Ingraham JL, Brooks Low K, Magasanik B, Reznikoff WS, Riley M, Schaechter M, Umberger HE, vol. 1, 2 edn. Washington D.C.: American Society for Microbiology; 1996: 1035-1063.
84. Steeghs L, den Hartog R, den Boer A, Zomer B, Roholl P, van der Ley P. 1998. Meningitis bacterium is viable without endotoxin. Nature 392:449-450.
85. Steeghs L: Lipid A engineering in vaccine development against *Neisseria meningitidis*. Utrecht: Utrecht University; 2001.
86. Pavliak V, Brisson JR, Michon F, Uhrin D, Jennings HJ. 1993. Structure of the sialylated L3 lipopolysaccharide of *Neisseria meningitidis*. J Biol Chem 268:14146-14152.
87. van der Ley P, van der Biezen J, Poolman JT. 1995. Construction of *Neisseria meningitidis* strains carrying multiple chromosomal copies of the *porA* gene for use in the production of a multivalent outer membrane vesicle vaccine. Vaccine 13:401-407.
88. Jennings MP, van der Ley P, Wilks KE, Maskell DJ, Poolman JT, Moxon ER. 1993. Cloning and molecular analysis of the *galE* gene of *Neisseria meningitidis* and its role in lipopolysaccharide biosynthesis. Mol Microbiol 10:361-369.
89. Jennings MP, Srikhanta YN, Moxon ER, Kramer M, Poolman JT, Kuipers B, van der LP. 1999. The genetic basis of the phase variation repertoire of lipopolysaccharide immunotypes in *Neisseria meningitidis*. Microbiology 145 (Pt 11):3013-3021.
90. Kulshin VA, Zahringer U, Lindner B, Frasch CE, Tsai CM, Dmitriev BA, Rietschel ET. 1992. Structural characterization of the lipid A component of pathogenic *Neisseria meningitidis*. J Bacteriol 174:1793-1800.
91. Rebeil R, Ernst RK, Gowen BB, Miller SI, Hinnebusch BJ. 2004. Variation in lipid A structure in the pathogenic yersiniae. Mol Microbiol 52:1363-1373.
92. Trent MS, Pabich W, Raetz CR, Miller SI. 2001. A PhoP/PhoQ-induced Lipase (PagL) that catalyzes 3-O-deacylation of lipid A precursors in membranes of *Salmonella typhimurium*. J Biol Chem 276:9083-9092.
93. Raetz CR. 2001. Regulated covalent modifications of lipid A. J Endotoxin Res 7:73-78.
94. Bos MP, Tefsen B, Geurtsen J, Tommassen J. 2004. Identification of an outer membrane protein required for the transport of lipopolysaccharide to the bacterial cell surface. Proc Natl Acad Sci U S A 101:9417-9422.
95. Estabrook MM, Griffiss JM, Jarvis GA. 1997. Sialylation of *Neisseria meningitidis* lipooligosaccharide inhibits serum bactericidal activity by masking lacto-N-neotetraose. Infect Immun 65:4436-4444.
96. Kahler CM, Martin LE, Shih GC, Rahman MM, Carlson RW, Stephens DS. 1998. The (alpha2-->8)-linked polysialic acid capsule and lipooligosaccharide structure both contribute to the ability of serogroup B *Neisseria meningitidis* to resist the bactericidal activity of normal human serum. Infect Immun 66:5939-5947.
97. Blacklow RS, Warren L. 1962. Biosynthesis of sialic acids by *Neisseria meningitidis*. J Biol Chem 237:3520-3526.
98. Varki A. 1997. Sialic acids as ligands in recognition phenomena. Faseb J 11:248-255.
99. Gotschlich EC, Fraser BA, Nishimura O, Robbins JB, Liu TY. 1981. Lipid on capsular polysaccharides of gram-negative bacteria. J Biol Chem 256:8915-8921.

100. Bos MP, Tommassen J. 2005. Viability of a capsule- and lipopolysaccharide-deficient mutant of *Neisseria meningitidis*. *Infect Immun* 73:6194-6197.
101. Antignac A, Rousselle JC, Namane A, Labigne A, Taha MK, Boneca IG. 2003. Detailed structural analysis of the peptidoglycan of the human pathogen *Neisseria meningitidis*. *J Biol Chem* 278:31521-31528.
102. Burroughs MH, Chang YS, Gage DA, Tuomanen EI. 1993. Composition of the peptidoglycan of *Haemophilus influenzae*. *J Biol Chem* 268:11594-11598.
103. Glauner B, Holtje JV, Schwarz U. 1998. The composition of the murein of *Escherichia coli*. *J Biol Chem* 263:10088-10095.
104. Quintela JC, Caparros M, de Pedro MA. 1995. Variability of peptidoglycan structural parameters in gram-negative bacteria. *FEMS Microbiol Lett* 125:95-100.
105. Tuomanen E, Schwartz J, Sande S, Light K, Gage D. 1989. Unusual composition of peptidoglycan in *Bordetella pertussis*. *J Biol Chem* 264:11093-11098.
106. Clarke AJ, Dupont C. 1992. O-acetylated peptidoglycan: its occurrence, pathobiological significance, and biosynthesis. *Can J Microbiol* 38:85-91.
107. Girardin SE, Boneca IG, Viala J, Chamaillard M, Labigne A, Thomas G, Philpott DJ, Sansonetti PJ. 2003. Nod2 is a general sensor of peptidoglycan through muramyl dipeptide (MDP) detection. *J Biol Chem* 278:8869-8872.
108. Inohara N, Ogura Y, Fontalba A, Gutierrez O, Pons F, Crespo J, Fukase K, Inamura S, Kusumoto S, Hashimoto M et al. 2003. Host recognition of bacterial muramyl dipeptide mediated through NOD2. Implications for Crohn's disease. *J Biol Chem* 278:5509-5512.
109. Dougherty TJ. 1985. Analysis of *Neisseria gonorrhoeae* peptidoglycan by reverse-phase, high-pressure liquid chromatography. *J Bacteriol* 163:69-74.
110. Martin SA, Rosenthal RS, Biemann K. 1987. Fast atom bombardment mass spectrometry and tandem mass spectrometry of biologically active peptidoglycan monomers from *Neisseria gonorrhoeae*. *J Biol Chem* 262:7514-7522.
111. The Comprehensive Microbial Resource (<http://cmr.tigr.org>)
112. TransportDB: Genomic Comparisons of Membrane Transport Systems (<http://www.membranetransport.org/>)
113. Vriezen N: Physiology of mammalian cells in suspension culture. Ph.D. thesis. Delft, The Netherlands: Technical University Delft; 1998.
114. Lange HC, Heijnen JJ. 2001. Statistical reconciliation of the elemental and molecular biomass composition of *Saccharomyces cerevisiae*. *Biotechnol Bioeng* 75:334-344.
115. Sariyar B, Perk S, Akman U, Hortacsu A. 2006. Monte Carlo sampling and principal component analysis of flux distributions yield topological and modular information on metabolic networks. *J Theor Biol* 242:389-400.
116. Wittmann C, Heinzle E. 2002. Genealogy profiling through strain improvement by using metabolic network analysis: metabolic flux genealogy of several generations of lysine-producing corynebacteria. *Appl Environ Microbiol* 68:5843-5859.
117. van der Heijden RTJM, Romein B, Heijnen JJ, Hellinga C, Luyben KCAM. 1994. Linear constraint relations in biochemical reaction systems: I. Classification of the calculability and the balanceability of conversion rates. *Biotechnol Bioeng* 43:3-10.
118. van der Heijden RTJM, Romein B, Heijnen JJ, Hellinga C, Luyben KCAM. 1994. Linear constraint relations in biochemical reaction systems: II. Diagnosis and estimation of gross errors. *Biotechnol Bioeng* 43:11-20.
119. Bonarius HPJ: Metabolic-Flux Analysis of mammalian-Cell Culture. Ph.D. thesis. Wageningen, The Netherlands: Wageningen University; 1998.
120. Grunden AM, Self WT, Villain M, Blalock JE, Shanmugam KT. 1999. An analysis of the binding of repressor protein ModE to modABCD (molybdate transport) operator/promoter DNA of *Escherichia coli*. *J Biol Chem* 274:24308-24315.
121. Fiesko J, Ritch T. 1986. Production of human alpha consensus interferon in recombinant *Escherichia coli*. *Chem Eng Commun* 45:229-240.
122. Kayser A, Weber J, Hecht V, Rinas U. 2005. Metabolic flux analysis of *Escherichia coli* in glucose-limited continuous culture. I. Growth-rate-dependent metabolic efficiency at steady state. *Microbiology* 151:693-706.
123. Akesson M, Forster J, Nielsen J. 2004. Integration of gene expression data into genome-scale metabolic models. *Metab Eng* 6:285-293.

124. Covert MW, Knight EM, Reed JL, Herrgard MJ, Palsson BO. 2004. Integrating high-throughput and computational data elucidates bacterial networks. *Nature* 429:92-96.
125. Patil KR, Nielsen J. 2005. Uncovering transcriptional regulation of metabolism by using metabolic network topology. *Proc Natl Acad Sci U S A* 102:2685-2689.
126. Badino Jr AC, Cândida MCR, Schmidell W. 2000. Improving $k_L a$ determination in fungal fermentation, taking into account electrode response time. *J Chem Technol Biotechnol* 75:469-474.
127. Dorresteyn RC, Berwald LG, Zomer G, de Gooijer CD, Wieten G, Beuvery EC. 1996. Determination of amino acids using o-phthalaldehyde-2-mercaptoethanol derivatization effect of reaction conditions. *Journal of Chromatography A* 724:159-167.
128. Welch DF. 1991. Applications of cellular fatty acid analysis. *Clin Microbiol Rev* 4:422-438.
129. White MA, Simmons MD, Bishop A, Chandler HA. 1988. Microbial identification by gas chromatography. *J R Nav Med Serv* 74:141-146.
130. Jantzen E, Bryn K, Bergan T, Bovre K. 1974. Gas chromatography of bacterial whole cell methanolysates; V. Fatty acid composition of *Neisseriae* and *Moraxellae*. *Acta Pathol Microbiol Scand [B]* Microbiol Immunol 82:767-779.
131. Westphal O, Jann JK. 1965. Bacterial lipopolysaccharide extraction with phenol-water and further application of the procedure. *Meth Carbohydr Chem* 5:83-91.
132. van der Ley P, Steeghs L, Hamstra HJ, ten Hove J, Zomer B, van Alphen L. 2001. Modification of lipid A biosynthesis in *Neisseria meningitidis* lpxL mutants: influence on lipopolysaccharide structure, toxicity, and adjuvant activity. *Infect Immun* 69:5981-5990.
133. Benthin S, Nielsen J, Villadsen J. 1991. A simple and reliable method for the determination of cellular RNA content. *Biotech Techn* 5:39-42.
134. Gerhardt P, Murray RGE, Wood WA, Krieg NR. Methods for general and molecular bacteriology. Washington D.C.: American Society for Microbiology; 1994.
135. Edwards JS, Ibarra RU, Palsson BO. 2001. *In silico* predictions of *Escherichia coli* metabolic capabilities are consistent with experimental data. *Nat Biotechnol* 19:125-130.
136. Edwards JS, Ramakrishna R, Schilling CH, Palsson BO. Metabolic flux balance analysis. In: *Metabolic Engineering*. Edited by Lee SY, Papoutsakis ET. New York: Marcel Dekker Inc.; 1999: 13-57.
137. Forster J, Gombert AK, Nielsen J. 2002. A functional genomics approach using metabolomics and *in silico* pathway analysis. *Biotechnol Bioeng* 79:703-712.
138. Vallino JJ, Stephanopoulos G. Flux determination in cellular bioreaction networks: applications to lysine fermentations. In: *Frontiers in bioprocessing*. Edited by Sikdar SK, Bier M, Todd P. Boca Raton, Fla: CRC press; 1990: 205-219.
139. Wang NS, Stephanopoulos G. 1983. Application of macroscopic balances to the identification of gross measurement errors. *Biotechnol Bioeng* 25:2177-2208.
140. Pramanik J, Keasling JD. 1997. Stoichiometric model of *Escherichia coli* metabolism: Incorporation of growth-rate dependent biomass composition and mechanistic energy requirements. *Biotechnol Bioeng* 56:398-421.
141. Thisted RA: Elements of statistical computing. New York: Chapman and Hall; 1989.
142. Bremer H, Dennis PP: Modulation of chemical composition and other parameters of the cell by growth rate. In: *Escherichia coli* and *Salmonella typhimurium*: Cellular and Molecular Biology. Edited by Neidhardt FC, Curtiss R, Ingraham JL, Brooks Low K, Magasanik B, Reznikoff WS, Riley M, Schaechter M, Umbarger HE, vol. 1, 2 edn. Washington D.C.: American Society for Microbiology; 1996: 1553-1569.
143. Pramanik J, Keasling JD. 1998. Effect of *Escherichia coli* biomass composition on central metabolic fluxes predicted by a stoichiometric model. *Biotechnol Bioeng* 60:230-238.
144. Neidhardt FC, Umbarger HE: Chemical composition of *Escherichia coli*. In: *Escherichia coli* and *Salmonella typhimurium*: Cellular and Molecular Biology. Edited by Neidhardt FC, Curtiss R, Ingraham JL, Brooks Low K, Magasanik B, Reznikoff WS, Riley M, Schaechter M, Umbarger HE, vol. 1, 2 edn. Washington D.C.: American Society for Microbiology; 1996: 13-16.
145. Neidhardt FC, Umbarger HE, Schaechter M: Physiology of the bacterial cell. Sunderland, MA: Sinauer Associates; 1990.
146. van der Werf MJ, Jellema RH, Hankemeier T. 2005. Microbial metabolomics: replacing trial-and-error by the unbiased selection and ranking of targets. *J Ind Microbiol Biotechnol* 32:234-252.

APPENDIX 2.1

A. Biomass composition

A1. Overall cellular composition of *N. meningitidis*

In a specific medium for growth, the overall cellular composition of bacterial cells depends on the growth rate of the cells [142, 143]. The overall cellular composition of *N. meningitidis* stain HB-1, grown in minimal medium at a specific growth rate of 0.04 h^{-1} is shown in Table 2.1.1.

Table 2.1.1 Overall cellular composition of *N. meningitidis*

% (w/w)	<i>E. coli</i> ²	<i>N. meningitidis</i> ¹	
		Average \pm SD	RSD assay (%)
Protein ³	55	71.0 ± 3.6	5
RNA ⁴	20.5	8.5 ± 2.2	25
DNA	3.1	0.7 ± 0.2	15
Lipids ⁵	9.1	11.4 ± 0.6	5
LPS ⁶	3.4	5.9 ± 0.3	5
Peptidoglycan ⁷	2.5	2.5 ± 0.3	10
Glycogen	2.5	-	-
Polyamines	0.4	-	-
Metabolites, cofactors, ions	3.5	-	-

¹ The analytical results were derived from two separate independent chemostat experiments. The standard deviation values (SD) represent the standard deviation between the two experiments and include the relative mean standard deviation (RSD) of the used analytical assay. All macromolecules and their composition were measured unless stated otherwise.

² Average chemical composition of *Escherichia coli* [144].

³ Total biomass protein was quantified by summation of the individual measured amino acid concentrations measured in biomass after acid hydrolysis as described in the text. The methods recovery was determined as $0.85 \pm 4 \%$ based on measurements of pure Bovine Serum Albumin and corrections were made accordingly.

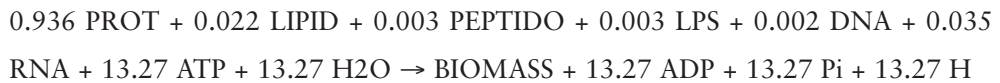
⁴ The measured macromolecules in the biomass accounted for $100 \pm 6 \%$ (w/w). The unmeasured content can be explained by a too low measured RNA content. Accurate measurement of total cellular RNA is complicated due to poor stability of RNA. The measured RNA content was multiplied by a factor of 1.2 to correct for unstable RNA [144]. The remaining unmeasured biomass content can account for at least 6.4% as indicated by the average chemical composition of *E. coli*.

⁵ The fatty acids present in biomass were individually quantified and equally distributed over the different phospholipids using the overall composition of Rahman and co-workers [75] as described in the text. Although the resulting model lipid structures are deviant from the actual structures as described by Rahman and co-workers its impact for modeling purposes is negligible.

⁶ LPS was quantified based on the measured amount of 3-hydroxydodecanoic acid (C12:0-3OH), a unique LPS related fatty acid. The LPS value possesses high uncertainty and may need to be readjusted as described in section A4.

⁷ Peptidoglycan amount in *N. meningitidis* was estimated based on *E. coli* [144] and the composition was based on the average of the peptidoglycan structures present in *N. meningitidis* [101]. For modeling purposes a relative mean standard deviation of 10% was assumed.

The biosynthesis of biomass was set as a linear combination of the macromolecules: protein, DNA, RNA, lipid, peptidoglycan and LPS which were considered to account for the overall biomass composition. The growth-associated ATP for maintenance was estimated to be 13.27 mol ATP / mol biomass. The accuracy of the estimation is, however, quite low. This value was calculated using linear regression of available $1/Y_{x/ATP}$ vs growth rate data from *E. coli* [122] using the growth rate applied in this study in the obtained equation followed by conversion to the desired unit using the molecular weight of biomass. One mole of biomass is defined by the reaction equation for this compound (reaction 128 in the simplified model) and is equivalent to 140 g dry weight with an elemental composition given in Table 2.1.7. Incorporation of the energy requirement yields the biomass biosynthesis reaction:



A2. Protein composition and biosynthesis

The energy requirement for Protein biosynthesis and processing was assumed identical to *E. coli*: 4.306 mol ATP / mol protein [145]. Incorporation of this energy requirement yields the final reaction for protein biosynthesis:



In which 1 AA is the sum of molar fractions of the various amino acids present in *N. meningitidis*.

Table 2.1.2 Protein composition *N. meningitidis*

% (mol AA/mol protein)	<i>N. meningitidis</i> ¹	
	genome ¹	Average ² ± SD
Aspartate (Asp)	5.3	5.1 ± 0.3
Glutamate (Glu)	6.4	7.6 ± 0.4
Serine (Ser)	5.4	4.4 ± 0.2
Histidine (His)	2.3	1.8 ± 0.1
Glycine (Gly)	6.9	9.3 ± 0.5
Threonine (Thr)	5.2	4.7 ± 0.2
Alanine (Ala)	9.5	14.9 ± 0.7
Arginine (Arg)	5.8	5.1 ± 0.3
Tyrosine (Tyr)	3.2	1.9 ± 0.1
Valaline (Val)	6.8	7.2 ± 0.4
Methionine (Met)	2.6	2.6 ± 0.1
Phenylalanine (Phe)	4.3	3.3 ± 0.2
Isoleucine (Ile)	5.9	4.8 ± 0.2
Leucine (Leu)	10.0	7.6 ± 0.4
Lysine (Lys)	5.8	5.4 ± 0.3
Proline (Pro)	4.2	3.5 ± 0.2
Asparagine (Asn) ⁴	4.1	4.0 ± 0.2
Tryptophan (Trp) ³	1.3	1.2 ± 0.1
Cysteine (Cys) ³	1.1	0.9 ± 0.1
Glutamine (Gln) ⁴	4.1	4.8 ± 0.2

1 Amino acid composition predicted by the genome [21]. For all genes, a random expression level between 0 - 100000 was used resulting in an identical (random) expression level of the corresponding proteins and their amino acid composition.

2 The standard deviation values (SD) represent the standard deviation between two independent chemostat experiments and includes the relative mean standard deviation (RSD) of the used analytical assay.

3 The amino acids Cys and Trp (AA) that were destructured during acid hydrolysis were calculated based on the predicted amino acid composition in the genome and the measured threonine quantity by using the formula below.

$$AA = \frac{Thr_{measured} \cdot AA_{genome}}{Thr_{genome}}$$

4 The amino acids Gln and Asn (AAn) that were converted to respectively Glu and Asp (AA) during acid hydrolysis were calculated based on the predicted amino acid composition in the genome and the measured Glx and Asx (AAx) quantity by using the formula:

$$AAn = \frac{AAx_{measured} \cdot AAn_{genome}}{AA_{genome}} \quad \text{in which} \quad AAx_{measured} = (AA + AAn)_{measured}$$

In this way, the ratio of *Glu:Gln* and *Asp:Asn* predicted by the genome is incorporated. This provides a more solid point of departure for flux mass balancing in comparison with the traditional applied 1:1 ratio.

A3. Nucleotide composition and biosynthesis

The DNA composition was derived from the complete nucleotide composition present in the genome sequence [21]. For RNA the Uridine content was based on the Thymine content in the genome sequence [23].

Table 2.1.3 DNA composition in *N. meningitidis*

	DNA composition
	% (mol/mol)
dTTP	24.24
dCTP	25.76
dGTP	25.76
dATP	24.24
Molecular weight DNA (g/mol)	324.96

The energy requirement for DNA biosynthesis and processing was assumed identical to *E. coli*: 1.372 mol ATP / mol DNA [145]. Incorporation of this energy requirement yields the final reaction for DNA biosynthesis:



In which dNTP is the sum of molar fractions of the various desoxyribonucleotides present in *N. meningitidis*.

Table 2.1.4 RNA composition in *N. meningitidis*

	RNA composition
	% (mol/mol)
UTP	24.27
CTP	25.56
GTP	25.97
ATP	24.20
Molecular weight DNA (g/mol)	337.63

The energy requirement for RNA biosynthesis and processing was assumed identical *E. Coli*: 0.4 mol ATP / mol RNA [145]. Incorporation of this energy requirement yields the final reaction for RNA biosynthesis:



In which NTP is the sum of molar fractions of the various ribonucleotides present in *N. meningitidis*.

A4. Lipid composition and biosynthesis

The fatty acids present in biomass were individually quantified using a modified gas chromatography method as described in the text. The quantified fatty acids were equally distributed over the different phospholipids using the overall composition of Rahman and co-workers [75].

Table 2.1.5 Lipid composition in *N. meningitidis*

% (w/w)	<i>N. gonorrhoeae</i>	<i>N. meningitidis</i>
	Senff et al. ² Average \pm SD	Rahman et al. ¹ Average \pm SD
phosphatidate (PA)	-	10.2 \pm 1.1
phosphatidylethanolamine (PE)	77 \pm 1	71.5 \pm 4.2
phosphatidylglycerol (PG)	18 \pm 2	18.3 \pm 4.1
lysophosphatidylethanolamine (LPE)	2 \pm 1	-
cardiolipin (CL)	2 \pm 1	-

1 FAB-MS determined average lipid composition of *N. meningitidis* strains NMB, 6940, M7, SS3, CMK2, R6, CMK1 and 469 cultivated in GC broth at 37 °C for 16-18 hours in an aerobic humid atmosphere supplemented with 3.5% CO₂ [75]. For modeling purposes 10.23 % PA, 71.46 % PE and 18.31 % PG were used.

2 Thin layer chromatography (TLC) determined average lipid composition of *N. gonorrhoeae* strain 2686 colonial types 1 and 4 cultivated in Mayer broth at 37 °C for 18 hours in an aerobic humid atmosphere [78]. Earlier, Sud and Feingold [79] determined a comparable composition.

Table 2.1.6 Fatty acid composition in *N. meningitidis*

% (mol/mol)	Jantzen et al. ¹ Average \pm SD	Average \pm SD ²
dodecanoic acid (C12:0)	3.5 \pm 0.7	8.6 \pm 0.9
3-hydroxydodecanoic acid (C12:0-3OH)3	6.0 \pm 2.8	9.6 \pm 0.2
tetradecanoic acid (C14:0)	7.0 \pm 0.0	3.5 \pm 0.5
3-hydroxytetradecanoic acid (C14:0-3OH)	4.5 \pm 2.1	4.2 \pm 1.1
hexadecenoic acid (C16:1)	29.0 \pm 5.7	26.8 \pm 1.7
hexadecanoic acid (C16:0)	39.0 \pm 2.8	40.6 \pm 2.1
octadecenoic acid (C18:1)	9.0 \pm 1.4	10.3 \pm 0.2
octadecanoic acid (C18:0)	2.0 \pm 0.0	1.1 \pm 0.1
octadecadienoic acid (C18:2)	1.0 \pm 1.0	-

1 Gaschromatography (GC) determined fatty acid composition of *N. meningitidis* strains M1 and B8152/66 cultivated on blood agar plates at 37 °C for 20 hours in an aerobic humid atmosphere supplemented with CO₂ [130].

2 GC determined fatty acid composition of *N. meningitidis* strain HB-1 as described in the text. The standard deviation values (SD) represent the standard deviation of two independent experiments and does not include the relative mean standard deviation (RSD) of the used analytical assay. Rahman and co-workers [75] additionally identified presence of tetradecenoic acid (C14:1) and hexadecadienoic acid (C16:2) in lipids.

3 Based on the measured lipopolysaccharide (LPS) structure, the molar ratio of C12:0/C12:0-3OH/C14:0-3OH is constant 1/1/1. However, a ratio of approximately 2/2/1 was measured using the GC method. As mentioned in the text, LPS was quantified based on the measured amount of C12:0-3OH (GC), thus neglecting the measured amount of C14:0-3OH. The remaining C12:0 quantity was used in lipid biosynthesis. When the LPS amount is quantified based on the measured amount of C14:0-3OH more C12:0 can be incorporated into lipid but a relatively large amount of C12:0-3OH is left over. Although it is possible that C12:0-3OH is synthesized faster than C14:0-3OH and accumulates in the cell we assumed that this was unlikely and therefore based the LPS amount on C12:0-3OH. Therefore, the LPS value possesses high uncertainty and may need to be readjusted.

A5. Elemental composition**Table 2.1.7** Elemental composition

	C	H	N	O	P	S	+	-
Amino Acids								
GLU	5	8	1	4	0	0	0	1
GLN	5	9	2	3	0	0	0	1
PRO	5	8	1	2	0	0	0	1
ASP	4	6	1	4	0	0	0	1
ASN	4	7	2	3	0	0	0	1
ARG	6	15	4	2	0	0	1	0
THR	4	8	1	3	0	0	0	1
LYS	6	15	2	2	0	0	1	0
ILE	6	12	1	2	0	0	0	1
MET	5	10	1	2	0	1	0	1
SER	3	6	1	3	0	0	0	1
CYS	3	6	1	2	0	1	0	1
GLY	2	4	1	2	0	0	0	1
VAL	5	10	1	2	0	0	0	1
LEU	6	12	1	2	0	0	0	1
ALA	3	6	1	2	0	0	0	1
HIS	6	10	3	2	0	0	1	0
PHE	9	10	1	2	0	0	0	1
TYR	9	10	1	3	0	0	0	1
TRP	11	11	2	2	0	0	0	1
DNA								
dATP	10	12	5	12	3	0	0	4
dCTP	9	12	3	13	3	0	0	4
dGTP	10	12	5	13	3	0	0	4
dTTP	10	13	2	14	3	0	0	4
RNA								
ATP	10	12	5	13	3	0	0	4
CTP	9	12	3	14	3	0	0	4
GTP	10	12	5	14	3	0	0	4
UTP	9	11	2	15	3	0	0	4
Fatty Acids								
C12:0-3OHACP	12	23	0	2	0	0	0	0
C12:0ACP	12	23	0	1	0	0	0	0
C14:0-3OHACP	14	27	0	2	0	0	0	0
C14:0ACP	14	27	0	1	0	0	0	0
C16:0ACP	16	31	0	1	0	0	0	0
C18:0ACP	18	35	0	1	0	0	0	0
C16:1ACP	16	29	0	1	0	0	0	0
C18:1ACP	18	33	0	1	0	0	0	0
Macromolecules								
PA	35.3	65.9	0.0	8.0	1.0	0.0	0.0	0.0
PE	37.3	69.9	1.0	8.0	1.0	0.0	0.0	0.0
PG	38.3	71.9	0.0	10.0	1.0	0.0	0.0	0.0
Peptidoglycan	55.8	88.2	12.2	27.7	0.0	0.0	0.0	1.0
LPS	134.0	245.0	4.0	67.0	3.0	0.0	0.0	4.0
DNA	9.7	12.2	3.8	7.0	1.0	0.0	0.0	2.0
RNA	9.5	11.8	3.8	8.0	1.0	0.0	0.0	2.0
Protein	4.7	7.5	1.3	1.5	0.0	0.0	0.0	0.0
Lipid	37.3	69.8	0.7	8.4	1.0	0.0	0.0	0.0
BIOMASS	6.3	10.3	1.5	2.2	0.1	0.0	0.0	0.0

Based on the measurements an approximate elemental biomass composition was determined:

$\text{CH}_{1.62}\text{O}_{0.35}\text{N}_{0.25}\text{P}_{0.013}\text{S}_{0.005}$. This yields a molecular weight on C-mole basis of ~23 g/C-mole which is comparable with other gram negative organisms like *E. coli*.

B. Metabolites measured in the culture supernatant and off-gas

Table 2.1.8 Metabolites measured in the culture supernatant and off-gas¹

Metabolite	Average \pm SD ²
Protein ³ (g.L ⁻¹)	0.063 \pm 0.019
Asp	0.029 \pm 0.012
Glu	0.020 \pm 0.009
Ser	0.001 \pm 0.001
His	0.030 \pm 0.043
Gly	0.004 \pm 0.001
Thr	0.041 \pm 0.012
Ala	0.011 \pm 0.010
Arg	0.012 \pm 0.010
Tyr	0.018 \pm 0.007
Val	0.002 \pm 0.001
Met	0.002 \pm 0.001
Phe	0.205 \pm 0.058
Ile	0.000 \pm 0.000
Leu	0.007 \pm 0.008
Lys	0.050 \pm 0.020
Pro	0.000 \pm 0.000
Asn	0.000 \pm 0.000
Trp	0.000 \pm 0.000
Cys	0.000 \pm 0.000
Gln	0.000 \pm 0.001
lactate	0.00 \pm 0.00
acetate	0.19 \pm 0.04
ethanol	1.80 \pm 0.22
NH ₃	4.87 \pm 0.97
glucose	0.00 \pm 0.00
off-gas O ₂ %(v/v)	31.8 \pm 4.70
off-gas CO ₂ %(v/v)	0.25 \pm 0.04
k _L a (h ⁻¹) ⁴	13.41 \pm 0.56

1 All metabolites were measured (mM) unless stated otherwise.

2 The standard deviation values (SD) represent the standard deviation between two independent experiments and includes the relative mean standard deviation (RSD) of the used analytical assay.

3 The composition of the supernatant protein was assumed to be identical to the cellular protein composition.

4 The volumetric oxygen transfer coefficient, k_La, in the bioreactor was determined accurately at 37 °C using a steady state set-up and a phosphate buffered saline solution (NVI, Z3000) as reference liquid. As mentioned in the text, the k_La values were confirmed using the dynamic method. The determined k_La using the dynamic method was 15.73 \pm 2.28 h⁻¹.

APPENDIX 2.2

A. Simplified metabolic model

TCA CYCLE

- 1 $OXA + ACCOA + H_2O \rightleftharpoons CIT + COA + H$
- 2 $CIT + NADP \rightleftharpoons AKG + CO_2 + NADPH$
- 3 $AKG + COA + NAD + H \rightarrow SUCCOA + NADH + CO_2$
- 4 $SUCCOA + Pi + ADP \rightleftharpoons SUC + COA + ATP + H$
- 5 $SUC + FAD \rightleftharpoons FADH_2 + FUM$
- 6 $FUM + H_2O \rightleftharpoons MAL$
- 7 $MAL + FAD \rightarrow FADH_2 + OXA$

EMP PATHWAY (glycolysis, gluconeogenesis)

- 8 $GLC + ATP \rightleftharpoons G6P + ADP + H$
- 9 $G6P \rightleftharpoons F6P$
- 10 $GAP \rightleftharpoons GLP$
- 11 $GAP + GLP + H_2O \rightarrow F6P + Pi$
- 12 $GAP + Pi + NAD + ADP \rightleftharpoons 3PG + ATP + NADH$
- 13 $3PG \rightleftharpoons PEP + H_2O + H$
- 14 $PEP + ADP + H \rightleftharpoons PYR + ATP$
- 15 $PEP + CO_2 + H_2O \rightarrow OXA + Pi + H$
- 16 $PYR + ATP + H_2O \rightleftharpoons PEP + AMP + Pi + 2 H$

PENTOSE PHOSPHATE PATHWAY

- 17 $G6P + NADP + H_2O \rightarrow 6PG + NADPH + 2 H$
- 18 $6PG + NADP \rightleftharpoons RU5P + CO_2 + NADPH$
- 19 $RU5P \rightleftharpoons R5P$
- 20 $RU5P \rightleftharpoons X5P + H$
- 21 $X5P + R5P \rightleftharpoons S7P + GAP$
- 22 $F6P + GAP \rightleftharpoons E4P + X5P + H$
- 23 $S7P + GAP + H \rightleftharpoons E4P + F6P$

ENTNER DOUDOROFF

- 24 $6PG \rightleftharpoons HD6PG + H_2O$
- 25 $HD6PG \rightleftharpoons GAP + PYR$

PYRUVATE METABOLISM

- 26 $PYR + COA + NAD \rightarrow ACCOA + CO_2 + NADH$
- 27 $LAC + NAD \rightleftharpoons PYR + NADH + H$
- 28 $MAL + NAD \rightarrow PYR + CO_2 + NADH$
- 29 $ACCOA + Pi \rightleftharpoons AC-P + COA$
- 30 $AC-P + ADP \rightleftharpoons ACE + ATP$
- 31 $ACE + COA + ATP + H \rightleftharpoons ACCOA + AMP + PPi$

AMINO ACIDS

- 32 $2 H + AKG + NH_3 + NADPH \rightleftharpoons GLU + NADP + H_2O$
- 33 $GLU + NH_3 + ATP \rightleftharpoons GLN + Pi + ADP + H$
- 34 $GLN + CO_2 + 2 H_2O + 2 ATP \rightleftharpoons CARBP + GLU + Pi + 2 ADP + H$
- 35 $GLU + ATP + 2 NADPH + H \rightarrow PRO + ADP + Pi + 2 NADP + H_2O$
- 36 $OXA + GLU \rightleftharpoons ASP + AKG$
- 37 $FUM + NH_3 + H \rightleftharpoons ASP$
- 38 $ASP + O_2 + H_2O \rightleftharpoons OXA + H_2O_2 + NH_3 + H$

- 39 $\text{ASP} + \text{NH}_3 \leftrightarrow \text{ASN} + \text{H}_2\text{O}$
40 $\text{ASP} + 2 \text{ATP} + \text{CARBP} + \text{NADPH} + 2 \text{GLU} \leftrightarrow \text{ARG} + \text{FUM} + \text{AKG} + \text{AMP} + \text{PPi} + \text{H} + 2 \text{Pi} + \text{ADP} + \text{NADP}$
41 $\text{ASP} + \text{ATP} + \text{NADPH} + \text{H} \leftrightarrow \text{ASP4SA} + \text{Pi} + \text{NADP} + \text{ADP}$
42 $\text{ASP4SA} + \text{H} + \text{NADPH} \leftrightarrow \text{HSER} + \text{NADP}$
43 $\text{HSER} + \text{ATP} + \text{H}_2\text{O} \leftrightarrow \text{THR} + \text{Pi} + \text{ADP} + 2 \text{H}$
44 $\text{ASP4SA} + \text{PYR} + \text{NADH} + \text{SUCCOA} + \text{GLU} \rightarrow \text{mDAP} + \text{SUC} + \text{AKG} + \text{COA} + \text{H} + \text{NAD}$
45 $\text{mDAP} + \text{H} \rightarrow \text{LYS} + \text{CO}_2$
46 $\text{THR} \rightarrow \text{OBUT} + \text{NH}_3$
47 $\text{OBUT} + \text{NADPH} + \text{H} + \text{GLU} + \text{PYR} \leftrightarrow \text{ILE} + \text{AKG} + \text{NADP} + \text{H}_2\text{O} + \text{CO}_2$
48 $\text{HSER} + \text{ACCOA} + \text{H}_2\text{S} \leftrightarrow \text{HCYS} + \text{ACE} + \text{COA} + 2 \text{H}$
49 $5\text{MTHF} + \text{HCYS} \leftrightarrow \text{THF} + \text{MET}$
50 $\text{SER} + \text{ACCOA} + \text{H}_2\text{S} \leftrightarrow \text{CYS} + \text{ACE} + \text{COA} + \text{H}$
51 $\text{SO}_4 + 2 \text{ATP} + \text{H}_2\text{O} + \text{RTR} \rightarrow \text{SO}_3 + \text{H} + \text{ADP} + \text{Pi} + \text{AMP} + \text{PPi} + \text{OTR}$
52 $\text{THS} + \text{O}_2 + \text{H}_2\text{O} \rightarrow 2 \text{SO}_3 + 2 \text{H}$
53 $\text{SO}_3 + 3 \text{NADPH} + 5 \text{H} \leftrightarrow \text{H}_2\text{S} + 3 \text{NADP} + 3 \text{H}_2\text{O}$
54 $\text{SER} \rightarrow \text{PYR} + \text{NH}_3$
55 $3\text{PG} + \text{NAD} + \text{GLU} + \text{H}_2\text{O} \leftrightarrow \text{SER} + \text{AKG} + \text{Pi} + \text{NADH} + 3 \text{H}$
56 $\text{THF} + \text{SER} \leftrightarrow \text{METHF} + \text{GLY} + \text{H}_2\text{O}$
57 $2 \text{PYR} + \text{NADPH} + 2 \text{H} \leftrightarrow \text{IVA} + \text{H}_2\text{O} + \text{CO}_2 + \text{NADP}$
58 $\text{IVA} + \text{GLU} \leftrightarrow \text{VAL} + \text{AKG} + \text{H}$
59 $\text{IVA} + \text{ACCOA} + \text{H}_2\text{O} + \text{NAD} + \text{GLU} \rightarrow \text{LEU} + \text{AKG} + \text{COA} + \text{NADH} + 2 \text{H} + \text{CO}_2$
60 $\text{VAL} + \text{PYR} \leftrightarrow \text{IVA} + \text{ALA}$
61 $\text{R5P} + \text{ATP} \leftrightarrow \text{PRPP} + \text{AMP} + \text{H}$
62 $\text{PRPP} + \text{ATP} + 3 \text{H}_2\text{O} + \text{GLN} + 3 \text{NAD} \rightarrow \text{HIS} + 3 \text{NADH} + 2 \text{PPi} + \text{AICAR} + \text{AKG} + \text{Pi}$
63 $\text{E4P} + 2 \text{PEP} + \text{NADPH} + \text{ATP} \rightarrow \text{CHOR} + 4 \text{Pi} + \text{NADP} + \text{ADP}$
64 $\text{CHOR} \leftrightarrow \text{PRE}$
65 $\text{PRE} + \text{GLU} \rightarrow \text{PHE} + \text{AKG} + \text{CO}_2 + \text{H}_2\text{O}$
66 $\text{PRE} + \text{NAD} + \text{GLU} \rightarrow \text{TYR} + \text{AKG} + \text{H} + \text{CO}_2 + \text{NADH}$
67 $\text{CHOR} + \text{GLN} + \text{H} \leftrightarrow \text{ANT} + \text{GLU} + \text{PYR}$
68 $\text{PRPP} + \text{ANT} + \text{SER} + \text{H} \rightarrow \text{TRP} + 2 \text{H}_2\text{O} + \text{PPi} + \text{CO}_2 + \text{GAP}$

CARBOHYDRATES

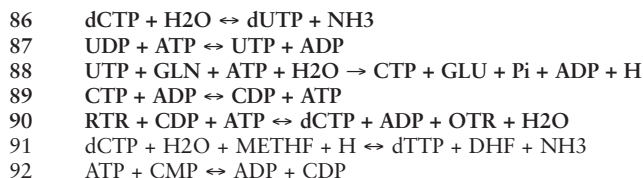
- 69 $\text{G6P} \leftrightarrow \text{G1P}$

ENERGY METABOLISM

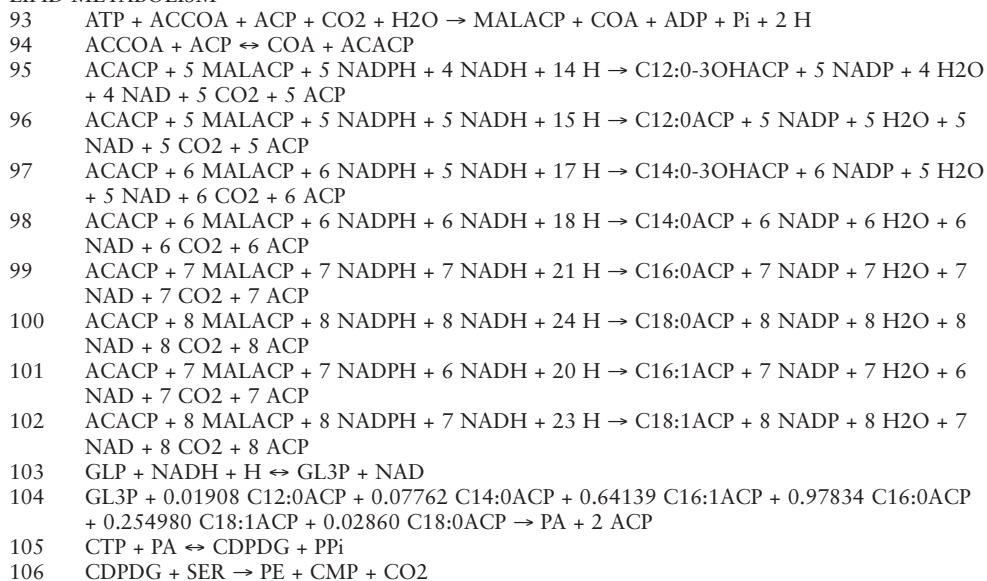
- 70 $\text{ATP} + \text{H}_2\text{O} \rightarrow \text{Pi} + \text{ADP} + \text{H}$
71 $\text{PPi} + \text{H}_2\text{O} \rightarrow 2 \text{Pi} + 2 \text{H}$
72 $\text{O}_2 + 4 \text{Pi} + 2 \text{NADH} + 4 \text{ADP} + 6 \text{H} \rightarrow 4 \text{ATP} + 6 \text{H}_2\text{O} + 2 \text{NAD}$
73 $\text{FADH}_2 + \text{NAD} \leftrightarrow \text{FAD} + \text{NADH} + \text{H}$
74 $\text{NADPH} + \text{NAD} \leftrightarrow \text{NADP} + \text{NADH}$

NUCLEOSIDES AND NUCLEOTIDES BIOSYNTHESIS

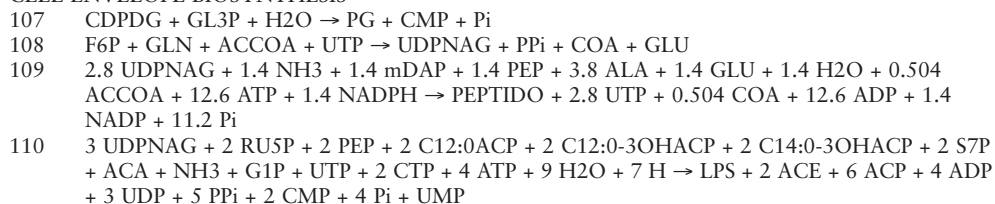
- 75 $\text{PRPP} + 2 \text{GLN} + 2 \text{H}_2\text{O} + \text{GLY} + 4 \text{ATP} + \text{FTHF} + \text{CO}_2 + \text{ASP} \rightarrow \text{AICAR} + \text{FUM} + 2 \text{GLU} + \text{PPi} + 4 \text{Pi} + 4 \text{ADP} + \text{THF} + 3 \text{H}$
76 $\text{AICAR} + \text{FTHF} \leftrightarrow \text{IMP} + \text{H}_2\text{O} + \text{THF}$
77 $\text{IMP} + \text{ASP} + \text{GTP} \leftrightarrow \text{FUM} + \text{AMP} + \text{GDP} + \text{Pi} + 2 \text{H}$
78 $\text{AMP} + \text{ATP} \leftrightarrow 2 \text{ADP}$
79 $\text{RTR} + \text{ATP} \leftrightarrow \text{dATP} + \text{OTR} + \text{H}_2\text{O}$
80 $\text{IMP} + \text{NAD} + 2 \text{H}_2\text{O} + 2 \text{ATP} + \text{GLN} \leftrightarrow \text{GDP} + \text{ADP} + \text{H} + \text{NADH} + \text{GLU} + \text{AMP} + \text{PPi}$
81 $\text{GDP} + \text{ATP} \leftrightarrow \text{GTP} + \text{ADP}$
82 $\text{RTR} + \text{GDP} + \text{ATP} \rightarrow \text{dGTP} + \text{ADP} + \text{OTR} + \text{H}_2\text{O}$
83 $\text{CARBP} + \text{ASP} + \text{O}_2 + \text{PRPP} + \text{H} \leftrightarrow \text{UMP} + \text{CO}_2 + \text{Pi} + \text{H}_2\text{O} + \text{H}_2\text{O}_2 + \text{PPi}$
84 $\text{UMP} + \text{ATP} \leftrightarrow \text{UDP} + \text{ADP}$
85 $\text{RTR} + \text{UDP} + \text{ATP} \leftrightarrow \text{dUTP} + \text{ADP} + \text{OTR} + \text{H}_2\text{O}$



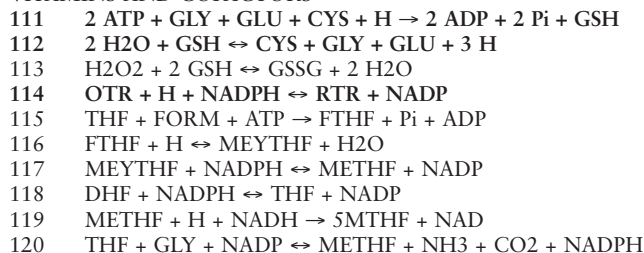
LIPID METABOLISM



CELL ENVELOPE BIOSYNTHESIS



VITAMINS AND COFACTORS



OTHERS

- 121 $\text{ACA} + \text{H} + \text{NADH} \rightleftharpoons \text{ETH} + \text{NAD}$
122 $\text{ACE} + \text{NADH} + 2 \text{H} \rightleftharpoons \text{ACA} + \text{H}_2\text{O} + \text{NAD}$
123 $2 \text{H}_2\text{O}_2 \rightleftharpoons \text{O}_2 + 2 \text{H}_2\text{O}$

MACROMOLECULES AND BIOMASS ASSEMBLY

- 124 $0.24236 \text{ dTTP} + 0.25764 \text{ dCTP} + 0.25764 \text{ dGTP} + 0.24236 \text{ dATP} + 1.372 \text{ ATP} + 2.372 \text{ H}_2\text{O} \rightarrow$
 $\text{DNA} + \text{PPi} + 1.372 \text{ ADP} + 1.372 \text{ Pi} + 1.372 \text{ H}$
125 $0.24268 \text{ UTP} + 0.25557 \text{ CTP} + 0.25972 \text{ GTP} + 0.64204 \text{ ATP} + 1.4 \text{ H}_2\text{O} \rightarrow \text{RNA} + \text{PPi} + 0.4$
 $\text{ADP} + 0.4 \text{ Pi} + 0.4 \text{ H}$
126 $0.051 \text{ ASP} + 0.076 \text{ GLU} + 0.044 \text{ SER} + 0.018 \text{ HIS} + 0.093 \text{ GLY} + 0.047 \text{ THR} + 0.149 \text{ ALA} +$
 $0.051 \text{ ARG} + 0.019 \text{ TYR} + 0.072 \text{ VAL} + 0.026 \text{ MET} + 0.033 \text{ PHE} + 0.048 \text{ ILE} + 0.076 \text{ LEU} +$
 $0.054 \text{ LYS} + 0.035 \text{ PRO} + 0.04 \text{ ASN} + 0.012 \text{ TRP} + 0.009 \text{ CYS} + 0.048 \text{ GLN} + 4.306 \text{ ATP} +$
 $3.306 \text{ H}_2\text{O} \rightarrow 1 \text{ PROT} + 4.306 \text{ ADP} + 4.306 \text{ Pi} + 3.551 \text{ H}$
127 $0.10913 \text{ PA} + 0.71561 \text{ PE} + 0.17525 \text{ PG} \rightarrow \text{LIPID}$
128 $0.93555 \text{ PROT} + 0.022120 \text{ LIPID} + 0.00256 \text{ PEPTIDO} + 0.002624 \text{ LPS} + 0.002141 \text{ DNA} +$
 $0.034943 \text{ RNA} + 13.27 \text{ ATP} + 13.27 \text{ H}_2\text{O} \rightarrow \text{BIOMASS} + 13.27 \text{ ADP} + 13.27 \text{ Pi} + 13.27 \text{ H}$

MEMBRANE TRANSPORT (exchange reactions)

- 129 $\text{GLC}_{\text{ext}} + \text{H}_{\text{ext}} \rightarrow \text{GLC} + \text{H}$
130 $\text{CO}_2 \rightarrow \text{CO}_{2,\text{ext}}$
131 $\text{H} \rightleftharpoons \text{H}_{\text{ext}}$
132 $\text{NH}_3 \rightleftharpoons \text{NH}_{3,\text{ext}}$
133 $\text{O}_{2,\text{ext}} \rightarrow \text{O}_2$
134 $\text{Pi}_{\text{ext}} + \text{H}_{\text{ext}} \rightleftharpoons \text{Pi} + \text{H}$
135 $\text{THS}_{\text{ext}} + \text{ATP} + \text{H}_2\text{O} \rightarrow \text{THS} + \text{ADP} + \text{Pi} + \text{H}$
136 $\text{SO}_4_{\text{ext}} + \text{ATP} + \text{H}_2\text{O} \rightarrow \text{SO}_4 + \text{ADP} + \text{Pi} + \text{H}$
137 $\text{H}_2\text{S} \rightleftharpoons \text{HS}_{\text{ext}} + \text{H}_{\text{ext}}$
138 $\text{GLU}_{\text{ext}} + \text{H}_{\text{ext}} \rightleftharpoons \text{GLU} + \text{H}$
139 $\text{GLN}_{\text{ext}} + \text{H}_{\text{ext}} \rightleftharpoons \text{GLN} + \text{H}$
140 $\text{PRO}_{\text{ext}} + \text{H}_{\text{ext}} \rightleftharpoons \text{PRO} + \text{H}$
141 $\text{ASP}_{\text{ext}} + \text{H}_{\text{ext}} \rightleftharpoons \text{ASP} + \text{H}$
142 $\text{ASN}_{\text{ext}} + \text{H}_{\text{ext}} \rightleftharpoons \text{ASN} + \text{H}$
143 $\text{ARG}_{\text{ext}} + \text{H}_{\text{ext}} \rightleftharpoons \text{ARG} + \text{H}$
144 $\text{THR}_{\text{ext}} + \text{H}_{\text{ext}} \rightleftharpoons \text{THR} + \text{H}$
145 $\text{LYS}_{\text{ext}} + \text{H}_{\text{ext}} \rightleftharpoons \text{LYS} + \text{H}$
146 $\text{ILE}_{\text{ext}} + \text{H}_{\text{ext}} \rightleftharpoons \text{ILE} + \text{H}$
147 $\text{MET}_{\text{ext}} + \text{H}_{\text{ext}} \rightleftharpoons \text{MET} + \text{H}$
148 $\text{SER}_{\text{ext}} + \text{H}_{\text{ext}} \rightleftharpoons \text{SER} + \text{H}$
149 $\text{CYS}_{\text{ext}} + \text{H}_{\text{ext}} \rightleftharpoons \text{CYS} + \text{H}$
150 $\text{GLY}_{\text{ext}} + \text{H}_{\text{ext}} \rightleftharpoons \text{GLY} + \text{H}$
151 $\text{VAL}_{\text{ext}} + \text{H}_{\text{ext}} \rightleftharpoons \text{VAL} + \text{H}$
152 $\text{LEU}_{\text{ext}} + \text{H}_{\text{ext}} \rightleftharpoons \text{LEU} + \text{H}$
153 $\text{ALA}_{\text{ext}} + \text{H}_{\text{ext}} \rightleftharpoons \text{ALA} + \text{H}$
154 $\text{HIS}_{\text{ext}} + \text{H}_{\text{ext}} \rightleftharpoons \text{HIS} + \text{H}$
155 $\text{PHE}_{\text{ext}} + \text{H}_{\text{ext}} \rightleftharpoons \text{PHE} + \text{H}$
156 $\text{TYR}_{\text{ext}} + \text{H}_{\text{ext}} \rightleftharpoons \text{TYR} + \text{H}$
157 $\text{TRP}_{\text{ext}} + \text{H}_{\text{ext}} \rightleftharpoons \text{TRP} + \text{H}$
158 $\text{LAC}_{\text{ext}} + \text{H}_{\text{ext}} \rightleftharpoons \text{LAC} + \text{H}$
159 $\text{ETH} \rightarrow \text{ETH}_{\text{ext}}$
160 $\text{ACE} + \text{H} \rightleftharpoons \text{ACE}_{\text{ext}} + \text{H}_{\text{ext}}$
161 $\text{PROT} \rightarrow \text{PROT}_{\text{ext}}$

Underdetermined reactions isolated using singular value decomposition are displayed in bold. Due to slight differences in measured biomass composition, stoichiometric coefficients in assembly reactions are slightly different between the two experiments. Fluxes were calculated using the reaction set of the corresponding experiment. The reaction set of experiment 1 is given above.

B. Abbreviations

3PG	3-Phospho-D-glycerate	DHF	Dihydrofolate
5MTHF	5-Methyltetrahydrofolate	DNA	deoxyribonucleic acid
6PG	6-Phospho-D-gluconate	dTTP	Deoxy thymidine triphosphate
ACA	Acetaldehyde	dUTP	Deoxy UTP
ACA_ext	Acetaldehyde (extracellular)	E4P	Erythrose-4-phosphate
ACACP	Acetyl-ACP	ETH	Ethanol
ACCOA	Acetyl-CoA	ETH_ext	Ethanol (extracellular)
ACE	Acetate	F16P	Fructose 1,6-bisphosphate
ACE_ext	Acetate (extracellular)	F6P	Fructose-6-phosphate
ACP	Acyl-carrier protein	FAD	Flavin adenine dinucleotide oxidized
AC-P	Acetyl phosphate	FADH2	Flavin adenine dinucleotide reduced
ADP	Adenosine diphosphate	FTHF	10-Formyltetrahydrofolate
AICAR	1-(5'-Phosphoribosyl)-5-amino-4-imidazolecarboxamide	FUM	Fumarate
AKG	2-Oxoglutarate (alpha-ketoglutarate)	G1P	Glucose-1-phosphate
ALA	Alanine	G6P	Glucose-6-phosphate
ALA_ext	Alanine (extracellular)	GAP	Glyceraldehyde 3-phosphate
AMP	Adenosine monophosphate	GDP	Guanosine diphosphate
ANT	Anthrnilate	GL3P	Glycerol 3-phosphate
ARG	Arginine	GLC	Glucose
ARG_ext	Arginine (extracellular)	GLC_ext	Glucose (extracellular)
ASN	Asparagine	GLN	Glutamine
ASN_ext	Asparagine (extracellular)	GLN_ext	Glutamine (extracellular)
ASP	Aspartate	GLP	Glycerone phosphate, dihydroxyacetone-phosphate
ASP_ext	Aspartate (extracellular)	GLU	Glutamate
ASP4SA	Aspartate-4-semialdehyde	GLU_ext	Glutamate (extracellular)
ATP	Adenosine triphosphate	GLY	Glycine
BIOMASS	Biomass	GLY_ext	Glycine (extracellular)
C12:0-3OHACP	3-Hydroxydodecanoyl-ACP	GSH	Glutathione
C12:0ACP	Dodecanoyl-ACP	GSSG	Oxidized glutathione (glutathionedisulfide)
C14:0-3OHACP	3-Hydroxytetradecanoyl-ACP	GTP	Guanosine triphosphate
C14:0ACP	Tetradecanoyl-ACP	H	Proton H+
C16:0ACP	Hexadecanoyl-ACP	H_ext	H+ (extracellular)
C16:1ACP	trans-Hexadec-2-enoyl-ACP	H2O	Water
C18:0ACP	Octadecanoyl-ACP	H2O2	Hydrogen peroxide
C18:1ACP	cis-11-octadecenoate-ACP	H2S	Hydrogen sulfide
CARBP	Carbamoyl phosphate	HCYS	L-Homocysteine
CDP	Cytidine diphosphate	HD6PG	2-Dehydro-3-deoxy-6-phospho-D-gluconate
CDPDG	CDP-diacylglycerol	HIS	Histidine
CHOR	Chorismate	HIS_ext	Histidine (extracellular)
CIT	Citrate	HS_ext	Hydrosulfide anion (extracellular)
CMP	Cytidine monophosphate	HSER	Homoserine
CO2	Carbondioxide	ILE	Isoleucine
CO2_ext	Carbondioxide (extracellular)	ILE_ext	Isoleucine (extracellular)
COA	Coenzyme A	IMP	Inosine monophosphate
CTP	Cytidine triphosphate	IVA	2-Oxoisovalerate
CYS	Cysteine	LAC	Lactate
CYS_ext	Cysteine (extracellular)	LAC_ext	Lactate (extracellular)
dATP	Deoxy ATP	LEU	Leucine
dCTP	Deoxy CTP	LEU_ext	Leucine (extracellular)
dGTP	Deoxy GTP		

LIPID	Lipid	SO4_ext	Sulfate (extracellular)
LPS	Lipopolysaccharide	SUC	Succinate
LYS	Lysine	SUCCOA	Succinyl Coenzyme A
LYS_ext	Lysine (extracellular)	THF	Tetrahydrofolate
MAL	Malate	THR	Threonine
MALACP	Malonyl-ACP	THR_ext	Threonine (extracellular)
mDAP	meso-2,6-diaminopimelate		
MET	Methionine		
MET_ext	Methionine (extracellular)		
METHF	N5,N10 Methylene tetrahydrofolate	THS	Thiosulfate
MEYTHF	5,10-Methenyl tetrahydrofolate	THS_ext	Thiosulfate (extracellular)
NAD	Nicotinamide adenine dinucleotide oxidized	TRP	Tryptophan
		TRP_ext	Tryptophan (extracellular)
NADH	Nicotinamide adenine dinucleotide reduced	TYR	Tyrosine
		TYR_ext	Tyrosine (extracellular)
NADP	Nicotinamide adenine dinucleotide phosphate oxidized	UDP	Uridine diphosphate
		UDPNAG	UDP-N-acetyl-D-glucosamine
NADPH	Nicotinamide adenine dinucleotide phosphate reduced	UMP	Uridine monophosphate
		UTP	Uridine triphosphate
NH3	Ammonia	VAL	Valine
NH3_ext	Ammonia (extracellular)	VAL_ext	Valine (extracellular)
O2	Oxygen	X5P	Xylulose-5-phosphate
O2_ext	Oxygen (extracellular)		
OBUT	2-Oxobutanoate		
OTR	Oxidized thioredoxin		
OXA	Oxaloacetate		
PA	Phosphadidate		
PE	Phosphatidylethanolamine		
PEP	Phosphoenolpyruvate		
PEPTIDO	Crosslinked peptidoglycan (40%)		
PG	Phosphatidylglycerol		
PHE	Phenylalanine		
PHE_ext	Phenylalanine (extracellular)		
Pi	Orthophosphate		
Pi_ext	Orthophosphate (extracellular)		
PPi	Pyrophosphate		
PRE	Prephenate		
PRO	Proline		
PRO_ext	Proline (extracellular)		
PROT	Protein		
PROT_ext	Protein (extracellular)		
PRPP	5-Phospho-alpha-D-ribose 1-diphosphate		
PYR	Pyruvate		
R5P	Ribose 5-phosphate		
RNA	ribonucleic acid		
RTR	Reduced thioredoxin		
RU5P	Ribulose-5-phosphate		
S7P	Sedoheptulose-7-phosphate		
SER	Serine		
SER_ext	Serine (extracellular)		
SO3	Sulfite		
SO4	Sulfate		

C. Measured production rates

The measured and balanced production rates are shown in the two tables below. #: The + sign indicates if a balance was used to calculate the true measurement rate vector (r_t), r_m : measured production rate ($\text{mol.g}^{-1}.\text{h}^{-1}$) calculated using Monte Carlo simulation as described in the text, V: variance ($\text{mol.g}^{-1}.\text{h}^{-1}$) calculated using Monte Carlo simulation as described in the text. r_t : true measurement rate ($\text{mol.g}^{-1}.\text{h}^{-1}$) used to calculate the unknown fluxes and production rates. h_e : statistical test value [38], P: allowed 95% chi-square value [38].

EXPERIMENT 1						
C balance #			+	-	+	
N balance #			-	+	+	
h_e			1.456	0.117		1.598
P			3.842	3.842		5.992
Compounds	r_m	V	r_t	r_t	r_t	V
CO2_ext	2.02E-03	8.78E-08	2.28E-03	2.02E-03	2.28E-03	4.26E-08
NH3_ext	-4.50E-04	7.86E-10	-4.50E-04	-4.59E-04	-4.60E-04	7.84E-11
O2_ext	-2.20E-03	1.59E-07	-2.20E-03	-2.20E-03	-2.20E-03	1.59E-07
BIOMASS	2.95E-04	3.50E-11	2.96E-04	2.94E-04	2.95E-04	3.18E-11
GLC_ext	-7.59E-04	2.26E-09	-7.19E-04	-7.59E-04	-7.19E-04	1.18E-09
H_ext	5.16E-04	1.54E-09	5.16E-04	5.16E-04	5.16E-04	1.54E-09
GLU_ext	4.86E-07	1.03E-14	4.86E-07	4.86E-07	4.86E-07	1.03E-14
GLN_ext	1.01E-07	4.54E-16	1.01E-07	1.01E-07	1.01E-07	4.54E-16
PRO_ext	0.00E+00	0.00E+00	0.00E+00	0.00E+00	0.00E+00	0.00E+00
ASP_ext	0.00E+00	0.00E+00	0.00E+00	0.00E+00	0.00E+00	0.00E+00
ASN_ext	0.00E+00	0.00E+00	0.00E+00	0.00E+00	0.00E+00	0.00E+00
ARG_ext	2.11E-07	1.98E-15	2.11E-07	2.11E-07	2.11E-07	1.98E-15
THR_ext	1.07E-06	5.00E-14	1.07E-06	1.07E-06	1.07E-06	5.00E-14
LYS_ext	2.59E-06	2.98E-13	2.60E-06	2.58E-06	2.59E-06	2.98E-13
ILE_ext	0.00E+00	0.00E+00	0.00E+00	0.00E+00	0.00E+00	0.00E+00
MET_ext	1.18E-07	6.06E-16	1.18E-07	1.18E-07	1.18E-07	6.06E-16
SER_ext	7.71E-08	2.59E-16	7.71E-08	7.71E-08	7.71E-08	2.59E-16
CYS_ext	0.00E+00	0.00E+00	0.00E+00	0.00E+00	0.00E+00	0.00E+00
GLY_ext	1.90E-07	1.58E-15	1.90E-07	1.90E-07	1.90E-07	1.58E-15
VAL_ext	8.92E-08	3.55E-16	8.92E-08	8.92E-08	8.92E-08	3.55E-16
LEU_ext	1.12E-07	5.64E-16	1.12E-07	1.12E-07	1.12E-07	5.64E-16
ALA_ext	1.90E-07	1.57E-15	1.90E-07	1.90E-07	1.90E-07	1.57E-15
HIS_ext	0.00E+00	0.00E+00	0.00E+00	0.00E+00	0.00E+00	0.00E+00
PHE_ext	5.30E-06	1.23E-12	5.33E-06	5.29E-06	5.32E-06	1.23E-12
TYR_ext	9.37E-07	3.92E-14	9.38E-07	9.37E-07	9.38E-07	3.92E-14
TRP_ext	0.00E+00	0.00E+00	0.00E+00	0.00E+00	0.00E+00	0.00E+00
LAC_ext	4.81E-06	1.01E-12	4.82E-06	4.81E-06	4.82E-06	1.01E-12
ETH_ext	3.84E-05	2.02E-11	3.85E-05	3.84E-05	3.85E-05	2.02E-11
ACE_ext	4.81E-06	1.01E-12	4.82E-06	4.81E-06	4.82E-06	1.01E-12
PROT_ext	1.18E-05	6.25E-12	1.19E-05	1.17E-05	1.18E-05	6.17E-12

EXPERIMENT 2

C balance #			+	-	+	
N balance #			-	+	+	
h _e			1.038	0.324	1.391	
P			3.842	3.842	5.992	
Compounds	r _m	V	r _t	r _t	r _t	V
CO2_ext	2.13E-03	1.02E-07	2.37E-03	2.13E-03	2.37E-03	4.67E-08
NH3_ext	-4.56E-04	1.46E-09	-4.56E-04	-4.77E-04	-4.78E-04	1.13E-10
O2_ext	-2.45E-03	1.79E-07	-2.45E-03	-2.45E-03	-2.45E-03	1.79E-07
BIOMASS	2.94E-04	3.59E-11	2.95E-04	2.93E-04	2.94E-04	3.39E-11
GLC_ext	-7.79E-04	2.34E-09	-7.46E-04	-7.79E-04	-7.46E-04	1.29E-09
H_ext	5.35E-04	1.81E-09	5.35E-04	5.35E-04	5.35E-04	1.81E-09
GLU_ext	5.66E-07	5.58E-14	5.67E-07	5.65E-07	5.66E-07	5.58E-14
GLN_ext	2.34E-07	4.15E-14	2.34E-07	2.33E-07	2.33E-07	4.15E-14
PRO_ext	0.00E+00	0.00E+00	0.00E+00	0.00E+00	0.00E+00	0.00E+00
ASP_ext	1.54E-06	1.04E-13	1.54E-06	1.54E-06	1.54E-06	1.04E-13
ASN_ext	0.00E+00	0.00E+00	0.00E+00	0.00E+00	0.00E+00	0.00E+00
ARG_ext	3.96E-07	6.42E-14	3.97E-07	3.92E-07	3.93E-07	6.42E-14
THR_ext	1.11E-06	5.27E-14	1.11E-06	1.11E-06	1.11E-06	5.27E-14
LYS_ext	0.00E+00	0.00E+00	0.00E+00	0.00E+00	0.00E+00	0.00E+00
ILE_ext	0.00E+00	0.00E+00	0.00E+00	0.00E+00	0.00E+00	0.00E+00
MET_ext	0.00E+00	0.00E+00	0.00E+00	0.00E+00	0.00E+00	0.00E+00
SER_ext	0.00E+00	0.00E+00	0.00E+00	0.00E+00	0.00E+00	0.00E+00
CYS_ext	0.00E+00	0.00E+00	0.00E+00	0.00E+00	0.00E+00	0.00E+00
GLY_ext	0.00E+00	0.00E+00	0.00E+00	0.00E+00	0.00E+00	0.00E+00
VAL_ext	0.00E+00	0.00E+00	0.00E+00	0.00E+00	0.00E+00	0.00E+00
LEU_ext	2.61E-07	5.16E-14	2.62E-07	2.60E-07	2.61E-07	5.16E-14
ALA_ext	3.94E-07	6.28E-14	3.94E-07	3.93E-07	3.94E-07	6.28E-14
HIS_ext	1.63E-06	1.34E-12	1.65E-06	1.57E-06	1.59E-06	1.33E-12
PHE_ext	5.42E-06	1.30E-12	5.45E-06	5.40E-06	5.43E-06	1.30E-12
TYR_ext	0.00E+00	0.00E+00	0.00E+00	0.00E+00	0.00E+00	0.00E+00
TRP_ext	0.00E+00	0.00E+00	0.00E+00	0.00E+00	0.00E+00	0.00E+00
LAC_ext	5.12E-06	1.14E-12	5.13E-06	5.12E-06	5.13E-06	1.14E-12
ETH_ext	5.62E-05	4.40E-11	5.64E-05	5.62E-05	5.64E-05	4.40E-11
ACE_ext	5.12E-06	1.14E-12	5.13E-06	5.12E-06	5.13E-06	1.14E-12
PROT_ext	1.87E-05	1.59E-11	1.89E-05	1.84E-05	1.86E-05	1.56E-11

D. Fluxdistributions

The calculated fluxes (r_c) and calculated production rates ($\text{mol.g}^{-1}.\text{h}^{-1}$) using the mass balances over intracellular compounds and balanced measured rates (r_t) using both the carbon and nitrogen balance are shown in the table below. The calculated values of the underdetermined reactions (see Appendix 2.2 B), isolated using singular value decomposition provide the minimum norm solution. SD: Standard deviation of calculated fluxes and rates ($\text{mol.g}^{-1}.\text{h}^{-1}$).

RNo. / Flux	EXPERIMENT 1		EXPERIMENT 2	
	r_c	SD	r_c	SD
1	6.25E-04	7.89E-05	6.77E-04	8.36E-05
2	6.25E-04	7.89E-05	6.77E-04	8.36E-05
3	5.62E-04	7.89E-05	6.14E-04	8.36E-05
4	5.43E-04	7.89E-05	5.95E-04	8.36E-05
5	5.62E-04	7.89E-05	6.14E-04	8.36E-05
6	1.92E-04	4.98E-05	2.19E-04	5.29E-05
7	1.87E-04	7.08E-05	2.18E-04	7.50E-05
8	7.19E-04	3.44E-05	7.46E-04	3.59E-05
9	-1.67E-04	1.33E-04	-1.40E-04	1.40E-04
10	-4.55E-06	4.46E-05	2.18E-05	4.73E-05
11	-1.22E-05	4.46E-05	1.34E-05	4.73E-05
12	6.75E-04	5.66E-05	6.73E-04	5.97E-05
13	3.87E-04	1.64E-04	3.29E-04	1.74E-04
14	3.45E-04	2.51E-05	3.69E-04	2.66E-05
15	1.53E-04	2.43E-05	1.52E-04	2.56E-05
16	1.63E-04	1.59E-04	2.46E-04	1.69E-04
17	8.85E-04	1.56E-04	8.85E-04	1.64E-04
18	3.12E-04	2.54E-04	2.33E-04	2.68E-04
19	1.25E-04	8.46E-05	1.01E-04	8.95E-05
20	1.85E-04	1.69E-04	1.31E-04	1.79E-04
21	1.06E-04	8.46E-05	7.90E-05	8.95E-05
22	-7.94E-05	8.46E-05	-5.21E-05	8.95E-05
23	1.04E-04	8.46E-05	7.80E-05	8.95E-05
24	5.73E-04	1.18E-04	6.51E-04	1.25E-04
25	5.73E-04	1.18E-04	6.51E-04	1.25E-04
26	8.29E-04	7.89E-05	9.00E-04	8.36E-05
27	-4.82E-06	1.00E-06	-5.13E-06	1.07E-06
28	4.20E-06	2.45E-05	4.07E-07	2.59E-05
29	2.56E-04	4.65E-05	2.95E-04	4.95E-05
30	2.56E-04	4.65E-05	2.95E-04	4.95E-05
31	2.23E-04	4.64E-05	2.43E-04	4.93E-05
32	7.00E-04	5.09E-04	9.36E-04	5.39E-04
33	1.75E-04	1.09E-04	2.36E-04	1.15E-04
34	2.03E-05	3.92E-07	2.33E-05	5.43E-07
35	1.01E-05	2.01E-07	1.08E-05	2.44E-07
36	1.87E-04	3.97E-04	3.62E-04	4.21E-04
37	3.99E-04	3.78E-05	4.29E-04	3.98E-05

RNo. / Flux	EXPERIMENT 1		EXPERIMENT 2	
	r_c	SD	r_c	SD
38	4.71E-04	4.13E-04	6.69E-04	4.38E-04
39	1.15E-05	2.30E-07	1.14E-05	2.57E-07
40	1.49E-05	2.96E-07	1.73E-05	4.57E-07
41	5.52E-05	1.18E-06	5.53E-05	1.24E-06
42	3.60E-05	7.30E-07	3.55E-05	8.10E-07
43	2.84E-05	5.90E-07	2.88E-05	6.66E-07
44	1.92E-05	6.33E-07	1.97E-05	4.39E-07
45	1.81E-05	6.24E-07	1.87E-05	4.22E-07
46	1.38E-05	2.76E-07	1.37E-05	3.10E-07
47	1.38E-05	2.76E-07	1.37E-05	3.10E-07
48	7.60E-06	1.51E-07	6.71E-06	1.52E-07
49	7.60E-06	1.51E-07	6.71E-06	1.52E-07
50	2.59E-06	5.17E-08	2.63E-06	5.93E-08
51	-5.17E-04	3.93E-05	-5.35E-04	4.27E-05
52	4.68E-04	2.28E-04	4.05E-04	2.41E-04
53	4.18E-04	4.51E-04	2.75E-04	4.77E-04
54	2.36E-04	1.11E-04	2.90E-04	1.18E-04
55	2.88E-04	1.11E-04	3.44E-04	1.18E-04
56	2.82E-05	5.42E-07	2.94E-05	8.18E-07
57	4.28E-05	8.51E-07	4.23E-05	9.75E-07
58	6.67E-05	1.32E-06	6.60E-05	1.48E-06
59	2.20E-05	4.38E-07	2.19E-05	5.37E-07
60	4.59E-05	9.07E-07	4.56E-05	1.03E-06
61	1.96E-05	3.72E-07	2.24E-05	1.22E-06
62	5.18E-06	1.03E-07	6.84E-06	1.16E-06
63	2.47E-05	1.18E-06	2.59E-05	1.22E-06
64	2.12E-05	1.16E-06	2.24E-05	1.20E-06
65	1.48E-05	1.12E-06	1.48E-05	1.16E-06
66	6.40E-06	2.26E-07	7.59E-06	1.71E-07
67	3.45E-06	6.90E-08	3.50E-06	7.90E-08
68	3.45E-06	6.90E-08	3.50E-06	7.90E-08
69	7.74E-07	1.48E-08	5.15E-07	1.02E-08
70	4.22E-04	3.81E-04	6.21E-04	4.04E-04
71	-2.26E-04	5.17E-05	-2.18E-04	5.51E-05
72	1.12E-03	3.33E-04	1.29E-03	3.53E-04
73	3.75E-04	7.15E-05	4.16E-04	7.59E-05
74	6.93E-05	5.04E-04	2.51E-04	5.34E-04
75	5.49E-06	1.05E-07	6.04E-06	1.20E-07
76	1.07E-05	2.03E-07	1.29E-05	1.17E-06
77	7.83E-06	1.51E-07	9.76E-06	1.16E-06
78	-8.56E-05	2.04E-04	6.31E-06	2.17E-04
79	1.53E-07	2.93E-09	3.13E-07	6.20E-09
80	2.84E-06	5.43E-08	3.12E-06	6.19E-08
81	1.05E-05	2.00E-07	1.25E-05	1.17E-06
82	1.63E-07	3.11E-09	3.32E-07	6.59E-09

RNo. / Flux	EXPERIMENT 1		EXPERIMENT 2	
	r_c	SD	r_c	SD
83	5.45E-06	1.04E-07	6.00E-06	1.19E-07
84	6.22E-06	1.19E-07	6.52E-06	1.29E-07
85	-1.11E-04	1.09E-04	-1.67E-04	1.15E-04
86	1.11E-04	1.09E-04	1.67E-04	1.15E-04
87	1.19E-04	1.09E-04	1.75E-04	1.15E-04
88	1.14E-04	1.09E-04	1.70E-04	1.15E-04
89	1.04E-04	1.09E-04	1.60E-04	1.15E-04
90	1.11E-04	1.09E-04	1.68E-04	1.15E-04
91	1.53E-07	2.93E-09	3.13E-07	6.20E-09
92	7.38E-06	1.41E-07	7.43E-06	1.47E-07
93	1.18E-04	2.25E-06	1.18E-04	2.34E-06
94	1.77E-05	3.39E-07	1.75E-05	3.46E-07
95	1.55E-06	2.96E-08	1.03E-06	2.04E-08
96	1.67E-06	3.20E-08	1.08E-06	2.14E-08
97	1.55E-06	2.96E-08	1.03E-06	2.04E-08
98	5.08E-07	9.72E-09	6.39E-07	1.27E-08
99	6.41E-06	1.22E-07	7.05E-06	1.40E-07
100	1.87E-07	3.58E-09	1.77E-07	3.51E-09
101	4.20E-06	8.03E-08	4.71E-06	9.33E-08
102	1.67E-06	3.19E-08	1.75E-06	3.46E-08
103	7.70E-06	1.47E-07	8.45E-06	1.67E-07
104	6.55E-06	1.25E-07	7.19E-06	1.42E-07
105	5.83E-06	1.12E-07	6.40E-06	1.27E-07
106	4.69E-06	8.96E-08	5.14E-06	1.02E-07
107	1.15E-06	2.19E-08	1.26E-06	2.50E-08
108	4.44E-06	8.48E-08	3.68E-06	7.29E-08
109	7.55E-07	1.44E-08	7.62E-07	1.51E-08
110	7.74E-07	1.48E-08	5.15E-07	1.02E-08
111	4.22E-04	3.81E-04	6.21E-04	4.04E-04
112	4.22E-04	3.81E-04	6.21E-04	4.04E-04
113	0.00E+00	0.00E+00	0.00E+00	0.00E+00
114	-5.17E-04	3.93E-05	-5.34E-04	4.27E-05
115	0.00E+00	0.00E+00	0.00E+00	0.00E+00
116	-1.62E-05	3.06E-07	-1.89E-05	1.19E-06
117	-1.62E-05	3.06E-07	-1.89E-05	1.19E-06
118	1.53E-07	2.93E-09	3.13E-07	6.20E-09
119	7.60E-06	1.51E-07	6.71E-06	1.52E-07
120	-4.27E-06	9.79E-08	-3.47E-06	5.92E-07
121	3.85E-05	4.49E-06	5.64E-05	6.63E-06
122	3.93E-05	4.49E-06	5.69E-05	6.63E-06
123	2.38E-04	2.07E-04	3.37E-04	2.19E-04
124	6.31E-07	1.21E-08	1.29E-06	2.56E-08
125	1.03E-05	1.97E-07	1.07E-05	2.13E-07
126	2.88E-04	5.75E-06	2.92E-04	6.59E-06
127	6.55E-06	1.25E-07	7.19E-06	1.42E-07

RNo. / Flux	EXPERIMENT 1		EXPERIMENT 2	
	r_c	SD	r_c	SD
128	2.95E-04	5.64E-06	2.94E-04	5.82E-06
129	7.19E-04	3.44E-05	7.46E-04	3.59E-05
130	2.28E-03	2.06E-04	2.37E-03	2.16E-04
131	8.26E-04	4.35E-04	1.01E-03	4.61E-04
132	-4.60E-04	8.86E-06	-4.78E-04	1.06E-05
133	2.20E-03	3.99E-04	2.45E-03	4.23E-04
134	1.98E-05	3.79E-07	2.08E-05	4.12E-07
135	4.68E-04	2.28E-04	4.05E-04	2.41E-04
136	-5.17E-04	3.93E-05	-5.35E-04	4.27E-05
137	4.08E-04	4.51E-04	2.66E-04	4.77E-04
138	-4.86E-07	1.01E-07	-5.66E-07	2.36E-07
139	-1.01E-07	2.13E-08	-2.33E-07	2.04E-07
140	0.00E+00	0.00E+00	0.00E+00	0.00E+00
141	0.00E+00	0.00E+00	-1.54E-06	3.22E-07
142	0.00E+00	0.00E+00	0.00E+00	0.00E+00
143	-2.11E-07	4.45E-08	-3.93E-07	2.53E-07
144	-1.07E-06	2.24E-07	-1.11E-06	2.30E-07
145	-2.59E-06	5.46E-07	0.00E+00	0.00E+00
146	0.00E+00	0.00E+00	0.00E+00	0.00E+00
147	-1.18E-07	2.46E-08	0.00E+00	0.00E+00
148	-7.71E-08	1.61E-08	0.00E+00	0.00E+00
149	0.00E+00	0.00E+00	0.00E+00	0.00E+00
150	-1.90E-07	3.97E-08	0.00E+00	0.00E+00
151	-8.92E-08	1.88E-08	0.00E+00	0.00E+00
152	-1.12E-07	2.37E-08	-2.61E-07	2.27E-07
153	-1.90E-07	3.96E-08	-3.94E-07	2.51E-07
154	0.00E+00	0.00E+00	-1.59E-06	1.15E-06
155	-5.32E-06	1.11E-06	-5.43E-06	1.14E-06
156	-9.38E-07	1.98E-07	0.00E+00	0.00E+00
157	0.00E+00	0.00E+00	0.00E+00	0.00E+00
158	-4.82E-06	1.00E-06	-5.13E-06	1.07E-06
159	3.85E-05	4.49E-06	5.64E-05	6.63E-06
160	4.82E-06	1.00E-06	5.13E-06	1.07E-06
161	1.18E-05	2.48E-06	1.86E-05	3.95E-06
H2O	2.86E-03	2.28E-04	3.03E-03	2.42E-04
Pi_ext	-1.98E-05	3.79E-07	-2.08E-05	4.12E-07
THS_ext	-4.68E-04	2.28E-04	-4.05E-04	2.41E-04
SO4_ext	5.17E-04	3.93E-05	5.35E-04	4.27E-05
HS_ext	4.08E-04	4.51E-04	2.66E-04	4.77E-04

Chapter 3

Modeling *Neisseria meningitidis* B metabolism at different specific growth rates

This chapter has been published as: Baart GJE, Willemsen M, Khatami E, de Haan A, Zomer B, Beuvery EC, Tramper J, Martens DE. 2008. Modeling *Neisseria meningitidis* B metabolism at different specific growth rates. *Biotechnology and Bioengineering*. Accepted.

ABSTRACT

Neisseria meningitidis is a human pathogen that can infect diverse sites within the human host. The major diseases caused by *N. meningitidis* are responsible for death and disability, especially in young infants. At the Netherlands Vaccine Institute (NVI) a vaccine against serogroup B organisms is currently being developed. This study describes the influence of the growth rate of *N. meningitidis* on its macro-molecular composition and its metabolic activity and was determined in chemostat cultures. In the applied range of growth rates, no significant changes in RNA content and protein content with growth rate were observed in *N. meningitidis*. The DNA content in *N. meningitidis* was somewhat higher at the highest applied growth rate. The phospholipid and lipopolysaccharide content in *N. meningitidis* changed with growth rate but no specific trends were observed. The cellular fatty acid composition and the amino acid composition did not change significantly with growth rate. Additionally, it was found that the PorA content in outer membrane vesicles was significantly lower at the highest growth rate. The metabolic fluxes at various growth rates were calculated using Flux Balance Analysis. Errors in fluxes were calculated using Monte Carlo Simulation and the reliability of the calculated flux distribution could be indicated, which has not been reported for this type of analysis. The yield of biomass on substrate ($Y_{x/s}$) and the maintenance coefficient (m_s) were determined as $0.44 (\pm 0.04) \text{ g.g}^{-1}$ and $0.04 (\pm 0.02) \text{ g.g}^{-1}.\text{h}^{-1}$, respectively. The growth associated energy requirement ($Y_{x/ATP}$) and the non-growth associated ATP requirement for maintenance (m_{ATP}) were estimated as $0.13 (\pm 0.04) \text{ mol.mol}^{-1}$ and $0.43 (\pm 0.14) \text{ mol.mol}^{-1}.\text{h}^{-1}$, respectively. It was found that the split ratio between the Entner-Doudoroff and the pentose phosphate pathway, the sole glucose utilizing pathways in *N. meningitidis*, had a minor effect on ATP formation rate but a major effect on the fluxes going through for instance the citric-acid cycle. For this reason, we presented flux ranges for underdetermined parts of metabolic network rather than presenting single flux values, which is more commonly done in literature.

INTRODUCTION

The species *Neisseria meningitidis* is only found in humans and colonizes mucosal surfaces of the nasopharynx (nose and throat) as a harmless commensal organism and, as such, is carried by five to ten percent of the adult population [1, 2]. Some strains are able to cross the mucosa into the bloodstream from where they can cause the diseases meningitis or septicaemia. These diseases are responsible for death and disability especially in young infants. Several genetic loci have been associated with disease [3, 4], but for most strains the mechanism of virulence is not well defined. There are different pathogenic *N. meningitidis* isolates of which five serogroups (A, B, C, Y, and W135) are responsible for most of the disease. Serogroup B and C organisms cause the majority of infections in Europe and America, whereas strains of group A and C dominate in Africa and Asia[5]. Effective polysaccharide and conjugate vaccines have been developed against serogroups A, C, Y and W135 strains. However, effective global prevention of meningococcal disease will not be achievable without the development of a vaccine against serogroup B meningitis, which causes about 50% of meningococcal disease cases worldwide [6]. Since the polysaccharide of the serogroup B meningococcus is poorly immunogenic [7], alternative vaccine approaches are needed for this bacterium. Current vaccine development against serogroup B organisms has mainly focussed on subcapsular protein antigens that are contained in outer membrane vesicles (OMVs) [6]. The outer membrane protein PorA has been identified as a major inducer of, and target for serum bactericidal antibodies and is expressed by almost all meningococci, which pinpoints PorA as a promising vaccine candidate [8]. However, PorA appears heterogeneous, requiring the development of a multivalent vaccine in which various PorA subtypes are present in order to induce sufficient protection. At the Netherlands Vaccine Institute (NVI) a vaccine against serogroup B organisms, including different PorA subtypes contained in OMVs is currently being developed. The process development focuses on cultivation of the organism, extraction of OMVs and subsequent purification of the porA containing OMVs [9].

The specific growth rate of bacteria is an important parameter in biotechnological processes, since it determines the macromolecular composition of the bacterial cell and its metabolic activity [10-13]. Knowledge about metabolism is essential for the development of an efficient cultivation process. Notably, product quality and quantity are primarily determined in the cultivation process.

Metabolism can be studied using metabolic network models, which contain all relevant metabolic reactions. The best approach would be to model the dynamic behaviour of the individual metabolic reactions using rate equations [14, 15]. However, this requires many kinetic parameters that are difficult to measure. As an alternative cell metabolism can be studied in steady state using the reaction stoichiometry in combination with mass balancing of the fluxes [11, 16-20]. An advantage of steady state stoichiometric modeling is that it is based on well-known stoichiometric coefficients and that it does not require determination of parameters like kinetic constants. However, stoichiometric metabolic models are usually underdetermined. Therefore additional experimental data or assumptions are required to calculate all metabolic fluxes in the network. The metabolic capabilities of the constructed network may be calculated using constraint-based computer simulation methods like metabolic flux analysis (MFA), flux balance analysis (FBA), elementary flux modes [21] or extreme pathways [22].

Genome-scale metabolic network models of micro-organisms such as *Haemophilus influenzae* [23], *Escherichia coli* [24-26], *Helicobacter pylori* [27], *Saccharomyces cerevisiae* [28, 29], *Lactococcus lactis* [11], *Lactobacillus plantarum* [10, 30], *Staphylococcus aureus* [31, 32], *Streptomyces coelicolor* [33], *Methanosarcina barkeri* [34] and recently *Mannheimia succiniciproducens* [35], *Mycobacterium tuberculosis* [36] and *Neisseria meningitidis* [37], have proven to be very useful to study metabolism in a systemic manner.

MFA has been used to analyze the metabolism of many organisms and is based on

metabolite balancing. MFA combined with ^{13}C -labelled metabolic flux analysis to analyze the labeling distribution of intracellular metabolites provides additional constraints and can yield a determined model system for which a unique solution can be calculated. Solid estimates of the intracellular flux distribution have been obtained using this method [38]. FBA is also based on metabolite balancing but lacks information related to the label distribution of intracellular metabolites and instead uses linear optimization (i.e. linear programming, LP) to find a single, unique, optimal value for a particular objective function. As a result the original solution space of the under-determined parts of the model system is reduced to a single solution. Notably, this single solution is not necessarily unique and there can be more than one flux distribution that reaches the optimal value of the objective function. Some examples of objective functions described in literature are maximize biomass formation, maximize ATP production, minimize glucose uptake and minimize the production of NADH, NADPH [11, 25, 39]. Both MFA and FBA limit the range of individual flux values based on available biochemical and thermodynamic literature of the enzymatic reactions (e.g. directional constraints). Successful prediction of growth rate and metabolite secretion rate has been done using the FBA approach combined with maximization of biomass formation as an objective function [40-43]. Nevertheless, the calculated intracellular flux distribution in these cases may not represent the true values. ^{13}C -constrained metabolic flux analysis allows a more accurate determination of intracellular fluxes, but is in general restricted to smaller metabolic networks. This restriction to smaller metabolic networks is determined by the amount of measurable (intracellular) metabolites and the requirement of a more complicated mathematical formulation. Recently, a strategy for employing partial ^{13}C -labeling information as additional constraint in FBA was presented by Choi and co-workers [44] and allowed a more accurate estimation of intracellular metabolic fluxes, as demonstrated in both the small-scale and the genome-scale *Escherichia coli* metabolic network. In addition, an extensive comparison of FBA-based *in silico* flux predictions, using different objective/constraint combinations, with *in vivo* fluxes from ^{13}C -experiments demon-

strated that prediction of flux distributions is, within limits, possible. The essential element in this case is to identify the most relevant objective for a specific condition, since no single objective predicted the experimental data for wild-type *E. coli* under all conditions [39].

The aim of this study was to further characterize the metabolism of *N. meningitidis* by determining the influence of the specific growth rate on its macromolecular composition and the distribution of metabolic fluxes.

In the present study, the metabolic fluxes at various growth rates were calculated using FBA with maximization of ATP yield as objective function. Errors in fluxes were calculated using Monte Carlo simulation (MCS). The advantage of this approach is that the reliability of the calculated flux distribution can be indicated for the determined parts of the metabolic network. To our knowledge this has not been done before. This combined procedure led to the calculation of the energy parameters of *N. meningitidis* grown aerobically on minimal medium. Furthermore, analysis of the ratio between the Entner-Doudoroff pathway and the pentose phosphate pathway provided more insight in the influence of this ratio on the estimation of the energy parameters.

MATERIALS AND METHODS

Strain, media & chemostat cultures

All experiments were conducted using *N. meningitidis* strain HB-1, a non-encapsulated, non-piliated variant of the group B isolate H44/76 [45]. Stock cultures of strain HB-1 were stored at $-135\text{ }^{\circ}\text{C}$ and when required a 500 mL shake flask, containing 150 mL medium was inoculated with 10 mL stock culture that contained 0.5 g/L biomass. After approximately 8 hours of incubation at $35\text{ }^{\circ}\text{C}$ with shaking at 200 rpm in an aerobic humid atmosphere, the culture was used to inoculate the bioreactor. Bacteria were grown on minimal chemically defined medium consisting of glucose, NH_4Cl , NaCl , MgSO_4 , K_2HPO_4 , KH_2PO_4 , FeCl_3 , $\text{Na}_2\text{S}_2\text{O}_3$ and trace elements [37] in a 3-L autoclavable ADI bioreactor (Applikon, Schiedam, The Netherlands), operated in chemostat mode, with a working volume of 1.4 L. The maximum growth rate on the minimal medium is $0.17 \pm 0.01\text{ /h}$ and was calculated using OD_{590} measurements from the batch phases of the chemostat cultures and three additional batch cultivations. Temperature, pH, dissolved oxygen (DO) concentration and stirrer speed were controlled at $37\text{ }^{\circ}\text{C}$, 7.0, 30% and 500-600 rpm respectively.

The sensors were connected to ADI control systems (Applikon, Schiedam, the Netherlands), which in turn were connected to a UNIX computer with BCSV (Compec, Belgium). BCSV-software carried out all the control-loops (dissolved oxygen, temperature, pH, stirrer rate and gas flow rate) and logged all data. The total gas flow rate was kept constant at $1.0\text{ L}\cdot\text{min}^{-1}$. The oxygen concentration was controlled by changing the oxygen fraction in the gas flow using headspace aeration only. The growth rate was controlled at 0.041, 0.082 or 0.161 h^{-1} and all chemostat cultures were done in duplicate. After at least four residence times physiological steady state was assumed based on online measurements (constant DO signal, O_2 and CO_2 -concentration in the off gas) and offline measurements (constant optical density, zero glucose concentration). In steady state, a small sample was taken for extraction of

OMVs, and a large 1.0 L sample was taken, which was divided into portions and processed as described before [37].

Extraction of OMVs

The OMV extractions were carried out in duplicate starting from a single culture sample that was divided into portions. OMVs were extracted from the live bacteria with 0.5% sodium deoxycholate and 10 mM EDTA in 0.1 M Tris-HCl at pH 8.6 [46] during 30 minutes at room temperature. Bacterial debris was removed by centrifugation (1h, 20000g, 4 °C). OMVs were separated from the extraction buffer using ultra-centrifugation (2 h, 125000 g, 4 °C). To remove as much extraction buffer as possible, the UC-tubes were turned upside-down and placed on a tissue. Next, a buffer containing 3% sucrose, 0.002% NaN₃ in 0.01 mM Tris (pH 7.4) was added and the solution was homogenized by pipetting up and down. It is worth noting that NaN₃ was added to the buffer to prevent contamination. Prior to further analysis, the OMV samples were stored at 4 °C for one month. Under these storage conditions OMVs are stable for at least one year [47]. All chemicals were from Merck (Merck, Darmstadt, Germany).

Analytical Procedures

Dry biomass concentration was determined in fourfold for each steady state sample by centrifugation (8000 g) of 50-200 mL of culture broth in preweighed tubes followed by drying (24 h, 80 °C). Before weighing, the tubes were cooled in a dessiccator for at least 1 h and dry cell weight was corrected for salts present in the medium. The O₂ and CO₂ concentrations in the exhaust gas from the chemostat cultures were measured with a mass spectrometer (Prima White Box 600, Thermo Electron, Winsford, United Kingdom). The volumetric oxygen transfer coefficient, k_{La} , in the bioreactors was determined accurately at 37 °C using a steady state set-up similar to the set-up described by Dorresteyn and co-workers [48]. Glucose, lactate, acetate, ethanol and other possible metabolites present in the culture supernatant [49] were determined by ¹H-NMR and ammonium was determined with an enzymatic kit (Boehringer, Mannheim, Germany)

as described before [37]. The molecular and macromolecular composition of biomass was determined in detail as described before [37]. Briefly, the amino acid composition of biomass protein was determined after hydrolysis (6 M HCl, 24 h, 110 °C) and subsequent amino acid analysis using an HPLC method as described before [50]. Free amino acids in the culture supernatant were determined using the same method. The amount of total fatty acids and the fatty acid composition was analyzed using a modified gaschromatography method [51]. First, fatty acids were liberated from cellular lipid using a saponification reagent (1.2 ml of 3.75 M NaOH in 50/50 v/v methanol/water) and incubation at 100 °C for 30 min. Second, the liberated fatty acids were methylated using a reagent (3.25 M HCl in methanol). After incubation (80 °C for 20 min.) samples were cooled down to room temperature and the fatty acid methyl esters were extracted by adding 1.5 ml hexane reagent (50/50 v/v hexane/methyl tertiary butyl ether) during mixing (15 min.). The aqueous layer was removed and the organic phase was washed by adding 3.0 ml of washing agent (0.3 M NaOH). Finally, the organic phase was finally transferred to a GC-vial and analyzed using a 6890 Agilent gas-chromatograph [52]. Fatty acid methylesters were identified by their retention times in comparison to those of a commercial standard (Microbial, Newark, DE, USA). Quantification of hydroxy-fatty acids has been done using C12:0-2OH as an internal standard whereas non-hydroxy-fatty acids have been quantified using C15:0 as an internal standard. The LPS content in biomass was quantified on the basis of 3-hydroxydodecanoic acid (C12:0-3OH) using the above described GC method. The measured molar ratio of the lipid A fatty acids: dodecanoic acid (C12:0), 3-hydroxydodecanoic acid (C12:0-3OH) and 3-hydroxytetradecanoic acid (C14:0-3OH) ranged from 2:2:1 to 3:3:1. However, structural analysis by mass spectroscopy of lipid A (results not shown) revealed that monophosphorylated hexa-acylated lipid A was present in *N. meningitidis* grown at all dilution rates which means that the molar ratio of the lipid A fatty acids C12:0, C12:0-3OH and C14:0-3OH was constant 1:1:1. Therefore, the measured amount of C14:0-3OH was neglected in all experiments and instead the C14:0-3OH quantity was based on the corresponding measured

C12:0-3OH quantity. Therefore, the LPS quantity possesses some uncertainty and may need to be readjusted. We found no particular reason for the apparently too low measured C14:0-3OH quantity using the GC method. As mentioned above, the structure of the lipid A part of LPS was measured. This was done as follows: LPS was isolated from biomass by hot phenol extraction [53] and the lipid A fraction was obtained after acid hydrolysis in 2% acetic acid followed by chloroform/methanol extraction [54]. Lipid A was analyzed by multiple-step nano-electrospray ionization mass spectrometry (nano-ESI) using an ion trap mass spectrometer (Finnigan Mat LCQ, Bremen, Germany) set in negative ion mode. The used overall phospholipid composition was based on the information provided by Rahman and co-workers [55], including 11% phosphatidate, 71% phosphatidylethanol-amine and 18% phosphatidylglycerol. The biomass RNA content was determined as described before [56] and the biomass DNA content was determined colorimetrically as described before [57]. The DNA composition was derived from the complete nucleotide composition in the genome sequence. For RNA the Uridine content was based on the Thymine content in the genome sequence [32]. Biomass biosynthesis was set as a linear combination of the macromolecules: protein, DNA, RNA, lipid, peptidoglycan and LPS which were considered to account for the overall biomass composition.

The protein content of the OMVs was measured according to Peterson [58]. Briefly, samples were diluted to a total volume of 500 mL with MilliQ water and 50 mL of 0.15% sodiumdesoxycholate (DOC) was added. After mixing, the samples were allowed to stand for 10 min at room temperature. Next, 50 ml of 72% TCA, was added and after mixing, the samples were centrifuged (15 min, 3000 g). After centrifugation, the supernatant was discarded by decanting immediately and turning the tube upside down over absorbent paper in a rack. The protein pellets were resuspended in 500 ml MilliQ and 500 ml reagent A was added. Reagent A was prepared by mixing equal amounts of copper carbonate tartrate solution (0.1% copper sulphate, 0.2% sodium potassium tartrate and 10% sodium carbonate in MilliQ water), NaOH solution

(0.8 M), 10% sodiumdodecylsulfate (SDS) and MilliQ water. After mixing, the samples were incubated (10 min, room temperature) and 250 μ L Reagent B (16.6% Folin Ciocaltue's phenol reagent in MilliQ water) was added and the samples were mixed. After incubation (30 min, room temperature) the absorbance was read at 750 nm and protein concentration was calculated. Bovin serum albumin was used as a standard. The relative PorA content was measured by SDS gel electrophoresis (SDS-PAGE) under denaturing conditions [59]. Prior to electrophoresis, the samples were prepared in 0.0625 M Tris-HCl, pH 6.8, containing SDS (2%), glycerol (10%), bromophenol blue (0.001%), 2-mercaptoethanol (5%) and OMV protein (0.5-1.0 mg/ml). These samples were incubated for 5 min at 100 °C. After cooling to room temperature, 20 μ L of sample were applied per slot on the gel (Biorad, Hercules, CA, USA). Electrophoresis was carried out at room temperature using a constant current of 100 mA and 100 V. The electrophoresis was stopped when the tracking dye (Bromophenol blue) reached the bottom of the gel. One slot per gel was used for prestained low range SDS-PAGE markers (Biorad, USA). After running and staining with Coomassie brilliant blue, the gels were scanned using an Agfa Fotolook 3.5 scanner and analyzed with Phoretix 1D Quantifier software (version 5.10, Biozym, Landgraaf, The Netherlands) for determination of the relative PorA content. The relative standard deviation of this analytical method was validated to be 5%.

Modeling Aspects

Methods for solving a metabolic network or set of linear equations are discussed extensively elsewhere [20, 25, 37, 60-62]. Briefly, first the genome-scale metabolic network was simplified as described before [37]. To reduce the number of parallel pathways, the reactions Phosphoenolpyruvate synthase, Acetate-CoA ligase and L-aspartate oxidase were removed in addition to the previously described simplifications [37]. Furthermore, the formate-tetrahydrofolate ligase reaction was removed (dead-end) and the hydrogen peroxide oxidoreductase (catalase) reaction was removed based on micro array data (unpublished results). These reactions are listed as ## in the

additional datafile. The simplified metabolic network used for FBA included 158 reactions (123 intracellular reactions, 35 transport fluxes) and 131 intracellular metabolites (Appendix 3 A). Biomass biosynthesis was set as a linear combination of the macromolecules: protein, DNA, RNA, lipid, peptidoglycan and LPS, which were considered to account for the overall biomass composition. The energy requirements for biomass formation and maintenance were estimated as explained in the results and discussion section. The matrix containing the mass balances over the intracellular compounds was checked for network sensitivity problems by performing singular value decomposition. In this way the combinations of fluxes and unknown exchange rates that can not be uniquely identified (i.e. calculated from the measurements) were isolated. Next, the redundancy matrix, R , for the measured rates, r_m , was calculated [63]. It was necessary to calculate the redundancy matrix for each dataset, because the biomass composition was slightly different for each set. The specific measured rates and the corresponding variances were calculated using mass balances and Monte Carlo simulation (MCS) as described before [37]. Then it was checked using the chi-square test variable whether the residuals obtained after multiplication of the redundancy matrix and the measured rates could be explained on the basis of measurement variances. After verification that this was the case and no gross errors were present, the measured rates were balanced (i.e. adjusted until all residuals were zero). The resulting balanced true rate vector, r_t , was used for FBA. The most important constraint in steady state metabolic modeling is that the mass balance for each metabolite must be closed and no accumulation of metabolites is allowed. Mathematically:

$$A \cdot x = b \quad (3.1)$$

Where A is the stoichiometric matrix including exchange reactions, x is the flux vector that contains the unknown fluxes and the unknown exchange rates, and b is the vector that contains the known (measured) exchange rates. If the system given in equation 3.1 is partly determined and redundant and partly underdetermined, which

is the case in the present study, the solution given with the pseudo inverse yields a unique least squares solution for the determined part while the minimum norm solution [37, 64] is calculated for the underdetermined fluxes. The minimum norm solution is only one of the infinite possible solutions. To determine which elements of x are calculable and have a unique solution and, which elements of x are not calculable and have an infinite amount of solutions the nullspace can be calculated. The nullspace is defined as the set of linear independent vectors that fulfil the equation:

$$A \cdot x_n = 0 \quad (3.2)$$

In other words, the null space vectors contain combinations of reactions of which the sum is always zero. Thus, the complete solution of equation 3.1 is:

$$x = A^\# \cdot b + \text{null space}(A) \cdot \lambda \quad (3.3)$$

Where $A^\#$ is the pseudo inverse of A and λ is a vector with as many elements as there are columns in the nullspace of A . For all possible values of λ the solution remains valid. Parallel pathways in the metabolic model typically yield null space vectors. The nullspace of the simplified metabolic model contains 7 columns (Additional datafile). To reduce the solution space of the underdetermined parts to a single solution, a linear objective function can be defined and the fluxes and unknown exchange reaction rates can be calculated by linear programming (LP). The objective function maximization of ATP yield, next to the objective function maximize biomass yield, were found to result in biologically meaningful predictions in nutrient limited continuous cultures [39]:

$$Z = r_{ATP} \rightarrow \text{maximize} \quad (3.4)$$

In combination with LP, lower (α) and upper boundaries (β) for fluxes, x , can be set on the basis of available biochemical and thermodynamic literature for the enzymatic

reactions (specification of reaction irreversibility):

$$\alpha \leq x \leq \beta \tag{3.5}$$

In the present study, LP was combined with MCS using the measured rate vectors and their corresponding variances as input for optimization with maximization of ATP hydrolysis (reaction 67 of the model, equation 3.4) as an objective function. Since ATP is an intermediate metabolite that cannot accumulate, maximization of the hydrolysis reaction automatically means that in the rest of the network ATP production is maximized. The Monte Carlo approach was used in order to estimate the errors in the determined parts of the metabolic model. The common FBA approach yields a single solution and lacks error estimates. The complete MCS-LP procedure is as follows: First, for each measured rate a random value was randomly computed within its allowed standard deviation interval. Second, the redundancy relations, in this case a carbon and nitrogen balance, were checked and when closing the rates were balanced. When the mass balance did not close, the rate vector was discarded and a new random rate vector was computed (back to the first step). Third, the resulting calculated true rates were used as input for the linear optimization. For every dataset this procedure was repeated 10000 times and the resulting flux distributions were stored in a temporary matrix. After completion of the simulations, a total of about 3830 optimized flux distributions were present in the temporary matrix for each data set, which were used to calculate the average optimized flux values and their corresponding variances. This procedure was done for all six separate data sets. In the simulations, the true production rates of excreted metabolites that were smaller than 0.1% of the total glucose consumption rate on C-molar basis ($\text{Cmol.g}^{-1}.\text{h}^{-1}$) were neglected in order to reduce calculation time. The stoichiometric matrices were constructed from the set of reactions using a self-made computer program running in Visual Basic (Microsoft, Seattle, WA, USA). MCS, FBA and weighted least squares linear regressions were done in self-made computer programs running in Matlab (version 6.5 r13; Mathworks, Natick, MA, USA).

RESULTS AND DISCUSSION

Growth rate dependent biomass composition

The macromolecular biomass composition was determined on three duplicate aerobic glucose-limited chemostat cultures grown at dilution rates of 0.041, 0.082 and 0.161 h⁻¹ and is shown in Table 3.1. Although observations in other micro-organisms showed that the RNA content increases with growth rate and the protein content decreases with growth rate [13, 65, 66], no significant changes in RNA content and protein content with growth rate were observed in *N. meningitidis*. The DNA content in *N. meningitidis* was constant between growth rates of 0.041 and 0.082 h⁻¹ and somewhat higher at a growth rate of 0.161 h⁻¹. The DNA content decreases with growth rate in *Escherichia coli* [13] and *Paracoccus denitrificans* [65], while in *Saccharomyces cerevisiae* the DNA content remains constant with growth rate [66]. For the Phospholipid and LPS content in *N. meningitidis* no growth rate specific (i.e. linear) trends were observed. However, both the phospholipid and the LPS content decreased with growth rate. In contrast, in *Neisseria gonorrhoeae* an increasing hexose content, which is proportional to the LPS content, with growth rate was observed [67]. The latter study also showed that LPS from *Neisseria gonorrhoeae* grown at dilution rates above 0.3 h⁻¹ contained ca. eightfold less serotype antigen than the LPS from cells grown at dilution rates below 0.3 h⁻¹ and the observed shift coincided with acetate excretion above 0.3 h⁻¹. The cellular amino acid composition of *N. meningitidis* did not change significantly with growth rate (Table 3.2). Similar results were found in carbon-limited *E. coli* cultures [12]. In the latter study, it was also observed that the fatty acid composition of *E. coli* was strongly dependent on growth rate while we observed no significant differences in fatty acid composition at different growth rates in *N. meningitidis* (Table 3.3).

Error diagnosis, balancing and FBA

Next to the determination of the biomass composition, the culture supernatant was

Table 3.1 Measured macromolecular composition (% w/w) of *N. meningitidis* at different specific growth rates, μ , including the standard deviation.

Macromolecule	μ (h ⁻¹)		
	0.041	0.082	0.161
Protein	71.55 ± 8.54	70.30 ± 8.35	64.48 ± 8.36
RNA	8.53 ± 2.13	8.5 ± 2.14	12.83 ± 3.21
DNA	0.75 ± 0.11	0.65 ± 0.10	2.21 ± 0.33
Phospholipids ¹	11.30 ± 0.20	7.71 ± 0.14	9.62 ± 0.17
LPS ²	5.84 ± 0.29	3.85 ± 0.42	4.94 ± 0.28
Peptidoglycan ³	2.50 ± 0.25	2.50 ± 0.25	2.50 ± 0.25
Total	100.47 ± 8.82	93.55 ± 8.64	96.57 ± 8.97

¹ The overall phospholipid composition used in the present study was assumed to be independent of growth rate and based on the values provided by Rahman and co-workers [55], including 11 % phosphatidate (PA), 71 % phosphatidylethanolamine (PE) and 18% phosphatidylglycerol (PG).

² LPS was quantified based on the measured amount of C12:0-3OH and possesses uncertainty as explained in the results and discussion.

³ Peptidoglycan amount in *N. meningitidis* was estimated based on *E. coli* [68] and the composition was based on the average of the peptidoglycan structures present in *N. meningitidis* [69]. For modeling purposes a relative mean standard deviation of 10% was assumed.

analyzed for excreted metabolites and the gas phase was analyzed for carbon dioxide production and oxygen consumption. These primary measurements were translated to measured conversion rates using mass balances. Next, all measurement errors were translated to errors (i.e. variances) in measured conversion rates using MCS as described before [37]. The redundancy matrix expressing the redundancy relations between the measured rates was calculated for each individual dataset and contained 2 independent equations. Inspection of these equations indicated a carbon, and a nitrogen balance. The residuals obtained after multiplication of the redundancy matrix with the measured rates could be explained on the basis of random measurement variances with test values that were lower than the 95% chi-square critical value of 5.992. In addition, the individual carbon and nitrogen balance could be closed for all datasets. Next, the measured rates were balanced and balanced true rate vector, r_t , was calculated. As explained in the materials and methods section, a solution for the underdetermined parts of the

Table 3.2 Measured amino acid composition (% w/w) of *N. meningitidis* at different specific growth rates, μ , including the standard deviation (% w/w).

Amino acid	μ (h ⁻¹)		
	0.041	0.082	0.161
Aspartate	5.45 ± 0.24	5.67 ± 0.16	5.81 ± 0.26
Glutamate	8.40 ± 0.60	8.84 ± 0.20	8.30 ± 1.48
Serine	3.67 ± 0.17	3.77 ± 0.08	4.03 ± 0.19
Histidine	2.10 ± 0.11	2.17 ± 0.07	2.15 ± 0.13
Glycine	5.50 ± 0.26	5.57 ± 0.12	5.59 ± 0.28
Threonine	4.49 ± 0.22	4.60 ± 0.12	4.53 ± 0.20
Alanine	10.41 ± 0.44	9.68 ± 0.37	8.83 ± 0.43
Arginine	7.65 ± 0.56	6.99 ± 0.20	7.95 ± 0.32
Tyrosine	3.22 ± 0.53	2.80 ± 0.13	3.61 ± 0.18
Valine	6.65 ± 0.31	6.76 ± 0.19	6.75 ± 0.28
Methionine	2.85 ± 0.18	2.21 ± 0.12	2.08 ± 0.31
Phenylalanine	4.20 ± 0.15	4.36 ± 0.08	4.54 ± 0.15
Isoleucine	4.93 ± 0.19	5.02 ± 0.13	5.12 ± 0.20
Leucine	7.84 ± 0.31	8.14 ± 0.16	8.29 ± 0.30
Lysine	6.95 ± 1.14	7.07 ± 1.39	7.03 ± 1.03
Proline	3.32 ± 0.29	3.48 ± 0.16	3.71 ± 0.29
Asparagine	4.18 ± 0.22	4.34 ± 0.13	4.45 ± 0.23
Tryptophan	1.87 ± 0.47	1.90 ± 0.21	1.99 ± 0.49
Cysteine	0.96 ± 0.29	0.99 ± 0.12	0.97 ± 0.30
Glutamine	5.36 ± 0.45	5.64 ± 0.16	4.89 ± 0.39

Table 3.3 Measured cellular fatty acid composition (FA) of *N. meningitidis* at different specific growth rates, μ , including the standard deviation.

FA (% w/w)	μ (h ⁻¹)		
	0.041	0.082	0.161
dodecanoic acid (C12:0)	6.19 ± 0.64	6.55 ± 0.48	6.80 ± 0.48
3-hydroxydodecanoic acid (C12:0-3OH)	7.66 ± 0.57	7.39 ± 0.88	7.54 ± 0.59
3-hydroxytetradecanoic acid (C14:0-3OH)*	8.65 ± 1.98	8.35 ± 1.20	8.52 ± 1.25
tetradecanoic acid (C14:0)	2.82 ± 0.36	2.99 ± 0.20	3.13 ± 0.26
hexadecenoic acid (C16:1 trans-9)	24.33 ± 2.02	24.33 ± 1.83	22.30 ± 1.82
hexadecenoic acid (C16:1 ω -7-cis)	0.52 ± 0.07	0.55 ± 0.04	0.56 ± 0.05
hexadecanoic acid (C16:0)	37.96 ± 2.89	37.48 ± 2.93	38.45 ± 2.77
octadecenoic acid (C18:1 ω -7-cis)	10.71 ± 0.73	11.32 ± 1.01	11.60 ± 1.18
octadecanoic acid (C18:0)	1.17 ± 0.15	1.04 ± 0.07	1.11 ± 0.10

* The C14:0-3OH quantity was calculated from the corresponding measured C12:0-3OH quantity as explained in the results and discussion section.

metabolic network was calculated using MCS-LP with maximize ATP as objective function. As mentioned in the introduction section, several objective functions can be chosen (e.g. minimization of glucose uptake, maximize ATP production). Recently, Schuetz and co-workers [39] showed that the objective function maximization of ATP yield, next to the objective function maximize biomass yield, were found to result in biologically meaningful predictions in nutrient limited continuous cultures. Since we measured both the glucose uptake rate and the biomass production rate we chose maximization of ATP yield as objective function. Since ATP plays a role in the under-determined parts, this objective function constrains all underdeterminacies which results in a unique solution for each dataset. The resulting flux distributions are provided in the additional datafile (worksheet flux distributions) and discussed in more detail below.

Growth yield and Energy requirements

According to the maintenance model of Pirt [70], the specific rates of substrate uptake and product formation, q_j , can be expressed as linear functions of the specific growth rate, μ , by ascribing the consumption of a substrate to a growth- and non-growth associated process:

$$q_j = \frac{\mu}{Y_{ij}} + m_j \quad (3.6)$$

Where Y_{ij} is the yield coefficient not including any maintenance associated processes and m_j the maintenance coefficient. Notably, the above equation is an algebraic modification of the original Pirt equation by Tempest and Neijssel [71]. The yield of biomass on substrate ($Y_{x/s}$) and the maintenance coefficient (m_s) were determined according to equation 6 as $0.44 (\pm 0.04) \text{ g}_{\text{biomass}} \cdot \text{g}_{\text{glucose}}^{-1}$ and $0.04 (\pm 0.02) \text{ g}_{\text{glucose}} \cdot \text{g}_{\text{biomass}}^{-1} \cdot \text{h}^{-1}$, respectively, using weighted least squares linear regression of the balanced specific glucose consumption rates and their corresponding variances at the different growth rates as input (Figure 3.1). The calculated $Y_{x/s}$ value is in range with values reported for aerobic glucose-limited grown *E. coli*, which range from $0.44 - 0.56 \text{ g}_{\text{biomass}} \cdot \text{g}_{\text{glucose}}^{-1}$, while the calculated m_s value is about twice as high compared to *E. coli* [17, 70].

For calculation of the percentage of glucose carbon flow towards biomass, carbon dioxide and excreted metabolites the true rates were expressed on a molar basis of carbon atoms (Figure 3.2). This analysis showed a decreasing flux of glucose carbon towards carbon dioxide and an increasing flux towards biomass, suggesting a more energy-efficient utilization of carbon substrate for biomass formation with increasing growth rate. In other words, the maintenance term in equation 3.6 becomes less important when the growth rate increases.

In order to estimate the growth- ($Y_{x/ATP}$) and non-growth (m_{ATP}) associated energy requirement for biomass formation, the ATP requirement in the biomass biosynthesis

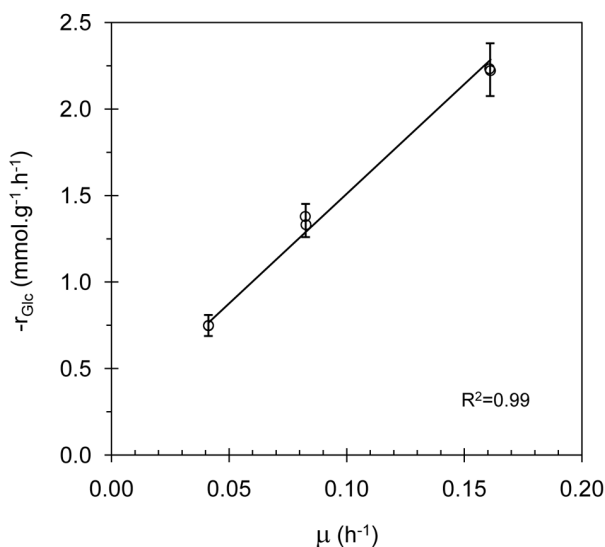


Figure 3.1 Estimation of $Y_{x/s}$ and m_s . The yield and maintenance were determined from six separate (o) aerobic glucose-limited chemostat cultures of *N. meningitidis* using weighted least squares linear regression (solid line). Error bars represent the standard deviation between duplicate balanced glucose consumption rates.

reaction (i.e. growth associated energy requirement, reaction 123 in the model) was set to zero, while the energy requirement for DNA, RNA and protein assembly were assumed to be 1.372, 0.4 and 4.306 mol ATP/mol macromolecule, respectively [72]. For the P/O ratio, describing the efficiency of the oxidative phosphorylation, a constant value was assumed. This was done since the P/O ratio, $Y_{x/\text{ATP}}$ and m_{ATP} can neither be measured directly nor evaluated independently. Vanrolleghem and co-workers [73] showed both theoretically and practically that the P/O ratio and a growth-related maintenance factor k , which includes both $Y_{x/\text{ATP}}$ and m_{ATP} , can be calculated using chemostat cultivations with different mixtures of substrates. Since cultivation on different substrates to determine unique values for the energetic parameters was beyond the scope of this study, a constant P/O ratio of 1.33 [74-76] was

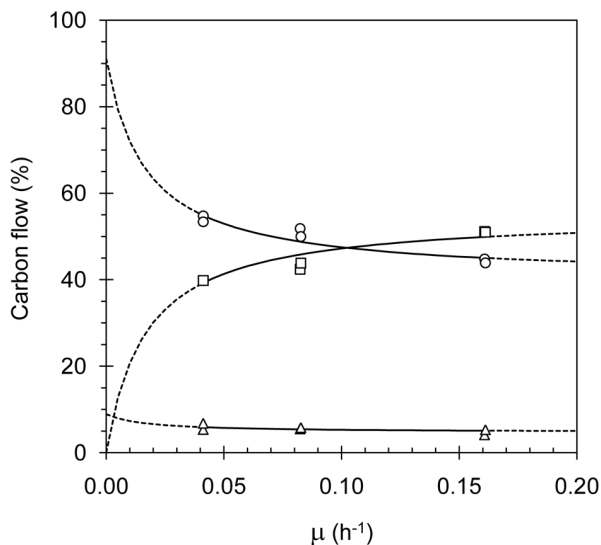


Figure 3.2 Carbon mass balance during glucose-limited aerobic chemostats of *N. meningitidis*. The percentage of glucose carbon flow towards biomass (\square), carbon dioxide (\circ) and total excreted metabolites (Δ) being the sum of acetate, ethanol, amino acids and extracellular protein. Lines represent predictions based on the calculated yield and maintenance values from Figure 3.1.

assumed. With the settings mentioned above and the measured conversion rates and their corresponding variances as an input, MCS in combination with linear optimization (MCS-LP) was done as explained in the materials and methods section. The unknown energy requirements expressed in ATP of the assimilatory reactions ($Y_{x/ATP}$) and the amount of ATP spent on maintaining the current state of the bacterium (m_{ATP}) were estimated using weighted least squares linear regression of the obtained q_{ATPh} values in analogy to the maintenance model of Pirt (equation 6) for which the MCS-LP calculated q_{ATPh} values and their corresponding variances at the different growth rates were used as input (Figure 3.3a). The total amount of ATP hydrolyzed (including ATP for maintenance) per mole of biomass formed (y_{ATP}) decreases with increasing growth rate (Figure 3.3b) indicating more energy-efficient biomass formation at higher growth

rates (i.e. less importance of maintenance). A similar trend was found in aerobic glucose-limited chemostat *E. coli* cultures [17, 75].

The growth associated energy requirement ($Y_{x/ATP}$) and the non-growth associated ATP requirement for maintenance (m_{ATP}) were calculated as $0.13 (\pm 0.04) \text{ mol}_{\text{biomass}} \cdot \text{mol}_{ATP}^{-1}$ ($0.81 \text{ Cmol}_{\text{biomass}} \cdot \text{mol}_{ATP}^{-1}$) and $0.43 (\pm 0.14) \text{ mol}_{ATP} \cdot \text{mol}_{\text{biomass}}^{-1} \cdot \text{h}^{-1}$ ($0.07 \text{ mol}_{ATP} \cdot \text{Cmol}_{\text{biomass}}^{-1} \cdot \text{h}^{-1}$), respectively (Figure 3.3). The calculated m_{ATP} value is within range of reported *E. coli* values that were obtained from aerobic glucose-limited chemostat cultures: 0.07 [17], 0.12 [77] and $0.15 \text{ mol}_{ATP} \cdot \text{Cmol}_{\text{biomass}}^{-1} \cdot \text{h}^{-1}$ [75]. The $Y_{x/ATP}$ value is higher than reported values obtained from aerobic glucose-limited chemostat *E. coli* cultures: 0.60 [75], 0.50 [17], $0.38 \text{ Cmol}_{\text{biomass}} \cdot \text{mol}_{ATP}^{-1}$. Since in these *E. coli* studies the assumed ATP requirement for DNA, RNA and protein assembly was the same as in our model, this indicates that *N. meningitidis* is more energy-

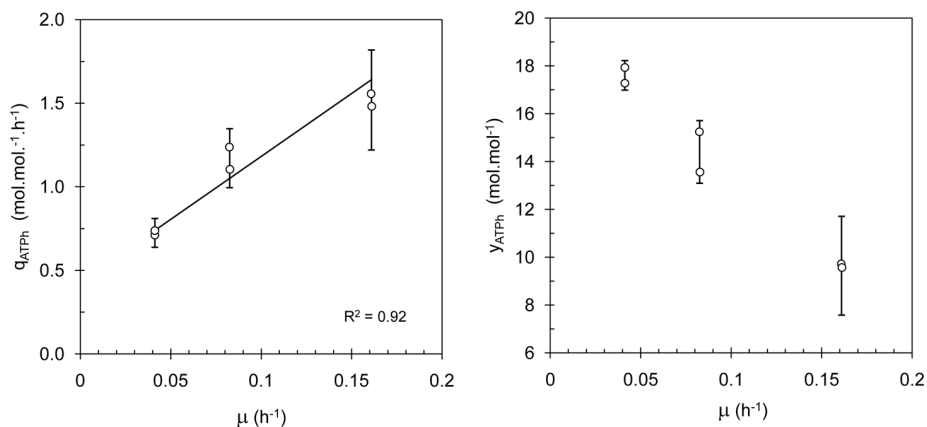


Figure 3.3 Energy parameters estimation. (a) The growth- and non-growth associated energy requirements determined from six separate (o) aerobic glucose-limited chemostat cultures of *N. meningitidis* using weighted least squares linear regression (solid line). (b) The total amount of ATP hydrolyzed per mole of biomass formed (y_{ATPh}) decreases with increasing growth rate indicating more energy-efficient biomass formation at higher growth rates. Error bars represent the standard deviations obtained from MCS-LP as explained in the text.

efficient in biomass formation. It is worth noting that the difference in assumed P/O ratios in these *E. coli* studies influenced the obtained $Y_{x/ATP}$ values, i.e. a higher P/O ratio results in a somewhat lower $Y_{x/ATP}$ value. Varma and Palsson [76] calculated that within the limits of P/O ratio from 2/3 to 2 the maximum calculated *E. coli* biomass yield varied within a 19% range. This illustrates as stated before that when accurate estimation of energy parameters is desired, multiple substrate chemostat studies [73] are an absolute requirement.

The FBA flux distribution results obtained from MCS-LP using maximize ATP as objective function showed that all the produced glucose-6-phosphate is processed solely through the Entner-Doudoroff pathway. This mathematical solution for the given *N. meningitidis* metabolic network is discussed in more detail below.

Influence of the EDP:PPP split ratio on estimation of energy parameters

In *N. meningitidis* glucose can be completely catabolized through the Entner-Doudoroff pathway (EDP) or the pentose phosphate pathway (PPP). The Embden-Meyerhof-Parnas glycolytic pathway (EMP) is not functional, because the gene coding for phosphofructokinase (*pfkA*) is not present in the genome [78]. As mentioned earlier, the flux distribution results obtained from MCS-LP using maximize ATP as objective function showed that all the produced glucose-6-phosphate is processed solely through the EDP. By comparing the total energy production of the PPP and the EDP (both including TCA cycle), one can calculate that the EDP can yield slightly more energy per consumed glucose. The partial degradation through the PPP yields 2 ATP, 7 NADPH, 3 NADH and 2 FADH₂ per mole of glucose consumed, while complete degradation of glucose to CO₂ in the PPP yields 12 NADPH at the cost of 1 ATP. Degradation through the EDP yields 3 ATP, 3 NADPH, 4 NADH and 4 FADH₂ per mole of glucose. Thus, at the assumed P/O ratio of 1.33 the EDP can generate 5.6% more ATP per mole of glucose, which explains the flux distribution results. When the P/O ratio increases the differences between the theoretical ATP yield of the

EDP and the PPP become smaller. Although the objective function maximization of ATP yield was found to achieve a high predictive accuracy for ^{13}C -determined *in vivo* fluxes in *E. coli* [39], the obtained results for *N. meningitidis* using this objective function can be questioned. For this reason we calculated the flux distributions using MCS-LP and the same objective function, while incorporating different pre-set EDP:PPP ratios. The MCS-LP procedure was done as described in the materials and methods section with the addition that prior to the linear optimization the upper boundary of the EDP (β_{EDP}) was automatically stepwise adjusted to a fraction (f) of the balanced glucose consumption rate (r_{glc}), while maintaining the experimentally determined $Y_{\text{x/s}}$:

$$\beta_{\text{EDP},i} = f_i \cdot r_{\text{glc}} \quad \text{with} \quad 0 \leq f \leq 1 \quad (3.8)$$

The fraction was stepwise increased from 0 to 1 in 20 steps (i). For each dataset a total of 1000 simulations per fraction were done. After completion of the simulations, the average optimized flux values and their corresponding variances at each fraction were calculated. The results of the simulations show that the total amount of ATP that is hydrolyzed (q_{ATPh}) increases with increasing ED fraction at all growth rates (Figure 3.4) as expected.

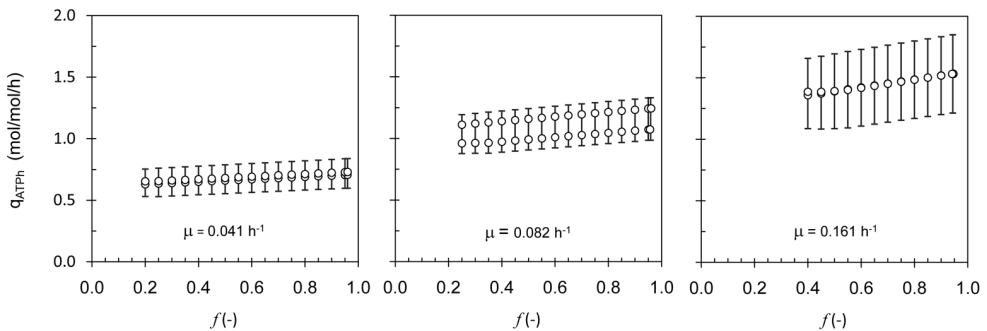


Figure 3.4 q_{ATPh} as function of the fraction of glucose channeled through the EDP (f). Error bars represent the standard deviation between simulation results (o) and were obtained from MCS-LP.

Below fractions of 0.2, 0.25 and 0.40 no feasible results were obtained for $\mu=0.041\text{ h}^{-1}$, $\mu=0.082\text{ h}^{-1}$ and $\mu=0.161\text{ h}^{-1}$, respectively. This means that a minimal flux through the EDP is required. This can be explained from the loss of CO_2 in the oxidative part of the PPP. Due to the fact that phosphofructokinase is not present fructose-6 phosphate (F6P) formed in the non-oxidative part of the PPP can only be converted back into glucose-6 phosphate (G6P) and must next be converted again through the oxidative part of the PPP, since the flux through the EDP is fixed. This means additional loss of CO_2 . Below a certain ED flux too much carbon is turned into CO_2 and a feasible solution cannot be found anymore since not enough carbon is left to form biomass. Because at higher growth rates the carbon flow to biomass increases (Figure 3.2) the minimum flux through the EDP also needs to increase, which explains the increasing minimum flux through the EDP at increasing growth rates. On the basis of ^{14}C studies in *N. meningitidis*, Jyssum [79] roughly calculated that the ED cleavage always synthesizes the major part of pyruvate (67-87%) while the PP pathway accounts for the remaining part. Morse and co-workers [80] found similar results for *Neisseria gonorrhoeae*.

At all growth rates the difference in calculated q_{ATPh} values from the lowest to the highest feasible fraction is only 10.4%, while the fluxes in for instance the citric acid cycle change significantly more. For example, the succinate dehydrogenase flux changes at least three fold from the lowest to the highest feasible fraction (Figure 3.5). However, even without exact knowledge of the split ratio between the energy generating pathways the energy parameters m_{ATP} and $Y_{\text{x/ATP}}$ can be determined quite accurately at a set P/O ratio. As stated, if exact determination of the energy parameters P/O ratio, $Y_{\text{x/ATP}}$ and m_{ATP} is desired, multiple substrate chemostat studies [73] could be combined with determination of the split ratios between energy generating pathways using ^{13}C labeled substrates. The results of such studies could lead to new objective functions with better predictive accuracy. In all cases, the definition of the metabolic model is crucial. For instance, neglecting metabolic reactions to remove parallel pathways could lead to

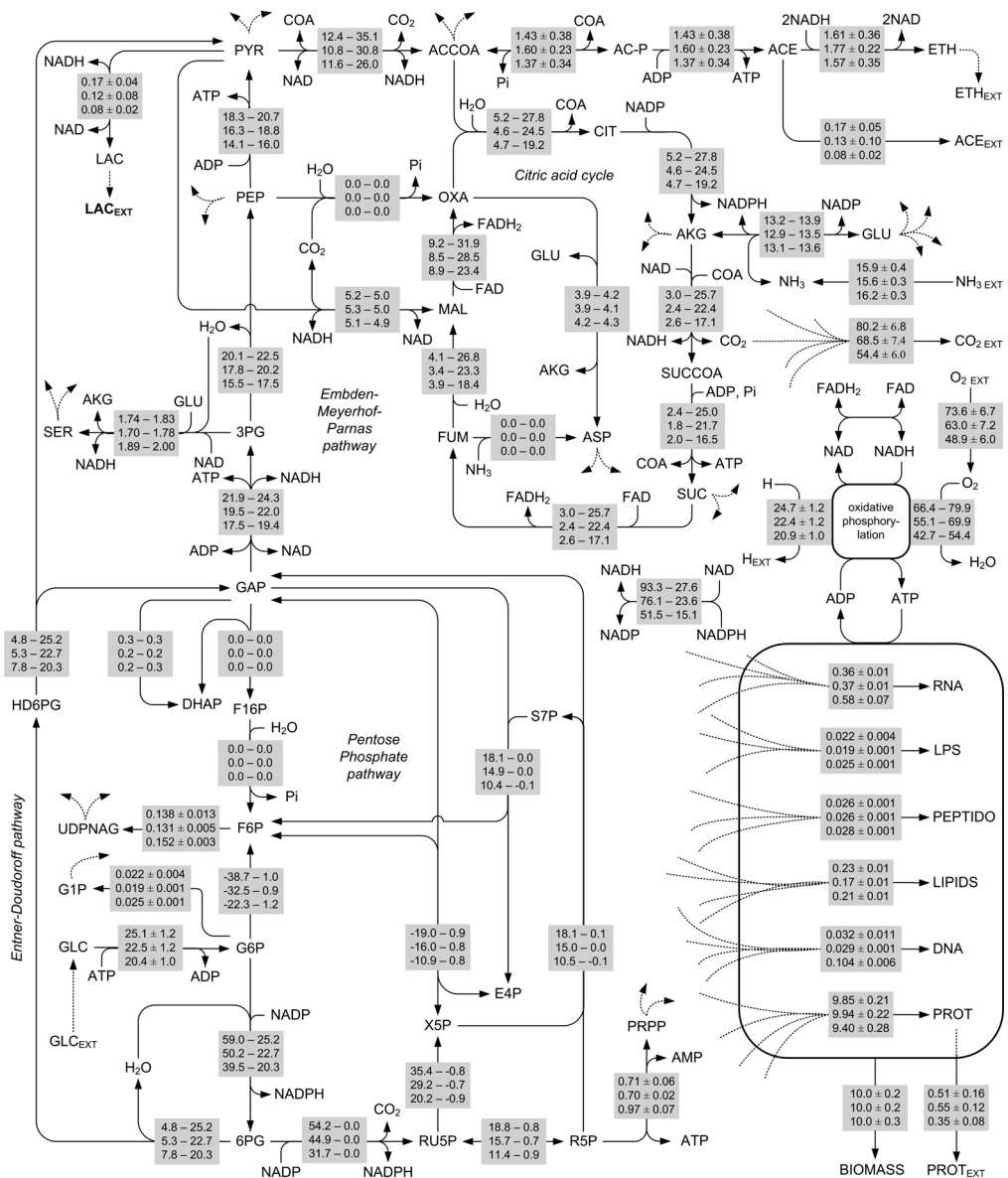


Figure 3.5 Overview of optimized metabolic flux distributions. Average flux values and ranges ($\text{mmol g}^{-1} \text{h}^{-1}$), normalized to biomass formation rate, are given in the black boxes in which the values from top to bottom correspond with $\mu=0.041 \text{ h}^{-1}$, $\mu=0.082 \text{ h}^{-1}$, and $\mu=0.161 \text{ h}^{-1}$, respectively. The determined fluxes are given with standard deviations calculated from the duplicate datasets. The underdetermined fluxes are presented as flux ranges which range from the lowest feasible EDP:PPP ratio to a EDP:PPP ratio of 1:0. The ranges represent the minimum calculated flux-1 SD (standard deviation) and the maximum calculated flux+1 SD.

a calculated flux distribution that is completely different from the true values. In turn, inclusion of a parallel pathway in a metabolic model automatically requires an objective function when solutions for flux values are desired. However, the question of which objective function is valid for the biological system under study and achieves the best predictive accuracy remains.

The split ratio analysis above illustrates that the ATP formation rate is insensitive to the split ratio between the EDP and the PPP. Thus the objective function maximization of ATP yield [39] to determine the split ratio between energy generating pathways and the fluxes in the remaining underdetermined parts of the metabolic model has limited accuracy in *N. meningitidis*. In other words the calculated fluxes in the underdetermined parts of the network might not represent the actual biological situation. For this reason, we have chosen to present flux ranges for underdetermined parts of the metabolic network rather than presenting single flux values (Figure 3.5 and Appendix 3 B).

Growth rate dependent PorA content in OMVs

As mentioned in the introduction section, the vaccine against serogroup B organisms developed at the NVI, focuses on the subcapsular protein antigen PorA. Both the Wilcoxon signed-rank test and the t-test indicated that the PorA content of OMVs extracted from biomass grown at a growth rate of 0.161 h^{-1} is significantly lower than the PorA content of OMVs extracted from biomass grown at lower growth rates ($p=0.0014$ when comparing $\mu=0.041\text{ h}^{-1}$ with $\mu=0.161\text{ h}^{-1}$ and $p=0.0019$ when comparing $\mu=0.082\text{ h}^{-1}$ with $\mu=0.161\text{ h}^{-1}$). The results are shown in Figure 3.6. In the regular vaccine production process bacteria are produced in batch culture. During batch cultivation the growth rate decreases [9] which indicates that the culture harvest point is a parameter that has an influence on the PorA content in extracted OMVs. Thus, for high PorA content, OMVs are best extracted from bacteria in the late growth phase. Similar indications were found in extracted OMVs from batch cultures of *N. meningitidis* serogroup B strain HP16215-2 [9]. Interestingly, the maximum

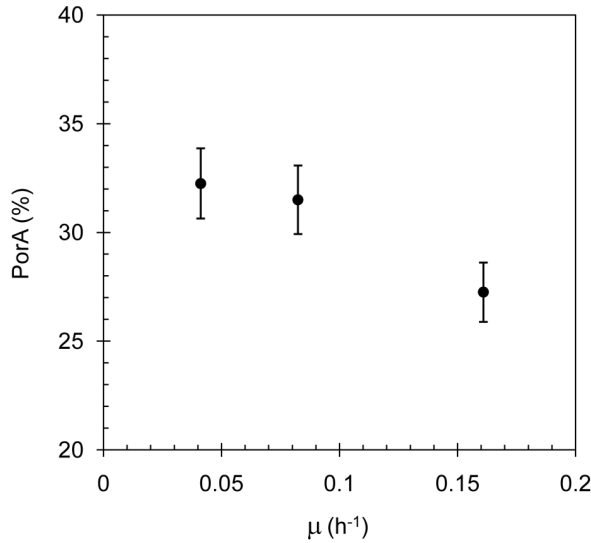


Figure 3.6 Average PorA content (% w/w, ●) in outer membrane vesicles that were extracted from *N. meningitidis* grown in steady state at different specific growth rates (μ). Error bars represent the standard deviations that were calculated from the four measurements at each growth rate.

amount of OMV protein obtained from batch cultivations using *N. meningitidis* serogroup B strain N44/89 [81] grown on modified Catlin medium [82], containing lactate instead of glucose, was achieved during stationary phase while Fu and co-workers [83] found that production of outer membrane protein complexes from *N. meningitidis* serogroup B strain B11 grown on modified Catlin medium can best be done in the late exponential phase, which is in line with our observations. These differences indicate that the composition, and thus extraction and isolation properties, of OMVs are strongly dependent on culture conditions and physiology.

CONCLUSIONS

The macromolecular composition of *N. meningitidis* changes little with growth rate. In the applied range of growth rates, no significant changes in RNA content and protein content with growth rate were observed while the DNA content in *N. meningitidis* was somewhat higher at the highest applied growth rate. The phospholipid and lipopolysaccharide content in *N. meningitidis* changed with growth rate but no specific trends were observed. In addition, the cellular fatty acid composition and the amino acid composition did not change significantly with growth rate. These observations show that *N. meningitidis* maintains its macromolecular composition even when its growth rate is changed fourfold.

Flux balance analysis combined with Monte Carlo simulation at different growth rates has been proven useful to calculate the errors in determined fluxes and to indicate the reliability of the obtained flux distributions. Split ratio analysis between the Entner-Doudoroff and the pentose phosphate pathway, indicated that given the measured rates a minimal flux through the Entner-Doudoroff pathway is required in *N. meningitidis*. Furthermore it was found that the split ratio had a minor effect on ATP formation rate but a major effect on the fluxes going through, for instance, the citric acid cycle. In other words, the mathematical result obtained from the objective function maximization of ATP yield may not reflect the biological situation for the underdetermined parts of the metabolic network. For this reason we presented the fluxes of the underdetermined parts of the metabolic network as flux ranges which were calculated from the EDP:PPP split ratio analysis.

At high growth rate the PorA content in outer membrane vesicles extracted from biomass was significantly lower in comparison with low growth rates, which indicates the importance of the culture harvest point in the regular vaccine production process.

ADDITIONAL DATA

The following additional data are available on CD-rom. The file named Additional data Chapter 3.xlsx is an excel file that includes 7 worksheets. The first worksheet named 'genome-scale model' includes the complete reaction database along with involved genes, enzyme numbers and metabolites. The second worksheet named 'simplified model' contains the simplified metabolic model. The third worksheet named 'abbreviations' contains a list of abbreviations of the metabolites. The fourth worksheet named 'null space' contains the null space vectors of the simplified model. The fifth worksheet named 'flux distributions' contains a table in which the flux distributions of the separate experiments are given. The sixth worksheet named 'split ratio' contains the calculated flux distributions at the different split ratios as explained in the main text. The seventh worksheet named 'final flux distributions' contains the complete flux distributions of which a part is shown in Figure 3.5.

ACKNOWLEDGEMENTS

We are grateful to Cor van Ingen for the freeze drying work, to Elly Verhagen for practical assistance and to Jan ten Hove and Tom Ploeger for LPS structural analysis.

REFERENCES

1. Rosenstein NE, Perkins BA, Stephens DS, Popovic T, Hughes JM. 2001. Meningococcal disease. *N Engl J Med* 344:1378-1388.
2. Stephens DS, Hoffman LH, McGee ZA. 1983. Interaction of *Neisseria meningitidis* with human nasopharyngeal mucosa: attachment and entry into columnar epithelial cells. *J Infect Dis* 148:369-376.
3. Snyder LA, Davies JK, Ryan CS, Saunders NJ. 2005. Comparative overview of the genomic and genetic differences between the pathogenic *Neisseria* strains and species. *Plasmid* 54:191-218.
4. Tzeng YL, Stephens DS. 2000. Epidemiology and pathogenesis of *Neisseria meningitidis*. *Microbes Infect* 2:687-700.
5. Morley SL, Pollard AJ. 2001. Vaccine prevention of meningococcal disease, coming soon? *Vaccine* 20:666-687.
6. Girard MP, Preziosi MP, Aguado MT, Kieny MP. 2006. A review of vaccine research and development: meningococcal disease. *Vaccine* 24:4692-4700.
7. Finne J, Bitter-Suermann D, Goridis C, Finne U. 1987. An IgG monoclonal antibody to group B meningococci cross-reacts with developmentally regulated polysialic acid units of glycoproteins in neural and extraneural tissues. *J Immunol* 138:4402-4407.
8. Vermont CL, van Dijken HH, Kuipers AJ, van Limpt CJ, Keijzers WC, van der Ende A, de Groot R, van Alphen L, van den Dobbelsteen GP. 2003. Cross-reactivity of antibodies against PorA after vaccination with a meningococcal B outer membrane vesicle vaccine. *Infect Immun* 71:1650-1655.
9. Baart GJE, de Jong G, Philippi M, Riet Kvt, van der Pol LA, Beuvery EC, Tramper J, Martens DE. 2007. Scale-up for bulk production of vaccine against meningococcal disease. *Vaccine* 25:6399-6408.
10. Teusink B, Wiersma A, Molenaar D, Francke C, de Vos WM, Siezen RJ, Smid EJ. 2006. Analysis of growth of *Lactobacillus plantarum* WCF51 on a complex medium using a genome-scale metabolic model. *J Biol Chem* 281:40041-40048.
11. Oliveira AP, Nielsen J, Forster J. 2005. Modeling *Lactococcus lactis* using a genome-scale flux model. *BMC Microbiol* 5:39.
12. Pramanik J, Keasling JD. 1998. Effect of *Escherichia coli* biomass composition on central metabolic fluxes predicted by a stoichiometric model. *Biotechnol Bioeng* 60:230-238.
13. Bremer H, Dennis PP. Modulation of chemical composition and other parameters of the cell by growth rate. In: *Escherichia coli* and *Salmonella typhimurium*: Cellular and Molecular Biology. Edited by Neidhardt FC, Curtiss R, Ingraham JL, Brooks Low K, Magasanik B, Reznikoff WS, Riley M, Schaechter M, Umberger HE, vol. 1, 2 edn. Washington D.C.: American Society for Microbiology; 1996: 1553-1569.
14. Mashego MR, van Gulik WM, Vinke JL, Visser D, Heijnen JJ. 2006. *In vivo* kinetics with rapid perturbation experiments in *Saccharomyces cerevisiae* using a second-generation BioScope. *Metab Eng* 8:370-383.
15. Steuer R, Gross T, Selbig J, Blasius B. 2006. Structural kinetic modeling of metabolic networks. *Proc Natl Acad Sci U S A* 103:11868-11873.
16. Furch T, Hollmann R, Wittmann C, Wang W, Deckwer WD. 2007. Comparative study on central metabolic fluxes of *Bacillus megaterium* strains in continuous culture using ¹³C labelled substrates. *Bioprocess Biosyst Eng* 30:47-59.
17. Kayser A, Weber J, Hecht V, Rinas U. 2005. Metabolic flux analysis of *Escherichia coli* in glucose-limited continuous culture. I. Growth-rate-dependent metabolic efficiency at steady state. *Microbiology* 151:693-706.
18. Edwards JS, Covert M, Palsson B. 2002. Metabolic modelling of microbes: the flux-balance approach. *Environ Microbiol* 4:133-140.
19. Henriksen CM, Christensen LH, Nielsen J, Villadsen J. 1996. Growth energetics and metabolic fluxes in continuous cultures of *Penicillium chrysogenum*. *J Biotechnol* 45:149-164.
20. van Gulik WM, Heijnen JJ. 1995. A metabolic network stoichiometry analysis of microbial growth and product formation. *Biotechnol Bioeng* 48:681-698.
21. Schuster S, Dandekar T, Fell DA. 1999. Detection of elementary flux modes in biochemical networks: a promising tool for pathway analysis and metabolic engineering. *Trends Biotechnol* 17:53-60.
22. Schilling CH, Schuster S, Palsson BO, Heinrich R. 1999. Metabolic pathway analysis: basic concepts and scientific applications in the post-genomic era. *Biotechnol Prog* 15:296-303.
23. Edwards JS, Palsson BO. 1999. Systems properties of the *Haemophilus influenzae* Rd metabolic

- genotype. *J Biol Chem* 274:17410-17416.
24. Edwards JS, Palsson BO. 2000. The *Escherichia coli* MG1655 *in silico* metabolic genotype: its definition, characteristics, and capabilities. *Proc Natl Acad Sci U S A* 97:5528-5533.
25. Edwards JS, Ibarra RU, Palsson BO. 2001. *In silico* predictions of *Escherichia coli* metabolic capabilities are consistent with experimental data. *Nat Biotechnol* 19:125-130.
26. Reed JL, Vo TD, Schilling CH, Palsson BO. 2003. An expanded genome-scale model of *Escherichia coli* K-12 (iJR904 GSM/GPR). *Genome Biol* 4:R54.
27. Schilling CH, Covert MW, Famili I, Church GM, Edwards JS, Palsson BO. 2002. Genome-scale metabolic model of *Helicobacter pylori* 26695. *J Bacteriol* 184:4582-4593.
28. Forster J, Famili I, Fu P, Palsson BO, Nielsen J. 2003. Genome-scale reconstruction of the *Saccharomyces cerevisiae* metabolic network. *Genome Res* 13:244-253.
29. Duarte NC, Herrgard MJ, Palsson BO. 2004. Reconstruction and validation of *Saccharomyces cerevisiae* iND750, a fully compartmentalized genome-scale metabolic model. *Genome Res* 14:1298-1309.
30. Teusink B, van Enckevort FH, Francke C, Wiersma A, Wegkamp A, Smid EJ, Siezen RJ. 2005. *In silico* reconstruction of the metabolic pathways of *Lactobacillus plantarum*: comparing predictions of nutrient requirements with those from growth experiments. *Appl Environ Microbiol* 71:7253-7262.
31. Becker SA, Palsson BO. 2005. Genome-scale reconstruction of the metabolic network in *Staphylococcus aureus* N315: an initial draft to the two-dimensional annotation. *BMC Microbiol* 5:8.
32. Heinemann M, Kummel A, Ruinatscha R, Panke S. 2005. *In silico* genome-scale reconstruction and validation of the *Staphylococcus aureus* metabolic network. *Biotechnol Bioeng* 92:850-864.
33. Borodina I, Krabben P, Nielsen J. 2005. Genome-scale analysis of *Streptomyces coelicolor* A3(2) metabolism. *Genome Res* 15:820-829.
34. Feist AM, Scholten JC, Palsson BO, Brockman FJ, Ideker T. 2006. Modeling methanogenesis with a genome-scale metabolic reconstruction of *Methanosarcina barkeri*. *Mol Syst Biol* 2:2006 0004.
35. Kim TY, Kim HU, Park JM, Song H, Kim JS, Lee SY. 2007. Genome-scale analysis of *Mannheimia succiniciproducens* metabolism. *Biotechnol Bioeng* 97:657-671.
36. Beste DJ, Hooper T, Stewart G, Bonde B, Avignone-Rossa C, Bushell ME, Wheeler P, Klamt S, Kierzek AM, McFadden J. 2007. GSMN-TB: a web-based genome-scale network model of *Mycobacterium tuberculosis* metabolism. *Genome Biol* 8:R89.
37. Baart GJ, Zomer B, de Haan A, van der Pol LA, Beuvery EC, Tramper J, Martens DE. 2007. Modeling *Neisseria meningitidis* metabolism: from genome to metabolic fluxes. *Genome Biol* 8:R136.
38. Christensen B, Gombert AK, Nielsen J. 2002. Analysis of flux estimates based on ¹³C-labelling experiments. *Eur J Biochem* 269:2795-2800.
39. Schuetz R, Kuepfer L, Sauer U. 2007. Systematic evaluation of objective functions for predicting intracellular fluxes in *Escherichia coli*. *Mol Syst Biol* 3 (article 119):1-15.
40. Edwards JS, Palsson BO. 2000. Metabolic flux balance analysis and the *in silico* analysis of *Escherichia coli* K-12 gene deletions. *BMC Bioinformatics* 1:1.
41. Edwards JS, Ramakrishna R, Palsson BO. 2002. Characterizing the metabolic phenotype: a phenotype phase plane analysis. *Biotechnol Bioeng* 77:27-36.
42. Famili I, Forster J, Nielsen J, Palsson BO. 2003. *Saccharomyces cerevisiae* phenotypes can be predicted by using constraint-based analysis of a genome-scale reconstructed metabolic network. *Proc Natl Acad Sci U S A* 100:13134-13139.
43. Forster J, Famili I, Palsson BO, Nielsen J. 2003. Large-scale evaluation of *in silico* gene deletions in *Saccharomyces cerevisiae*. *Omics* 7:193-202.
44. Choi HS, Kim TY, Lee DY, Lee SY. 2007. Incorporating metabolic flux ratios into constraint-based flux analysis by using artificial metabolites and converging ratio determinants. *J Biotechnol* 129:696-705.
45. Bos MP, Tommassen J. 2005. Viability of a capsule- and lipopolysaccharide-deficient mutant of *Neisseria meningitidis*. *Infect Immun* 73:6194-6197.
46. Fredriksen JH, Rosenqvist E, Wedege E, Bryn K, Bjune G, Froholm LO, Lindbak AK, Mogster B, Namork E, Rye U et al. 1991. Production, characterization and control of MenB-vaccine "Folkehelsen": an outer membrane vesicle vaccine against group B. *NIPH Ann* 14:67-79; discussion 79-80.
47. Arigita C, Jiskoot W, Wistdijk J, van Ingen C, Hennink WE, Crommelin DJ, Kersten GF. 2004. Stability of mono- and trivalent meningococcal outer membrane vesicle vaccines. *Vaccine* 22:629-642.
48. Dorrestijn RC, de Gooijer CD, Tramper J, Beuvery EC. 1994. A method for simultaneous determination of solubility and transfer coefficient of oxygen in aqueous media using off-gas mass spectrometry. *Biotechnol Bioeng* 43:149-154.

49. Baruque-Ramos J, Hiss H, Converti A, Goncalves VM, Raw I. 2006. Accumulation of organic acids in cultivations of *Neisseria meningitidis* C. *J Ind Microbiol Biotechnol* 33:869-877.
50. Dorresteyn RC, Berwald LG, Zomer G, de Gooijer CD, Wieten G, Beuvery EC. 1996. Determination of amino acids using o-phthalaldehyde-2-mercaptoethanol derivatization effect of reaction conditions. *Journal of Chromatography A* 724:159-167.
51. Welch DF. 1991. Applications of cellular fatty acid analysis. *Clin Microbiol Rev* 4:422-438.
52. White MA, Simmons MD, Bishop A, Chandler HA. 1988. Microbial identification by gas chromatography. *J R Nav Med Serv* 74:141-146.
53. Westphal O, Jann JK. 1965. Bacterial lipopolysaccharide extraction with phenol-water and further application of the procedure. *Methods Carbohydr Chem* 5:83-91.
54. van der Ley P, Steeghs L, Hamstra HJ, ten Hove J, Zomer B, van Alphen L. 2001. Modification of lipid A biosynthesis in *Neisseria meningitidis* lpxL mutants: influence on lipopolysaccharide structure, toxicity, and adjuvant activity. *Infect Immun* 69:5981-5990.
55. Rahman MM, Kolli VS, Kahler CM, Shih G, Stephens DS, Carlson RW. 2000. The membrane phospholipids of *Neisseria meningitidis* and *Neisseria gonorrhoeae* as characterized by fast atom bombardment mass spectrometry. *Microbiology* 146 (Pt 8):1901-1911.
56. Benthin S, Nielsen J, Villadsen J. 1991. A simple and reliable method for the determination of cellular RNA content. *Biotech Techn* 5:39-42.
57. Daniels L, Hanson RS, Phillips JA. Chemical analysis. In: *Methods for general and molecular bacteriology*. Edited by Gerhardt P, Murray RGE, Wood WA, Krieg NR, 2 edn. Washington D.C.: American Society for Microbiology; 1994: 534-535.
58. Peterson GL. 1977. A simplification of the protein assay method of Lowry et al. which is more generally applicable. *Anal Biochem* 83:346-356.
59. Lugtenberg B, Meijers J, Peters R, van der Hoek P, van Alphen L. 1975. Electrophoretic resolution of the "major outer membrane protein" of *Escherichia coli* K12 into four bands. *FEBS Lett* 58:254-258.
60. Edwards JS, Ramakrishna R, Schilling CH, Palsson BO. Metabolic flux balance analysis. In: *Metabolic Engineering*. Edited by Lee SY, Papoutsakis ET. New York: Marcel Dekker Inc.; 1999: 13-57.
61. Forster J, Gombert AK, Nielsen J. 2002. A functional genomics approach using metabolomics and *in silico* pathway analysis. *Biotechnol Bioeng* 79:703-712.
62. Vallino JJ, Stephanopoulos G. Flux determination in cellular bioreaction networks: applications to lysine fermentations. In: *Frontiers in bioprocessing*. Edited by Sikdar SK, Bier M, Todd P. Boca Raton, Fla: CRC press; 1990: 205-219.
63. van der Heijden RTJM, Romein B, Heijnen JJ, Hellinga C, Luyben KCAM. 1994. Linear constraint relations in biochemical reaction systems: I. Classification of the calculability and the balanceability of conversion rates. *Biotechnology and Bioengineering* 43:3-10.
64. Bonarius HPJ, Schmid G, Tramper J. 1997. Flux analysis of underdetermined metabolic networks: the quest for the missing constraints. *Trends in Biotechnol* 15:308-314.
65. Hanegraaf PP, Muller EB. 2001. The dynamics of the macromolecular composition of biomass. *J Theor Biol* 212:237-251.
66. Lange HC, Heijnen JJ. 2001. Statistical reconciliation of the elemental and molecular biomass composition of *Saccharomyces cerevisiae*. *Biotechnol Bioeng* 75:334-344.
67. Morse SA, Mintz CS, Sarafian SK, Bartenstein L, Bertram M, Apicella MA. 1983. Effect of dilution rate on lipopolysaccharide and serum resistance of *Neisseria gonorrhoeae* grown in continuous culture. *Infect Immun* 41:74-82.
68. Neidhardt FC, Umbarger HE. Chemical composition of *Escherichia coli*. In: *Escherichia coli and Salmonella typhimurium: Cellular and Molecular Biology*. Edited by Neidhardt FC, Curtiss R, Ingraham JL, Brooks Low K, Magasanik B, Reznikoff WS, Riley M, Schaechter M, Umbarger HE, vol. 1, 2 edn. Washington D.C.: American Society for Microbiology; 1996: 13-16.
69. Antignac A, Rousselle JC, Namane A, Labigne A, Taha MK, Boneca IG. 2003. Detailed structural analysis of the peptidoglycan of the human pathogen *Neisseria meningitidis*. *J Biol Chem* 278:31521-31528.
70. Pirt SJ. 1965. The maintenance energy of bacteria in growing cultures. *Proc R Soc Lond B Biol Sci* 163:224-231.
71. Tempest DW, Neijssel OM. 1984. The status of YATP and maintenance energy as biologically interpretable phenomena. *Ann Rev Microbiol* 38:459-486.
72. Neijssel OM, Teixeira de Mattos MJ, Tempest DW. Growth Yield and Energy Distribution. In: *Escherichia coli and Salmonella typhimurium: Cellular and Molecular Biology*. Edited by

- Neidhardt FC, Curtiss R, Ingraham JL, Brooks Low K, Magasanik B, Reznikoff WS, Riley M, Schaechter M, Umbarger HE, vol. 2, 2 edn. Washington D.C.: American Society for Microbiology; 1996: 1683-1692.
73. Vanrolleghem PA, de Jong-Gubbels P, van Gulik WM, Pronk JT, van Dijken JP, Heijnen S. 1996. Validation of a metabolic network for *Saccharomyces cerevisiae* using mixed substrate studies. *Biotechnol Prog* 12:434-448.
74. Gennis RB, Stewart V. Respiration. In: *Escherichia coli* and *Salmonella typhimurium*: Cellular and Molecular Biology. Edited by Neidhardt FC, Curtiss R, Ingraham JL, Brooks Low K, Magasanik B, Reznikoff WS, Riley M, Schaechter M, Umbarger HE, vol. 1, 2 edn. Washington D.C.: American Society for Microbiology; 1996: 217-261.
75. Lequeux G, Johansson L, Maertens J, Vanrolleghem PA, Liden G. 2006. MFA for overdetermined systems reviewed and compared with rna expression data to elucidate the difference in shikimate yield between carbon- and phosphate-limited continuous cultures of *E. coli* W3110.shik1. *Biotechnol Prog* 22:1056-1070.
76. Varma A, Palsson BO. 1993. Metabolic Capabilities of *Escherichia coli* II. Optimal Growth Patterns. *J Theor Biol* 165:503-522.
77. Carlson R, Sreenc F. 2004. Fundamental *Escherichia coli* biochemical pathways for biomass and energy production: creation of overall flux states. *Biotechnol Bioeng* 86:149-162.
78. Tettelin H, Saunders NJ, Heidelberg J, Jeffries AC, Nelson KE, Eisen JA, Ketchum KA, Hood DW, Peden JF, Dodson RJ et al. 2000. Complete genome sequence of *Neisseria meningitidis* serogroup B strain MC58. *Science* 287:1809-1815.
79. Jyssum K. 1962. Dissimilation of C14 labelled glucose by *Neisseria meningitidis* 2. The incorporation of 1-C14 and 6-C14 into pyruvate. *Acta Pathol Microbiol Immunol Scand [B]* 55:335-341.
80. Morse SA, Stein S, Hines J. 1974. Glucose metabolism in *Neisseria gonorrhoeae*. *J Bacteriol* 120:702-714.
81. Santos S, Baruque-Ramos J, Tanizaki MM, Lebrun I, Schenkman RPF. 2006. Production of outer membrane vesicles (OMV) in batch cultivation of *Neisseria meningitidis* serogroup B. *Brazilian Journal of Microbiology* 37:488-493.
82. Catlin BW. 1973. Nutritional profiles of *Neisseria gonorrhoeae*, *Neisseria meningitidis*, and *Neisseria lactamica* in chemically defined media and the use of growth requirements for gonococcal typing. *J Infect Dis* 128:178-194.
83. Fu J, Bailey FJ, King JJ, Parker CB, Robinett RS, Kolodin DG, George HA, Herber WK. 1995. Recent advances in the large scale fermentation of *Neisseria meningitidis* group B for the production of an outer membrane protein complex. *Biotechnology (N Y)* 13:170-174.

APPENDIX 3

A. Simplified model *Neisseria meningitidis* serogroup B

TCA CYCLE

- 1 OXA + ACCOA + H₂O ↔ CIT + COA
- 2 CIT + NADP → AKG + CO₂ + NADPH + H
- 3 AKG + COA + NAD → SUCCOA + NADH + H + CO₂
- 4 SUCCOA + Pi + ADP → SUC + COA + ATP
- 5 SUC + FAD ↔ FADH₂ + FUM
- 6 FUM + H₂O ↔ MAL
- 7 MAL + FAD ↔ FADH₂ + OXA

EMP PATHWAY (glycolysis, gluconeogenesis)

- 8 GLC + ATP ↔ G6P + ADP
- 9 G6P ↔ F6P
- 10 GAP ↔ DHAP
- 11 GAP + DHAP + H₂O → F6P + Pi
- 12 GAP + Pi + NAD + ADP ↔ 3PG + ATP + NADH + H
- 13 3PG ↔ PEP + H₂O
- 14 PEP + ADP ↔ PYR + ATP
- 15 PEP + CO₂ + H₂O → OXA + Pi

PENTOSE PHOSPHATE PATHWAY

- 16 G6P + NADP + H₂O → 6PG + NADPH + H
- 17 6PG + NADP ↔ RU5P + CO₂ + NADPH + H
- 18 RU5P ↔ R5P
- 19 RU5P ↔ X5P
- 20 X5P + R5P ↔ S7P + GAP
- 21 F6P + GAP ↔ E4P + X5P
- 22 S7P + GAP ↔ E4P + F6P

ENTNER DOUDOROFF

- 23 6PG ↔ HD6PG + H₂O
- 24 HD6PG ↔ GAP + PYR

PYRUVATE METABOLISM

- 25 PYR + COA + NAD → ACCOA + CO₂ + NADH + H
- 26 LAC + NAD ↔ PYR + NADH + H
- 27 MAL + NAD ↔ PYR + CO₂ + NADH + H
- 28 ACCOA + Pi ↔ AC-P + COA
- 29 AC-P + ADP ↔ ACE + ATP

AMINO ACIDS

- 30 AKG + NH₃ + NADPH + H ↔ GLU + NADP + H₂O
- 31 GLU + NH₃ + ATP ↔ GLN + Pi + ADP
- 32 GLN + CO₂ + 2 H₂O + 2 ATP ↔ CARBP + GLU + Pi + 2 ADP
- 33 GLU + ATP + 2 NADPH + 2 H → PRO + ADP + Pi + 2 NADP + H₂O
- 34 OXA + GLU ↔ ASP + AKG
- 35 FUM + NH₃ ↔ ASP
- 36 ASP + NH₃ ↔ ASN + H₂O
- 37 ASP + 2 ATP + CARBP + NADPH + H + 2 GLU ↔ ARG + FUM + AKG + AMP + PPi + 2 Pi + ADP + NADP
- 38 ASP + ATP + NADPH + H ↔ ASP4SA + Pi + NADP + ADP
- 39 ASP4SA + H + NADPH ↔ HSER + NADP
- 40 HSER + ATP + H₂O ↔ THR + Pi + ADP
- 41 ASP4SA + PYR + NADH + H + SUCCOA + GLU → mDAP + SUC + AKG + COA + NAD
- 42 mDAP → LYS + CO₂
- 43 THR → OBUT + NH₃
- 44 OBUT + NADPH + H + GLU + PYR ↔ ILE + AKG + NADP + H₂O + CO₂
- 45 HSER + ACCOA + H₂S ↔ HCYS + ACE + COA
- 46 SMTHF + HCYS ↔ THF + MET
- 47 SER + ACCOA + H₂S ↔ CYS + ACE + COA
- 48 SO₄ + 2 ATP + H₂O + RTR → SO₃ + ADP + Pi + AMP + PPi + OTR
- 49 THS + O₂ + H₂O → 2 SO₃ + 2 H
- 50 SO₃ + 3 NADPH + 5 H ↔ H₂S + 3 NADP + 3 H₂O
- 51 SER → PYR + NH₃
- 52 3PG + NAD + GLU + H₂O ↔ SER + AKG + Pi + NADH + H

53 THF + SER \leftrightarrow METHF + GLY + H₂O
 54 2 PYR + NADPH + H \leftrightarrow IVA + H₂O + CO₂ + NADP
 55 IVA + GLU \leftrightarrow VAL + AKG
 56 IVA + ACCOA + H₂O + NAD + GLU \rightarrow LEU + AKG + COA + NADH + H + CO₂
 57 VAL + PYR \leftrightarrow IVA + ALA
 58 R5P + ATP \leftrightarrow PRPP + AMP
 59 PRPP + ATP + 3 H₂O + GLN + 2 NAD \rightarrow HIS + 2 NADH + 2 H + 2 PPi + AICAR + AKG + Pi
 60 E4P + 2 PEP + NADPH + H + ATP \rightarrow CHOR + 4 Pi + NADP + ADP
 61 CHOR \leftrightarrow PRE
 62 PRE + GLU \rightarrow PHE + AKG + CO₂ + H₂O
 63 PRE + NAD + GLU \rightarrow TYR + AKG + CO₂ + NADH + H
 64 CHOR + GLN \leftrightarrow ANT + GLU + PYR
 65 PRPP + ANT + SER \rightarrow TRP + 2 H₂O + PPi + CO₂ + GAP

CARBOHYDRATES

66 G6P \leftrightarrow G1P

ENERGY METABOLISM

67 ATP + H₂O \rightarrow Pi + ADP
 68 PPi + H₂O \rightarrow 2 Pi
 69 O₂ + 2 NADH + 2 H + 2.67 ADP + 2.67 Pi \rightarrow 2.67 ATP + 4.67 H₂O + 2 NAD
 70 FADH₂ + NAD \leftrightarrow FAD + NADH + H
 71 NADPH + NAD \leftrightarrow NADP + NADH

NUCLEOSIDES AND NUCLEOTIDES BIOSYNTHESIS

72 PRPP + 2 GLN + 2 H₂O + GLY + 4 ATP + FTHF + CO₂ + ASP \rightarrow AICAR + FUM + 2 GLU + PPi + 4 Pi + 4 ADP + THF
 73 AICAR + FTHF \leftrightarrow IMP + H₂O + THF
 74 IMP + ASP + GTP \leftrightarrow FUM + AMP + GDP + Pi
 75 AMP + ATP \leftrightarrow 2 ADP
 76 RTR + ATP \leftrightarrow dATP + OTR + H₂O
 77 IMP + NAD + 2 H₂O + 2 ATP + GLN \leftrightarrow GDP + ADP + H + NADH + GLU + AMP + PPi
 78 GDP + ATP \leftrightarrow GTP + ADP
 79 RTR + GDP + ATP \rightarrow dGTP + ADP + OTR + H₂O
 80 CARBP + ASP + O₂ + PRPP \rightarrow UMP + CO₂ + Pi + H₂O + H₂O₂ + PPi
 81 UMP + ATP \leftrightarrow UDP + ADP
 82 UDP + ATP \leftrightarrow UTP + ADP
 83 RTR + UDP + ATP \leftrightarrow dUTP + ADP + OTR + H₂O
 84 dUTP + NH₃ \leftrightarrow dCTP + H₂O
 85 dCTP + ADP + OTR + H₂O \leftrightarrow RTR + CDP + ATP
 86 CDP + ATP \leftrightarrow CTP + ADP
 87 dUTP + H₂O + METHF + 2 ATP \leftrightarrow dTTP + DHF + PPi + 2 ADP
 88 ADP + CDP \leftrightarrow ATP + CMP

LIPID METABOLISM

89 ATP + ACCOA + ACP + CO₂ + H₂O \rightarrow MALACP + COA + ADP + Pi
 90 ACCOA + ACP \leftrightarrow COA + ACACP
 91 ACACP + 5 MALACP + 5 NADPH + 4 NADH + 9 H \rightarrow C12:0-3OHACP + 5 NADP + 4 H₂O + 4 NAD + 5 CO₂ + 5 ACP
 92 ACACP + 5 MALACP + 5 NADPH + 5 NADH + 10 H \rightarrow C12:0ACP + 5 NADP + 5 H₂O + 5 NAD + 5 CO₂ + 5 ACP
 93 ACACP + 6 MALACP + 6 NADPH + 5 NADH + 11 H \rightarrow C14:0-3OHACP + 6 NADP + 5 H₂O + 5 NAD + 6 CO₂ + 6 ACP
 94 ACACP + 6 MALACP + 6 NADPH + 6 NADH + 12 H \rightarrow C14:0ACP + 6 NADP + 6 H₂O + 6 NAD + 6 CO₂ + 6 ACP
 95 ACACP + 7 MALACP + 7 NADPH + 7 NADH + 14 H \rightarrow C16:0ACP + 7 NADP + 7 H₂O + 7 NAD + 7 CO₂ + 7 ACP
 96 ACACP + 8 MALACP + 8 NADPH + 8 NADH + 16 H \rightarrow C18:0ACP + 8 NADP + 8 H₂O + 8 NAD + 8 CO₂ + 8 ACP
 97 ACACP + 7 MALACP + 7 NADPH + 6 NADH + 13 H \rightarrow C16:1ACP + 7 NADP + 7 H₂O + 6 NAD + 7 CO₂ + 7 ACP
 98 ACACP + 8 MALACP + 8 NADPH + 7 NADH + 15 H \rightarrow C18:1ACP + 8 NADP + 8 H₂O + 7 NAD + 8 CO₂ + 8 ACP
 99 DHAP + NADH + H \leftrightarrow GL3P + NAD
 100 GL3P + a C12:0ACP + b C14:0ACP + c C16:1ACP + d C16:0ACP + e C18:1ACP + f C18:0ACP \rightarrow PA + 2 ACP

With stoichiometric coefficients (SC):

SC	$\mu = 0.041 \text{ h}^{-1}$		$\mu = 0.082 \text{ h}^{-1}$		$\mu = 0.161 \text{ h}^{-1}$	
	Exp. 1A	Exp. 1B	Exp. 2A	Exp. 2B	Exp. 3A	Exp. 3B
a	0.01908	0.00712	0	0.01622	0.0028	0.00321
b	0.07762	0.08894	0.08344	0.08271	0.08972	0.09383
c	0.64139	0.65521	0.63863	0.65568	0.59641	0.60579
d	0.97834	0.98099	0.98271	0.95530	0.99614	1.01082
e	0.25498	0.24308	0.27196	0.26676	0.28846	0.26078
f	0.02860	0.02467	0.02324	0.02334	0.02647	0.02556

101 CTP + PA \leftrightarrow CDPDG + PPi
 102 CDPDG + SER \rightarrow PE + CMP + CO₂
 103 CDPDG + GL3P + H₂O \rightarrow PG + CMP + Pi

CELL ENVELOPE BIOSYNTHESIS

- 104 $\text{F6P} + \text{GLN} + \text{ACCOA} + \text{UTP} \rightarrow \text{UDPNAG} + \text{PPi} + \text{COA} + \text{GLU}$
 105 $2.8 \text{ UDPNAG} + 1.4 \text{ NH}_3 + 1.4 \text{ mDAP} + 1.4 \text{ PEP} + 3.8 \text{ ALA} + 1.4 \text{ GLU} + 1.4 \text{ H}_2\text{O} + 0.504 \text{ ACCOA}$
 $+ 12.6 \text{ ATP} + 1.4 \text{ NADPH} + 1.4 \text{ H} \rightarrow \text{PEPTIDO} + 2.8 \text{ UTP} + 0.504 \text{ COA} + 12.6 \text{ ADP} + 1.4 \text{ NADP} + 11.2 \text{ Pi}$
 106 $3 \text{ UDPNAG} + 2 \text{ RUSP} + 2 \text{ PEP} + 2 \text{ C12:0ACP} + 2 \text{ C12:0-3OHACP} + 2 \text{ C14:0-3OHACP} + 2 \text{ S7P}$
 $+ \text{ACA} + \text{NH}_3 + \text{GIP} + \text{UTP} + 2 \text{ CTP} + 4 \text{ ATP} + 9 \text{ H}_2\text{O} \rightarrow \text{LPS} + 2 \text{ ACE} + 6 \text{ ACP} + 4 \text{ ADP} + 3 \text{ UDP}$
 $+ 5 \text{ PPi} + 2 \text{ CMP} + 4 \text{ Pi} + \text{UMP}$

VITAMINS AND COFACTORS

- 107 $2 \text{ ATP} + \text{GLY} + \text{GLU} + \text{CYS} \rightarrow 2 \text{ ADP} + 2 \text{ Pi} + \text{GSH}$
 108 $2 \text{ H}_2\text{O} + \text{GSH} \leftrightarrow \text{CYS} + \text{GLY} + \text{GLU}$
 109 $\text{H}_2\text{O}_2 + 2 \text{ GSH} \rightarrow \text{GSSG} + 2 \text{ H}_2\text{O}$
 110 $\text{GSSG} + \text{NADPH} + \text{H} \rightarrow 2 \text{ GSH} + \text{NADP}$
 111 $\text{OTR} + \text{NADPH} + \text{H} \leftrightarrow \text{RTR} + \text{NADP}$
 112 $\text{FTHF} \leftrightarrow \text{MEYTHF} + \text{H}_2\text{O}$
 113 $\text{MEYTHF} + \text{NADPH} + \text{H} \leftrightarrow \text{METHF} + \text{NADP}$
 114 $\text{DHF} + \text{NADPH} + \text{H} \leftrightarrow \text{THF} + \text{NADP}$
 115 $\text{METHF} + \text{H} + \text{NADH} \leftrightarrow \text{5MTHF} + \text{NAD}$
 116 $\text{THF} + \text{GLY} + \text{NAD} \rightarrow \text{METHF} + \text{NH}_3 + \text{CO}_2 + \text{NADH} + \text{H}$

OTHERS

- 117 $\text{ACA} + \text{H} + \text{NADH} \leftrightarrow \text{ETH} + \text{NAD}$
 118 $\text{ACE} + \text{NADH} + \text{H} \leftrightarrow \text{ACA} + \text{H}_2\text{O} + \text{NAD}$

MACROMOLECULES AND BIOMASS ASSEMBLY

- 119 $0.24236 \text{ dTTP} + 0.25764 \text{ dCTP} + 0.25764 \text{ dGTP} + 0.24236 \text{ dATP} + 1.372 \text{ ATP} + 2.372 \text{ H}_2\text{O} \rightarrow$
 $\text{DNA} + \text{PPi} + 1.372 \text{ ADP} + 1.372 \text{ Pi} + 1.372 \text{ H}$
 120 $0.24268 \text{ UTP} + 0.25557 \text{ CTP} + 0.25972 \text{ GTP} + 0.64204 \text{ ATP} + 1.4 \text{ H}_2\text{O} \rightarrow \text{RNA} + \text{PPi} + 0.4 \text{ ADP} + 0.4 \text{ Pi} + 0.4 \text{ H}$
 121 $\text{a ASP} + \text{b GLU} + \text{c SER} + \text{d HIS} + \text{e GLY} + \text{f THR} + \text{g ALA} + \text{h ARG} + \text{i TYR} + \text{j VAL} + \text{k MET}$
 $+ \text{l PHE} + \text{m ILE} + \text{n LEU} + \text{o LYS} + \text{p PRO} + \text{q ASN} + \text{r TRP} + \text{s CYS} + \text{t GLN} + 4.306 \text{ ATP}$
 $+ 3.306 \text{ H}_2\text{O} \rightarrow 1 \text{ PROT} + 4.306 \text{ ADP} + 4.306 \text{ Pi} + 3.551 \text{ H}$

With stoichiometric coefficients (SC):

SC	$\mu = 0.041 \text{ h}^{-1}$		$\mu = 0.082 \text{ h}^{-1}$		$\mu = 0.161 \text{ h}^{-1}$	
	Exp. 1A	Exp. 1B	Exp. 2A	Exp. 2B	Exp. 3A	Exp. 3B
a	0.051	0.051	0.053	0.054	0.056	0.054
b	0.076	0.068	0.076	0.075	0.067	0.066
c	0.044	0.044	0.045	0.045	0.048	0.048
d	0.018	0.018	0.018	0.018	0.018	0.018
e	0.093	0.092	0.092	0.094	0.095	0.095
f	0.047	0.048	0.048	0.049	0.048	0.048
g	0.149	0.145	0.134	0.139	0.128	0.122
h	0.051	0.058	0.050	0.051	0.057	0.058
i	0.019	0.026	0.019	0.020	0.025	0.025
j	0.072	0.070	0.072	0.073	0.073	0.072
k	0.026	0.023	0.018	0.019	0.015	0.020
l	0.033	0.032	0.033	0.033	0.034	0.035
m	0.048	0.047	0.048	0.049	0.049	0.051
n	0.076	0.074	0.078	0.078	0.080	0.081
o	0.054	0.064	0.068	0.054	0.061	0.061
p	0.035	0.037	0.038	0.038	0.040	0.042
q	0.040	0.039	0.041	0.041	0.043	0.042
r	0.012	0.012	0.012	0.013	0.011	0.011
s	0.009	0.009	0.010	0.010	0.010	0.010
t	0.048	0.044	0.049	0.048	0.043	0.042

- 122 $0.10913 \text{ PA} + 0.71561 \text{ PE} + 0.17525 \text{ PG} \rightarrow \text{LIPID}$

- 123 $\text{a PROT} + \text{b LIPID} + \text{c PEPTIDO} + \text{d LPS} + \text{e DNA} + \text{f RNA} + \text{g ATP} + \text{g H}_2\text{O} \rightarrow \text{BIOMASS} + \text{g ADP} + \text{g Pi} + \text{g H}$

With stoichiometric coefficients (SC):

SC	$\mu = 0.041 \text{ h}^{-1}$		$\mu = 0.082 \text{ h}^{-1}$		$\mu = 0.161 \text{ h}^{-1}$	
	Exp. 1A	Exp. 1B	Exp. 2A	Exp. 2B	Exp. 3A	Exp. 3B
a	0.93577	0.93043	0.94035	0.93817	0.91388	0.89632
b	0.02219	0.02447	0.01706	0.01652	0.02087	0.0215
c	0.00256	0.00259	0.00263	0.00265	0.00274	0.00285
d	0.00262	0.00175	0.00178	0.00202	0.00238	0.00254
e	0.00213	0.00437	0.00276	0.00302	0.00959	0.01116
f	0.03473	0.03639	0.03542	0.03762	0.05054	0.06564
g	13.27	13.27	12.46	12.46	12.56	12.56

MEMBRANE TRANSPORT

```

124     GLC_ext + H_ext → GLC + H
125     CO2 → CO2_ext
126     H ↔ H_ext
127     NH3_ext → NH3
128     O2_ext → O2
129     Pi_ext + H_ext ↔ Pi + H
130     THS_ext + ATP + H2O → THS + ADP + Pi
131     SO4_ext + ATP + H2O → SO4 + ADP + Pi
132     H2S ↔ HS_ext + H_ext
133     GLU + H ↔ GLU_ext + H_ext
134     GLN + H ↔ GLN_ext + H_ext
135     PRO + H ↔ PRO_ext + H_ext
136     ASP + H ↔ ASP_ext + H_ext
137     ASN + H ↔ ASN_ext + H_ext
138     ARG + H ↔ ARG_ext + H_ext
139     THR + H ↔ THR_ext + H_ext
140     LYS + H ↔ LYS_ext + H_ext
141     ILE + H ↔ ILE_ext + H_ext
142     MET + H ↔ MET_ext + H_ext
143     SER + H ↔ SER_ext + H_ext
144     CYS + H ↔ CYS_ext + H_ext
145     GLY + H ↔ GLY_ext + H_ext
146     VAL + H ↔ VAL_ext + H_ext
147     LEU + H ↔ LEU_ext + H_ext
148     ALA + H ↔ ALA_ext + H_ext
149     HIS + H ↔ HIS_ext + H_ext
150     PHE + H ↔ PHE_ext + H_ext
151     TYR + H ↔ TYR_ext + H_ext
152     TRP + H ↔ TRP_ext + H_ext
153     LAC + H ↔ LAC_ext + H_ext
154     ETH → ETH_ext
155     ACE + H ↔ ACE_ext + H_ext
156     PROT → PROT_ext

```

B. Fluxdistributions

The calculated fluxes and calculated production rates (x), normalised to biomass production rate, including their normalised standard deviation (SD) of the determined reactions are shown as: Value \pm SD (mmol.g⁻¹.h⁻¹). The calculated fluxes and calculated production rates, normalised to biomass production rate, of the under-determined reactions are shown as flux ranges: Value-1·SD - flux+1·SD (mmol.g⁻¹.h⁻¹). These range values are based on the split ratio analysis as described in the main text.

RNo. / flux	x ($\mu = 0.041$ h ⁻¹)			x ($\mu = 0.082$ h ⁻¹)			x ($\mu = 0.161$ h ⁻¹)		
1	5.17	-	27.83	4.57	-	24.52	4.65	-	19.16
2	5.17	-	27.80	4.56	-	24.55	4.66	-	19.14
3	3.04	-	25.68	2.38	-	22.39	2.64	-	17.13
4	2.38	-	25.01	1.78	-	21.70	2.04	-	16.52
5	3.03	-	25.69	2.39	-	22.36	2.64	-	17.14
6	4.08	-	26.76	3.38	-	23.33	3.89	-	18.39
7	9.18	-	31.88	8.53	-	28.51	8.93	-	23.40
8	25.07	\pm	1.17	22.46	\pm	1.19	20.45	\pm	1.00
9	-38.74	-	1.01	-32.55	-	0.93	-22.30	-	1.17
10	0.26	-	0.29	0.19	-	0.20	0.24	-	0.25
11	0.00	-	0.00	0.00	-	0.00	0.00	-	0.00
12	21.89	-	24.26	19.52	-	21.98	17.45	-	19.38
13	20.11	-	22.46	17.76	-	20.24	15.50	-	17.45
14	18.35	-	20.65	16.28	-	18.78	14.09	-	16.01
15	0.00	-	0.00	0.00	-	0.00	0.00	-	0.00
16	58.98	-	25.24	50.22	-	22.75	39.48	-	20.29
17	54.22	-	0.00	44.93	-	0.00	31.69	-	0.00
18	18.82	-	0.81	15.68	-	0.72	11.43	-	0.91
19	35.35	-	-0.77	29.20	-	-0.71	20.20	-	-0.87
20	18.13	-	0.07	14.97	-	0.00	10.46	-	-0.07
21	-19.01	-	0.89	-16.00	-	0.76	-10.89	-	0.84
22	18.07	-	0.02	14.94	-	-0.03	10.41	-	-0.12
23	4.77	-	25.23	5.30	-	22.75	7.81	-	20.30
24	4.77	-	25.24	5.30	-	22.75	7.81	-	20.31
25	12.38	-	35.12	10.83	-	30.78	11.61	-	26.03
26	-0.17	\pm	0.04	-0.12	\pm	0.08	-0.08	\pm	0.02
27	-5.21	-	-5.00	-5.28	-	-5.03	-5.14	-	-4.92
28	1.43	\pm	0.38	1.60	\pm	0.23	1.37	\pm	0.34
29	1.43	\pm	0.38	1.60	\pm	0.23	1.37	\pm	0.34
30	13.18	-	13.93	12.93	-	13.52	13.05	-	13.60
31	2.15	\pm	0.09	2.12	\pm	0.05	2.59	\pm	0.11
32	0.74	\pm	0.05	0.70	\pm	0.02	0.89	\pm	0.03
33	0.35	\pm	0.01	0.38	\pm	0.01	0.39	\pm	0.01
34	3.88	-	4.18	3.88	-	4.06	4.17	-	4.35
35	0.00	-	0.00	0.00	-	0.00	0.00	-	0.00
36	0.39	\pm	0.01	0.41	\pm	0.01	0.40	\pm	0.02
37	0.55	\pm	0.04	0.51	\pm	0.01	0.55	\pm	0.01
38	1.88	\pm	0.04	1.84	\pm	0.07	1.75	\pm	0.04
39	1.22	\pm	0.03	1.19	\pm	0.03	1.14	\pm	0.02

RNo. / flux	x ($\mu = 0.041 \text{ h}^{-1}$)			x ($\mu = 0.082 \text{ h}^{-1}$)			x ($\mu = 0.161 \text{ h}^{-1}$)		
40	0.97	\pm	0.02	1.00	\pm	0.02	0.97	\pm	0.03
41	0.66	\pm	0.02	0.65	\pm	0.07	0.61	\pm	0.02
42	0.63	\pm	0.02	0.61	\pm	0.07	0.57	\pm	0.02
43	0.47	\pm	0.01	0.48	\pm	0.01	0.47	\pm	0.01
44	0.47	\pm	0.01	0.48	\pm	0.01	0.47	\pm	0.01
45	0.24	\pm	0.02	0.19	\pm	0.01	0.16	\pm	0.02
46	0.24	\pm	0.02	0.19	\pm	0.01	0.16	\pm	0.02
47	0.09	\pm	0.00	0.10	\pm	0.00	0.09	\pm	0.00
48	0.00	-	0.00	0.00	-	0.00	0.00	-	0.00
49	0.16	-	0.17	0.14	-	0.15	0.12	-	0.14
50	0.32	-	0.35	0.28	-	0.29	0.24	-	0.28
51	0.00	-	0.00	0.00	-	0.00	0.00	-	0.00
52	1.74	-	1.83	1.70	-	1.78	1.89	-	2.00
53	0.98	\pm	0.03	0.95	\pm	0.03	1.15	\pm	0.06
54	1.45	\pm	0.03	1.50	\pm	0.03	1.44	\pm	0.04
55	2.26	\pm	0.04	2.19	\pm	0.06	1.98	\pm	0.09
56	0.75	\pm	0.01	0.78	\pm	0.02	0.76	\pm	0.02
57	1.56	\pm	0.03	1.47	\pm	0.04	1.30	\pm	0.06
58	0.71	\pm	0.06	0.70	\pm	0.02	0.97	\pm	0.07
59	0.21	\pm	0.04	0.18	\pm	0.00	0.18	\pm	0.01
60	0.86	\pm	0.05	0.70	\pm	0.02	0.67	\pm	0.02
61	0.74	\pm	0.05	0.57	\pm	0.02	0.57	\pm	0.01
62	0.50	\pm	0.04	0.37	\pm	0.01	0.33	\pm	0.01
63	0.24	\pm	0.02	0.20	\pm	0.01	0.23	\pm	0.01
64	0.12	\pm	0.00	0.12	\pm	0.01	0.10	\pm	0.00
65	0.12	\pm	0.00	0.12	\pm	0.01	0.10	\pm	0.00
66	0.022	\pm	0.004	0.019	\pm	0.001	0.025	\pm	0.001
67	136.08	-	197.17	104.70	-	167.11	67.81	-	115.56
68	2.28	-	2.56	2.19	-	2.33	2.89	-	3.21
69	66.41	-	79.95	55.07	-	69.90	42.67	-	54.38
70	12.21	-	57.54	10.91	-	50.84	11.58	-	40.55
71	93.26	-	27.61	76.07	-	23.60	51.53	-	15.12
72	0.19	\pm	0.01	0.20	\pm	0.01	0.34	\pm	0.04
73	0.40	\pm	0.05	0.38	\pm	0.01	0.52	\pm	0.03
74	0.30	\pm	0.04	0.27	\pm	0.01	0.35	\pm	0.02
75	1.51	-	1.81	1.53	-	1.62	1.94	-	2.14
76	0.01	\pm	0.00	0.01	\pm	0.00	0.03	\pm	0.00
77	0.10	\pm	0.01	0.10	\pm	0.00	0.18	\pm	0.02
78	0.39	\pm	0.05	0.37	\pm	0.01	0.50	\pm	0.03
79	0.01	\pm	0.00	0.01	\pm	0.00	0.03	\pm	0.00
80	0.19	\pm	0.01	0.20	\pm	0.01	0.34	\pm	0.04
81	0.22	\pm	0.01	0.22	\pm	0.01	0.37	\pm	0.04
82	0.17	\pm	0.02	0.16	\pm	0.01	0.24	\pm	0.02
83	0.11	\pm	0.01	0.11	\pm	0.00	0.20	\pm	0.02
84	0.10	\pm	0.01	0.10	\pm	0.00	0.17	\pm	0.02
85	0.09	\pm	0.00	0.09	\pm	0.00	0.15	\pm	0.02

RNo. / flux	x ($\mu = 0.041 \text{ h}^{-1}$)			x ($\mu = 0.082 \text{ h}^{-1}$)			x ($\mu = 0.161 \text{ h}^{-1}$)		
86	0.34	\pm	0.01	0.28	\pm	0.01	0.39	\pm	0.02
87	0.01	\pm	0.00	0.01	\pm	0.00	0.03	\pm	0.00
88	-0.25	\pm	0.00	-0.19	\pm	0.00	-0.24	\pm	0.00
89	4.00	\pm	0.07	2.99	\pm	0.06	3.80	\pm	0.07
90	0.60	\pm	0.01	0.45	\pm	0.01	0.57	\pm	0.01
91	0.04	\pm	0.01	0.04	\pm	0.00	0.05	\pm	0.00
92	0.05	\pm	0.01	0.04	\pm	0.00	0.05	\pm	0.00
93	0.04	\pm	0.01	0.04	\pm	0.00	0.05	\pm	0.00
94	0.02	\pm	0.00	0.01	\pm	0.00	0.02	\pm	0.00
95	0.23	\pm	0.01	0.16	\pm	0.01	0.21	\pm	0.00
96	0.01	\pm	0.00	0.00	\pm	0.00	0.01	\pm	0.00
97	0.15	\pm	0.01	0.11	\pm	0.00	0.13	\pm	0.00
98	0.06	\pm	0.00	0.05	\pm	0.00	0.06	\pm	0.00
99	0.27	\pm	0.01	0.20	\pm	0.00	0.25	\pm	0.00
100	0.23	\pm	0.01	0.17	\pm	0.00	0.21	\pm	0.00
101	0.21	\pm	0.01	0.15	\pm	0.00	0.19	\pm	0.00
102	0.17	\pm	0.01	0.12	\pm	0.00	0.15	\pm	0.00
103	0.04	\pm	0.00	0.03	\pm	0.00	0.04	\pm	0.00
104	0.138	\pm	0.013	0.131	\pm	0.005	0.152	\pm	0.003
105	0.026	\pm	0.000	0.026	\pm	0.001	0.028	\pm	0.001
106	0.022	\pm	0.004	0.019	\pm	0.001	0.025	\pm	0.001
107	0.00	-	0.00	0.00	-	0.00	0.00	-	0.00
108	0.00	-	0.00	0.00	-	0.00	0.00	-	0.00
109	0.19	\pm	0.01	0.20	\pm	0.01	0.34	\pm	0.04
110	0.19	\pm	0.01	0.20	\pm	0.01	0.34	\pm	0.04
111	0.02	-	0.04	0.03	-	0.03	0.10	-	0.11
113	-0.60	\pm	0.06	-0.57	\pm	0.02	-0.87	\pm	0.07
114	-0.60	\pm	0.06	-0.57	\pm	0.02	-0.87	\pm	0.07
115	0.01	\pm	0.00	0.01	\pm	0.00	0.03	\pm	0.00
116	0.24	\pm	0.02	0.19	\pm	0.01	0.16	\pm	0.02
117	-0.13	\pm	0.02	-0.18	\pm	0.00	-0.09	\pm	0.04
118	1.61	\pm	0.36	1.77	\pm	0.22	1.57	\pm	0.35
119	1.63	\pm	0.36	1.79	\pm	0.22	1.59	\pm	0.35
121	0.032	\pm	0.011	0.029	\pm	0.001	0.104	\pm	0.006
122	0.36	\pm	0.01	0.37	\pm	0.01	0.58	\pm	0.07
123	9.85	\pm	0.21	9.94	\pm	0.22	9.40	\pm	0.28
124	0.23	\pm	0.01	0.17	\pm	0.00	0.21	\pm	0.00
125	10.00	\pm	0.18	10.00	\pm	0.20	10.00	\pm	0.26
126	25.07	\pm	1.17	22.46	\pm	1.19	20.45	\pm	0.99
127	80.21	\pm	6.77	68.53	\pm	7.35	54.37	\pm	6.00
128	24.69	\pm	1.18	22.39	\pm	1.22	20.88	\pm	1.00
129	15.93	\pm	0.44	15.61	\pm	0.34	16.18	\pm	0.32
130	73.61	\pm	6.68	63.00	\pm	7.21	48.86	\pm	6.01
131	0.69	\pm	0.02	0.62	\pm	0.02	0.97	\pm	0.07
132	0.16	-	0.17	0.14	-	0.15	0.12	-	0.14
133	0.00	-	0.00	0.00	-	0.00	0.00	-	0.00

RNo. / flux	x ($\mu = 0.041 \text{ h}^{-1}$)			x ($\mu = 0.082 \text{ h}^{-1}$)			x ($\mu = 0.161 \text{ h}^{-1}$)		
134	0.00	-	0.00	0.00	-	0.00	0.00	-	0.00
135	0.02	\pm	0.01	0.01	\pm	0.00	0.01	\pm	0.00
136	0.01	\pm	0.01	0.00	\pm	0.00	0.00	\pm	0.00
137	0.00	\pm	0.00	0.00	\pm	0.00	0.00	\pm	0.00
138	0.03	\pm	0.00	0.02	\pm	0.00	0.01	\pm	0.00
139	0.00	\pm	0.00	0.00	\pm	0.00	0.00	\pm	0.00
140	0.01	\pm	0.01	0.00	\pm	0.00	0.01	\pm	0.00
141	0.04	\pm	0.01	0.04	\pm	0.01	0.05	\pm	0.01
142	0.04	\pm	0.00	0.00	\pm	0.00	0.00	\pm	0.00
143	0.00	\pm	0.00	0.00	\pm	0.00	0.00	\pm	0.00
144	0.00	\pm	0.00	0.00	\pm	0.00	0.00	\pm	0.00
145	0.00	\pm	0.00	0.00	\pm	0.00	0.00	\pm	0.00
146	0.00	\pm	0.00	0.00	\pm	0.00	0.00	\pm	0.00
147	0.00	\pm	0.00	0.00	\pm	0.00	0.00	\pm	0.00
148	0.00	\pm	0.00	0.00	\pm	0.00	0.00	\pm	0.00
149	0.01	\pm	0.01	0.00	\pm	0.00	0.00	\pm	0.00
150	0.01	\pm	0.01	0.01	\pm	0.00	0.01	\pm	0.01
151	0.03	\pm	0.00	0.00	\pm	0.00	0.01	\pm	0.00
152	0.18	\pm	0.04	0.05	\pm	0.01	0.01	\pm	0.00
153	0.02	\pm	0.00	0.00	\pm	0.00	0.00	\pm	0.00
154	0.00	\pm	0.00	0.00	\pm	0.00	0.00	\pm	0.00
155	0.17	\pm	0.04	0.12	\pm	0.08	0.08	\pm	0.02
156	1.61	\pm	0.36	1.77	\pm	0.22	1.57	\pm	0.35
157	0.17	\pm	0.04	0.13	\pm	0.08	0.08	\pm	0.02
158	0.51	\pm	0.16	0.55	\pm	0.12	0.35	\pm	0.08
H ₂ O (calculated)	108.50	-	122.43	95.17	-	109.84	84.74	-	96.44
H _{ext} (calculated)	-0.347	-	-0.316	-0.295	-	-0.278	-0.277	-	-0.239
P _i _{ext} (calculated)	-0.69	\pm	0.02	-0.62	\pm	0.02	-0.97	\pm	0.07
THS _{ext} (calculated)	-0.173	-	-0.158	-0.147	-	-0.143	-0.138	-	-0.120
SO ₄ _{ext} (calculated)	0.00	-	0.00	0.00	-	0.00	0.00	-	0.00
HS _{ext} (calculated)	0.00	-	0.00	0.00	-	0.00	0.00	-	0.00
CO ₂ _{ext} (measured)	80.21	\pm	6.76	68.53	\pm	7.31	54.37	\pm	6.03
NH ₃ _{ext} (measured)	-15.93	\pm	0.44	-15.61	\pm	0.34	-16.18	\pm	0.32
O ₂ _{ext} (measured)	-73.61	\pm	6.70	-63.00	\pm	7.28	-48.86	\pm	6.05
BIOMASS (measured)	10.00	\pm	0.18	10.00	\pm	0.20	10.00	\pm	0.26
GLC _{ext} (measured)	-25.07	\pm	1.19	-22.46	\pm	1.19	-20.45	\pm	1.00
GLU _{ext} (measured)	0.02	\pm	0.01	0.01	\pm	0.00	0.01	\pm	0.00
GLN _{ext} (measured)	0.01	\pm	0.01	0.00	\pm	0.00	0.00	\pm	0.00
PRO _{ext} (measured)	0.00	\pm	0.00	0.00	\pm	0.00	0.00	\pm	0.00
ASP _{ext} (measured)	0.03	\pm	0.00	0.02	\pm	0.00	0.01	\pm	0.00
ASN _{ext} (measured)	0.00	\pm	0.00	0.00	\pm	0.00	0.00	\pm	0.00
ARG _{ext} (measured)	0.01	\pm	0.01	0.00	\pm	0.00	0.01	\pm	0.00
THR _{ext} (measured)	0.04	\pm	0.01	0.04	\pm	0.01	0.05	\pm	0.01
LYS _{ext} (measured)	0.04	\pm	0.00	0.00	\pm	0.00	0.00	\pm	0.00
ILE _{ext} (measured)	0.00	\pm	0.00	0.00	\pm	0.00	0.00	\pm	0.00
MET _{ext} (measured)	0.00	\pm	0.00	0.00	\pm	0.00	0.00	\pm	0.00

RNo. / flux	x ($\mu = 0.041 \text{ h}^{-1}$)			x ($\mu = 0.082 \text{ h}^{-1}$)			x ($\mu = 0.161 \text{ h}^{-1}$)		
SER_ext (measured)	0.00	\pm	0.00	0.00	\pm	0.00	0.00	\pm	0.00
CYS_ext (measured)	0.00	\pm	0.00	0.00	\pm	0.00	0.00	\pm	0.00
GLY_ext (measured)	0.00	\pm	0.00	0.00	\pm	0.00	0.00	\pm	0.00
VAL_ext (measured)	0.00	\pm	0.00	0.00	\pm	0.00	0.00	\pm	0.00
LEU_ext (measured)	0.01	\pm	0.01	0.00	\pm	0.00	0.00	\pm	0.00
ALA_ext (measured)	0.01	\pm	0.01	0.01	\pm	0.00	0.01	\pm	0.01
HIS_ext (measured)	0.03	\pm	0.00	0.00	\pm	0.00	0.01	\pm	0.00
PHE_ext (measured)	0.18	\pm	0.04	0.05	\pm	0.01	0.01	\pm	0.00
TYR_ext (measured)	0.02	\pm	0.00	0.00	\pm	0.00	0.00	\pm	0.00
TRP_ext (measured)	0.00	\pm	0.00	0.00	\pm	0.00	0.00	\pm	0.00
LAC_ext (measured)	0.17	\pm	0.04	0.12	\pm	0.08	0.08	\pm	0.02
ETH_ext (measured)	1.61	\pm	0.36	1.77	\pm	0.22	1.57	\pm	0.35
ACE_ext (measured)	0.17	\pm	0.04	0.13	\pm	0.08	0.08	\pm	0.02
PROT_ext (measured)	0.51	\pm	0.16	0.55	\pm	0.12	0.35	\pm	0.08

Chapter 4

Heterologous expression of phosphofructokinase in *Neisseria meningitidis*

This chapter has been submitted for publication as: Baart GJE, Langenhof M, van de Waterbeemd B, Hamstra HJ, Zomer B, Beuvery EC, Tramper J, Martens DE. 2008. Heterologous expression of phosphofructokinase in *Neisseria meningitidis*.

ABSTRACT

At the Netherlands Vaccine Institute (NVI) a vaccine against serogroup B meningococci, a human pathogen that can infect diverse sites within the human host, is currently being developed. An important aspect in this development trajectory is the development of a consistent cultivation step. The consistency of the cultivation step, relies on the applied environmental conditions, which should be in accordance with the *N. meningitidis* (primary) metabolism. According to the genomic information for *N. meningitidis* and experimental observations glucose can be completely catabolized through the Entner-Doudoroff pathway (ED) and the pentose phosphate pathway (PP). The Embden-Meyerhof-Parnas glycolytic pathway (EMP) is not functional, because the gene for phosphofructokinase (*pfkA*) is not present. The phylogenetic distribution of phosphofructokinase (PFK) indicates that in most obligate aerobic organisms PFK is lacking. We conclude that this is because of the limited contribution of PFK to the energy supply in aerobically grown organisms in comparison with the energy generated through oxidative phosphorylation. Under anaerobic or microaerobic conditions the available energy is limiting and PFK provides an advantage, which explains the presence of PFK in many (facultative) anaerobic organisms. *In silico* flux balance analysis predicted an increase of biomass yield as a result of PFK expression. However, analysis of a genetically engineered *N. meningitidis* strain that expresses a heterologous PFK showed that the yield of biomass on substrate decreased in comparison with a *pfkA* deficient control strain which was compensated mainly by an increase in CO₂ production, whereas production of by-products was comparable between the two strains. This might explain why the *pfkA* gene is not obtained by horizontal gene transfer, since it is initially unfavourable for biomass yield. No large effects related to expression of *pfkA* were observed in the transcriptome. Although our results suggest that introduction of PFK does not contribute to a more efficient strain in terms of biomass yield, achievement of a robust, optimal metabolic network that enables a higher growth rate or a higher biomass yield, might be possible after adaptive evolution of the strain, which remains to be investigated.

INTRODUCTION

The species *Neisseria meningitidis* (meningococcus) is only found in humans and colonizes mucosal surfaces of the nasopharynx as a harmless commensal organism and, as such, is carried by at least five to ten percent of the adult population [1, 2]. Some strains are able to cross the mucosa into the bloodstream from where they can cause the diseases meningitis or septicaemia. There are different pathogenic *N. meningitidis* isolates of which five serogroups (A, B, C, Y, and W135) are responsible for most of the disease. Conjugate-polysaccharide vaccines that offer protection against infection with meningococcal serogroups A, C, Y and W-135 are effective and have been widely used [3, 4]. However, a broadly protective vaccine against infection by serogroup B *N. meningitidis* is not yet available, while this serogroup contributes significantly to the burden of meningococcal disease in many industrialized countries where both epidemic and endemic serogroup B infections occur [5].

Since the polysaccharide of the serogroup B meningococcus is poorly immunogenic [6], alternative vaccine approaches are needed for this bacterium. Current vaccine development against serogroup B strains has mainly focussed on subcapsular protein antigens that are contained in outer membrane vesicles [3]. The outer membrane protein porin A (PorA) has been identified as a major inducer of, and target for serum bactericidal antibodies and is expressed by almost all meningococci, pinpointing porA as a promising vaccine candidate [7]. Vaccines effective against specific strains responsible for serogroup B epidemic disease have been developed [5], but due to the heterogeneity of porA the development of a safe serogroup B vaccine that is cross protective against multiple strains and is effective in infants and young children is an absolute requirement. At the Netherlands Vaccine Institute (NVI) a cross-protective multivalent vaccine against serogroup B organisms, including different PorA subtypes contained in outer membrane vesicles (OMVs) is currently being developed. The vaccine process development focuses on cultivation of the organism, extraction of OMVs and

subsequent purification of the PorA containing OMVs [8]. Knowledge about the primary metabolism is essential for the development of a consistent cultivation step in the vaccine production process. For this reason a *N. meningitidis* serogroup B genome-scale metabolic model has been build and used to study primary metabolism [9, 10]. Earlier studies on glucose utilization in *N. meningitidis* confirm the presence of enzymes related to the glycolytic Embden-Meyerhof-Parnas (EMP) pathway, the Entner-Doudoroff (ED) pathway and the pentose phosphate (PP) pathway [11-16] (Figure 4.1). However, it was found that the EMP pathway does not contribute to pyruvate synthesis, indicating that, the EMP pathway is not functional. These observations were in accordance with the *N. meningitidis* serogroup B genome [17] in which a gene encoding phosphofructokinase (PFK) is not present. In order to possibly improve the efficiency of the cultivation step in the vaccine production process we extended the *N. meningitidis* metabolism with PFK. Furthermore, we used a comparative genomics approach to establish which factors determine the presence or absence of PFK in bacteria.

PFK (EC 2.7.1.11) is a key enzyme in glycolysis and is known to be regulated by allosteric effectors. The regulation of enzymes by allosteric effectors is a major mechanism of metabolic control, since it couples the activity of an enzyme to changes in the concentrations of metabolites produced by reactions that are distant in the metabolic network. PFK catalyzes the irreversible phosphorylation of fructose-6-phosphate (F6P) to fructose-1,6-bisphosphate (FBP) using ATP and is allosterically inhibited by phosphoenolpyruvate (PEP) and activated by ADP (or GDP) when the energy demand of the cell increases [18]. The ATP-PFK described above (PFK-1) is broadly distributed in Eukaryota and Bacteria, as indicated by homologous protein sequences and biochemical evidence [19], and is encoded by the *pfkA* gene. A second type of ATP-PFK enzyme (PFK-2), found strictly in *Escherichia coli* and encoded by the *pfkB* gene, has a minor activity (ca. 10% of the total) [20] and is inhibited by ATP at low concentrations of F6P [21]. The inorganic pyrophosphate (PPi) dependent phosphofructo-

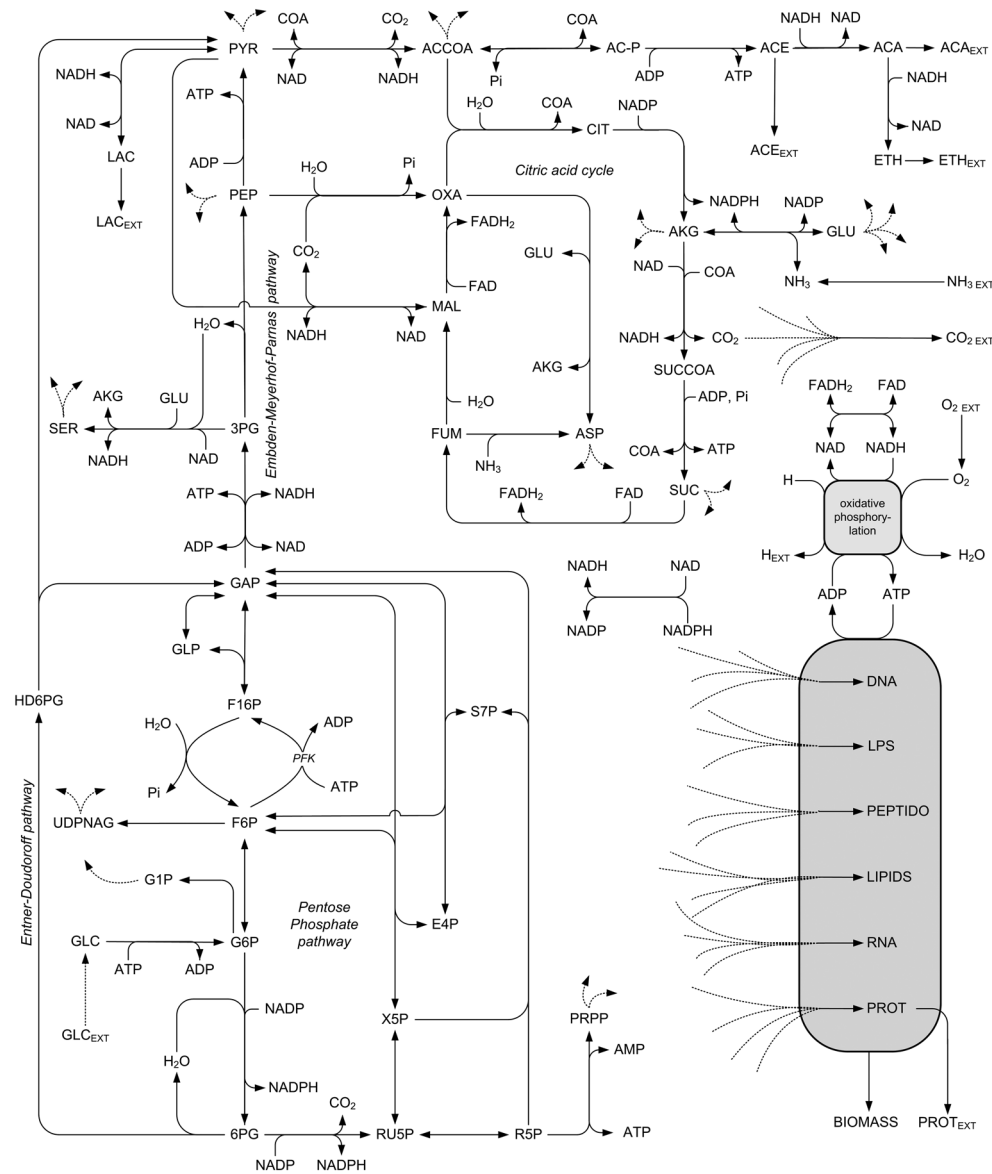


Figure 4.1 Overview of the *N. meningitidis* metabolism. The gene encoding phosphofructokinase (PFK) is not present in *N. meningitidis*. Abbreviations are listed in Appendix 2.2

kinase (PPi-PFK) catalyses the same reaction using PPi in a reversible way and can thus function in both glycolysis and gluconeogenesis. PPi-PFK (EC 2.7.1.90) has a more limited distribution, but is also found in Eukaryota and Bacteria [19]. ATP-PFK and PPi-PFK share a common ancestry, but phylogenies show a very complex evolutionary pattern [22, 23]. Some Archaea contain a unique ADP dependent PFK (ADP-PFK) that appears to be phylogenetically distinct and instead belongs to the glucokinase family of kinases [24, 25]. Baptiste and co-workers [19] addressed the taxonomic distribution of ATP- and PPi-dependent phosphofructokinases and concluded that numerous horizontal gene transfer events and substitution of amino acids in its catalytic sites appear to occur at high rate. In fact, a single point mutation can induce a change of the phospho-donor [26]. The presence of PFK in several bacterial species of which the genomes have been sequenced and the absence in closely related species strongly suggest that this enzyme can be lost during evolution [19]. None of the mentioned types of PFK are present in *N. meningitidis*.

If it is assumed that *N. meningitidis* once had a functional PFK and during the evolution of the species this activity was lost [19], the question why *N. meningitidis* lost PFK activity remains. In particular, since glucose is present within nasopharyngeal tissue [27] the presence of PFK can yield one additional ATP per unit consumed substrate, which is the case for all substrates that enter the level above fructose-6-phosphate in metabolism.

In each genus, transformation is discriminant in favor of its own and against foreign DNA through sequence specificity of DNA receptors. In pathogenic *Neisseria* species transformation mainly occurs to induce genetic variability. Pathogenic *Neisseria* species are naturally competent for DNA uptake from their environment [28] and transformation is the predominant source of new genetic information that is integrated into the genome [29]. Transformation of *Neisseria* is correlated with the presence of a 5'-GCCGTCTGAA-3' DNA uptake sequence (DUS) in the exogenous DNA, type IV

pilus expression and homologous recombination mediated by recombinase A (RecA) [30]. It has been shown that *Neisseria* species preferably take up DUS-containing DNA found within its own genus [30, 31] and this process of DNA exchange by horizontal gene transfer (HZT), also known as lateral gene transfer (LGT), has been implicated in the evolution of *argF* [32], alteration of *penA* resulting in penicillin resistance [33], pilin antigenic variation [34] and other genetic alterations. Since none of the *Neisseria* species, of which the complete genome sequences are publically available, contain PFK homologues [17, 35-38], HZT events within and between *Neisseria* species can never result in PFK functionality. However, DNA exchange between phylogenetically divergent species is possible [39] as shown by the acquisition of *sodC* in *N. meningitidis* from *Haemophilus influenza* by HZT [28]. Since *H. influenza* contains a gene encoding *pfkA* the possibility for *N. meningitidis* to obtain this gene exists. Hence, the question why *N. meningitidis* did not acquire the *pfkA* gene from for instance *H. influenza* in order to possibly enhance growth like in *E. coli* remains puzzling.

In order to establish what determines the presence or absence of PFK in an organism we used phylogenetic profiling and literature as a starting point. In addition, we engineered a recombinant *N. meningitidis* strain to determine the influence of heterologous expression of PFK on biomass yield and composition and analyzed the strain on the metabolic and transcriptomic level.

MATERIALS AND METHODS

Bacterial strains and growth conditions

Competent *E. coli* cells (Invitrogen, Carlsbad, CA, USA) were used for cloning purposes. Transformants of *E. coli* were grown overnight at 37 °C in an aerobic humid atmosphere containing 5% CO₂, on solid or liquid Luria–Bertani medium (BD, Franklin Lakes, NJ, USA) containing either 100 µg.mL⁻¹ kanamycin or 100 µg.mL⁻¹ ampicillin, and, when necessary, 1 mM IPTG and X-gal. *N. meningitidis* strain HB-1, a non-encapsulated, non-piliated variant of the group B isolate H44/76 [40] was used for genetic modification. Untransformed *N. meningitidis* HB-1 cells were grown overnight on GC medium base plates (BD, Franklin Lakes, NJ, USA) supplemented with IsoVitalX (BD, Franklin Lakes, NJ, USA) or in liquid meningococcal medium [41], while HB-1 derivatives were grown on the GC medium base plates containing kanamycin (100 µg.ml⁻¹). All incubations were done in a CO₂ incubator at 37 °C in a humid atmosphere containing 5% CO₂. The final *N. meningitidis* HB-1 mutants (HB-1+*kanR* and HB-1+*kanR+pfkA*) were used to generate bacterial stock-cultures using chemically defined medium [9] to ensure starting material of constant quality for the chemostat cultures. After the addition of glycerol (20%, final concentration) the stock cultures were stored at -135 °C and when required a 500 mL shake flask, containing 150 ml medium was inoculated with 10 ml stock culture that contained 0.5 g.L⁻¹ biomass. After approximately 8 hours of incubation at 35 °C with shaking at 200 rpm in an aerobic humid atmosphere, the culture was used to inoculate the bioreactor. Bacteria were grown on minimal chemically defined medium [9] in 3-L autoclavable ADI bioreactors (Applikon, Schiedam, The Netherlands), operated in chemostat mode, with a working volume of 1.4 L. Temperature, pH, dissolved oxygen (DO) concentration and stirrer speed were controlled at 37 °C, 7.0, 30% and 600 rpm, respectively. The total gas flow rate was kept constant at 1.0 L.min⁻¹. The oxygen concentration was controlled by changing the oxygen fraction in the gasflow using headspace aeration only. The growth rate was controlled at 0.13 h⁻¹. After at least

four residence times physiological steady state was assumed based on online measurements (constant DO signal, O₂ and CO₂-concentration in the offgas) and offline measurements (constant optical density, glucose concentration). In steady state, four small samples were taken using a rapid sampling procedure as described below, and a large 1.0 L sample was taken, divided into portions and processed as described before [9]. All chemostats were run in duplicate.

Analytical procedures

Dry biomass concentration was determined in fourfold for each steady state sample by centrifugation (8000 g) of 50-200 mL of culture broth in preweighed tubes followed by drying (24 h, 80 °C). Before weighing, the tubes were cooled in a dessicator for at least 1 h and dry cell weight was corrected for salts present in the medium. The O₂ and CO₂ concentrations in the exhaust gas from the chemostat cultures were measured with a mass spectrometer (Prima White Box 600, Thermo Electron, United Kingdom). The volumetric oxygen transfer coefficient, k_La , in the bioreactors was determined accurately at 37 °C using a steady state set-up similar to Dorresteyn [42]. Glucose, lactate and ammonium in the culture supernatant were determined as described before [9]. Acetate, ethanol and other possible metabolites present in the culture supernatant were determined by ¹H-NMR as described before [9]. The molecular and macro-molecular composition of biomass was determined experimentally as described before [9, 10], which is very important in mathematical modeling of cellular metabolism [43, 44]. PFK activity was measured enzymatically in cell-free extracts using a coupling enzyme assay [45]. Briefly, the cell-free extract was obtained by applying five freeze/thaw cycles to a concentrated cell suspension in MilliQ water, followed by centrifugation (8000 g, 30 min), to remove insoluble cellular fragments, and sterilization of the lysate by filtration (0.22 µm). To determine PFK-activity, 50 ml of cell-free extract was added to 900 ml of a 55.56 mM Tris-HCl buffer (pH 7.5) containing 5.56 mM MgCl₂, 55.56 mM KCl, 1.39 mM ATP, 0.17 mM NADH, 1.8 U.ml⁻¹ aldolase, 8.89 U.ml⁻¹ triose phosphate isomerase and 2.27 U.ml⁻¹ glycerol phosphate dehydro-

genase. The reaction was started by adding 50 ml of fructose-6-phosphate solution (100 mM). PFK-activity was determined by measuring the decrease in absorption at 340 nm (as a consequence of NADH-oxidation) during 10 min. *E. coli* cell-free extract was used as a positive control for PFK-activity, whereas cell-free extract of *N. meningitidis* HB-1+*kanR* was used as a negative control.

Recombinant DNA techniques

Since *E. coli* plasmids are not able to persist in *N. meningitidis* and because no high copy number plasmids exist for *N. meningitidis*, heterologous expression of a gene can only be achieved by homologous recombination. To use this strategy, the gene of interest has to be inserted into a vector between DNA-sequences homologous to the site at which the gene has to be inserted into the genome. Besides being used for homologous recombination, these homologous sequences must also contain a DUS as explained in the introduction section. A kanamycin resistance gene must be present between the homologous regions to select for transformants after transformation. The final plasmid constructed in this study that was used for transformation of *N. meningitidis* strain HB-1 contains a sequence homologous to a DNA sequence situated just downstream of the *rmpM* gene, which encodes a class 4 outer membrane protein. This is the location of choice, because of constitutive expression of genes from this site [46]. Incorporation of heterologous *pfkA* at this site leads to its expression by the *rmpM*-promoter. Although standard methods were used for DNA preparation, restriction enzyme analysis, cloning, and sequencing [47], the description of the cloning procedure (Figure 4.2) to obtain the *pfkA*⁺ phenotype (HB-1+*kanR*+*pfkA*) and the HB-1+*kanR* control phenotype is described briefly below.

PCR and sequencing

After identification of the location of the *pfkA* gene in *E. coli* K12 using the NCBI database [48], PCR was used to amplify an *E. coli* DNA-fragment containing *pfkA* with Taq polymerase. Sci Ed Clone Manager 6 (Scientific & Educational Software,

Cary, NC, USA) was used to design the forward oligonucleotide primer (5'-CAAG-AAGACTTCCGCAACA-3') and the reverse oligonucleotide primer (5'-TGA-TAAGCGAAGCGCATCAG-3'). Primers were synthesized by Sigma-Genosys (Dorset, United Kingdom). The forward primer anneals 55 bp upstream of the ATG start codon while the reverse primer anneals 79 bp downstream of the TAA stopcodon which results in a *pfkA* containing DNA-fragment of 1096 bp.

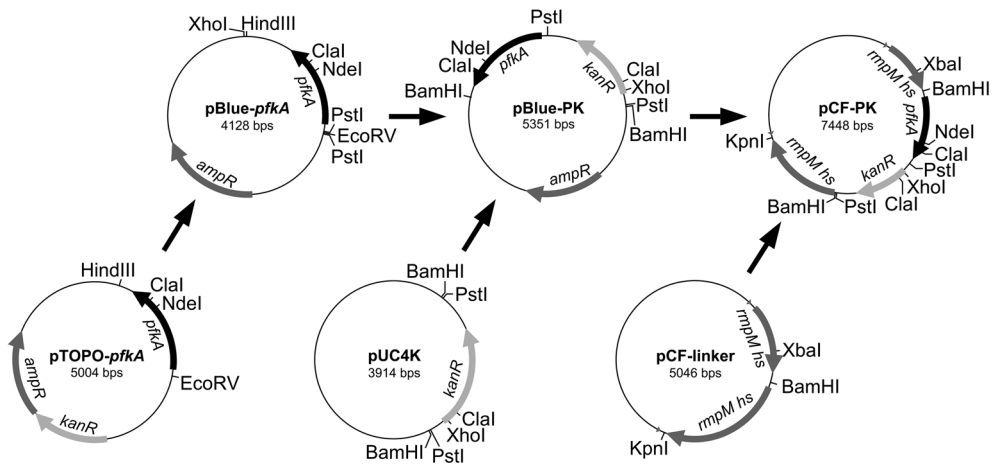


Figure 4.2 Plasmids and their relationships including relevant restriction enzyme sites.

The primers were diluted to a concentration of 1 mmol.mL⁻¹ and were added to puReTag ready-to-go PCR beads (Amersham Biosciences, Little Chalfont, United Kingdom) prior to the addition of *E. coli* cells. Using six combinations of mixtures containing various amounts of primers and *E. coli* cells, PCR was carried out (GeneAmp PCR system 9600, PerkinElmer, Waltham, MA, USA) using the following cycling conditions: Initial denaturation of the template DNA at 94 °C for 5 min followed by 30 cycles of 94 °C for 15 min, 55 °C for 30 seconds and 72 °C for 1 min and completed with 7 min at 72 °C and ∞ 4°C. From each reaction mixture, 10 µL was added to 4 µL of loading buffer (1 mM EDTA, 0.25 % bromophenol blue, 40% sucrose) and analysed on a 1% agarose gel using 1x TBE buffer (Biorad, Hercules,

CA, USA) at 100 V for 30 minutes, to check for sufficient amplification of the DNA-fragment. It was found that 10 mL primers in combination with 1-2 mL *E. coli* cells gave the best results (results not shown). The generated 1096 bp fragment was cloned into the pCR 2.1 TOPO plasmid, using the TOPO TA cloning kit (Invitrogen, Carlsbad, CA, USA), according to the manufacturer's protocol. The plasmids were purified from the culture using a miniprep kit (Promega, Madison, WI, USA) to obtain plasmid DNA of high purity. After digestion of the plasmid DNA (37 °C, 2 h) using HindIII and EcoRV samples were analysed for the presence of the *pfkA* gene by agarose gel electrophoresis and fragments were purified from the gel using the Promega Gel and PCR clean-up system (Promega, Madison, WI, USA) according to the manufacturer's protocol. Fragments were checked by sequencing using the ABI prism DNA sequencing kit (Applied Biosystems, Foster City, CA, USA) according to the manufacturer's protocol. In order to obtain reliable sequencing results a primer annealing at position 359 of the DNA-fragment was designed (5'-GGCGGTGACGGTTCCTACAT-3') and sequencing was performed on an ABI prism 310 genetic analyser (Applied Biosystems, Foster City, CA, USA). Sequencing of eight pCR-TOPO-*pfkA* constructs resulted in one usable construct (pTOPO-*pfkA*).

Constructs

A pCF-Linker plasmid, containing the sites necessary for DNA uptake and homologous recombination was available from previous studies [49]. Since a usable construct has to contain a kanamycin resistance gene (*kanR*) next to the *pfkA* gene and both genes have to be cloned in the BamHI site of the pCF-linker plasmid (Figure 4.2), a construct was prepared containing both the kanamycin resistance gene and *pfkA*. Shortly, the procedure was as follows: First the pTOPO-*pfkA* plasmid and a pBluescript vector which contains an ampicillin resistance gene (Stratagene, La Jolla, CA, USA) were digested by HindIII and EcoRV. Digestion of the pTOPO-*pfkA* by these enzymes resulted in an 1173 bp fragment containing *pfkA* which was purified as described above. Second, the purified fragment was ligated into the pBluescript vector (pBlue-*pfkA*)

and transformation was done in medium containing ampicillin. Third, a kanamycin resistance gene was obtained from an available pUC4K vector [49] by digestion with PstI and subsequent purification. The kanamycin resistance gene was ligated into the pBlue-*pfkA* vector (pBlue-PK) and transformant selection was done in medium containing kanamycin. After purification of the resulting plasmid DNA, the orientation of the kanamycin resistance gene was checked by XhoI digestion. Plasmids containing the correct orientation were selected yielding the required *pfkA-kanR* fragment. After ligation of the *pfkA-kanR* fragment into the BamHI site of pCF-Linker, transformation of competent *E. coli* cells was carried out and transformant selection was done in medium containing kanamycin, yielding the final pCF-linker-*pfkA-kanR* plasmid (pCF-PK). For correct expression by the *rmpM*-promoter the orientation of the fragment was checked by NdeI and XbaI digestion. Plasmids containing the fragment in the correct orientation were selected and used for transformation of *N. meningitidis* HB-1. After transformation, a PCR was done with the primers for *pfkA* which confirmed the presence of the inserted DNA-fragment. The control strain was created by cutting both pCF-linker and pUC4K with BamHI. After purification of the fragments, *kanR* was ligated into pCF-linker yielding the pCF-K plasmid. The orientation of *kanR* in this construct was checked by digestion with XbaI and ClaI. This construct was used for transformation of *N. meningitidis* HB-1.

Transformation

The plasmid-constructs (pCF-PK and pCF-K) were cut using KpnI and the linear DNA was used for transformation. Overnight grown *N. meningitidis* strain HB-1 were scraped from the GC agar plate using a swab and resuspended in 10 ml meningococcal medium containing 10 mM MgCl₂. The suspension was diluted 5 times in the same medium. 2.5 µl linear construct-DNA was added to 2.5 ml of the diluted suspension. After transformation (37 °C, 3 h), 250 µl of the suspension was plated on gonococcal (GC-) agar plates containing kanamycin. Plates were stored overnight in the CO₂-incubator. Colonies obtained this way were picked and plated again on kanamycin containing

GC-plates to get rid of untransformed cells, which stay alive, but cannot grow in the presence of kanamycin. This procedure was repeated once to get a total of three plating steps on kanamycin containing medium. The final *N. meningitidis* HB-1 mutants (HB-1+*kanR* and HB-1+*kanR*+*pfkA*) were used to generate stock-cultures.

Rapid sampling

When the chemostat cultures were run, a full genome *N. meningitidis* microarray was not yet available at the NVI. For this reason we decided to quench the culture broth using a rapid sampling procedure followed by low temperature storage to freeze bacterial metabolism and preserve RNA. The practical rapid sampling setup of Lange and co-workers [50] was adjusted by addition of air filters (0.2 mm) at the relevant points to construct a closed system that was suitable for working with pathogens. In steady state, four samples of 5 mL were taken in 35 mL, -40 °C quenching solution (60% w/w methanol buffered with 10 mM HEPES, pH 7.5) [50] and stored at -80 °C until further analysis. The quenched samples were stored for two years prior to RNA isolation.

Microarrays

Samples were analyzed using a full genome *N. meningitidis* microarray. Based on the genome sequence of *N. meningitidis* serogroup B strain MC58 [17], a set of 2078 70-mer oligonucleotides was developed at Operon (Cologne, Germany), covering 93% of all predicted open reading frames (ORFs). In addition, a single 70-mer *pfkA* oligonucleotide sequence from *E. coli* K-12 was added to the set. Oligonucleotide pellets were dissolved in 50% DMSO (v/v in water) to a concentration of 20 µM and spotted in triplicate on UltraGAPS II coated slides (Corning, New York, NJ, USA), using the Omnigrid 100 microarray spotter (GeneMachines, San Carlos, CA, USA).

In steady state a sample for RNA extraction was taken from each of the four chemostats (two duplicate experiments). For each microarray sample, the quenched bacterial culture samples were used directly for RNA isolation. Notably, RNase retarding

solution [51, 52] was not added to any sample. The amount of quenched bacterial culture used for RNA isolation was equal to 1.2 ml.O_D₅₉₀⁻¹ to ensure that an equal amount of bacteria were used as starting material. The samples were concentrated by centrifugation (3000 g, 15 min) and treated with Tris-EDTA buffer, containing 0.5 mg.ml⁻¹ lysozyme (Sigma-Aldrich, Zwijndrecht, The Netherlands) for 3 minutes. Total RNA was extracted with the SV Total RNA isolation system according to the manufacturer's protocol (Promega Benelux, Leiden, The Netherlands). Nucleic-acid concentration was adjusted by precipitation and spectral analysis was used to determine final nucleic-acid concentration and purity. RNA integrity was confirmed with the Bioanalyzer RNA6000 Nano assay (Agilent Technologies, Amstelveen, The Netherlands), according to the manufacturers' protocol. RNA integrity was predicted by calculation of the RNA integrity number (RIN) [53].

Total RNA from the three experimental samples (per strain) was reverse transcribed to cDNA and labeled with Cy3 dye using the Chipshot Indirect Labelling and Clean-up kit (Promega Benelux, Leiden, The Netherlands) according to manufacturer's protocol, with one deviation: 2 µl random primer and no oligo-dT primer was used per reaction to reverse transcribe the RNA. Common reference samples, containing equal amounts of total RNA from all three experimental samples, were labelled with Cy5. The labeled and purified cDNA samples were pooled in Cy3/Cy5 pairs and volumes were adjusted to 25 µl. An equal volume of hybridization buffer was added, to a final concentration of 25% formamide, 5x SSC and 0.1% SDS. Samples were applied to the microarray slides and placed in a hybridization chamber (GeneMachines, San Carlos, CA, USA) for 16-20 hours at 42 °C in the dark. Differential gene expression levels were calculated through comparison with a common reference sample, containing equal amounts of RNA from all experimental samples.

The microarrays were scanned with a ScanArray Express microarray scanner (Perkin Elmer, Groningen, The Netherlands) and median fluorescence intensities were quantified

for each spot using ArrayVision software (Imaging Research, Roosendaal, The Netherlands). The expression data were natural-log transformed, quantile normalized, and values of replicate spots were averaged. These data processing steps were done with the free statistical software R (WU, Wien, Austria), using an in-house developed script. The sample from duplicate 1 was tested twice to assess method reproducibility in relation to duplicate reproducibility.

Phylogenetic profiling

To determine the presence or absence of the *pfkA* gene and other genes related to glucose metabolism and glucose transport, in different species, the STRING database [54, 55] was used as a starting point. Notably, the orthology assignment between genes in different species that are present in the STRING database is mainly derived from the COG database [48] in which clusters of orthologous groups of proteins (COGs) are delineated by comparing protein sequences encoded in complete genomes. The protein sequences of the relevant genes of *E. coli* were used as an input. In the cases where no or very low homology was found in *N. meningitidis*, while functionality has been indicated elsewhere [56, 57], the protein sequences of the relevant genes of *N. meningitidis* were also used as input. In order to interpret the results obtained from the alignments more easily, the STRING scores were converted to a color scale that is based on four colors using a self-made computer program running in Visual Basic (Microsoft, Seattle, WA, USA). In this program the homology scores (bitscores) of the relevant protein sequence of a species, serve as an input. In the cases where no sequence homology was found, the color red was assigned. In the cases where some homology was found but the bitscore was below the general threshold value of 60 [54, 58], the color orange was assigned. The genes that are present are indicated by the color green and high homology (high scores) are indicated by a slightly darker green. The reliability of the color re-scaling was checked by cross-referencing using BlastP [59] and 2 randomly chosen protein sequences which confirmed the obtained results.

Metabolic modeling

Methods for solving a metabolic network or set of linear equations are discussed extensively elsewhere [60-64]. Briefly, first the genome-scale metabolic model [9] was simplified as described before [10]. Next, an acetaldehyde exchange reaction was added based on the measurement of acetaldehyde in the culture supernatant. In addition, for the HB-1+*kanR*+*pfkA* strain the irreversible PFK reaction was added to the model (see additional data, worksheet model). For both cases the primary measurements were translated to measured conversion rates using mass balances and all measurement errors were translated to errors (i.e. variances) in measured conversion rates using Monte Carlo simulation (MCS) as described before [9].

The redundancy matrix expressing the redundancy relations between the measured exchange rates was calculated for each individual dataset and contained 2 independent equations. Inspection of these equations indicated a carbon, and a nitrogen balance. Both metabolic models (HB-1+*kanR* and the HB-1+*kanR*+*pfkA*) are partly under-determined. Linear optimization (i.e. linear programming, LP) was combined with MCS and used to find a single, unique, optimal value for the objective function maximization of ATP hydrolysis as described before [10]. Since ATP is an intermediate metabolite that cannot accumulate, maximization of the hydrolysis reaction automatically means that in the rest of the network ATP production is maximized. Notably, this single solution is not necessarily unique and there can be more than one flux distribution that reaches the optimal value of the objective function.

Prior to balancing and LP (FBA) *in silico* FBA simulations were done in order to determine the possible increase in yield as a result of *pfkA* introduction. The protein, fatty acid and biomass biosynthesis reactions in the *in silico* FBA simulations were based on the measured average composition which was determined before [10]. The following external metabolites were allowed to freely enter and leave the system: ammonia, water, phosphate, thiosulfate, sulfate, carbon dioxide, oxygen, and protons. In addition,

amino acids, acetate, hydrogen sulfide, ethanol and extracellular protein were only allowed to leave the system. Glucose was the sole carbon source that was allowed to enter the system. The objective function used in *in silico* FBA was the maximization of biomass. This objective function was found to result in biologically meaningful predictions in nutrient limited continuous *E. coli* cultures [65]. *In silico* FBA was combined with Monte Carlo simulation (MCS) using previously determined substrate ($Y_{x/s}$, m_s) and energy parameters ($Y_{x/ATP}$, m_{ATP}) and their corresponding variances [10] as input for optimization at different chosen growth rates. The complete procedure was as follows: First a growth rate was chosen and at this growth rate a thousand values for the corresponding consumption rate of glucose, the growth associated ATP requirement for biomass and the flux through the non-growth-associated ATP-maintenance reaction (m_{ATP}) were calculated using MCS and stored as temporary data set. Second, each set of these simulated values was used as input for *in silico* FBA and the fluxdistribution results were stored in a temporary matrix. After completion of the simulations at the chosen growth rate, the average value and the corresponding variance of each flux and exchange rate were calculated. Then, the next growth rate was selected and the above described procedure was done again. After completion of the *in silico* FBA calculations for strain HB-1+*kanR*, the stoichiometric matrix corresponding to strain HB-1+*kanR*+*pfkA* was selected and the complete procedure was repeated using the same growth rates as inputs. The Monte Carlo approach was used in order to estimate the errors in the calculated *in silico* biomass on substrate yield values ($Y_{x/s}^{in\ silico}$) at the different growth rates in the two strains. The stoichiometric matrices used in this study were constructed from the set of reactions using a self-made computer program running in Visual Basic (Microsoft, Seattle, WA, USA). Both Monte Carlo simulations (MCS) and flux balance analysis (FBA) were executed in self-made computer programs running in Matlab (version 6.5 r13; Mathworks, Natick, MA, USA).

RESULTS & DISCUSSION

In silico FBA

A functional glycolysis in *N. meningitidis* by inclusion of PFK theoretically leads to an increase in the biomass yield as shown in Figure 4.3. The possible increase in biomass yield is higher when the growth rate is lower, as expected. Since a functional glycolysis only produces one additional ATP on a total of about 20 ATP in central metabolism, the impact of PFK when cells grow at a low growth becomes relatively more important, since the availability of ATP for biomass growth decreases with decreasing growth rates due to the maintenance requirements. In other words, the more limiting energy becomes for growth the more important it is to increase the yield of ATP on substrate and thus the more advantageous PFK becomes.

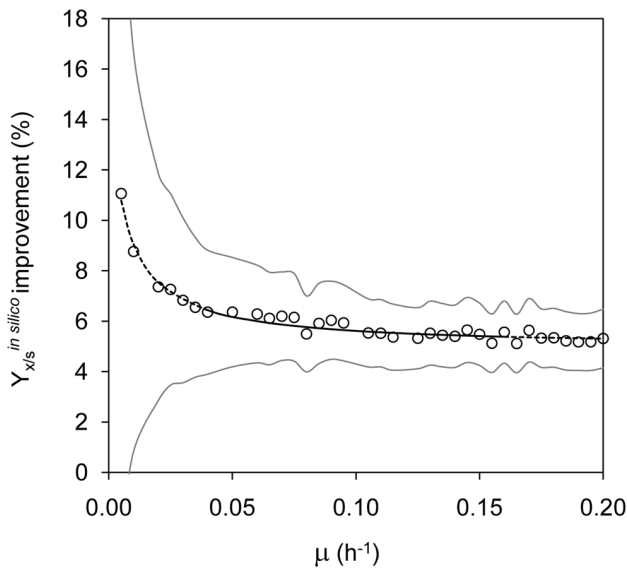


Figure 4.3 Percentage improvement of *in silico* biomass yield ($Y_{x/s}^{in\ silico}$) in the *pfkA*+ strain at various growth rates (μ) in comparison with the HB-1+*kanR* strain. The grey lines represent the standard deviation on the predictions (o). Since the substrate and energy parameters (see materials and methods section) were estimated in the 0.04-0.16 range of growth rates, the average line (black) is dashed outside this range.

Phylogenetic profiling

Phylogenetic profiling (see additional data, worksheet phylogenetic profiling) reveals that many genomes of both γ - and δ -proteobacteria, Acidobacteria, Firmicutes, Bacteroidetes, Actinobacteria, and some Cyanobacteria and all Eukaryota contain a *pfkA* gene (or a *pfkA* homolog), while it is absent in most α -, β -proteobacteria and Chlamydiae genomes and Archaea (Appendix 4). Notably, all listed Firmicutes, δ -proteobacteria and acidobacteria contain a *pfkA* homolog. The presence of *pfkA* in all listed families, except Archaea indicates that its origin is ancient. However, its phylogenetic distribution is patchy and complex. For instance, the genomes of two species within the listed β -proteobacteria (i.e. *Rhodoferrax ferrireducens* and *Chromobacterium violaceum*) contain a *pfkA* homolog, while all other species do not. Observations within all the classified families of bacterial species show similar results. In other words, there always seem to be one or more species within a classified family that contain a *pfkA* gene, so phylogenetic based discrimination to reconstruct the evolutionary history of *pfkA* does not seem possible. However, the patchy phylogenetic distribution suggests, as indicated earlier [19], that *pfkA* can be lost during evolution of a species. Phylogenetic profiling indicates that the genomes of most anaerobic organisms (e.g. *Clostridium* species) contain a *pfkA* gene, which is in agreement with the obtained *in silico* FBA results, since at low growth rate, increased yield is predicted. Since little energy is generated from substrate in anaerobically grown species, the relative gain in ATP yield increases significantly when the glycolytic pathway is present. Absence of a *pfkA* gene in anaerobic organisms goes together with absence of genes related to the EMP pathway and/or absence of glucose transport capabilities (e.g. *Psychrobacter* species). In facultative anaerobic species, the presence or absence of a *pfkA* gene is more variable. For instance, the genomes of *Escherichia* species, *Shigella* species, *Salmonella* species, *Haemophilus* species, *Mannheimia* succiniciproducens, *Staphylococcus* species, *Corynebacterium* species, *Listeria* species, *Yersinia* and *Vibrio* species contain a *pfkA* homolog, while the genomes of *Legionella* species, *Chlamydophila* species and *Chlamydia* species do not. In the genomes of the latter

three species, additional genes related to the EMP pathway are also not present. Similar to facultative anaerobic species, the distribution of the *pfkA* gene in obligate aerobic species is variable. However, obligate aerobic species seem to lack *pfkA* (e.g. *Burkholderia*, *Neisseria*, *Heliobacter* and *Bordetella* species). From an energy point of view, lack of *pfkA* in an obligate aerobe seems obvious, since the contribution of PFK to the energy supply in an aerobically grown organism is limited in comparison with the energy generated through oxidative phosphorylation, which might explain the absence of *pfkA* in the *N. meningitidis* genome. In other words, under aerobic conditions the substrate is more important for anabolism (i.e. supply of intermediates for growth), than for generating energy. Under anaerobic or microaerobic conditions this is just the other way around and the substrate is more important for energy generation than for anabolism and PFK provides an advantage. Therefore, in the case of limiting energy supply, the objective of an organism seems to be optimize the yield of energy on substrate (maximize $Y_{ATP/s}$). In contrast, in the case of sufficient available energy, it seems that the strategy of organisms is to consume this energy as fast as possible (maximize r_{ATP}) in order to outcompete other micro-organisms living in the same habitat. There always seems to be a trade-off between high biomass yield and high energy dissipation rates necessary for fast growth, as examined extensively by Von Stockar and co-workers [66, 67].

Scheutz and coworkers [65] found that under carbon (and energy) limitation in chemostat, *Escherichia coli* aims at maximization of biomass. In the case of excess availability of carbon (and energy), the *E. coli* metabolism operates in such a way that a minimal amount of biochemical reactions are being used to generate the required ATP. This typical over-flow metabolism (e.g. production of acetate) results in less efficient energy utilization of the carbon source. Nevertheless, the resulting suboptimal yields go hand in hand with dissipation of more energy and thereby enable higher catabolic rates [65], which might be a way to outcompete other organisms living in the same habitat. Furthermore, the excreted products like acetate and ethanol may inhibit

growth of other organisms. This shows that *E. coli* has developed a mechanism that compromises between growth efficiency (i.e. biomass yield) and metabolic rate (i.e. growth rate) and the environmental conditions (i.e. habitat) determine which mechanism is preferred. There is more experimental evidence showing that at carbon substrate limitation, high yield pathways are indeed adopted [68-70].

In the *N. meningitidis* genome, genes encoding a glucose/galactose transporter (NMB0535), a putative sugar transporter (NMB0388) and a glucokinase (glk, NMB1390) have been annotated. Since *N. meningitidis* does not have PFK, it seems that the maximal flux through the ED pathway in *N. meningitidis* can reach higher values than the maximum flux going through the EMP pathway if it would have been present. In *Staphylococcus* and *Streptococcus* genomes, known inhabitants of the nose and throat, *pfkA* is present while glucokinase is absent and glucose uptake proceeds via the PEP:carbohydrate phosphotransferase system (PTS system). PTS-mediated substrate uptake involves the transfer of the phosphoryl group of the high-energy metabolite phosphoenolpyruvate to the carbohydrate through a cascade of phosphotransfer proteins including EI, Hpr, and EIIB^{BC} [71, 72]. In *E. coli* the PTS proteins EI (encoded by *ptsI*), Hpr (encoded by *ptsH*), the glucose-specific component EIIB^{Glc} (encoded by *crr*), the glucose transporter EIICB^{Glc} (encoded by *ptsG*) are members of the carbon catabolite modulon that regulates the activity of most catabolic operons and carbohydrate transport in *E. coli*. In the *N. meningitidis* genome the genes encoding an EI protein (NMB2044, *ptsI*), a HPr protein (NMB2045, *ptsH*) and an EIIB mannose/sorbose specific subunit (NMB2046) have been annotated. The first two genes are part of a *ptsHI* operon while NMB2046 is located 69 bp upstream of *ptsH* [56, 73]. This suggests that transport of mannose/sorbose in *N. meningitidis* might proceed via a PTS system. Genes encoding a glucose specific EIIB component and a glucose specific PTS-transporter (EIIB^{Glc}) have not been found in the *N. meningitidis* genome, which suggests that glucose transport does not proceed via a PTS system.

In contrast with *N. meningitidis*, *E. coli* has a functional EMP pathway. *E. coli* mutants that lack the *pfkA* gene are impaired in growth on all carbon sources entering glycolysis at or above the level of F6P and the growth rate drastically decreases when grown on sugars, such as glucose, which are normally transported and phosphorylated by the PTS [74]. A strong decrease in growth rate was also observed in PFK mutants of *Lactococcus lactis*, in which the PFK activity was reduced by replacement of the natural promoter with weaker synthetic promoters [75]. Thus, it seems that the presence of PFK in an organism enables its ability to grow fast when grown on carbon sources (e.g. glucose, mannose, galactose, fructose etc.) that enter glycolysis above the level of F6P. However, in organisms that additionally lack a PTS system, this is not the case. It has been shown in *E. coli* that strains lacking PTS have pleiotropic phenotypes and are impaired in their capacity to grow on glucose and other PTS sugars [76, 77]. The significantly decreasing relative transcription level of *pfkA* in a PTS deficient *E. coli* mutant (Δ *ptsHlcr*), in comparison to the wild-type [78], suggests that there might be a correlation between PFK and PTS. Since a functional EMP pathway can generate twice as much PEP from glucose in comparison with the ED pathway, presence of PFK and the PTS system seem to go hand in hand. To illustrate the possible correlation between PFK and the PTS system, Figure 4.4 shows Venn diagrams for *pfkA*, *glk* (glucokinase, GK) and *ptsG* (glucose specific PTS-transporter EIIB^{Glc}) in γ - and β -proteobacteria, Firmicutes and Actinobacteria. No *ptsG* homologs have been found in α -, ϵ - and δ -proteobacteria, Acidobacteria, Chlamydiae, Bacteroidetes, Cyanobacteria and Spirochaetes species, whereas *pfkA* homologs, in some of these species are present (see Appendix 4). This suggests that the glucose specific PTS-transporter (EIIB^{Glc}) originated after *pfkA* in evolution. The only exception is found within the β -proteobacteria, in particular the *Burkholderia* species, in which a *pfkA* homolog has not been found, while the PTS system is functional. Notably, only the β -proteobacterium *Chromobacterium violaceum*, contains both a *pfkA* homolog and all homologs related to the PTS system.

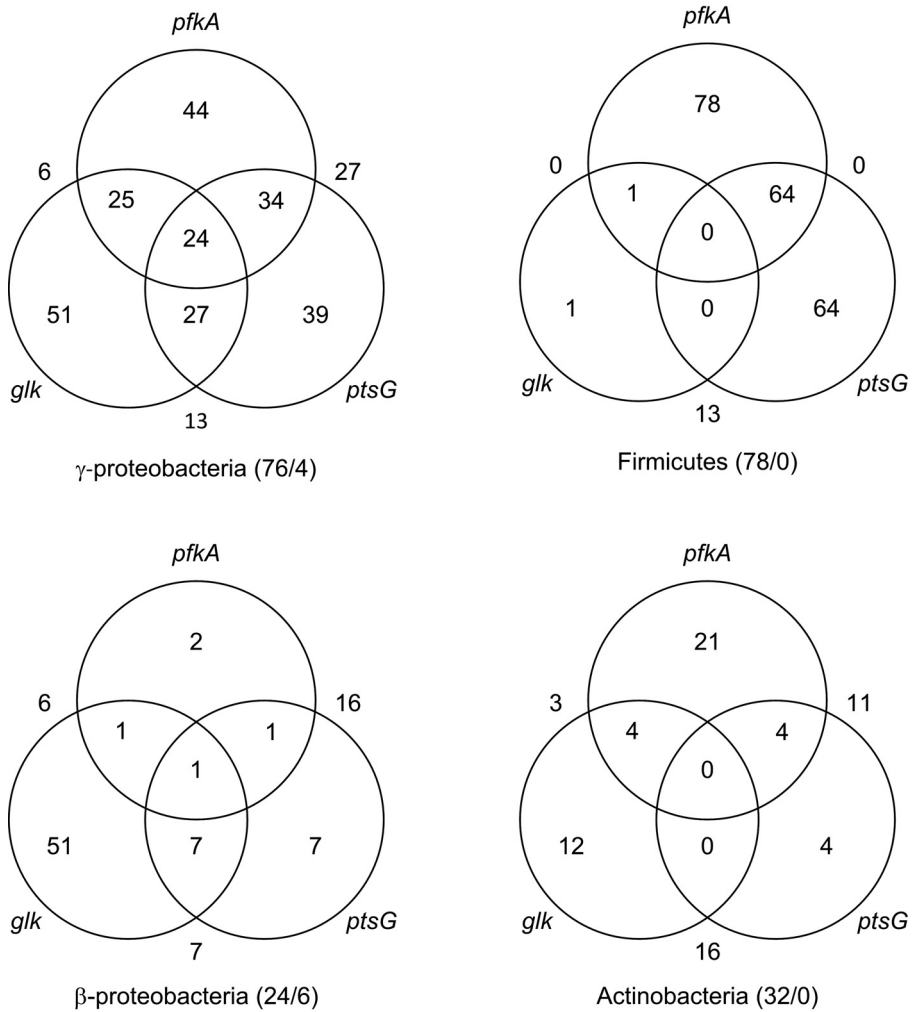


Figure 4.4 Venn diagrams indicating the relationship (numbers in the circles) between PFK (encoded by *pfkA*), the glucose specific PTS-transporter EIIB^{Glc} (encoded by *ptsG*) and glucokinase, GK, (encoded by *glk*) in γ -proteobacteria, β -proteobacteria, Firmicutes and Actinobacteria. For example, in 76 of the listed γ -proteobacteria, *pfkA*, *ptsG* and *glk* homologs are present in 44, 39 and 51 organisms, respectively. In 34 organisms *pfkA* and *ptsG* homologs are both present, whereas in 27 organisms *pfkA* and *ptsG* homologs are both absent (number outside the circles). Hence, in 61 (27+34) of the 76 cases (80%) PFK and EIIB^{Glc} are correlated. In 25 organisms *pfkA* and *glk* homologs are both present, whereas in 6 organisms *pfkA* and *glk* homologs are both absent. Therefore, in 31 cases (41%) PFK and GK are correlated. Notably, in 4 of the 76 γ -proteobacteria (76/4) *pfkA*, *ptsG* and *glk* homologs are absent.

From the Venn diagrams (Fig. 4.4) it can be calculated that in 157 of the 210 cases PFK and EIIB^{Glc} are correlated (75%), meaning they are either found together or both are not present at all, or stated differently in the 156 cases where either PFK or EIIB^{Glc} is present they are present together in 103 cases, which indicates that they are correlated. As a control the correlation with GK is included. PFK and GK are correlated in 30% of the cases. Notably, when the 312 bacterial species, listed in the phylogenetic profile (see additional data), are taken into consideration PFK and EIIB^{Glc} are correlated in 70% of the cases and PFK and GK in 30% of the cases (Appendix 4). This shows that the correlation between PFK and the PTS system is stronger than between PFK and GK, possibly, because of the mentioned fact that the EMP pathway, including PFK, generates more PEP, which is a substrate for the PTS system. Phylogenetic profiling indicates that the EI PTS protein (encoded by *ptsI*), is present in 92%, 20% and 96% of the Bacteria, Eukaryota and Archea, respectively, which clearly indicates more (ancient) functional roles for the PTS system.

Since the PTS system is typical for anaerobic and facultative aerobic organisms [72], the lack of a PTS system in *N. meningitidis* seems obvious. Although, during infection, pathogenic *N. meningitidis* encounters host anatomical sites with low oxygen levels, which indicates that anaerobic metabolism is required [79, 80], one can argue that this requirement is not a main determinant of *N. meningitidis* evolution. In particular, since natural evolution of *N. meningitidis* takes place in the aerobic nasopharyngeal mucosa. A PTS deficient *E. coli* mutant ($\Delta ptsHIcrr$) that underwent an adaptive evolution process [76], showed a higher relative *pfkA* expression level in comparison with the parental mutant strain and also grew faster on glucose (μ of 0.42 vs 0.1 h⁻¹), which indicates that *pfkA* also plays an important role when PTS is lacking. Nevertheless, the mutant (PB12) grew significantly slower than the wild-type strain (μ of 0.71 h⁻¹) [78] indicating the importance of the PTS for achieving a high growth rate. The possibility that other possible main nutrients for growth, (for example lactate), which are not processed via F6P and are present the natural habitat of *N. meningitidis*,

cannot be ignored and might also be determinants of *pfkA* deficiency in *N. meningitidis*. *In vitro* enzyme studies using *E. coli* enzymes [81] show that PFK, glucokinase and phosphoglucoisomerase are inhibited by ATP and PEP, which might be determinants of *pfkA* loss in PTS deficient organisms. In conclusion, for growth on hexose sugars the fact whether a micro-organism is strictly anaerobic or strictly aerobic seems to be the most important factor determining the presence, respectively absence of PFK and thus can also explain the absence of PFK in *Neisseria meningitidis*, which is an aerobic bacterium. A second factor, which can also be important is growth on substrates entering metabolism below the PFK level, like lactate.

RNA integrity and comparison of expression profiles

In total three samples were taken for RNA extraction (per strain). Two RNA extraction samples were taken from one chemostat and one sample was taken from the duplicate chemostat of that strain. The integrity of mRNA molecules is of great importance for experiments that try to reflect the snapshot of gene expression at the moment of RNA extraction [82]. A robust and reliable method for prediction of the RNA integrity is based on calculation of the RNA integrity number (RIN) of the extracted RNA sample, which provides a more reliable quality assessment than the common ribosomal RNA ratio method [53]. The RIN scores of the RNA samples from the two chemostats were 9.4 and 9.8 indicating that the RNA was of good quality and suitable for use in DNA microarray analysis. This shows that the rapid sampling protocol used in this study followed by storage of the quenched biomass at -80 °C prevents RNA degradation for a long period of time (at least two years). Kashara and co-workers [83] found that RNA in rat liver tissue can be preserved up to at least one year when samples are stored at -80 °C, but to our knowledge RNA preservation periods over one year have not been reported before. Comparison of the overall gene expression levels of two samples taken from the same chemostat culture may be a relevant indication for the reproducibility of the microarray analysis method. Two samples taken from one chemostat showed a good correlation between overall gene expression levels for both strains

(HB-1+*kanR*, $R^2 = 0.95$; HB-1+*kanR*+*pfkA*, $R^2 = 0.94$). Comparison of the overall gene expression levels of the two different chemostat cultures of the same strain may be a relevant indication for the biological reproducibility. The correlation between gene expression levels of the two separate chemostat cultures, calculated by weighted least squares linear regression, was also sufficient (HB-1+*kanR*, $R^2 = 0.94$; HB-1+*kanR*+*pfkA*, $R^2 = 0.99$). The results of these comparisons are provided in the additional data file (worksheet reproducibility). The correlation between the averaged gene expression levels of strain HB-1+*kanR* and HB-1+*kanR*+*pfkA* is shown in Figure 4.5. The gene expression values outside the 99% confidence interval of prediction indicate the genes that are up- or downregulated as a result of *pfkA* expression.

The averaged gene expression differences indicate that the heterologous *pfkA* gene is expressed in strain HB-1+*kanR*+*pfkA*. Introduction of the *pfkA* gene in *N. meningitidis* induced a change in the gene expression level of the *pfkA* gene (foldratio, FR = 2.9) and high gene expression changes (FR > 3.0) in the expression of only seven genes. These genes were upregulated in strain HB-1+*kanR*+*pfkA* and include the *pilE* gene (NMB0018) and six *pilS* genes (NMB0020, NMB0021, NMB0022, NMB0023, NMB0025 and NMB0026).

These virulence genes are phase-variable, which is reversible on/off switching of expression state [30]. Therefore it is possible that the ‘on’ expression state of these genes was selected during strain construction and upregulation of these genes might not be a result of heterologous *pfkA* expression. Due to the limited number of samples in the present study, the expression changes of the genes mentioned above were considered to be significant and reliable. Usually, gene expression changes above 2-, 3-, and 4-fold variation are considered significant [84]. However, a 1.6-fold difference to be detected at a level of confidence of above 99% has been indicated in the literature for *N. meningitidis* [85, 86]. If we apply this cut-off value, seven additional genes are indicated. Although the reliability of this set of additional indicated genes is lower, we

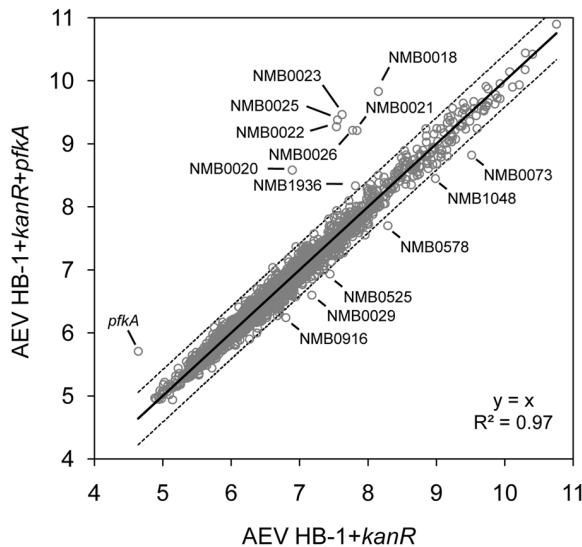


Figure 4.5 Linear regression of average expression values, AEV (o) of *N. meningitidis* strain HB-1+*kanR* and *N. meningitidis* strain HB-1+*kanR*+*pfkA* (black line). The dashed lines indicate the 99% confidence interval of prediction. Introduction of the *pfkA* gene induced a change in the gene expression level of the *pfkA* gene (FR = 2.9). High gene expression changes (FR > 3.0) include the *pilE* gene (NMB0018) and six *pilS* genes (NMB0020, NMB0021, NMB0022, NMB0023, NMB0025 and NMB0026). Small gene expression changes (FR>1.6) were observed for NMB0578, NMB1936, NMB0073, NMB0029, NMB0916, NMB1048, and NMB0525. However the latter set possesses uncertainty as explained in text.

found that two genes in this set are correlated with heterologous PFK expression. The copper ABC transporter periplasmic copper-binding protein gene (NMB0578) was found to be downregulated (FR=1.8), which can be explained by the fact that PFK is inhibited by copper [87]. The ATP synthase F1, alpha subunit gene (NMB1936) was found to be upregulated (FR=1.68), which can be explained by a higher oxygen consumption rate of strain HB-1+*kanR*+*pfkA* (see metabolic observations section). The relation of the other five downregulated genes in the additional indicated set (NMB0073 encoding the capsule polysaccharide export inner-membrane protein, FR=2.0; NMB0029 encoding glycerate dehydrogenase, FR=1.78; NMB0916 and NMB1048, both encoding hypothetical proteins, FR=1.75 and FR=1.71, respectively;

NMB0525 encoding a putative aluminum resistance protein, FR=1.66) with heterologous PFK expression, remains unclear.

Physiological and metabolic observations

Successful expression of PFK in *N. meningitidis* HB-1+*kanR*+*pfkA* was indicated by measuring the PFK activity using a coupling enzyme assay. A clear decrease in absorption is visible in cell lysate of the HB-1+*kanR*+*pfkA* strain, indicating the presence of active PFK (Fig. 4.6). Notably, the observed PFK activity was significantly lower (~100 fold) in comparison with identically prepared *E. coli* extracts (results not shown). This may be due to the use of the *rmpM* promoter site, due to the presence of allosteric inhibitors as explained in the introduction section or due to active fructose-1,6-bisphosphatase in the *N. meningitidis* cell-extract which might interfere with the determination [88]. Interference is unlikely in the *E. coli* cell-extract since fructose-1,6-bisphosphatase is not required when grown on hexoses and pentoses [89].

The macromolecular biomass composition was determined on the two duplicate aerobic glucose-limited chemostat cultures and is shown in Table 4.1. In strain HB-1+*kanR*+*pfkA*, the RNA content is significantly higher and the lipopolysaccharide (LPS) content is lower, whereas no significant changes were observed for the other components. The cellular amino acid composition of both strains did not differ significantly (Table 4.2). We observed small differences in fatty acid composition (Table 4.3). In particular, the unsaturated hexadecenoic acid (C16:1) content and the 3-hydroxydodecanoic acid (C12:0-3OH) content in strain HB-1+*kanR*+*pfkA* were somewhat higher. Overall the changes in the biomass composition were minimal.

The redundancy matrix expressing the redundancy relations between the measured exchange rates was calculated for each individual dataset and contained a carbon and a nitrogen balance. The residuals obtained after multiplication of the redundancy matrix with the measured exchange rates could be explained on the basis of random

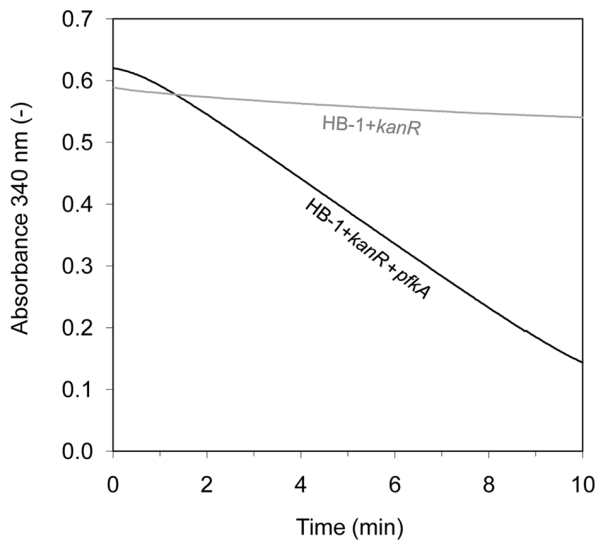


Figure 4.6 PFK activity measurements. Absorbance at 340 nm was measured in cell-free extracts of *N. meningitidis* strain HB-1+*kanR*+*pfkA* (black line) and the negative control strain HB-1+*kanR* (grey line) during 10 min. The decreasing black line indicates successful expression of PFK in *N. meningitidis*.

measurement variances with test values that were lower than the 95% chi-square critical value of 5.992 [93]. In addition, the individual carbon and nitrogen balance could be closed for all datasets. Hence, the carbon and nitrogen containing exchange rates were balanced. As explained in the materials and methods section, a single solution for the underdetermined parts of both metabolic networks was calculated using maximization of ATP yield (maxATP) as an objective function. It was found that in the HB-1+*kanR*+*pfkA* strain 24% of the total ATP was formed in the EMP pathway, the citric acid cycle and the acetate production reaction, whereas in the HB-1+*kanR* strain 16% of the total ATP was formed in the ED pathway, the citric acid cycle and the acetate production reaction. In both strains the remaining part of ATP was formed in oxidative phosphorylation (see Additional data file, worksheet fluxdistributions).

Table 4.1 Measured macromolecular composition (% w/w) of *N. meningitidis* strains HB-1+*kanR* (*pfkA*⁻) and HB-1+*kanR*+*pfkA* (*pfkA*⁺), different including the standard deviation.

Component	<i>pfkA</i> ⁻	<i>pfkA</i> ⁺
Protein	67.14 ± 7.85	69.41 ± 9.18
RNA	5.87 ± 1.47	9.97 ± 2.49
DNA	1.79 ± 0.27	1.78 ± 0.27
Phospholipids ¹	11.22 ± 0.16	10.69 ± 0.14
LPS ²	5.83 ± 0.16	4.88 ± 0.12
Peptidoglycan ³	2.50 ± 0.25	2.50 ± 0.25
Total	94.3 ± 8.0	99.2 ± 9.5

¹ The overall phospholipid composition used in the present study was based on the values provided by Rahman and co-workers [90], including 11 % phosphatidate (PA), 71 % phosphatidylethanolamine (PE) and 18% phosphatidylglycerol (PG).

² LPS was quantified based on the measured amount of C12:0-3OH and possesses uncertainty previously [10].

³ Peptidoglycan amount in *N. meningitidis* was estimated based on *E. coli* [91] and the composition was based on the average of the peptidoglycan structures present in *N. meningitidis* [92]. For modeling purposes a relative mean standard deviation of 10% was assumed.

As expected, the HB-1+*kanR* strain processes glucose-6-phosphate solely through the ED pathway using this objective function, since the ED pathway can yield slightly more energy per consumed glucose in comparison with the PP pathway [10]. It was found that the ATP hydrolysis flux (i.e. the flux that was maximized) was twice as high in the HB-1+*kanR*+*pfkA* strain (see additional data file, worksheet flux distributions). Even if it is assumed that the EMP pathway is not active in the PFK mutant due to a too low activity of the PFK and glucose is metabolised through the ED pathway, the ATP hydrolysis flux is still 1.6 times higher in the PFK mutant. The biomass composition of both strains is comparable, which indicates that it is unlikely that more ATP is required for HB-1+*kanR*+*pfkA* biomass formation. Possibly, heterologous expression of PFK induces stress and increases the ATP requirement for maintenance. In addition, introduction of *pfkA* in *N. meningitidis* may result in a futile cycle in combination with fructose-1,6 biphosphatase resulting in the loss of ATP. To compensate for this more ATP must be generated from glucose resulting in more CO₂ generation

Table 4.2 Measured cellular amino acid composition (% w/w) of *N. meningitidis* strains HB-1+*kanR* (*pfkA*⁻) and HB-1+*kanR*+*pfkA* (*pfkA*⁺), including the standard deviation.

Amino acid	<i>pfkA</i> ⁻	<i>pfkA</i> ⁺
Aspartate	5.68 ± 0.26	5.62 ± 0.27
Glutamate	7.78 ± 0.43	7.84 ± 0.45
Serine	3.79 ± 0.19	4.01 ± 0.21
Histidine	2.13 ± 0.14	2.05 ± 0.16
Glycine	5.45 ± 0.27	5.51 ± 0.28
Threonine	4.64 ± 0.21	4.46 ± 0.20
Alanine	8.75 ± 0.40	9.14 ± 0.42
Arginine	7.85 ± 0.33	8.05 ± 0.35
Tyrosine	3.72 ± 0.14	3.91 ± 0.15
Valine	6.60 ± 0.32	6.59 ± 0.30
Methionine	2.67 ± 0.15	2.57 ± 0.21
Phenylalanine	4.54 ± 0.16	4.45 ± 0.17
Isoleucine	5.11 ± 0.22	5.08 ± 0.22
Leucine	8.32 ± 0.32	8.16 ± 0.33
Lysine	6.96 ± 1.11	6.88 ± 1.16
Proline	3.72 ± 0.31	3.64 ± 0.30
Asparagine	4.35 ± 0.23	4.31 ± 0.24
Tryptophan	1.98 ± 0.54	1.91 ± 0.54
Cysteine	0.96 ± 0.33	0.83 ± 0.32
Glutamine	4.97 ± 0.39	5.00 ± 0.41

and a decrease in biomass yield. The measured (balanced) C-mol yield of biomass on substrate, $Y_{x/s}$, in strain HB-1+*kanR*+*pfkA* was found to be 0.45 ± 0.03 C-mol.C-mol⁻¹, while $Y_{x/s}$ in strain HB-1+*kanR* was found to be 0.52 ± 0.03 C-mol.C-mol⁻¹. Notably, predictions obtained from *in silico* FBA, at the same growth rate of 0.13 h⁻¹, showed opposite results (i.e. 0.47 ± 0.04 and 0.49 ± 0.04 for strain HB-1+*kanR* and strain

Table 4.3 Measured cellular fatty acid composition (% w/w) of *N. meningitidis* strains HB-1+*kanR* (*pfkA*⁻) and HB-1+*kanR*+*pfkA* (*pfkA*⁺), different including the standard deviation.

Fatty acid	<i>pfkA</i> ⁻	<i>pfkA</i> ⁺
dodecanoic acid (C12:0)	7.99 ± 0.33	6.93 ± 0.33
3-hydroxydodecanoic acid (C12:0-3OH)	7.54 ± 0.26	6.83 ± 0.24
3-hydroxytetradecanoic acid (C14:0-3OH)*	3.31 ± 0.27	3.50 ± 0.12
tetradecanoic acid (C14:0)	8.53 ± 0.26	7.72 ± 0.25
hexadecenoic acid (C16:1 trans-9)	20.92 ± 0.83	23.29 ± 0.75
hexadecenoic acid (C16:1 ω-7-cis)	0.40 ± 0.02	0.46 ± 0.02
hexadecanoic acid (C16:0)	39.53 ± 1.4	38.98 ± 1.43
octadecenoic acid (C18:1 ω-7-cis)	10.52 ± 0.44	11.40 ± 0.72
octadecanoic acid (C18:0)	1.26 ± 0.06	0.89 ± 0.06

* The C14:0-3OH quantity was calculated from the corresponding measured C12:0-3OH quantity as explained previously [10].

HB-1+*kanR*+*pfkA*, respectively). This might explain why the *pfkA* gene is not obtained by HZT, since it is initially unfavourable for biomass yield. The lower $Y_{x/s}$ in strain HB-1+*kanR*+*pfkA* means less carbon is assimilated in biomass, which was compensated mainly by an increase in CO₂ production (i.e. 0.52 ± 0.06 C-mol.C-mol⁻¹ for strain HB-1+*kanR*+*pfkA* and 0.44 ± 0.04 C-mol.C-mol⁻¹ for strain HB-1+*kanR*), while the production of byproducts (i.e. ethanol, acetate, acetahdehyde, lactate, amino acids and protein) was low and comparable between the two strains (i.e. 0.03 ± 0.01 C-mol.C-mol⁻¹ for strain HB-1+*kanR*+*pfkA* and 0.05 ± 0.01 C-mol.C-mol⁻¹ for strain HB-1+*kanR*). No significant differences between the maximum growth rates of both strains were observed during the batch phase preceding the chemostat phase (results not shown). Theoretically, a higher yield would be expected and due to the earlier mentioned trade off between high biomass yield and high energy dissipation rates a lower maximum growth rate would be expected. As mentioned it seems plausible that introduction of *pfkA* in *N. meningitidis* resulted in a futile cycle. This results in loss of ATP (and dissipation of energy), more CO₂ production and a lower yield of bio-

mass on substrate. The extra dissipation of energy can explain why no lower growth rate has been found, which is thus in line with the theory. Adaptive evolution to achieve a robust, optimal metabolic network that enables a higher growth rate [94] or a higher yield, might be possible.

Schoen and co-workers [95] suggested that a fast replication rate upon colonization of a new host by *N. meningitidis* might constitute a selective advantage. However, from an economical point of view, efficiency should be more important than rate. Colonization of the nasopharynx by *N. meningitidis* is a complex series of events that requires both efficient scavenging of nutrients and evasion of innate immune killing. The levels of lactate and glucose in homogenates of nasopharyngeal tissue are constant and range from 0.6 to 2.4 mmol.l⁻¹ and 3.9 to 5.8 mmol.l⁻¹, respectively [27] and these levels were not affected by infection either with wild-type meningococci or *lctP*-deficient meningococci, which illustrates chemostat-like (constant) environmental conditions within the nasopharynx in terms of carbon source. This suggests that selection for efficiency might be more important than selection for growth rate. However, the concentrations of both carbon sources in the nasopharynx are still significantly higher in comparison with concentrations in a C-limited chemostat. Furthermore, the concentrations measured in the nasopharynx are far beyond the K_s , which ranges for glucose from $4 \cdot 10^{-4}$ – 0.1 mmol.l⁻¹ [96] and indicates that selection for growth rate is possible.

The variable environmental conditions of an organisms' habitat seems to be the most important determinant of its survival (optimization) strategy and its corresponding physiological evolution. In *E. coli* this is reflected by the vast amount of genes that are related to physiological adaption (~ 20% of the genes in the *E. coli* genome). In contrast, only ~ 2% of the genes in the *N. meningitidis* genome, is related to physiological adaption [30], whereas ~ 100 genes in the meningococcal genome are related to phase and antigenic variation (in *E. coli* < 10 genes) [30]. Therefore, it seems that the gene-

rating of genetic variability [30, 37, 95], to cope with the host immune defense systems [30, 97, 98], is the main survival strategy of *N. meningitidis*, which is reflected by the vast amount of different tools that are specifically designed for this purpose. For instance, *N. meningitidis* is equipped with secretory proteins that are involved in the adherence to host cells or required to suppress the host's defence mechanisms [99], of which the site-specific proteases to cleave human immunoglobulin A1 (IgA1) [100], the first line of defense at mucosal membranes, and the generation of surface antigen variants [37] are two examples. Both examples are strong indications that growth rate is indeed the main strategy of *N. meningitidis* in order to outcompete other micro-organisms living in the same habitat, since the faster its replication rate, the faster new genotypes are generated (genetic variability) and the faster specific proteases are available (suppress immune defence). However, the nature of *N. meningitidis* remains complex as illustrated by the presence of a polysaccharide capsule, one of the essential meningococcal attributes for virulence and pathogenesis. This capsule negatively affects bacterial adhesion and, consequently, entry but is fundamental for intracellular survival [101]. The capsule also prevents phagocytic killing of bacteria present in the circulation during infection [101, 102]. Since genetic variability is dominated by random events [30], the influence of environmental factors on the natural evolution of the primary metabolism of meningococci might be limited.

CONCLUSIONS

The phylogenetic distribution of PFK indicates that in most obligate aerobic organisms PFK is lacking. In many (facultative) anaerobic organisms PFK is present and seems to go hand in hand with the presence of a PTS system. A competitive advantage under anaerobic conditions seems the most important factor for the presence of PFK. In the case of limiting energy availability due to the absence of oxidative phosphorylation, the objective of an organism seems to be to optimize the yield of energy on substrate (maximize $Y_{ATP/s}$) favoring PFK. In the case sufficient energy can be liberated from the substrate due to oxidative phosphorylation, the objective of an organism seems to be to optimize the rate of energy generation (maximize r_{ATP}) in order to outcompete other micro-organisms living in the same habitat. Since the natural evolution of *N. meningitidis* takes place in the aerobic nasopharyngeal mucosa, the absence of *pfkA* in the *N. meningitidis* genome can be explained. *In silico* FBA predicts an increase in biomass yield upon inclusion of PFK. However, experimentally a lower biomass yield is found in the presence of PFK as compared to the control without PFK. Possibly this is caused by the fact that phosphatases are active, creating futile cycles and dissipation of energy. This makes clear that no initial advantage is gained when PFK is expressed in *N. meningitidis*, which illustrates that possible HZT events to obtain the *pfkA* gene are unlikely.

ADDITIONAL DATA

The following additional data are available on CD-rom. The file named Additional data Chapter 4.xlsx is an excel file that includes 7 worksheets. The first worksheet named 'model' contains the simplified metabolic model. The second worksheet named 'abbreviations' contains a list of abbreviations of the metabolites. The third worksheet named 'flux distributions' contains the calculated flux distributions of all experimental data sets. The fourth worksheet named 'phylogenetic profiling' contains the phylogenetic profile of 373 species. The fifth worksheet named 'phylo reactions' contains the relevant reactions list and the used amino acid sequences for the phylogenetic profiling. The sixth worksheet named 'transcriptome' contains the gene expression data. The seventh worksheet named 'reproducibility' contains the linear regressions of the gene expression data.

ACKNOWLEDGEMENTS

We thank Jeroen Pennings for his help with the microarray analysis and data processing, Marieke Willemsen, Elly Verhagen and Jan van den IJssel for practical assistance, Alex de Haan for HPLC and GC measurements, Martin Hamzink for NMR measurements, Marcel Hoefnagel for sharing his knowlegde on determination of phosphofructokinase activity in cell-free extracts and Christoph Schoen for sharing his view on this subject.

REFERENCES

1. Rosenstein NE, Perkins BA, Stephens DS, Popovic T, Hughes JM. 2001. Meningococcal disease. *N Engl J Med* 344:1378-1388.
2. Stephens DS, Hoffman LH, McGee ZA. 1983. Interaction of *Neisseria meningitidis* with human nasopharyngeal mucosa: attachment and entry into columnar epithelial cells. *J Infect Dis* 148:369-376.
3. Girard MP, Preziosi MP, Aguado MT, Kieny MP. 2006. A review of vaccine research and development: meningococcal disease. *Vaccine* 24:4692-4700.
4. Trotter CL, Ramsay ME. 2007. Vaccination against meningococcal disease in Europe: review and recommendations for the use of conjugate vaccines. *FEMS Microbiology Reviews* 31:101-107.
5. Zimmer SM, Stephens DS. 2006. Serogroup B meningococcal vaccines. *Curr Opin Investig Drugs* 7:733-739.
6. Finne J, Bitter-Suermann D, Goridis C, Finne U. 1987. An IgG monoclonal antibody to group B meningococci cross-reacts with developmentally regulated polysialic acid units of glycoproteins in neural and extraneural tissues. *J Immunol* 138:4402-4407.
7. Vermont CL, van Dijken HH, Kuipers AJ, van Limpt CJ, Keijzers WC, van der Ende A, de Groot R, van Alphen L, van den Dobbelsteen GP. 2003. Cross-reactivity of antibodies against PorA after vaccination with a meningococcal B outer membrane vesicle vaccine. *Infect Immun* 71:1650-1655.
8. Baart GJE, de Jong G, Philippi M, Riet Kvt, van der Pol LA, Beuvery EC, Tramper J, Martens DE. 2007. Scale-up for bulk production of vaccine against meningococcal disease. *Vaccine* 25:6399-6408.
9. Baart GJ, Zomer B, de Haan A, van der Pol LA, Beuvery EC, Tramper J, Martens DE. 2007. Modeling *Neisseria meningitidis* metabolism: from genome to metabolic fluxes. *Genome Biol* 8:R136.
10. Baart GJE, Willemsen M, Khatami E, de Haan A, Zomer B, Beuvery EC, Tramper J, Martens DE. 2008. Modeling *Neisseria meningitidis* B metabolism at different specific growth rates. *Biotechnol Bioeng* Accepted.
11. Holten E. 1974. 6-Phosphogluconate dehydrogenase and enzymes of the Entner-Doudoroff pathway in *Neisseria*. *Acta Pathol Microbiol Scand [B] Microbiol Immunol* 82:207-213.
12. Holten E. 1975. Radiorespirometric studies in genus *Neisseria*. I. The catabolism of glucose. *Acta Pathol Microbiol Scand [B]* 83:353-366.
13. Jysum K. 1962. Dissimilation of C14 labelled glucose by *Neisseria meningitidis* 1. The formation of CO₂ and acetate from glucose carbon. *Acta Pathol Microbiol Immunol Scand [B]* 55:319-324.
14. Jysum K. 1962. Dissimilation of C14 labelled glucose by *Neisseria meningitidis* 2. The incorporation of 1-C14 and 6-C14 into cellular components in short time experiments. *Acta Pathol Microbiol Immunol Scand [B]* 55:325-334.
15. Jysum K. 1962. Dissimilation of C14 labelled glucose by *Neisseria meningitidis* 2. The incorporation of 1-C14 and 6-C14 into pyruvate. *Acta Pathol Microbiol Immunol Scand [B]* 55:335-341.
16. Jysum K, Borchgrevink B, Jysum S. 1961. Glucose catabolism in *Neisseria meningitidis*. 1. Glucose oxidation and intermediate reactions of the Embden-Meyerhof pathway. *Acta Pathol Microbiol Scand* 53:71-83.
17. Tettelin H, Saunders NJ, Heidelberg J, Jeffries AC, Nelson KE, Eisen JA, Ketchum KA, Hood DW, Peden JF, Dodson RJ et al. 2000. Complete genome sequence of *Neisseria meningitidis* serogroup B strain MC58. *Science* 287:1809-1815.
18. Blangy D, Buc H, Monod J. 1968. Kinetics of the allosteric interactions of phosphofructokinase from *Escherichia coli*. *Journal of Molecular Biology* 31:13-35.
19. Baptiste E, Moreira D, Philippe H. 2003. Rampant horizontal gene transfer and phospho-donor change in the evolution of the phosphofructokinase. *Gene* 318:185-191.
20. Fraenkel DG. Glycolysis. In: *Escherichia coli* and *Salmonella typhimurium*: Cellular and Molecular Biology. Edited by Neidhardt FC, Curtiss R, Ingraham JL, Brooks Low K, Magasanik B, Reznikoff WS, Riley M, Schaechter M, Umberger HE, vol. 1, 2 edn. Washington D.C.: American Society for Microbiology; 1996: 189-198.
21. Guixé V, Babul J. 1985. Effect of ATP on phosphofructokinase-2 from *Escherichia coli*. A mutant enzyme altered in the allosteric site for MgATP. *J Biol Chem* 260:11001-11005.
22. Muller M, Lee JA, Gordon P, Gaasterland T, Sensen CW. 2001. Presence of prokaryotic and eukaryotic species in all subgroups of the PP(i)-dependent group II phosphofructokinase protein family. *J Bacteriol* 183:6714-6716.
23. Siebers B, Klenk HP, Hensel R. 1998. PPI-dependent phosphofructokinase from *Thermoproteus*

- tenax*, an archaeal descendant of an ancient line in phosphofructokinase evolution. J Bacteriol 180:2137-2143.
24. Ito S, Fushinobu S, Yoshioka I, Koga S, Matsuzawa H, Wakagi T. 2001. Structural basis for the ADP-specificity of a novel glucokinase from a hyperthermophilic archaeon. Structure 9:205-214.
 25. Verhees CH, Tuininga JE, Kengen SW, Stams AJ, van der Oost J, de Vos WM. 2001. ADP-dependent phosphofructokinases in mesophilic and thermophilic methanogenic archaea. J Bacteriol 183:7145-7153.
 26. Chi A, Kemp RG. 2000. The primordial high energy compound: ATP or inorganic pyrophosphate? J Biol Chem 275:35677-35679.
 27. Exley RM, Shaw J, Mowe E, Sun YH, West NP, Williamson M, Botto M, Smith H, Tang CM. 2005. Available carbon source influences the resistance of *Neisseria meningitidis* against complement. J Exp Med 201:1637-1645.
 28. Kroll JS, Wilks KE, Farrant JL, Langford PR. 1998. Natural genetic exchange between *Haemophilus* and *Neisseria*: intergeneric transfer of chromosomal genes between major human pathogens. Proc Natl Acad Sci U S A 95:12381-12385.
 29. Chen I, Dubnau D. 2004. DNA uptake during bacterial transformation. Nat Rev Microbiol 2:241-249.
 30. Davidsen T, Tonjum T. 2006. Meningococcal genome dynamics. Nat Rev Microbiol 4:11-22.
 31. Elkins C, Thomas CE, Seifert HS, Sparling PF. 1991. Species-specific uptake of DNA by gonococci is mediated by a 10-base-pair sequence. J Bacteriol 173:3911-3913.
 32. Zhou J, Spratt BG. 1992. Sequence diversity within the *argF*, *fbp* and *recA* genes of natural isolates of *Neisseria meningitidis*: interspecies recombination within the *argF* gene. Mol Microbiol 6:2135-2146.
 33. Spratt BG, Bowler LD, Zhang QY, Zhou J, Smith JM. 1992. Role of interspecies transfer of chromosomal genes in the evolution of penicillin resistance in pathogenic and commensal *Neisseria* species. J Mol Evol 34:115-125.
 34. Seifert HS, Ajioka RS, Marchal C, Sparling PF, So M. 1988. DNA transformation leads to pilin antigenic variation in *Neisseria gonorrhoeae*. Nature 336:392-395.
 35. Parkhill J, Achtman M, James KD, Bentley SD, Churcher C, Klee SR, Morelli G, Basham D, Brown D, Chillingworth T et al. 2000. Complete DNA sequence of a serogroup A strain of *Neisseria meningitidis* Z2491. Nature 404:502-506.
 36. *Neisseria gonorrhoeae* Genome Sequencing Strain FA 1090 (<http://www.genome.ou.edu/gono.html>).
 37. Bentley SD, Vernikos GS, Snyder LA, Churcher C, Arrowsmith C, Chillingworth T, Cronin A, Davis PH, Holroyd NE, Jagels K et al. 2007. Meningococcal genetic variation mechanisms viewed through comparative analysis of serogroup C strain FAM18. PLoS Genet 3:e23.
 38. Peng J, Yang L, Yang F, Yang J, Yan Y, Nie H, Zhang X, Xiong Z, Jiang Y, Cheng F et al. 2008. Characterization of ST-4821 complex, a unique *Neisseria meningitidis* clone. Genomics 91:78-87.
 39. Omelchenko MV, Makarova KS, Wolf YI, Rogozin IB, Koonin EV. 2003. Evolution of mosaic operons by horizontal gene transfer and gene displacement in situ. Genome Biol 4:R55.
 40. Bos MP, Tommassen J. 2005. Viability of a capsule- and lipopolysaccharide-deficient mutant of *Neisseria meningitidis*. Infect Immun 73:6194-6197.
 41. van der Ley P, van der Biezen J, Hohenstein P, Peeters C, Poolman JT. 1993. Use of transformation to construct antigenic hybrids of the class 1 outer membrane protein in *Neisseria meningitidis*. Infect Immun 61:4217-4224.
 42. Dorresteyn RC, de Gooijer CD, Tramper J, Beuvery EC. 1994. A method for simultaneous determination of solubility and transfer coefficient of oxygen in aqueous media using off-gas mass spectrometry. Biotechnol Bioeng 43:149-154.
 43. Lange HC, Heijnen JJ. 2001. Statistical reconciliation of the elemental and molecular biomass composition of *Saccharomyces cerevisiae*. Biotechnol Bioeng 75:334-344.
 44. Vriezen N. Physiology of mammalian cells in suspension culture. Ph.D. thesis. Delft, The Netherlands: Technical University Delft; 1998.
 45. Fordyce AM, Moore CH, Pritchard GG. 1982. Phosphofructokinase from *Streptococcus lactis*. Methods Enzymol 90 Pt E:77-82.
 46. van der Ley P, van Alphen L. Construction of *porA* Mutants. In: Meningococcal Vaccines. Humana Press; 2001: 145-154.
 47. Sambrook J, Fritsch EF, Maniatis T. Molecular cloning: a laboratory manual, 2 edn. Cold Spring Harbor, N.Y.: Cold Spring Harbor Laboratory Press; 1989.
 48. National Center for Biotechnology Information (NCBI) (<http://www.ncbi.nlm.nih.gov/>).
 49. van der Ley P, van der Biezen J, Poolman JT. 1995. Construction of *Neisseria meningitidis* strains carrying multiple chromosomal copies of the *porA* gene for use in the production of a multivalent

- outer membrane vesicle vaccine. Vaccine 13:401-407.
50. Lange HC, Eman M, van Zuijlen G, Visser D, van Dam JC, Frank J, de Mattos MJ, Heijnen JJ. 2001. Improved rapid sampling for in vivo kinetics of intracellular metabolites in *Saccharomyces cerevisiae*. Biotechnol Bioeng 75:406-415.
 51. Mutter GL, Zahrieh D, Liu C, Neuberg D, Finkelstein D, Baker HE, Warrington JA. 2004. Comparison of frozen and RNALater solid tissue storage methods for use in RNA expression microarrays. BMC Genomics 5:88.
 52. Ramalho AS, Beck S, Farinha CM, Clarke LA, Heda GD, Steiner B, Sanz J, Gallati S, Amaral MD, Harris A et al. 2004. Methods for RNA extraction, cDNA preparation and analysis of CFTR transcripts. J Cyst Fibros 3 Suppl 2:11-15.
 53. Schroeder A, Mueller O, Stocker S, Salowsky R, Leiber M, Gassmann M, Lightfoot S, Menzel W, Granzow M, Ragg T. 2006. The RIN: an RNA integrity number for assigning integrity values to RNA measurements. BMC Mol Biol 7:3.
 54. STRING (Search Tool for the Retrieval of Interacting Genes/Proteins) (<http://string.embl.de/>).
 55. von Mering C, Jensen LJ, Snel B, Hooper SD, Krupp M, Foglierini M, Jouffre N, Huynen MA, Bork P. 2005. STRING: known and predicted protein-protein associations, integrated and transferred across organisms. Nucleic Acids Res 33:D433-437.
 56. The BioCyc collection of Pathway/Genome Databases (<http://www.biocyc.org/>).
 57. KEGG: Kyoto Encyclopedia of Genes and Genomes (<http://www.genome.ad.jp/kegg/>).
 58. STRING (Search Tool for the Retrieval of Interacting Genes/Proteins) (<http://string.embl.de/>).
 59. BLAST Frequently Asked Questions (FAQ) (http://www.ncbi.nlm.nih.gov/blast/blast_FAQs.shtml).
 60. Edwards JS, Ibarra RU, Palsson BO. 2001. In silico predictions of *Escherichia coli* metabolic capabilities are consistent with experimental data. Nat Biotechnol 19:125-130.
 61. Edwards JS, Ramakrishna R, Schilling CH, Palsson BO. Metabolic flux balance analysis. In: Metabolic Engineering, Edited by Lee SY, Papoutsakis ET. New York: Marcel Dekker Inc.; 1999: 13-57.
 62. Forster J, Gombert AK, Nielsen J. 2002. A functional genomics approach using metabolomics and *in silico* pathway analysis. Biotechnol Bioeng 79:703-712.
 63. van Gulik WM, Heijnen JJ. 1995. A metabolic network stoichiometry analysis of microbial growth and product formation. Biotechnol Bioeng 48:681-698.
 64. Vallino JJ, Stephanopoulos G. Flux determination in cellular bioreaction networks: applications to lysine fermentations. In: Frontiers in bioprocessing. Edited by Sikdar SK, Bier M, Todd P. Boca Raton, Fla: CRC press; 1990: 205-219.
 65. Schuetz R, Kuepfer L, Sauer U. 2007. Systematic evaluation of objective functions for predicting intracellular fluxes in *Escherichia coli*. Mol Syst Biol 3 (article 119):1-15.
 66. Liu J-S, Vojinovic V, Patino R, Maskow T, von Stockar U. 2007. A comparison of various Gibbs energy dissipation correlations for predicting microbial growth yields. Thermochimica Acta 458:38-46.
 67. von Stockar U, Maskow T, Liu J, Marison IW, Patino R. 2006. Thermodynamics of microbial growth and metabolism: an analysis of the current situation. J Biotechnol 121:517-533.
 68. Brauer MJ, Saldanha AJ, Dolinski K, Botstein D. 2005. Homeostatic adjustment and metabolic remodeling in glucose-limited yeast cultures. Mol Biol Cell 16:2503-2517.
 69. Postma E, Verduyn C, Scheffers WA, Van Dijken JP. 1989. Enzymic analysis of the crabtree effect in glucose-limited chemostat cultures of *Saccharomyces cerevisiae*. Appl Environ Microbiol 55:468-477.
 70. Vulic M, Kolter R. 2001. Evolutionary cheating in *Escherichia coli* stationary phase cultures. Genetics 158:519-526.
 71. Deutscher J, Francke C, Postma PW. 2006. How phosphotransferase system-related protein phosphorylation regulates carbohydrate metabolism in bacteria. Microbiol Mol Biol Rev 70:939-1031.
 72. Postma PW, Lengeler JW, Jacobson GR. 1993. Phosphoenolpyruvate:carbohydrate phosphotransferase systems of bacteria. Microbiol Rev 57:543-594.
 73. The BioCyc collection of Pathway/Genome Databases (<http://www.biocyc.org/>).
 74. Roehl RA, Vinopal RT. 1976. Lack of glucose phosphotransferase function in phosphofructokinase mutants of *Escherichia coli*. J Bacteriol 126:852-860.
 75. Andersen HW, Solem C, Hammer K, Jensen PR. 2001. Twofold reduction of phosphofructokinase activity in *Lactococcus lactis* results in strong decreases in growth rate and in glycolytic flux. J Bacteriol 183:3458-3467.
 76. Flores N, Xiao J, Berry A, Bolivar F, Valle F. 1996. Pathway engineering for the production of aromatic compounds in *Escherichia coli*. Nat Biotechnol 14:620-623.
 77. Flores S, Gosset G, Flores N, de Graaf AA, Bolivar F. 2002. Analysis of carbon metabolism in

- Escherichia coli* strains with an inactive phosphotransferase system by (13)C labeling and NMR spectroscopy. *Metab Eng* 4:124-137.
78. Flores N, Flores S, Escalante A, de Anda R, Leal L, Malpica R, Georgellis D, Gosset G, Bolivar F. 2005. Adaptation for fast growth on glucose by differential expression of central carbon metabolism and gal regulon genes in an *Escherichia coli* strain lacking the phosphoenolpyruvate:carbohydrate phosphotransferase system. *Metab Eng* 7:70-87.
 79. Bartolini E, Frigimelica E, Giovinazzi S, Galli G, Shaik Y, Genco C, Welsch JA, Granoff DM, Grandi G, Grifantini R. 2006. Role of FNR and FNR-regulated, sugar fermentation genes in *Neisseria meningitidis* infection. *Mol Microbiol* 60:963-972.
 80. Nassif X, Pujol C, Morand P, Eugene E. 1999. Interactions of pathogenic *Neisseria* with host cells. Is it possible to assemble the puzzle? *Mol Microbiol* 32:1124-1132.
 81. Ogawa T, Mori H, Tomita M, Yoshino M. 2007. Inhibitory effect of phosphoenolpyruvate on glycolytic enzymes in *Escherichia coli*. *Res Microbiol* 158:159-163.
 82. Strand C, Enell J, Hedenfalk I, Ferno M. 2007. RNA quality in frozen breast cancer samples and the influence on gene expression analysis--a comparison of three evaluation methods using microcapillary electrophoresis traces. *BMC Mol Biol* 8:38.
 83. Kasahara T, Miyazaki T, Nitta H, Ono A, Miyagishima T, Nagao T, Urushidani T. 2006. Evaluation of methods for duration of preservation of RNA quality in rat liver used for transcriptome analysis. *J Toxicol Sci* 31:509-519.
 84. Wodicka L, Dong H, Mittmann M, Ho MH, Lockhart DJ. 1997. Genome-wide expression monitoring in *Saccharomyces cerevisiae*. *Nat Biotechnol* 15:1359-1367.
 85. Dietrich G, Kurz S, Hubner C, Aepinus C, Theiss S, Guckenberger M, Panzner U, Weber J, Frosch M. 2003. Transcriptome analysis of *Neisseria meningitidis* during infection. *J Bacteriol* 185:155-164.
 86. Guckenberger M, Kurz S, Aepinus C, Theiss S, Haller S, Leimbach T, Panzner U, Weber J, Paul H, Unkmeier A et al. 2002. Analysis of the heat shock response of *Neisseria meningitidis* with cDNA- and oligonucleotide-based DNA microarrays. *J Bacteriol* 184:2546-2551.
 87. Gebhard S, Ronimus RS, Morgan HW. 2001. Inhibition of phosphofructokinases by copper(II). *FEMS Microbiol Lett* 197:105-109.
 88. Uyeda K, Luby LJ. 1974. Studies on the effect of fructose diphosphatase on phosphofructokinase. *J Biol Chem* 249:4562-4570.
 89. Fraenkel DG, Horecker BL. 1965. Fructose-1, 6-diphosphatase and acid hexose phosphatase of *Escherichia coli*. *J Bacteriol* 90:837-842.
 90. Rahman MM, Kolli VS, Kahler CM, Shih G, Stephens DS, Carlson RW. 2000. The membrane phospholipids of *Neisseria meningitidis* and *Neisseria gonorrhoeae* as characterized by fast atom bombardment mass spectrometry. *Microbiology* 146 (Pt 8):1901-1911.
 91. Neidhardt FC, Umbarger HE. Chemical composition of *Escherichia coli*. In: *Escherichia coli* and *Salmonella typhimurium*: Cellular and Molecular Biology. Edited by Neidhardt FC, Curtiss R, Ingraham JL, Brooks Low K, Magasanik B, Reznikoff WS, Riley M, Schaechter M, Umbarger HE, vol. 1, 2 edn. Washington D.C.: American Society for Microbiology; 1996: 13-16.
 92. Antignac A, Rousselle JC, Namane A, Labigne A, Taha MK, Boneca IG. 2003. Detailed structural analysis of the peptidoglycan of the human pathogen *Neisseria meningitidis*. *J Biol Chem* 278:31521-31528.
 93. van der Heijden RTJM, Romein B, Heijnen JJ, Hellings C, Luyben KCAM. 1994. Linear constraint relations in biochemical reaction systems: II. Diagnosis and estimation of gross errors. *Biotechnology and Bioengineering* 43:11-20.
 94. Hua Q, Joyce AR, Palsson BO, Fong SS. 2007. Metabolic characterization of *Escherichia coli* strains adapted to growth on lactate. *Appl Environ Microbiol* 73:4639-4647.
 95. Schoen C, Joseph B, Claus H, Vogel U, Frosch M. 2007. Living in a changing environment: insights into host adaptation in *Neisseria meningitidis* from comparative genomics. *Int J Med Microbiol* 297:601-613.
 96. van 't Riet K, Tramper J. Basic Bioreactor Design. New York, USA: Marcel Dekker Inc.; 1991.
 97. Taha MK, Deghmane AE, Antignac A, Zarantonelli ML, Larribe M, Alonso JM. 2002. The duality of virulence and transmissibility in *Neisseria meningitidis*. *Trends Microbiol* 10:376-382.
 98. Alexander HL, Richardson AR, Stojiljkovic I. 2004. Natural transformation and phase variation modulation in *Neisseria meningitidis*. *Mol Microbiol* 52:771-783.
 99. van Ulsen P, Tommassen J. 2006. Protein secretion and secreted proteins in pathogenic *Neisseriaceae*. *FEMS Microbiol Rev* 30:292-319.

100. Vitovski S, Sayers JR. 2007. Relaxed cleavage specificity of an immunoglobulin A1 protease from *Neisseria meningitidis*. *Infect Immun* 75:2875-2885.
101. Spinosa MR, Progida C, Tala A, Cogli L, Alifano P, Bucci C. 2007. The *Neisseria meningitidis* capsule is important for intracellular survival in human cells. *Infect Immun* 75:3594-3603.
102. Stephens DS, Greenwood B, Brandtzaeg P. 2007. Epidemic meningitis, meningococcaemia, and *Neisseria meningitidis*. *Lancet* 369:2196-2210.

APPENDIX 4

Phylogenetic correlations

The relationships between PFK (encoded by *pfkA*), the glucose specific PTS-transporter EIIB^{Glc} (encoded by *ptsG*) and glucokinase, GK, (encoded by *glk*) in bacterial species are shown in the table below. Table 4.1.1 shows the number of cases where homologs of the relevant genes (or a combinations of these genes) are present within a subclass (including the percentage of the total within that subclass). Table 4.1.2 shows the number of cases where homologs of the relevant genes (or combinations) are absent. Table 4.1.3 shows the possible correlations between PFK, EIIB^{Glc} and GK. #species, number of species within the subclass.

Table 4.1.1 Homologs present

Species	# species	<i>pfkA</i>	<i>ptsG</i>	<i>glk</i>	<i>pfkA+ptsG</i>	<i>pfkA+glk</i>	<i>glk+ptsG</i>	<i>pfkA+ptsG+glk</i>
γ-proteobacteria	76	44 (58%)	39 (51%)	51 (67%)	34 (45%)	25 (33%)	27 (36%)	24 (32%)
β-proteobacteria	24	2 (8%)	7 (29%)	17 (71%)	1 (4%)	1 (4%)	7 (29%)	1 (4%)
α-proteobacteria	43	5 (12%)	0 (0%)	23 (53%)	0 (0%)	4 (9%)	0 (0%)	0 (0%)
ε-proteobacteria	8	3 (38%)	0 (0%)	2 (25%)	0 (0%)	0 (0%)	0 (0%)	0 (0%)
δ-proteobacteria	9	9 (100%)	0 (0%)	2 (22%)	0 (0%)	2 (22%)	0 (0%)	0 (0%)
Acidobacteria	2	2 (100%)	0 (0%)	0 (0%)	0 (0%)	0 (0%)	0 (0%)	0 (0%)
Firmicutes	78	78 (100%)	64 (82%)	1 (1%)	64 (82%)	1 (1%)	0 (0%)	0 (0%)
Chlamydiae	12	1 (8%)	0 (0%)	0 (0%)	0 (0%)	0 (0%)	0 (0%)	0 (0%)
Bacteroidetes	8	7 (88%)	0 (0%)	0 (0%)	0 (0%)	0 (0%)	0 (0%)	0 (0%)
Actinobacteria	32	21 (66%)	4 (13%)	12 (38%)	4 (13%)	4 (13%)	0 (0%)	0 (0%)
Cyanobacteria	5	3 (60%)	0 (0%)	5 (100%)	0 (0%)	3 (60%)	0 (0%)	0 (0%)
Spirochaetes	6	4 (67%)	0 (0%)	0 (0%)	0 (0%)	0 (0%)	0 (0%)	0 (0%)
Other bacteria	9	7 (78%)	1 (11%)	0 (0%)	1 (11%)	0 (0%)	0 (0%)	0 (0%)
Bacteria	312	186 (60%)	115 (37%)	113 (36%)	104 (33%)	40 (13%)	34 (11%)	25 (8%)

Table 4.1.2 Homologs absent

Species	# species	<i>pfkA</i>	<i>ptsG</i>	<i>glk</i>	<i>pfkA+ptsG</i>	<i>pfkA+glk</i>	<i>glk+ptsG</i>	<i>pfkA+ptsG+glk</i>
γ-proteobacteria	76	32 (42%)	37 (49%)	25 (33%)	27 (36%)	6 (8%)	13 (17%)	4 (5%)
β-proteobacteria	24	22 (92%)	17 (71%)	7 (29%)	16 (67%)	6 (25%)	7 (29%)	6 (25%)
α-proteobacteria	43	38 (88%)	43 (100%)	20 (47%)	38 (88%)	19 (44%)	20 (47%)	19 (44%)
ε-proteobacteria	8	5 (63%)	8 (100%)	6 (75%)	5 (63%)	3 (38%)	6 (75%)	3 (38%)
δ-proteobacteria	9	0 (0%)	9 (100%)	7 (78%)	0 (0%)	0 (0%)	7 (78%)	0 (0%)
Acidobacteria	2	0 (0%)	2 (100%)	2 (100%)	0 (0%)	0 (0%)	2 (100%)	0 (0%)
Firmicutes	78	0 (0%)	14 (18%)	77 (99%)	0 (0%)	0 (0%)	13 (17%)	0 (0%)
Chlamydiae	12	11 (92%)	12 (100%)	12 (100%)	11 (92%)	11 (92%)	12 (100%)	11 (92%)
Bacteroidetes	8	1 (13%)	8 (100%)	8 (100%)	1 (13%)	1 (13%)	8 (100%)	1 (13%)
Actinobacteria	32	11 (34%)	28 (88%)	20 (63%)	11 (34%)	3 (9%)	16 (50%)	3 (9%)
Cyanobacteria	5	2 (40%)	5 (100%)	0 (0%)	2 (40%)	0 (0%)	0 (0%)	0 (0%)
Spirochaetes	6	2 (33%)	6 (100%)	6 (100%)	2 (33%)	2 (33%)	6 (100%)	2 (33%)
Other	9	2 (22%)	8 (89%)	9 (100%)	2 (22%)	2 (22%)	8 (89%)	2 (22%)
Bacteria	312	126 (40%)	197 (63%)	199 (64%)	115 (37%)	53 (17%)	118 (38%)	51 (16%)

Table 4.1.3 Correlations

Species	# species	<i>pfkA+ptsG</i>	<i>pfkA+glk</i>	<i>glk+ptsG</i>	<i>pfkA+ptsG+glk</i>
γ-proteobacteria	76	61 (80%)	31 (41%)	40 (53%)	28 (37%)
β-proteobacteria	24	17 (71%)	7 (29%)	14 (58%)	7 (29%)
α-proteobacteria	43	38 (88%)	23 (53%)	20 (47%)	19 (44%)
ε-proteobacteria	8	5 (63%)	3 (38%)	6 (75%)	3 (38%)
δ-proteobacteria	9	0 (0%)	2 (22%)	7 (78%)	0 (0%)
Acidobacteria	2	0 (0%)	0 (0%)	2 (100%)	0 (0%)
Firmicutes	78	64 (82%)	1 (1%)	13 (17%)	0 (0%)
Chlamydiae	12	11 (92%)	11 (92%)	12 (100%)	11 (92%)
Bacteroidetes	8	1 (13%)	1 (13%)	8 (100%)	1 (13%)
Actinobacteria	32	15 (47%)	7 (22%)	16 (50%)	3 (9%)
Cyanobacteria	5	2 (40%)	3 (60%)	0 (0%)	0 (0%)
Spirochaetes	6	2 (33%)	2 (33%)	6 (100%)	2 (33%)
Other	9	3 (33%)	2 (22%)	8 (89%)	2 (22%)
Bacteria	312	219 (70%)	93 (30%)	152 (49%)	76 (24%)

Chapter 5

Scale-up for bulk production of vaccine against meningococcal disease

This chapter has been published as: Baart GJE, de Jong G, Philippi M, Riet Kvt, van der Pol LA, Beuvery EC, Tramper J, Martens DE. 2007. Scale-up for bulk production of vaccine against meningococcal disease. *Vaccine* 25:6399-6408.

ABSTRACT

At the Netherlands Vaccine Institute (NVI) a vaccine against *Neisseria meningitidis* serogroup B organisms based on different porA subtypes contained in outer membrane vesicles (OMVs) is in advanced stage of development and will be evaluated in clinical trial studies in the near future. In order to meet the expected demand for product, the current biopharmaceutical production process is being scaled-up. This study describes the scale-up approach for the upstream process and the resulting bioreactor design and operation strategy leading towards a feasible solution for bulk production of a vaccine against meningococcal disease. The technically realized 1.2 m³ bioreactor, equipped with a turbine impeller for gas dispersion, was complemented with an upward pumping impeller and a rotary plate foam breaker to contain foam inside the bioreactor. Aeration and ventilation in the culture broth were controlled by increasing the stirrer speed and gas flow rate simultaneously at increasing oxygen demand. The scale-up was successful and comparable growth curves and nutrient consumption profiles were reached on 0.06 and 1.2 m³.

NOMENCLATURE

CER	$[\text{mol.m}^{-3}.\text{s}^{-1}]$	carbon evolution rate
C_{ol}	$[\text{mol.m}^{-3}]$	dissolved oxygen concentration
C_{ol}^*	$[\text{mol.m}^{-3}]$	interface oxygen concentration
D	$[\text{m}]$	impeller diameter
g	$[\text{m.s}^{-2}]$	gravitational acceleration
H	$[\text{m}]$	liquid height in bioreactor
He	$[\text{Pa}.\text{(mol.m}^{-3})^{-1}]$	Henry's law constant
k_{La}	$[\text{s}^{-1}]$	volumetric gas-liquid mass transfer coefficient
N	$[\text{s}^{-1}]$	impeller speed
N_{p}	$[-]$	impeller power number
OTR	$[\text{mol.m}^{-3}.\text{s}^{-1}]$	oxygen transfer rate
OUR	$[\text{mol.m}^{-3}.\text{s}^{-1}]$	oxygen uptake rate
P	$[\text{Pa}]$	total pressure
P_{g}	$[\text{W}]$	gassed power input
P_{u}	$[\text{W}]$	ungassed power input
Q_{g}	$[\text{vvm}]$	volumetric gas flow rate
q_{g}	$[\text{m}^3.\text{s}^{-1}]$	gas flow rate
T	$[\text{m}]$	bioreactor diameter
t_{mt}	$[\text{s}]$	characteristic time for mass transfer
t_{oc}	$[\text{s}]$	critical time for oxygen depletion
t_{m}	$[\text{s}]$	mixing time
V	$[\text{m}^3]$	volume
x_1	$[\text{m}]$	disc thickness Rushton turbine
y_{O_2}	$[-]$	oxygen mole fraction in outlet gas
ν	$[\text{m}^2.\text{s}^{-1}]$	kinematic viscosity
ρ	$[\text{kg.m}^{-3}]$	density

INTRODUCTION

Vaccine development against *Neisseria meningitidis*

The current status of research and development of vaccines against meningococcal disease due to *Neisseria meningitidis*, which is a major cause of severe meningitis and septicemia with epidemic potential, especially striking infants, has been reviewed recently [2]. There are different pathogenic *N. meningitidis* isolates of which five serogroups (A, B, C, Y, and W135) are responsible for most of the disease cases. Serogroup B and C organisms cause the majority of infections in Europe and America, whereas strains of group A and C dominate in Africa and Asia [3]. Effective polysaccharide vaccines have been developed against serogroups A, C, Y and W135 strains [2]. However, effective global prevention of meningococcal disease will not be achievable without the development of a vaccine against serogroup B meningitis (MenB), which causes about 50% of meningococcal disease cases worldwide. Development of a safe and effective vaccine based on the serogroup B polysaccharide is complicated by its poor immunogenicity [4]. This is most probably caused by its homology to epitopes present on the polysialic acidcarrying neural cell adhesion molecules in humans [5]. In addition, this similarity has been suggested to induce autoimmunity [6], although, no definite signs of autoimmunity in adult vaccination trials have been reported in literature [4]. Consequently, vaccine research against serogroup B organisms has mostly focused on subcapsular proteins contained in outer membrane vesicles (OMVs). The outer membrane protein PorA has been identified as a major inducer of, and target for serum bactericidal antibodies and is expressed by almost all meningococci, which pinpoints PorA as a promising vaccine candidate [7]. However, PorA appears heterogeneous, requiring the development of a multivalent vaccine in which various PorA subtypes are present in order to induce sufficient protection. Although various approaches can be used in the development of a multivalent vaccine, use of genetic-engineered strains expressing more than one PorA subtype to overcome the problem of heterogeneity seems promising [8].

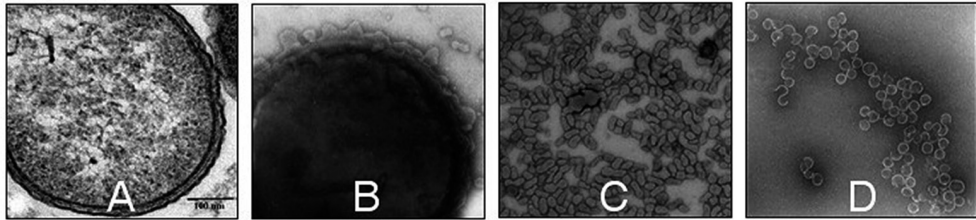


Figure 5.1 The MenB vaccine production process visualized by electron microscopy[34]. At the end of the culture step bacteria (A) are concentrated and OMVs are extracted from the bacteria using an extraction buffer (B). Once the OMV extraction process is completed, the bacterial debris is separated from the OMVs and the OMVs (C) are further purified yielding an OMV bulk product (D). The purified OMV bulk products of three different recombinant strains, each expressing three *porA* subtypes, are mixed and formulated [8] to obtain the final vaccine product. Hence, the vaccine contains nine different *PorA* subtypes [35] and will offer wide-spread protection against meningococcal disease caused by serogroup B organisms [36].

At the Netherlands Vaccine Institute (NVI) a vaccine based on different *porA* subtypes contained in OMVs is in advanced stage of development and will be evaluated in phase I clinical trial studies in the near future. The vaccine production process consists of different steps as shown in Figure 5.1. In order to meet the expected demand for product the current biopharmaceutical production process is being scaled-up. This paper describes the scale-up of the culture step of the production process and is focused on bioreactor design and operation.

Scale-up

Scale-up can be defined as a procedure for the design and construction of a large-scale system on the basis of the results of experiments with small-scale equipment. It is an important step in process development that must overcome several difficulties. To prevent or minimize non-scale related problems during scale-up an established small-scale process with defined culture conditions needs to be available. For this it is essential that the starting material (seedlot or cell bank) for the process is of the required quality. The quality of the inoculum can have a substantial impact on process consistency and performance in terms of productivity, product quality and

process control [9]. To prevent possible introduction of transmissible spongiform encephalopathies (TSEs) [10] the use of raw materials of animal origin in any part of the process must be avoided. Even more because the quality of animal originating materials is hard to control and could easily have impact on process performance. Therefore, defined synthetic media are preferred in biopharmaceutical production processes to ensure reproducible growth and prevent regulatory difficulties. Kinetic information related to the metabolism of the micro-organism obtained at small-scale is independent of scale (for a given pH, dissolved oxygen concentration (DO), temperature, medium composition and quality of the starting materials present in this medium) and does not need to be taken into account for determination of the scale-up strategy. In fact, transport phenomena are the only phenomena that are dependent on scale [11] and therefore become the basis of every scale-up procedure. Method-based procedures for scale-up and optimization of processes in large-scale stirred-tank reactors include: fundamental methods, semifundamental methods (computational fluid dynamics), dimensional analysis and scale-down, regime analysis and scale-down, rules of thumb and finally trial and error [12]. The rules-of-thumb for bio-reactor scale-up is basically an extension of the rules of thumb for scale-up of chemical reactors and is based on parameters that can be kept constant between scales. The scale-up parameters most frequently used are: constant specific power input (P/V), constant volumetric oxygen transfer coefficient (k_La), constant tip speed of the agitator, and constant dissolved oxygen concentration [13]. Application of the different scale-up parameters normally result in entirely different process conditions at scale-up to production scale and it is impossible to maintain all the parameters in the same ratio to one another. Nevertheless, the rules of thumb are commonly used in industry [13, 14]. In practice often combinations of methods are used for adequate scale-up of a bioreactor. No scale-up strategy as such is generally established, so for each product, process and facility a suitable scale-up strategy needs to be determined [15]. Many factors like overall production yields, costs, efficiency, time, knowledge, experience, equipment availability and good-manufacturing-practice compliance play

an important role in scale-up. Additionally, the downstream process (DSP) must be taken into account and preferably scaled-up interactively with the up-stream process, since enlarged volumes and/or higher product concentrations may affect the DSP strategy and vice-versa limitations in scale-up of DSP may affect choices in the up-stream process.

For the scale-up of aerobic cultivations of organisms that are not sensitive to shear like *N. meningitidis*, gas-liquid mass transport is the most significant factor [16]. Therefore, the value of the oxygen uptake rate, OUR ($\text{mol.m}^{-3}.\text{h}^{-1}$), which is scale independent, becomes the most important parameter. To keep the oxygen concentration constant in a growing system the oxygen transfer rate, OTR ($\text{mol.m}^{-3}.\text{h}^{-1}$), should always equal the OUR. The OTR is mainly determined by the k_La (h^{-1}), the dissolved oxygen concentration, C_{ol} (mol.m^{-3}) and the top pressure, P (Pa) in the vessel as given by:

$$\text{OUR} = \text{OTR} = k_La(C_{ol}^* - C_{ol}) \quad (5.1)$$

Where C_{ol}^* is the oxygen concentration in equilibrium with the gas-phase (mol.m^{-3}), which is given by:

$$C_{ol}^* = \frac{y_{O_2}P}{H_e} \quad (5.2)$$

Where y_{O_2} is the oxygen fraction in the gas (mole.mole^{-1}) and H_e is the Henry coefficient ($\text{Pa.m}^3.\text{mole}^{-1}$). Both the C_{ol} and P can be kept constant. By requiring that the C_{ol} is constant between scales, scale-up can be done on the basis of the maximum oxygen uptake rate (OUR) attained in the small-scale process and oxygen limitation can be prevented. The peak OUR of the culture on small-scale is then defined as the oxygen transfer rate that needs to be at least achievable in the large-scale system. In practice, scale-up of an aerobic process is often done on the basis of keeping the value

of $k_L a$ constant between scales. The $k_L a$ value in large bioreactors (liquid height, $H > 1$ m) can be determined during cultivation using the method that is based on the mass-transfer equation (Eq.1) [17], where the C_{ol} is the known setpoint, C_{ol}^* is the oxygen concentration in the medium in equilibrium with the outgoing oxygen concentration in the gas-phase and OTR is calculated from the difference in ingoing and outgoing amount of oxygen per unit time divided by the liquid volume.

Although gas-liquid mass transport is the most significant factor in scale-up of an aerobic cultivation process, the mixing time cannot be neglected. At increasing scale, mixing times also increase, which can lead to, for instance, low dissolved oxygen concentrations or high pH control agent concentrations in certain regions of the bioreactor [17]. Therefore, mixing time analysis should also be included in the scale-up analysis. The carbon evolution rate (CER), linked to the OUR by the respiration coefficient, is also important in scale-up. High carbon dioxide concentrations in the cultivation broth can cause growth inhibition [18, 19]. This inhibitory effect can be circumvented by using a sufficient high gas flow for venting out excess carbon dioxide.

Next to the effects of gas-liquid mass transfer, foam formation can become an important factor during scale-up of aerobic cultivations. Vortex mixing in combination with head-space aeration ensures foam entrapment into the liquid phase and can be applied for shear insensitive organisms on small scale. However, at increasing scale, head-space aeration becomes limiting and air, whether or not enriched with pure oxygen needs to be sparged directly into the liquid to achieve the required gas-liquid mass transfer rates. Sparging results in increased foaming of the broth, which in principle can easily be controlled using antifoaming agents. However, current requirements for production of human biologicals (<http://www.emea.eu.int>) mandate strict control of all aspects of the process including the validated proof of removal of undesired compounds like antifoaming agents from the final product. Hydrophobic interactions between the lipid fraction of the biological and the antifoaming agents

can not be avoided and may result in the incorporation of the antifoaming agent into the membrane. Although selective removal of the antifoaming agent may be possible, the antifoam itself as well as the removal step may affect the integrity of the membrane structure and in this way have a negative effect on the product(s) contained in the membrane. Therefore, for whole-cell products or products contained in outer membrane vesicles or outer membrane fragments, use of antifoaming agents is not recommended and another solution must be found for foam control. Therefore mechanical foam control using stirring [20], hydromechanical force [21] or rotary plate foam breakers [22] is preferable when processing products that are contained in the outer membrane or outer membrane structures. In this way, regulatory difficulties are prevented.

MATERIALS AND METHODS

Strain

N. meningitidis strain HP16215-2, a recombinant non-encapsulated, non-piliated variant of the group B isolate H44/76 containing three different PorA subtypes, was used throughout this study. Before experimental scale-up work was started a bacterial seedbank for continued manufacturing of the product was produced using the two-tiered concept in which the master seedbank was used to generate the working seedbank. The media used in the process of seedbank development as well as the cultivation medium were completely chemically defined and contained no compounds of animal origin. Each manufacturing run started with inoculation from the working seedbank followed by the usual extension to increasing pre-culture volumes using inoculation percentages between 1 and 3%.

Batch cultures

Bacteria were grown in three different bioreactors: a small-scale 5 L unbaffled autoclavable glass bioreactor with 3 L working volume (control), a 0.06 m³ in-situ sterilisable stainless steel bioreactor with 0.04 m³ working volume and a 1.2 m³ in-situ sterilisable stainless steel bioreactor with 0.8 m³ working volume. All bioreactors (Applikon, Schiedam, the Netherlands) were operated in batch mode and equipped with one Rushton 6-blade impeller for mixing and gas dispersion. The DO, temperature and pH were controlled at 30±3%, 35±0.1 °C and 7.0±0.4 (using 12 N phosphoric acid), respectively. In the 5 L control experiments pH control was omitted, while DO was controlled (using headspace aeration only) by first increasing the stirrer speed from 300-600 rpm followed by changing the oxygen fraction in the gas flow. This gas flow was kept constant at 1 L.min⁻¹. Since the 5 L bioreactors were not equipped with baffles, a liquid vortex occurred as a result of mixing. This vortex prevented build-up of foam originating from the broth since both the liquid flow and the flow of foam are directed towards the impeller and mixed back into the liquid. In the large-

scale experiments DO was controlled by changing the stirrer speed and gas flow simultaneously as described in the results section to maximum levels of 250 rpm and 200 L.min⁻¹ in the 1.2 m³ bioreactor and 500 rpm and 10 L.min⁻¹ in the 0.06 m³ bioreactor. Foam was controlled mechanically using a rotary plate foam breaker (Type AA, Bioengineering AG, Wald, Switzerland) on both the 0.06 m³ and 1.2 m³ scale. Additionally the 1.2 m³ bioreactor was equipped with a Scaba 3SHP1 upward pumping impeller (Scanpump AB, Mölndal, Sweden) for primary foam containment.

Analytical procedures

The optical density (OD) of the cultures was determined at 590 nm in a Vitalab 01 spectrophotometer (Vital Scientific, Dieren, The Netherlands) in 1 cm light path plastic cuvettes (Greiner Labortechnik, Frickenhausen, Germany). Samples were diluted below 0.3 OD units to fit the linear range of the spectrophotometer. Biomass dry weight was calculated on the basis of optical density measurements using a factor of 0.48 g_{dry weight}.L⁻¹ (g_{dw}.L⁻¹) per OD unit. This linear relationship between optical density measurements and dry biomass weight was determined in small-scale experiments (results not shown). The oxygen and carbondioxide concentration in the gas flow (in- and out) were measured with a mass spectrometer (Prima White Box 600, Thermo Electron, Winsford, United Kingdom) on small- and 0.06 m³ scale and with a paramagnetic oxygen and carbondioxide gas analyser (Type 4100, Servomex BV, Zoetermeer, The Netherlands) on 1.2 m³ scale.

Glucose was determined with a YSI 2700 glucose/lactate analyser (Yellow Springs Instruments, Yellow Springs, USA). Glutamate was determined with a YSI 2700 glutamate/glutamine analyser (Yellow Springs Instruments). DNA in the culture supernatant was quantified with fluorescence spectroscopy using ethidium bromide (MP biochemicals, Illkirch, France) as described before [23].

Software

The sensors were connected to ADI control systems (Applikon, Schiedam, the Netherlands), which were connected to a UNIX computer with BCSV software (Compex, Belgium). BCSV software carried out all the control-loops (DO, temperature, pH, stirrer rate and gas flow rate) and logged all data [24]. Tablecurve 2D (Jandel Scientific, San Rafael, USA) was used for curve fitting the cell density data points, of the 0.06 m³ experiments, with a sigmoidal function describing the bacterial growth curve according to Gompertz as described before [25].

RESULTS

Regime analysis

Regime analysis can be used to identify the rate-limiting subprocesses from a set of relevant subprocesses using characteristic times as described in detail elsewhere [12]. As mentioned before, for the scale-up of aerobic cultivations gas-liquid mass transport is the most significant factor [16]. A limited oxygen supply can lead to an undesired fermentative process. In general, the two causes for oxygen limitation in an aerated stirred vessel are insufficient mixing or insufficient oxygen mass transfer. In order to identify the possible limiting factor at scale-up (i.e. mixing or gas-liquid mass transfer) regime analysis was used. Empirical formulas were used to calculate the characteristic time for mixing, t_m (s), and for oxygen transfer, $(k_La)^{-1}$ (s), as a function of design parameters, like reactor dimensions, impeller speed, gas-flow rate and type of impeller. These, system related characteristic times were next compared to the characteristic time for oxygen mass transfer, t_{mt} (s) of the process (biomass growth), as defined in Table 5.1. Many empirical formulas exist for calculating mixing time and k_La , which were all obtained from specific bioreactor configurations at specific modes of operation. This means that their accuracy, when generally applied, is somewhat limited. Nevertheless, for a given system, most of the empirical formulas yield comparable results by order of magnitude. Ideally, the choice of empirical relations to be used should be based on actual measurements in the system under study, in this case the 0.06 and 1.2 m³ bioreactors. However, often this is not possible, because the reactor still has to be built or is not available in the correct configuration yet. If for practical reasons measurements are not possible, one should use those formulas that are obtained for systems that closest resemble the system under study. Here the last approach had to be taken and the empirical formulas expected to be most adequate for our systems are given in Table 5.1. In all calculations a standard bioreactor configuration was assumed (1 Rushton six-blade turbine placed 1 turbine diameter from the bottom, $T/D = 3:1$, $H/T = 1:1$ and 4 baffles). For the 0.06 m³ system the actual k_La value was

Table 5.1 Empirical formulas

no.	parameter	formula	reference
1	$k_L a$ (volumetric oxygen transfer coefficient)	$k_L a \left(\frac{v}{g^2} \right)^{\frac{1}{3}} = 7.94 \cdot 10^{-4} \left[\frac{P_g V^{-1}}{1000 \rho (v g^2)^{\frac{1}{3}}} \right]^{0.62} \left[\frac{q_g}{V} \left(\frac{v}{g^2} \right)^{\frac{1}{3}} \right]^{0.23}$	Schlüter and Deckwer [25]
2	P_g (gassed power dissipation)	$1- \frac{P_g}{P_u} = 9.9 \left(\frac{q_g N^{0.25}}{D^2} \right)$ when $\frac{q_g N^{0.25}}{D^2} \leq 0.055$ $1- \frac{P_g}{P_u} = 0.52 + 0.62 \left(\frac{q_g N^{0.25}}{D^2} \right)$ when $\frac{q_g N^{0.25}}{D^2} > 0.055$	Cui et al. [26]
3	t_m (mixing time, single Rushton turbine)	$t_m = \frac{5.3 T^2}{N D^2 N_p^{\frac{1}{3}}}$	Nienow [28]
4	t_m (mixing time, dual Rushton turbine)	$t_m = \frac{3.3}{N N_p^{\frac{1}{3}}} \left(\frac{H}{D} \right)^{2.43}$	Cooke et al. [29]
5	t_{circ} (circulation time)	$t_{circ} = \frac{t_m}{4}$	van 't Riet and Tramper [16]
6	N_p (power number impeller)	$N_p = 2.512 \left(\frac{x_1}{D} \right)^{-0.195} T^{0.0628}$	Bujalski et al. [27]
7	P_u (ungassed power dissipation)	$P_u = \rho N_p N^3 D^5$	van 't Riet and Tramper [16]
8	t_{mt} (characteristic time for mass transfer)	$t_{mt} = \frac{C_{ol}^* - C_{ol}}{OUR}$	Sweere et al. [11]
9	t_{oc} (critical time oxygen depletion)	$t_{oc} = \frac{C_{ol}}{OUR}$	van 't Riet and Tramper [16]

calculated from measurements at the maximum point of operation ($P_g \cdot V^{-1} = 2.3 \text{ W} \cdot \text{kg}^{-1}$, $Q_G = 0.25 \text{ vvm}$), using the mass-transfer equation (Eq. 5.1) [17]. As can be seen in Figure 5.2, the measured values correspond well with the estimated value using the formula of Schlüter and Deckwer [26], where the ‘gassed power input (P_g)’ was calculated using the formula of Cui and co-workers [27] and the ungassed power input from the equation of van 't Riet and Tramper.

To identify the possible rate limiting factor (i.e. mixing or gas-liquid mass transfer) at scale-up to an available 1.2 m³ vessel, both t_m and $(k_L a)^{-1}$ were calculated using the formulas mentioned in Table 5.1 (formula 3 and 1 respectively) and compared to the characteristic time for mass transfer of the process (t_{mt}). Standardly this done for the oxygen limitation case ($C_{oi}=0$), however in this case the dissolved oxygen concentration was kept constant at 30%. As can be seen in Table 5.1, $k_L a$ is a function of $P_g V^{-1}$ and $q_g \cdot V^{-1}$. The volumetric gas flow rate was kept constant between scales, at a value of 0.25 vvm. Therefore the $k_L a$ only becomes a function of $P_g V^{-1}$ and is thus the same for both the 0.06 m³ and the 1.2 m³ bioreactors. The results of the regime analysis are shown in Figure 5.2. Figure 5.2 shows that between scales the changes in characteristic mixing times are limited. Furthermore, it is shown that in the region where both t_m

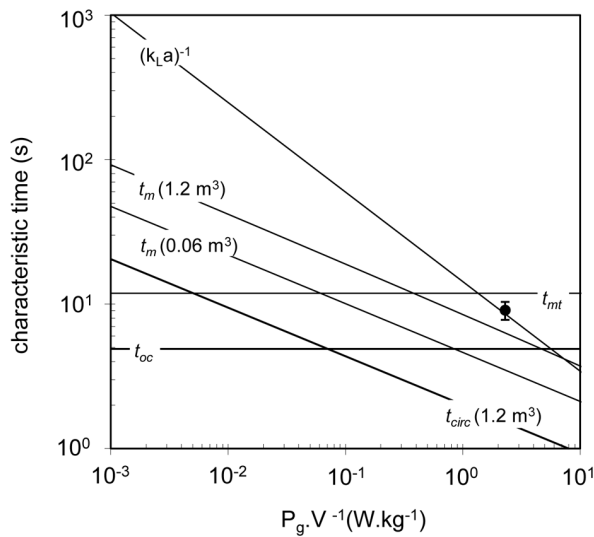


Figure 5.2 Regime analysis in the 0.06 m³ and the 1.2 m³ bioreactors at a volumetric gas flow of 0.25 vvm. Black square: $(k_L a)^{-1}$ in the 0.06 m³ bioreactor calculated from measurements as described in the text. Within the above plotted $P_g \cdot V^{-1}$ range $(k_L a)^{-1}$ is greater than t_m indicating that design can, in principle, be done on the bases of gas-liquid mass transfer.

and $(k_L a)^{-1}$ are smaller than t_{mt} ($P_g V^{-1} > 1.5 \cdot 10^0$) the characteristic time for oxygen transfer of the system $(k_L a)^{-1}$ is larger than the characteristic time mixing (t_m) meaning design can, in principle, be done on the basis of gas-liquid mass transfer.

Scale-up and Bioreactor design

Scale-up was done on the basis of keeping both the maximum OUR and the dissolved oxygen concentration constant between scales. As stated, the dissolved oxygen concentration was kept constant at a value of 30% of the value at saturation with air at atmospheric conditions ($DO=30\%$). This needs to be taken into account, since at dissolved oxygen concentrations greater than zero the actual driving force for gas-liquid mass transfer decreases considerably. By using the peak OUR value from the 0.06 m^3 experiments and a dissolved oxygen concentration of 30% air saturation at atmospheric conditions, the required $k_L a$ value in the 1.2 m^3 bioreactor was calculated to be 0.092 s^{-1} using the mass-transfer equation (Eq. 5.1) [17]. The required gassed power input at a volumetric gas flow rate of 0.25 vvm was then calculated using the formula of Schlüter and Deckwer [26]. Next, the equation derived by Cui and co-workers [27] was combined with the equation of van 't Riet and Tramper to calculate the agitation rate and the ungassed power consumption. The turbine impeller power number was calculated using the formula derived by Bujalski and co-workers [28]. Calculation of the ungassed power consumption is important, because power consumption should not exceed the maximum capacity of the engine. For example, when unexpectedly the gas flow fails during operation at maximum impeller speed, the power uptake by the impeller increases rapidly (factor 2 by order of magnitude [27]). If the installed engine power is insufficient, because it was based on the gassed situation, this may in the worst case lead to overheating or even break down of the engine. For very large scales ($>20 \text{ m}^3$) it may not be feasible to install an engine based on the ungassed power input. In this case some kind of emergency procedure should be installed that turns down the engine in case of too high power consumption. At a maximum gas-flow rate of $200 \text{ L} \cdot \text{min}^{-1}$, the maximum required agitation rate was calculated to be 220 rpm .

The maximum gassed power consumption in this case was $1.6 \text{ kW}\cdot\text{m}^{-3}$ and the ungassed power consumption $2.7 \text{ kW}\cdot\text{m}^{-3}$.

Next, using the calculated agitation speed, the liquid mixing time (t_m) was calculated to be 7.2 s using the formula derived by Nienow [29], which is valid for a single impeller system and is independent of the impeller type [29]. In this study we have applied a dual impeller system. The bottom impeller was a standard Rushton turbine, suitable for gas-liquid mass transfer and the top impeller was an upward pumping Scaba 3SHP1 as described later. Cooke and co-workers [30] derived a formula for mixing time for a system with two Rushton impellers of the same size. As summarized by Vrabel and co-workers [31], the form of the formula derived by Cooke and co-workers was also found to apply for axial down- and upward-pumping impellers but t_m was typically reduced by a factor of 2. All t_m formulas mentioned above did not take into account the contribution of pneumatic power [31]. At higher aeration rates, the pneumatic contribution to liquid mixing becomes more important and compensates for the loss of mechanical power. Therefore, in large bioreactors the pneumatic contribution to liquid mixing should be taken into account. However, Vrabel and co-workers [31] found that overall there is a minimal change in the quality of liquid mixing. Based on the above and not taking into account the pneumatic contribution, the t_m of the system was estimated to be between 3.5 and 6.9 s.

An important process related characteristic time for bioreactor design is the critical time of oxygen depletion, t_{oc} (s) [17]. The t_{oc} of the process was calculated to be 5 s using formula 9 in Table 5.1. This value is in the same order of magnitude as the t_m . If no oxygen gradients in the liquid broth are allowed, the t_m should be smaller than the t_{oc} and if oxygen gradients (but no oxygen depletion) in the liquid broth are allowed, the circulation time, t_{circ} (s), should be smaller than the t_{oc} . This means that for our system oxygen depletion will not occur, but oxygen gradients might be present depending on the actual value of t_m .

The actual installed engine power was higher than the calculated required power to take the order of magnitude calculations, energy losses and possible desired future improvement of performance into consideration. The actual installed engine power was 4 kW and the maximum gas-flow rate was set to a maximum level 200 L.min⁻¹. The final configuration of the 1.2 m³ bioreactor is shown in Figure 5.3.

To keep foam, which originates from the culture broth during cultivation, inside the bioreactor, a two-stage mechanical foam containment approach was used. First, stirring as foam disruption (SAFD) [28] was applied for primary foam containment using a Scaba 3SHP1 upward pumping impeller (tank diameter : 3SHP1diameter = 2:1, Scaba 3SHP1 impeller power number = 0.65 [31]), which was placed just below the ungassed liquid surface. As mentioned above, this upward pumping axial impeller reduces the mixing time considerably.

Secondly, a rotary plate foam breaker placed in the exhaust gas line served as additional foam containment measure. Below a gas flow rate of approximately 90 L_{air}.min⁻¹ ($Cx \approx 1.7 \text{ g}_{\text{dry biomass}} \cdot \text{L}^{-1}$), SAFD was sufficient to keep foam inside the bioreactor.

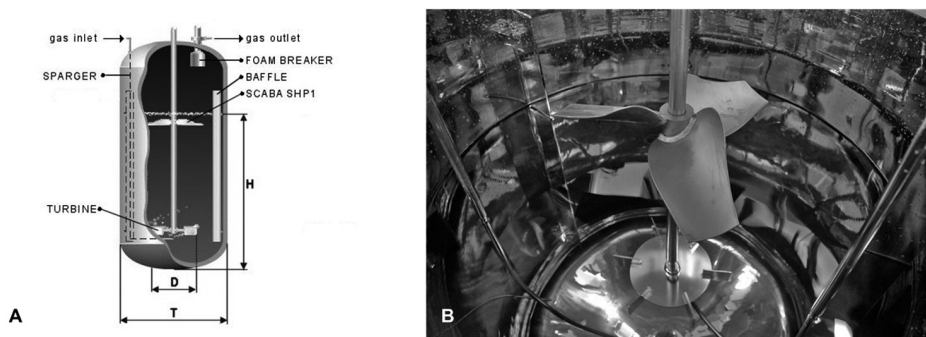


Figure 5.3 A) Schematic overview of the 1.2 m³ production bioreactor with a working volume of 0.8 m³, liquid height, H, tank diameter, T and Rushton turbine diameter D. The geometric ratios were $H=T=1 \text{ m}$, $D=T/3$, $D_{\text{SHP1}}=T/2$ and baffle width = $0.08 \cdot T$. B) Inside view of the 1.2 m³ production bioreactor showing the Rushton turbine for mixing and gas dispersion and the Scaba 3SHP1 upward pumping impeller[20] for foam disruption.

Bioreactor operation: Aeration and ventilation

To control aeration and ventilation in the culture broth a controller was developed that increases the stirrer speed (N) and gas flow rate (q_g) simultaneously at increasing oxygen demand. The stirrer speed was controlled on the basis of the measured dissolved oxygen concentration (DO), while the gas-flow rate was controlled on the basis of the measured oxygen concentration difference in the inflow- and exhaust gas (ΔO_2). By using this approach, the gas-flow rate is determined by the pre-set ventilation requirement (ΔO_2) and the stirrer speed is adjusted to maintain the setpoint. In this way, accumulation of carbon-dioxide is effectively prevented. In all experiments the ΔO_2 was set to 5 %. Based on the positive results at the start of the scale-up experiments with this ΔO_2 value, no additional research was done to determine a possible optimal ΔO_2 value. A schematic of both controllers is shown in Figure 5.4.

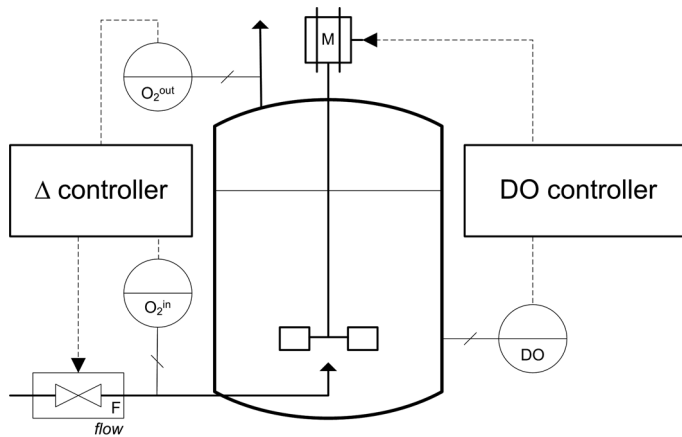


Figure 5.4 Schematic presentation of the aeration and ventilation control. The Δ controller generates a setpoint for the gas mass flow controller (F) based on the measured oxygen concentration difference between the in- and exhaust gas. The DO controller generates a setpoint for the stirrer rate (M) based on the measured dissolved oxygen concentration in the culture broth.

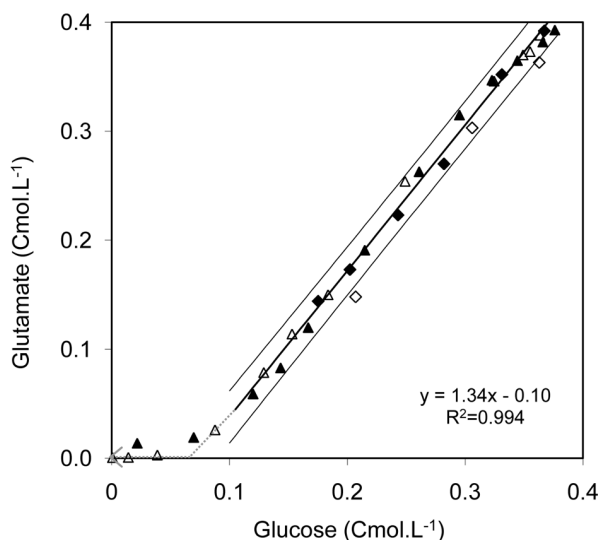


Figure 5.5 Stoichiometry of substrate consumption during cultivation of *N. meningitidis* strain HP16215-2 on two scales. From the start of the cultivation (high glucose and high glutamate concentration) consumption of glutamate and glucose occurs in a constant ratio of 1.34:1 until glutamate depletion. Open and closed triangles: 60 L scale experiments, open and closed diamonds: 1.2 m³ scale experiments. Solid bold black line, fitted straight line based on the 0.06 m³ data points; solid thin black lines, 95% confidence interval of prediction for the fitted straight line.

Biomass growth, substrate consumption and product quality

Under controlled cultivation conditions using chemically defined medium without compounds of animal origin, growth in the bioreactors at all scales was consistent with a yield on carbon substrates (glucose and glutamate) of $0.6 \pm 0.02 \text{ g}_{\text{dw}} \cdot \text{g}_{\text{carbon}}^{-1}$. During cultivation the C-molar consumption ratio of glutamate:glucose was constant 1.34:1 in both the 0.06 m³ and the 1.2 m³ experiments (Figure 5.5). The bacterial growth curves (Figure 5.6) were comparable and can be described by a sigmoidal function according to Gompertz [25]. The bacteria grew to a final density C_x of $5.4 \pm 0.6 \text{ g}_{\text{dw}} \cdot \text{L}^{-1}$ with an estimated [24] growth rate of $0.55 \pm 0.1 \text{ h}^{-1}$ initially, towards $0.1 \pm 0.1 \text{ h}^{-1}$ at the end of the cultivations. Preliminary experiments on 0.06 m³ scale showed (results not shown) that the composition of the outer membrane vesicle product was constant

when bacteria were harvested above a cell density of $1.0 \text{ g}_{\text{dw}}\cdot\text{L}^{-1}$. The total PorA content of the outer membrane vesicle products, produced from bacteria that were harvested above this cell density, was above 70%. These values were in agreement with values found on small scale (5 L). The determination of the distribution of the different PorA subtypes present in the outer membrane vesicle products was beyond the scope of this study. At this moment, no vesicle products have been produced from 1.2 m^3 scale cultures. Therefore, the effect of scale on parameters like product yield and antigenic composition remains to be investigated. The amount of DNA in the culture super-

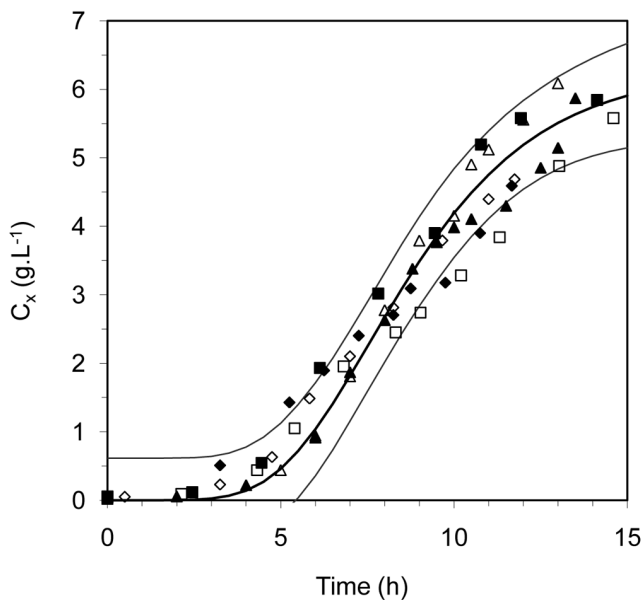


Figure 5.6 Growth curves of *N. meningitidis* strain HP16215-2 on various scales. Differences caused by differences in used inoculum percentages were corrected. Open and closed squares: Control experiments (5 L), open and closed triangles: 0.06 m^3 scale experiments, open and closed diamonds: 1.2 m^3 scale experiments. Solid bold black line, fitted sigmoidal function according to Gompertz [25], using the 0.06 m^3 cell density data points; solid thin black lines, 95% confidence interval of prediction for the fitted function.

natant, is correlated with the degree of cell lysis [32]. After 10 h of cultivation ($Cx \geq 4.0 \text{ g}_{\text{dw}} \cdot \text{L}^{-1}$) we observed a small, neglectable increase in the culture supernatant DNA concentration on both 0.06 m^3 and 1.2 m^3 scale (Figure 5.7). This small increase is most probably related to the higher shear forces that are present at large scale. As soon as carbon substrates for growth become limiting, as occurred at the end of the 0.06 m^3 cultivations, the DNA concentration in the supernatant increases rapidly. Therefore, to maintain the integrity of the bacteria, harvesting needs to be done before substrate limitation occurs.

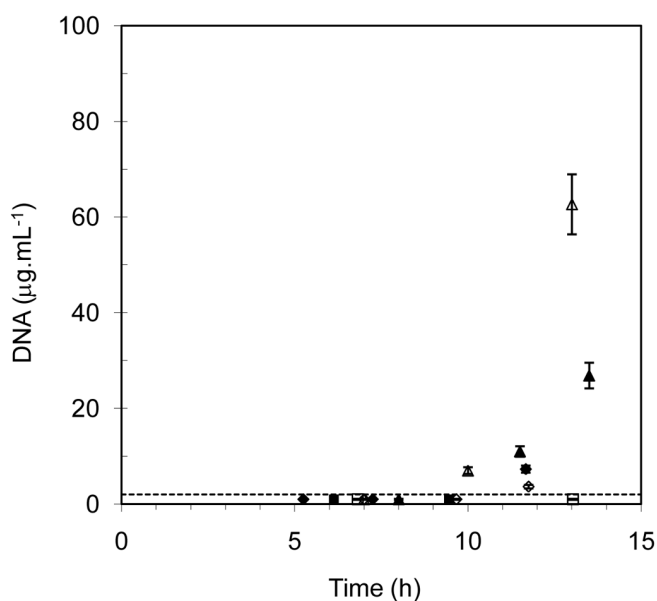


Figure 5.7 DNA concentration in the culture supernatant on three scales. The amount of DNA is correlated with the degree of cell lysis. Values below the detection limit of 2 µg/mL (dotted line) were set to 1. Open and closed squares: Control experiments (5 L), open and closed triangles: 0.06 m^3 scale experiments, open and closed diamonds: 1.2 m^3 scale experiments.

DISCUSSION

The used scale-up approach and the resulting bioreactor design and operation strategy has led to a feasible solution for bulk production of *N. meningitidis* serogroup B organisms for production of an outer membrane vesicle vaccine against meningococcal disease. This work illustrates that the combination of regime analysis, OUR as scale-up parameter followed by a bioreactor design based on empirical relations and a defined mode of operation is an effective strategy that can be adopted for scale-up of aerobic cultivation processes in general. Furthermore, mechanical foam control using stirring in combination with a rotary plate foam breaker proved to be an effective way to contain foam inside the 1.2 m³ bioreactor.

In this way the use of antifoaming agents was not required and complex validation studies to show proof of removal of these agents from the final product could be prevented. It must be emphasized that the success of this scale-up was assisted by the availability of a consistent small-scale process in which culture conditions (e.g. pH, DO, temperature and medium composition) were determined. Additionally, detailed information related to the metabolism of the micro-organism was available from our earlier research [33].

The measured constant stoichiometry of substrate consumption (Figure 5.5) as well as the comparable growth curves on both 0.06 m³ and 1.2 m³ scale (Figure 5.6) indicate that metabolism is identical between scales. As mentioned before, preliminary experiments on 0.06 m³ scale showed that the total porA content of the outer membrane vesicle products was above 70% when bacteria were harvested above a cell density of 1.0 g_{dw}·L⁻¹. Since, no vesicle products have been produced from 1.2 m³ scale cultures, parameters like product yield and antigenic composition still need to be studied at this scale. However, we expect no differences in this respect since the medium composition and the mode of bioreactor operation are kept constant between scales. The data shown in this study relate to strain HP16215-2. For the production of the nonavalent

vaccine product two other recombinant strains (HP10124 and HP1416) are required. On small scale, both these strains show the same growth behaviour and metabolism as strain HP16215-2. Important factors for scale-up like final biomass yield on substrate and specific oxygen demand are identical between all three strains. Therefore, we expect that the described scale-up conditions will also apply for the other strains.

The upstream production process described in this study yields at the least a sufficient amount of biomass for production of the vaccine for the Dutch market. Next to the active component (PorA) the final outer membrane vesicle vaccine contains other components that influence the protective action in humans. In this respect, the vesicle vaccine is an exceptional product. Optimization of the present upstream process needs to be focussed on monitoring and control of the critical process parameters that affect the composition of the final product and determine the product quality. Optimization can be done until clinical phase III production (market scale). No changes will be implemented with respect to bacterial strains and starting materials that might change the impurity profile of the vaccine product. Nevertheless, the process characteristics and relevant assays on intermediate and purified product will have to demonstrate that the process at phase III/market scale is comparable to the smaller scale phase I/II process and meets the pre-set criteria for process and product as specified according to cGMP guidelines.

REFERENCES

1. Girard MP, Preziosi MP, Aguado MT, Kiény MP. 2006. A review of vaccine research and development: meningococcal disease. *Vaccine* 24(22):4692-700.
2. Morley SL, Pollard AJ. 2001. Vaccine prevention of meningococcal disease, coming soon? *Vaccine* 20(5-6):666-87.
3. Bruge J, Bouveret-Le Cam N, Danve B, Rougon G, Schulz D. 2004. Clinical evaluation of a group B meningococcal N-propionylated polysaccharide conjugate vaccine in adult, male volunteers. *Vaccine* 22:1087-96.
4. Finne J, Bitter-Suermann D, Goridis C, Finne U. 1987. An IgG monoclonal antibody to group B meningococci cross-reacts with developmentally regulated polysialic acid units of glycoproteins in neural and extraneural tissues. *J Immunol* 138(12):4402-7.
5. Frasch CE. Vaccines for prevention of meningococcal disease. 1989. *Clin Microbiol Rev* 2:134-8.
6. Vermont CL, van Dijken HH, Kuipers AJ, van Limpt CJ, Keijzers WC, van der Ende A, et al. 2003. Cross-reactivity of antibodies against PorA after vaccination with a meningococcal B outer membrane vesicle vaccine. *Infect Immun* 71(4):1650-5.
7. de Kleijn E, van Eijndhoven L, Vermont C, Kuipers B, van Dijken H, Rumke H, et al. 2001. Serum bactericidal activity and isotype distribution of antibodies in toddlers and schoolchildren after vaccination with RIVM hexavalent PorA vesicle vaccine. *Vaccine* 20(3-4):352-8.
8. Okonkowski J, Kizer Bentley L, Listner K, Robinson D, Chartrain M. 2005. Development of a robust, versatile, and scalable inoculum train for the production of a DNA vaccine. *Biotechnol Prog* 21(4):1038-47.
9. Thiry M, Cingolani D. 2002. Optimizing scale-up fermentation processes. *Trends Biotechnol* 20(3):103-5.
10. Mavituna F. Strategies for Bioreactor scale-up. In: Moreira AR, Wallace KK, editors. *Computer and Information Science Application in Bioprocess Engineering*. Dordrecht, The Netherlands: Kluwer Academic Publishers, 1996.
11. Sweere APJ, Luyben KCAM, Kossen NWF. 1987. Regime analysis and scale-down: Tools to investigate the performance of bioreactors. *Enz Microb Technol* 9(7):386-98.
12. Kossen NWF, Oosterhuis NMG. Modelling and Scaling-up of Bioreactors. In: Rehm HJ, Reed G, editors. *Biotechnology*. 2 ed. Weinheim, Germany: VGH-Verlag, 1985.
13. Junker BH. 2004. Scale-up Methodologies for *Escherichia coli* and Yeast fermentation Processes. *J Biosc Bioeng* 97:347-64.
14. Schmidt FR. 2005. Optimization and scale up of industrial fermentation processes. *Appl Microbiol Biotechnol* 68(4):425-35.
15. Hubbard DW, Ledger SE, Hoffman JA. Scaling-up aerobic fermentation which produce non-newtonian, viscoelastic broths In: Galindo E, Ramirez OT, editors. *Advances in Bioprocess Engineering*. Dordrecht, The Netherlands: Kluwer Academic Publishers, 1994: 95-110.
16. van 't Riet K, Tramper J. *Basic Bioreactor Design*. New York, USA: Marcel Dekker Inc., 1991.
17. Chen SL, Gutmans F. 1976. Carbon dioxide inhibition of yeast growth in biomass production. *Biotechnol Bioeng* 18(10):1455-62.
18. Forkman A, Laurell AB. 1966. Growth inhibition of *Neisseriae* by a carbonic anhydrase inhibitor. Influence of CO₂-concentration. *Acta Pathol Microbiol Scand* 67(4):542-6.
19. Hoeks FW, Boon LA, Studer F, Wolff MO, van-der-Schot F, Vrabel P, et al. 2003. Scale-up of stirring as foam disruption (SAFD) to industrial scale. *J Ind Microbiol Biotechnol* 30(2):118-28.
20. Vetoshkin A. Design of devices for mechanical foam suppression (Hydromechanical foam suppressors). *Chemical and Petroleum Engineering* 1998; 34(3):180-6.
21. Vetoshkin AG. Modeling of Centrifugal Rotary Plate Foam Breakers. 2003. *Theo Found of Chem Eng* 37(4):372-7.
22. Gerhardt P, Murray RGE, Wood WA, Krieg NR. *Methods for general and molecular bacteriology*. Washington D.C.: American Society for Microbiology, 1994.
23. Neeleman R, van Boxtel T. 2001. Estimation of specific growth rate from cell density measurements. *Bioproc Biosys Eng* 24(3):179-85.
24. Zwietering MH, Jongensburger I, Rombouts FM, van 't Riet K. 1990. Modeling of the Bacterial Growth Curve. *Appl Environ Microbiol* 66(6):1875-81.
25. Schluter V, Deckwer WD. 1992. Gas/liquid mass transfer in stirred vessels. *Chem Eng Sci* 47(9-11):2357-62.

26. Cui YQ, van der Lans RGJM, Luyben KCAM. 1996. Local power uptake in gas-liquid systems with single and multiple rushton turbines. *Chem Eng Sci* 51(11):2631-6.
27. Bujalski W, Nienow AW, Chatwin S, Cooke M. 1987. The dependency on scale of power numbers of Rushton disc turbines. *Chem Eng Sci* 42(2):317-26.
28. Nienow AW. 1997. On impeller circulation and mixing effectiveness in the turbulent flow regime. *Chem Eng Sci* 52(15):2557-65.
29. Cooke M, Middleton JC, Bush JR. Mixing and mass transfer in filamentous fermentations. In: King R, editor. Second international conference on bioreactors and fluid dynamics; 1988; Cranfield, UK.: BHR Group; 1988. p. 37-64.
30. Vrabel P, van der Lans RGJM, Luyben KCAM, Boon L, Nienow AW. 2000. Mixing in large-scale vessels stirred with multiple radial or radial and axial up-pumping impellers: modelling and measurements. *Chem Eng Sci* 55(23):5881-96.
31. Bylund F, Castan A, Mikkola R, Veide A, Larsson G. 2000. Influence of scale-up on the quality of recombinant human growth hormone. *Biotechnol Bioeng* 69(2):119-28.
32. Baart GJ, Zomer B, de Haan A, van der Pol LA, Beuvery EC, Tramper J, Martens DE. 2007. Modeling *Neisseria meningitidis* metabolism: from genome to metabolic fluxes. *Genome Biol* 8(7):R136.
33. Claassen I, Meylis J, van der Ley P, Peeters C, Brons H, Robert J, et al. 1996. Production, characterization and control of a *Neisseria meningitidis* hexavalent class 1 outer membrane protein containing vesicle vaccine. *Vaccine* 14(10):1001-8.
34. Bos JM, Rumke HC, Welte R, Spanjaard L, van Alphen L, Postma MJ. 2006. Combination vaccine against invasive meningococcal B and pneumococcal infections: potential epidemiological and economic impact in the Netherlands. *Pharmacoeconomics* 24(2):141-53.
35. Borrow R, Carlone GM, Rosenstein N, Blake M, Feavers I, Martin D, et al. 2005. *Neisseria meningitidis* group B correlates of protection and assay standardization-International Meeting Report Emory University, Atlanta, Georgia, United States, 16-17 March 2005. *Vaccine* 24(24):5093-107.

Chapter 6

General Discussion

Emerging infectious diseases

Today's highly mobile, interdependent and interconnected world provides many opportunities for the rapid spread of infectious diseases and other public health threats. Severe Acute Respiratory Syndrome (SARS), the first severe new disease of this century, clearly illustrated that it spread easily along the routes of international air travel, to cause not just death and disability, but also significant social and economic disruption. Infectious diseases are now spreading geographically much faster than at any time in history and they appear to be emerging more quickly than ever before. Since the 1970s, newly emerging diseases have been identified at the rate of one or more per year, which means there are now nearly 40 diseases that were unknown a generation ago [1]. In addition, during the last five years, the World Health Organisation (WHO) has verified more than 1100 epidemic events worldwide [1]. Cholera, yellow fever and epidemic meningococcal diseases made a comeback in the last quarter of the 20th century and call for renewed efforts in surveillance, prevention and control [1]. Every year, 4 million people die of acute respiratory infections, 2 million die of diarrhoeal disease and another 2 million people die from tuberculosis [2]. Added to this list is the increasing threat of infections as a result of treatment in a hospital or a healthcare service unit, that are caused by staphylococci, enterococci, *Escherichia coli*, *Pseudomonas aeruginosa*, *Klebsiella pneumoniae* and other bacterial pathogens. In addition, the increasing incidence of multidrug-resistant bacteria and viruses, like methicillin-resistant *Staphylococcus aureus* (MRSA) and HIV [3], respectively, and the threat of an avian influenza pandemic (e.g. H5N1), is becoming a major concern [1]. Recently, the first analytical evidence on the increasing threat of emerging infectious diseases to global health was demonstrated [4]. The emergence of infectious diseases indicate non-random global patterns [4] and is correlated with socio-economic, environmental and ecological factors. Taking the above into consideration, it seems that one of the most important improvements in the field of vaccine development is to significantly shorten the development time from vaccine candidate to vaccine, which is currently 15-20 years. Due to the application of genome-based bioinformatics

approaches [5] and the related systems biology tools, including transcriptomics, metabolomics and proteomics in the development process, it is likely that the total development period from vaccine candidate to vaccine can be shortened significantly.

Systems biology

The advent of whole-genome sequencing of bacteria and advances in bioinformatics has revolutionized the study of bacterial pathogenesis already over the last years, enabling the targeting of possible vaccine candidates starting from genomic information [5]. The information provided by the genome can also be used to obtain information on the metabolic capabilities of the organism. This is done by screening the genome for genes that code for enzymes present in the primary metabolism yielding a genome-scale metabolic network. This process of network reconstruction, followed by the synthesis of *in silico* models describing their functionalities, is the essence of systems biology [6]. Commonly, this process of metabolic network reconstruction is a fully automated process and the presence of a particular reaction is inferred if an ortholog of the corresponding enzyme is encoded in the genome. In most cases this results in networks that contain gaps due to the incomplete or incorrect annotation of the genome. Various bioinformatic approaches have been proposed to fill in the gaps by taking into account genomic correlations (e.g. mRNA co-expression, chromosomal clustering across genomes and protein fusions) between known and missing parts of metabolic networks. In addition, using biochemical literature, transcriptome data or by direct measurements, the presence of missing enzymatic reactions may be proven and the network can be completed. Mostly, such a complete metabolic network contains underdetermined parts due to the presence of parallel or cyclic pathways. This means that for certain parts of the network the flux values cannot be determined. In order to narrow down the number of possible solutions for these parts, constraints can be set on certain enzymatic reactions based on biochemical and thermodynamic information found in literature or determined experimentally. In addition, an optimal solution that optimizes a particular objective function for the underdetermined reactions can be

found using linear programming. This constraints-based metabolic modeling technique is often referred to as flux-balance analysis (FBA). The computational reconstruction and analysis of metabolic models, starting from genomic information, is an essential aspect of systems biology and can be used for vaccine process development purposes as described in Chapter 2. In particular, knowledge about metabolism is essential for the development of an efficient cultivation process, since product quality and quantity are primarily determined in this process.

An extensive literature study on the primary metabolism of *N. meningitidis* in combination with the publically available genome sequence of *N. meningitidis* serogroup B [7] led to the construction of a genome-scale metabolic model. The validity of a simplified metabolic network derived from the genome-scale metabolic network was checked using flux-balance analysis using data from chemostat cultures and several useful predictions were obtained from *in silico* experiments, including substrate preference. The genome-scale model is valuable, because it offers a framework to study the *N. meningitidis* metabolism as a whole, or certain aspects of it. In the present study it was used to design a chemically defined, minimal synthetic medium for growth of *N. meningitidis*, which was tested successfully in batch and chemostat cultures.

The specific growth rate of bacteria is an important parameter in biotechnological processes, since it determines the macro-molecular composition of the bacterial cell and its metabolic activity [8-11]. In Chapter 3 the model was used to study the influence of the growth rate of *N. meningitidis* on its macro-molecular composition and its metabolic activity in chemostat cultures. It was found that *N. meningitidis* maintains its macromolecular composition even when its growth rate is changed fourfold. At high growth rate the PorA content in outer membrane vesicles extracted from biomass was significantly lower in comparison with low growth rates, which indicates the importance of the culture harvest point in the regular vaccine production process. The yield and maintenance parameters related to growth yield on substrate ($Y_{x/s}$ and

m_s) and energy requirements for biomass formation ($Y_{x/ATP}$ and m_{ATP}) were estimated and are in the same order of magnitude as the values found in literature for *Escherichia coli*. The metabolic fluxes at various growth rates were calculated using FBA with maximization of ATP yield as objective function and errors in fluxes were calculated using Monte Carlo Simulation (MCS). Using this MCS approach, the reliability of the calculated flux distribution could be calculated for the determined parts of the metabolic network. The flux values obtained for the underdetermined parts using maximization of ATP as objective function showed that all the produced glucose-6-phosphate is processed solely through the Entner-Doudoroff pathway (EDP), since the EDP can yield slightly more energy per consumed glucose in comparison with the pentose phosphate pathway (PPP). Notably, the Embden-Meyerhof-Parnas glycolytic pathway (EMP) is not functional in *N. meningitidis*. Although the objective function ‘maximization of ATP yield’ was found to achieve a relatively high predictive accuracy for ^{13}C -determined *in vivo* fluxes in *E. coli* [12], the obtained results using this objective function can be questioned. For this reason the flux values were re-calculated using the same objective function, while incorporating different pre-set EDP:PPP ratios. This split ratio analysis between the Entner-Doudoroff (EDP) and the pentose phosphate pathway (PPP), the sole glucose utilizing pathways in *N. meningitidis*, indicated that, given the measured rates, a minimal flux through the Entner-Doudoroff pathway is required in *N. meningitidis*. In addition, based on the minor effect of the split ratio on the ATP formation rate, it was concluded that the mathematical result obtained from the objective function ‘maximization of ATP yield’ may not reflect the actual biological situation for the underdetermined parts of the metabolic network. Therefore, the fluxes of the underdetermined parts of the metabolic network were presented as flux ranges, which were calculated from the EDP:PPP split ratio analysis.

Genetic engineering

Genetic engineering has been applied in *N. meningitidis* in order to express different PorA serosubtypes in one strain [13] or to detoxify LPS [14], but it has not been used

to improve production strains from a manufacturing point of view (e.g. increase the yield of biomass on substrate or reduce by-product formation). The research described in Chapter 4 is a first step in this direction. In accordance with the *N. meningitidis* serogroup B genome [7] and studies on glucose utilization in *N. meningitidis* [15-20], it was found previously that the Embden-Meyerhof-Parnas glycolytic pathway is not functional in *N. meningitidis* because a single gene, *pfkA*, encoding phosphofructokinase (PFK), is missing from the *N. meningitidis* genome. In Chapter 4, based on the model developed in Chapter 2 and 3, *in silico* FBA indicated that expression of PFK in *N. meningitidis* results in an increased yield of biomass on substrate. The predicted increase in yield was relatively higher at low growth rates. This poses the question why PFK is not present in *N. meningitidis*. A comparative genomics approach to establish which factors determine the presence or absence of PFK in an organism indicated that in most obligate aerobic organisms, like *N. meningitidis*, PFK is lacking. In many (facultative) anaerobic organisms PFK is present and seems to go hand in hand with the presence of a phosphoenolpyruvate:carbohydrate phosphotransferase system (PTS system). A competitive advantage under anaerobic conditions seems the most important factor for the presence of PFK. In the case of limiting energy availability, due to the absence of oxidative phosphorylation, the objective of an organism seems to be optimization of energy yield on substrate (maximize $Y_{ATP/s}$) favoring PFK. In the case sufficient energy can be liberated from the substrate due to oxidative phosphorylation, the objective of an organism seems to be to optimize the rate of energy generation (maximize r_{ATP}) in order to outcompete other micro-organisms living in the same habitat. Natural evolution of *N. meningitidis* takes place in the aerobic nasopharyngeal mucosa, which can explain absence of *pfkA* in the *N. meningitidis* genome. Although *in silico* FBA predicted an increase in biomass yield upon inclusion of PFK, a genetically engineered recombinant *N. meningitidis* strain that expresses a heterologous phosphofructokinase from *E. coli*, grown in glucose limited chemostat, gave a lower biomass yield as compared to the genetically engineered control strain without PFK. Based on the experimental observations it was concluded that this was possibly caused

by phosphatase activity, creating a futile cycle (dissipation of energy). In addition, this made clear that no initial advantage is gained when PFK is expressed in *N. meningitidis*, which illustrates that possible (intra-species) horizontal gene transfer events [21, 22] to obtain the *pfkA* gene are unlikely.

Scale-up

The gathered knowledge on the *N. meningitidis* serogroup B metabolism led to the development of a small-scale cultivation process, including the development of a chemically defined medium for high cell-density cultivation and defined culture conditions, in parallel with the development of a reproducible and robust cell bank procedure for the three trivalent [23] vaccine production strains (unpublished results). As described in Chapter 5, this provided the starting point for scale-up of the upstream part of the vaccine production process in which regime analysis [24] identified oxygen uptake rate as the rate-limiting subprocess. Hence, the primary bioreactor design was done on the basis of gas-liquid mass transfer and an aeration and ventilation controller, which increases the stirrer speed and gas flow rate simultaneously at increasing oxygen demand, was developed and successfully implemented. In order to prevent the use of antifoaming agents and thus complex validation studies to show proof of removal of these agents from the final product, mechanical foam control using stirring in combination with a rotary plate foam breaker proved to be an effective way to contain foam inside the bioreactor. The 1.2 m³ bioreactor was technically realized following cGMP guidelines and is appropriate for bulk production of the vaccine for phase III clinical trials and for the vaccine after licensing of the product. In addition, the design of the bioreactor allows production of other bacterial vaccines (e.g. diphtheria) without the need for fundamental changes (i.e. multi-purpose). This work illustrates that the combination of regime analysis, OUR as scale-up parameter followed by a bioreactor design based on empirical relations and a defined mode of operation is an effective strategy that can be adopted for scale-up of aerobic cultivation processes in general. Notably, the upstream production process described in this study yields at least a

sufficient amount of biomass for production of the *N. meningitidis* serogroup B vaccine for the Dutch market, which indicates the potentially meaningful impact on public health in The Netherlands and beyond.

Outlook

The metabolic model of *N. meningitidis* presented in this thesis can be used for further optimization of the cultivation process which can lead to higher biomass concentrations. In addition, genetic engineering of *N. meningitidis* from a manufacturing point of view has been hardly investigated and the presented metabolic model of *N. meningitidis* can be used as a starting point to identify suitable targets for this purpose. It is worth noting that various success stories have been reported in the literature [25-27], where a metabolic model was used *in silico*, to determine the effect of knocking-out a gene or a set of genes and their corresponding biochemical pathways on biomass yield. This illustrates the potential of whole cell modeling and simulation [28-30]. Obtaining various system-level, or so-called ‘omics’, datasets, together with existing data, presented in this thesis and the literature, will facilitate the further development of the vaccine production process and the development of analytical tools needed for the characterization of the vaccine candidates and in a later stage for quality control of the licensed vaccines [31].

The availability of hundreds of *N. meningitidis* genomes enables identification of their genetic differences and shows an unexpected high degree of intra-species diversity. This suggests that in many cases, a universal vaccine is possible only by including a combination of antigens and this combination must take into account the population structure of the pathogen [32]. In order to make the bulk production of such a combination vaccine feasible, genetic engineering is required and at the Netherlands Vaccine Institute (NVI), genetic engineering has been applied in *N. meningitidis* in order to express different PorA serosubtypes in one strain [13]. However, some PorAs appear to be weakly immunogenic [33] and an adjusted immu-

nization schedule [34] is required to overcome this problem. Obtaining a higher cellular concentration of these weakly immunogenic PorAs in recombinant *N. meningitidis* strains, and thus in the final product (i.e. outer membrane vesicles), by controlling the expression level of the different PorAs is an interesting alternative. The feasibility of such approach has been demonstrated in *E. coli*, where a partial least squares model (PLS) found good correlations between the sequence of a promoter and its strength [35], which resulted in the ability to control the expression level of an enzyme in central metabolism by changing the promoter of the gene encoding this enzyme in the *E. coli* genome (unpublished results).

The computational reconstruction and analysis of metabolic models of microbial metabolism is one of the first success stories of systems biology. Nevertheless, the extent and quality of metabolic network reconstructions and thus also the model developed in Chapter 2 and 3 is still limited by the current state of biochemical knowledge and analytical methods. For example, even in *E. coli*, one of the most studied bacteria, a new metabolic pathway of glucose metabolism was discovered in 2003 [36] and a previously undescribed pathway for pyrimidine catabolism was discovered in 2006 [37]. In addition, large-scale metabolite profiling indicates an abundance of unknown compounds in metabolism [38], which illustrates that metabolomic measurements provide a wealth of information about the biochemical status of cells, tissues or organisms and play an increasing role to elucidate the function of unknown and novel genes [39, 40]. Hence, experimental high-throughput data can be used to improve and expand metabolic network reconstructions to include unexplored areas of metabolism. Advances in experimental technology and analytical methodologies [41] bring this aim an important step closer to realization. The processing and integration of datasets, obtained from the different system-levels of information that are present in an organism (i.e. the ‘omes’), will play an important part in exploiting the new experimental opportunities for vaccine and vaccine process development (e.g. the design of growth media). Therefore, setting up a systems biology platform in the research and

development department of biopharmaceutical companies, and institutes like the NVI is an absolute requirement in order to significantly shorten the development time of a vaccine. Knowledge gathered from such a systems biology platform can be used in the complete development trajectory of a vaccine, starting from identification and selection of vaccine candidates, to the design of growth media and the identification of genetic engineering targets to possibly improve the organism. Notably, increasing the level of understanding of the immunological mechanisms of protection [42] will also contribute to a more focused and faster vaccine development track.

REFERENCES

1. WHO. The world health report 2007: a safer future : global public health security in the 21st century. Geneva: World Health Organization; 2007.
2. Kaufmann SH. 2007. The contribution of immunology to the rational design of novel antibacterial vaccines. *Nat Rev Microbiol* 5:491-504.
3. Shafer RW, Schapiro JM. 2008. HIV-1 Drug Resistance Mutations: an Updated Framework for the Second Decade of HAART. *AIDS Rev* 10:67-84.
4. Jones KE, Patel NG, Levy MA, Storeygard A, Balk D, Gittleman JL, Daszak P. 2008. Global trends in emerging infectious diseases. *Nature* 451:990-993.
5. Rappuoli R. 2001. Reverse vaccinology, a genome-based approach to vaccine development. *Vaccine* 19:2688-2691.
6. Palsson BO. *Systems Biology: Properties of Reconstructed Networks*. New York: Cambridge University Press; 2006.
7. Tettelin H, Saunders NJ, Heidelberg J, Jeffries AC, Nelson KE, Eisen JA, Ketchum KA, Hood DW, Peden JF, Dodson RJ et al. 2000. Complete genome sequence of *Neisseria meningitidis* serogroup B strain MC58. *Science* 287:1809-1815.
8. Teusink B, Wiersma A, Molenaar D, Francke C, de Vos WM, Siezen RJ, Smid EJ. 2006. Analysis of growth of *Lactobacillus plantarum* WCFS1 on a complex medium using a genome-scale metabolic model. *J Biol Chem* 281:40041-40048.
9. Oliveira AP, Nielsen J, Forster J. 2005. Modeling *Lactococcus lactis* using a genome-scale flux model. *BMC Microbiol* 5:39.
10. Pramanik J, Keasling JD. 1998. Effect of *Escherichia coli* biomass composition on central metabolic fluxes predicted by a stoichiometric model. *Biotechnol Bioeng* 60:230-238.
11. Bremer H, Dennis PP. Modulation of chemical composition and other parameters of the cell by growth rate. In: *Escherichia coli* and *Salmonella typhimurium*: Cellular and Molecular Biology. Edited by Neidhardt FC, Curtiss R, Ingraham JL, Brooks Low K, Magasanik B, Reznikoff WS, Riley M, Schaechter M, Umberger HE, vol. 1, 2 edn. Washington D.C.: American Society for Microbiology; 1996: 1553-1569.
12. Schuetz R, Kuepfer L, Sauer U. 2007. Systematic evaluation of objective functions for predicting intracellular fluxes in *Escherichia coli*. *Mol Syst Biol* 3 (article 119):1-15.
13. van der Ley P, van der Biezen J, Poolman JT. 1995. Construction of *Neisseria meningitidis* strains carrying multiple chromosomal copies of the porA gene for use in the production of a multivalent outer membrane vesicle vaccine. *Vaccine* 13:401-407.
14. Ley Pvd, Steeghs L, Hamstra HJ, Hove Jt, Zomer B, Alphen Lv. Modification of lipid A biosynthesis in *Neisseria meningitidis* lpxL1 mutants: influence on lipopolysaccharide structure, toxicity, and adjuvant activity. In: *Infection and Immunity*. vol. 69 2005: 5981-5990.
15. Holten E. 1974. 6-Phosphogluconate dehydrogenase and enzymes of the Entner-Doudoroff pathway in *Neisseria*. *Acta Pathol Microbiol Scand [B] Microbiol Immunol* 82:207-213.
16. Holten E. 1975. Radiorespirometric studies in genus *Neisseria*. I. The catabolism of glucose. *Acta Pathol Microbiol Scand [B]* 83:353-366.
17. Jyssum K. 1962. Dissimilation of C14 labelled glucose by *Neisseria meningitidis* 1. The formation of CO₂ and acetate from glucose carbon. *Acta Pathol Microbiol Immunol Scand [B]* 55:319-324.
18. Jyssum K. 1962. Dissimilation of C14 labelled glucose by *Neisseria meningitidis* 2. The incorporation of 1-C14 and 6-C14 into cellular components in short time experiments. *Acta Pathol Microbiol Immunol Scand [B]* 55:325-334.
19. Jyssum K. 1962. Dissimilation of C14 labelled glucose by *Neisseria meningitidis* 2. The incorporation of 1-C14 and 6-C14 into pyruvate. *Acta Pathol Microbiol Immunol Scand [B]* 55:335-341.
20. Jyssum K, Borchgrevink B, Jyssum S. 1961. Glucose catabolism in *Neisseria meningitidis*. 1. Glucose oxidation and intermediate reactions of the Embden-Meyerhof pathway. *Acta Pathol Microbiol Scand* 53:71-83.
21. Omelchenko MV, Makarova KS, Wolf YI, Rogozin IB, Koonin EV. 2003. Evolution of mosaic operons by horizontal gene transfer and gene displacement in situ. *Genome Biol* 4:R55.
22. Kroll JS, Wilks KE, Farrant JL, Langford PR. 1998. Natural genetic exchange between *Haemophilus* and *Neisseria*: intergeneric transfer of chromosomal genes between major human pathogens. *Proc Natl Acad Sci U S A* 95:12381-12385.

23. Bos JM, Rumke HC, Welte R, Spanjaard L, van Alphen L, Postma MJ. 2006. Combination vaccine against invasive meningococcal B and pneumococcal infections: potential epidemiological and economic impact in the Netherlands. *Pharmacoeconomics* 24:141-153.
24. Sweere APJ, Luyben KCAM, Kossen NWF. 1987. Regime analysis and scale-down: Tools to investigate the performance of bioreactors. *Enzyme and Microbial Technology* 9:386-398.
25. Hua Q, Joyce AR, Fong SS, Pálsson BO. 2006. Metabolic analysis of adaptive evolution for *in silico*-designed lactate-producing strains. *Biotechnol Bioeng* 95:992-1002.
26. Fong SS, Burgard AP, Herring CD, Knight EM, Blattner FR, Maranas CD, Pálsson BO. 2005. *In silico* design and adaptive evolution of *Escherichia coli* for production of lactic acid. *Biotechnol Bioeng* 91:643-648.
27. Smid EJ, Molenaar D, Hugenholtz J, de Vos WM, Teusink B. 2005. Functional ingredient production: application of global metabolic models. *Curr Opin Biotechnol* 16:190-197.
28. Joyce AR, Pálsson BO. 2007. Toward whole cell modeling and simulation: comprehensive functional genomics through the constraint-based approach. *Prog Drug Res* 64:265, 267-309.
29. Joyce AR, Pálsson BO. 2008. Predicting gene essentiality using genome-scale *in silico* models. *Methods Mol Biol* 416:433-457.
30. Gianchandani EP, Oberhardt MA, Burgard AP, Maranas CD, Papin JA. 2008. Predicting biological system objectives de novo from internal state measurements. *BMC Bioinformatics* 9:43.
31. Streefland M, van de Waterbeemd B, Happe H, van der Pol LA, Beuvery EC, Tramper J, Martens DE. 2007. PAT for vaccines: the first stage of PAT implementation for development of a well-defined whole-cell vaccine against whooping cough disease. *Vaccine* 25:2994-3000.
32. Mora M, Donati C, Medini D, Covacci A, Rappuoli R. 2006. Microbial genomes and vaccine design: refinements to the classical reverse vaccinology approach. *Curr Opin Microbiol* 9:532-536.
33. Luijckx TA, van Dijken H, Hamstra HJ, Kuipers B, van der Ley P, van Alphen L, van den Dobbelsteen G. 2003. Relative immunogenicity of PorA subtypes in a multivalent *Neisseria meningitidis* vaccine is not dependent on presentation form. *Infect Immun* 71:6367-6371.
34. Luijckx T, van Dijken H, van Els C, van den Dobbelsteen G. 2006. Heterologous prime-boost strategy to overcome weak immunogenicity of two serosubtypes in hexavalent *Neisseria meningitidis* outer membrane vesicle vaccine. *Vaccine* 24:1569-1577.
35. De Mey M, Maertens J, Lequeux GJ, Soetaert WK, Vandamme EJ. 2007. Construction and model-based analysis of a promoter library for *E. coli*: an indispensable tool for metabolic engineering. *BMC Biotechnol* 7:34.
36. Fischer E, Sauer U. 2003. A novel metabolic cycle catalyzes glucose oxidation and anaplerosis in hungry *Escherichia coli*. *J Biol Chem* 278:46446-46451.
37. Loh KD, Gyaneshwar P, Markenscoff Papadimitriou E, Fong R, Kim KS, Parales R, Zhou Z, Inwood W, Kustu S. 2006. A previously undescribed pathway for pyrimidine catabolism. *Proc Natl Acad Sci U S A* 103:5114-5119.
38. Fiehn O, Weckwerth W. 2003. Deciphering metabolic networks. *Eur J Biochem* 270:579-588.
39. Hollywood K, Brison DR, Goodacre R. 2006. Metabolomics: current technologies and future trends. *Proteomics* 6:4716-4723.
40. Kell DB. 2004. Metabolomics and systems biology: making sense of the soup. *Curr Opin Microbiol* 7:296-307.
41. van der Werf MJ, Overkamp KM, Muilwijk B, Coulter L, Hankemeier T. 2007. Microbial metabolomics: toward a platform with full metabolome coverage. *Anal Biochem* 370:17-25.
42. Lambert PH, Liu M, Siegrist CA. 2005. Can successful vaccines teach us how to induce efficient protective immune responses? *Nat Med* 11:S54-62.

Summary

The species *Neisseria meningitidis* is only found in humans and colonizes mucosal surfaces of the nasopharynx (nose and throat) as a harmless commensal organism and, as such, is carried by five to ten percent of the adult population. Some strains are able to cross the mucosa into the bloodstream from where they can cause the diseases meningitis or septicaemia. These diseases are responsible for death and disability especially in young infants. There are different pathogenic *N. meningitidis* isolates of which five serogroups (A, B, C, Y, and W135) are responsible for most of the disease. Serogroup B and C organisms cause the majority of infections in Europe and America, whereas strains of group A and C dominate in Africa and Asia. Effective polysaccharide and conjugate vaccines have been developed against serogroups A, C, Y and W135 strains. However, effective global prevention of meningococcal disease will not be achievable without the development of a vaccine against serogroup B meningitis, which causes about 50% of meningococcal disease cases worldwide. Since the polysaccharide of the serogroup B meningococcus is poorly immunogenic, current vaccine development against serogroup B organisms has mainly focussed on subcapsular protein antigens that are contained in outer membrane vesicles (OMVs). The outer membrane protein PorA has been identified as a major inducer of, and target for serum bactericidal antibodies and is expressed by almost all meningococci, which pinpoints PorA as a promising vaccine candidate. However, PorA appears heterogeneous, requiring the development of a multivalent vaccine in which various PorA serosubtypes are present in order to induce sufficient protection.

At the Netherlands Vaccine Institute (NVI) a vaccine against serogroup B organisms, including different PorA serosubtypes contained in OMVs is currently being developed. The process development focuses on cultivation of the organism, extraction of OMVs and additional purification steps. The aim of the research described in this thesis was the development and scale-up of the cultivation process for a vaccine against *N. meningitidis* serogroup B organisms based upon PorA entrapped in outer membrane vesicles.

Working from the genomic database of *Neisseria meningitidis* serogroup B together with biochemical and physiological information provided in literature, a genome-scale flux model for primary metabolism of *Neisseria meningitidis* was constructed as described in Chapter 2. The validity of a simplified metabolic network that was derived from the genome-scale metabolic network was checked using flux-balance analysis with data obtained from chemostat cultures. Several useful predictions were obtained from in silico experiments, including substrate preference, and a minimal medium for growth of *Neisseria meningitidis*. The medium was tested successfully in batch and chemostat cultures. The genome-scale model is valuable, because it offers a framework to study *N. meningitidis* metabolism as a whole or certain aspects of it and can also be used for vaccine process development purposes (e.g. design of growth media).

Chapter 3 describes the influence of the growth rate of *N. meningitidis* on its macromolecular composition and its metabolic activity using chemostat cultures. In the applied range of growth rates, no significant changes in RNA content and protein content with growth rate were observed in *N. meningitidis*. The DNA content was somewhat higher at the highest applied growth rate. The phospholipid and lipopolysaccharide content in *N. meningitidis* changed with growth rate, but no specific trends were observed. The cellular fatty acid composition and the amino acid composition did not change significantly with growth rate. At high growth rate the PorA content in outer membrane vesicles extracted from biomass was significantly lower in comparison with low growth rates, which indicates the importance of the culture harvest point in the regular vaccine production process. The metabolic fluxes at various growth rates were calculated using Flux Balance Analysis. Errors in fluxes were calculated using Monte Carlo simulation and the reliability of the calculated flux distribution could be indicated. The yield of biomass on substrate ($Y_{x/s}$) and the maintenance coefficient (m_s) were determined as $0.44 (\pm 0.04) \text{ g.g}^{-1}$ and $0.04 (\pm 0.02) \text{ g.g}^{-1}.\text{h}^{-1}$, respectively. The growth associated energy requirement ($Y_{x/ATP}$) and the non-growth associated ATP requirement for maintenance (m_{ATP}) were estimated as $0.13 (\pm 0.04) \text{ mol.mol}^{-1}$

and $0.43 (\pm 0.14) \text{ mol} \cdot \text{mol}^{-1} \cdot \text{h}^{-1}$, respectively. Split ratio analysis between the Entner-Doudoroff (EDP) and the pentose phosphate pathway (PPP), the sole glucose utilizing pathways in *N. meningitidis*, indicated that, given the measured rates, a minimal flux through the Entner-Doudoroff pathway is required in *N. meningitidis*. Furthermore, it was found that the split ratio between the Entner-Doudoroff and the pentose phosphate pathway, the sole glucose utilizing pathways in *N. meningitidis*, had a minor effect on ATP formation rate but a major effect on the fluxes going through, for instance, the citric-acid cycle. For this reason, flux ranges were presented for underdetermined parts of metabolic network rather than presenting single flux values.

According to the genomic information for *N. meningitidis* and experimental observations, glucose can be completely catabolized through the Entner-Doudoroff pathway (ED) and the pentose phosphate pathway (PP). The Embden-Meyerhof-Parnas glycolytic pathway (EMP) is not functional, because the gene for phosphofructokinase (*pfkA*) is not present. As described in Chapter 4, the phylogenetic distribution of phosphofructokinase (PFK) obtained from 312 bacterial species indicates that in most obligate aerobic organisms PFK is lacking and it was concluded that this is because of the limited contribution of PFK to the energy supply in aerobically grown organisms in comparison with the energy generated through oxidative phosphorylation. Under anaerobic or microaerobic conditions the available energy is limiting and PFK provides an advantage, which explains the presence of PFK in many (facultative) anaerobic organisms. In accordance with this, *in silico* flux balance analysis predicted an increase in biomass yield as a result of PFK expression. Analysis of a genetically engineered *N. meningitidis* strain that expresses a heterologous phosphofructokinase from *Escherichia coli* (encoded by the *pfkA* gene) showed that the yield of biomass on substrate ($Y_{x/s}$) decreased in comparison with a *pfkA* deficient control strain, which was compensated mainly by an increase in CO_2 production, whereas production of by-products was comparable between the *pfkA* mutant and a control strain. It was concluded that this is possibly caused by the fact that phosphatases are

active, creating futile cycles and dissipation of energy. This might explain why the *pfkA* gene is not obtained by horizontal gene transfer, since it is initially unfavourable for biomass yield. No large effects related to heterologous expression *pfkA* were observed in the transcriptome and overall the changes in the biomass composition were minimal.

The gathered knowledge on the *N. meningitidis* serogroup B metabolism led to the development of a small-scale cultivation process, including the development of a chemically defined medium for high cell-density cultivation and defined culture conditions. In addition a reproducible and robust cell bank procedure was developed for the three trivalent vaccine production strains. In order to meet the expected demand for product, the biopharmaceutical production process was scaled-up. Chapter 5 describes the scale-up approach for the upstream process and the resulting bioreactor design and operation strategy leading to a feasible solution for bulk production of a vaccine against meningococcal disease. The combination of regime analysis, oxygen uptake rate as scale-up parameter followed by a bioreactor design based on empirical relations and a defined mode of operation was an effective strategy that can be adopted for scale-up of aerobic cultivation processes in general.

The technically realized 1.2 m³ bioreactor, equipped with a turbine impeller for gas dispersion, was complemented with an upward pumping impeller and a rotary plate foam breaker to contain foam inside the bioreactor. Hence, the use of antifoaming agents, and thus complex validation studies to show proof of removal of these agents from the final product, could be prevented. Aeration and ventilation in the culture broth were controlled by increasing the stirrer speed and gas flow rate simultaneously at increasing oxygen demand. The scale-up was successful and comparable growth curves and nutrient consumption profiles were reached on 0.06 and 1.2 m³. The upstream production process, including the realized manufacturing bioreactor configuration is compliant with current good manufacturing practices and yields at the least a sufficient amount of biomass for production of the *N. meningitidis* serogroup B vaccine for the Dutch market.

The work described in this thesis illustrates that the application of systems biology tools provides a new and effective way for vaccine process development against *N. meningitidis* serogroup B organisms. The application of systems biology in vaccine and vaccine process development will lead to a significant shortening of the development time from vaccine candidate to vaccine, which is an absolute requirement in order to deal with the rapidly emerging infectious diseases.

Samenvatting

Neisseria meningitidis, ofwel meningokok, is een Gram-negatieve bacterie, die alleen voorkomt in de mens. De natuurlijke habitat van deze bacterie is het slijmvlies van de nasopharynx (neus-keelholte) in de mens. Ongeveer 10% van de bevolking draagt de meningokok in de nasopharynx zonder ziekteverschijnselen te vertonen. Sommige meningokokken stammen zijn in staat om de slijmvliesen te passeren en in de bloedsomloop terecht te komen, vanwaar ze de ziektes hersenvliesontsteking (meningitis) of bloedvergiftiging (sepsis) kunnen veroorzaken. Deze ziektes treffen vooral jonge kinderen en zijn verantwoordelijk voor sterfte en invaliditeit. Er komen verschillende pathogene meningokokken voor waarvan vijf serogroepen (A, B, C, Y en W135) verantwoordelijk zijn voor de meeste ziektegevallen. In Europa worden de meeste infecties veroorzaakt door serogroep B en C meningokokken, terwijl groep A en C meningokokken domineren in Afrika en Azië. Vaccins tegen serogroep A, C, Y en W135 meningokokken, die gebaseerd zijn op polysacchariden (suikerketens) uit het kapsel van de bacterie en gebonden kunnen zijn aan een eiwit (polysaccharide-conjugaat), zijn beschikbaar en werkzaam. Echter, wereldwijde bescherming tegen meningokokkenziekte is niet haalbaar zonder de ontwikkeling van een vaccin tegen serogroep B meningokokken, die wereldwijd ongeveer 50% van de ziektegevallen veroorzaken. Polysacchariden van serogroep B meningokokken zijn nauwelijks immunogeen en dus niet werkzaam. Om deze reden spitst vaccinontwikkeling tegen serogroep B meningokokken zich toe op eiwitten, die door het buitenmembraan (en het kapsel) van de bacterie heen steken. Het porievormend buitenmembraaneiwit, PorA, is in staat om bacteriedodende antistoffen op te wekken in de mens en komt voor in bijna alle meningokokken. Deze bacteriedodende antistoffen bieden bescherming tegen meningokokkenziekte en daarom is PorA een veelbelovende vaccinkandidaat. Niet in elke meningokok is het PorA eiwit hetzelfde (heterogeen), waardoor verschillende PorA eiwitten in het vaccin opgenomen moeten worden om bescherming te bieden tegen de verschillende meningokokkenstammen. Daarnaast is het belangrijk dat de PorA eiwitten in de juiste conformatie gepresenteerd worden. Bij het Nederlands Vaccin Instituut wordt een vaccin tegen serogroep B meningokokken ontwikkeld op basis van

genetisch gemodificeerde meningokokken stammen, die geen kapsel hebben en meerdere PorA eiwitten tot expressie brengen. Door het buitenmembraan van deze stammen te destabiliseren met een zeepachtige stof worden blaasjes (*vesicles*) van het buitenmembraan afgescheiden. Deze zogenaamde buitenmembraan*vesicles* (in het Engels *outer membrane vesicles*, OMVs) bevatten de PorA eiwitten in de juiste conformatie en vormen de basis van het vaccin. In totaal worden drie recombinante meningokokken stammen, die elk drie verschillende PorA eiwitten tot expressie brengen, gebruikt voor het vaccin, dat om deze reden een multivalent OMV vaccin wordt genoemd. De procesontwikkeling van het vaccin richt zich op: het kweken van de recombinante meningokokken-stammen, de extractie van de OMVs en de zuivering van de OMVs.

Het onderwerp van dit proefschrift is de ontwikkeling en de opschaling van het kweekproces, voor de productie van het multivalente OMV vaccin tegen serogroep B meningokokken.

Kennis van de stofwisseling (het metabolisme) van de bacterie is erg belangrijk voor het ontwikkelen van een efficiënt kweekproces. Het kweekproces is de bepalende factor voor de productkwaliteit en -kwantiteit. De informatie, die in het genoom van *Neisseria meningitidis* serogroep B aanwezig is, kan gebruikt worden voor de ontwikkeling van het kweekproces door in het genoom de genen op te zoeken die coderen voor enzymen, die aanwezig zijn in het primair metabolisme. De reacties, die deze enzymen uitvoeren, vormen tezamen een metabool netwerk.

Op basis van het genoom van *N. meningitidis* serogroep B en biochemische en fysiologische informatie uit de literatuur werd een dergelijk, genoom-gebaseerd, metabolisch netwerk opgesteld, zoals beschreven staat in hoofdstuk 2. De geldigheid van een vereenvoudigd metabolisch netwerk, dat werd afgeleid van het genoom-gebaseerde netwerk, werd vastgesteld met behulp van flux balans analyse (FBA). FBA is een wiskundige techniek, waarmee de intracellulaire omzettingssnelheden van de meta-

bolieten, oftewel de metabolische fluxen, en de productie- en consumptiesnelheden van de extracellulaire metabolieten, berekend kunnen worden. Zonder experimentele metingen wordt FBA *in silico* FBA genoemd. In dit geval kunnen de fluxen berekend worden door het stellen van bepaalde randvoorwaarden (bijvoorbeeld een maximale substraat consumptiesnelheid) en door gebruik te maken van een optimaliteitscriterium, oftewel doelfunctie. Een voorbeeld van een doelfunctie is bijvoorbeeld ‘maximaliseer biomassa’. Door het toepassen van een doelfunctie worden fluxwaarden berekend die optimaal zijn voor de doelfunctie. Met andere woorden, er worden fluxwaarden berekend die de doelfunctie optimaliseren. In beide gevallen (met en zonder metingen) is het vastleggen van de richting waarin irreversibele reacties verlopen belangrijk, omdat op deze manier het aantal mogelijke oplossingen wordt beperkt. Op de gemeten metaboliet concentraties, de concentratie bacteriën, de samenstelling van de bacteriën, de stoffen in de gasfase etc. zit een bepaalde variantie. Deze varianties kunnen gebruikt worden om de variantie in de omzettingssnelheden te berekenen. De variantie in de omzettingssnelheden kan vervolgens gebruikt worden om de zogenaamde redundante omzettingssnelheden op elkaar af te stemmen. Dit afstemmen wordt balanceren van de omzettingssnelheden genoemd en heeft als resultaat dat de gemeten omzettingssnelheden nauwkeuriger worden geschat, waardoor ook de fluxen nauwkeuriger berekend worden.

Zoals beschreven staat in hoofdstuk 2, kan Monte Carlo simulatie gebruikt worden om bovengenoemde varianties te berekenen. De omzettingssnelheden voor de FBA beschreven in hoofdstuk 2 werden experimenteel gemeten in continu culturen (chemostat) en volgens bovengenoemde technieken verwerkt. Daarnaast werden verschillende bruikbare *in silico* voorspellingen gedaan waaronder substraat-voorkeur hetgeen heeft geleid tot een minimaal groeimedum voor *N. meningitidis* serogroep B. De specifieke groeisnelheid van bacteriën is een belangrijke parameter in biotechnologische processen omdat deze de macromoleculaire samenstelling en metabolische activiteit van de bacterie bepaalt. Hoofdstuk 3 beschrijft de invloed van de specifieke groeisnelheid van

N. meningitidis op de macromoleculaire samenstelling en metabolische activiteit. In het toegepaste bereik van groeisnelheden werden geen significante verschillen waargenomen in RNA- en eiwit-gehalten. Het DNA-gehalte was enigszins hoger bij de hoogste groeisnelheid. De fosfolipid- en lipopolysaccharidegehalten veranderden met de groeisnelheid, maar er werden geen specifieke trends waargenomen. De vetzuur- en eiwit-samenstellingen veranderden niet significant met de groeisnelheid. Bij de hoogste groeisnelheid was het PorA gehalte in buitenmembraanvesicles significant lager in vergelijking met de lagere groeisnelheden. Dit is een belangrijke indicatie voor het oogstmoment in het reguliere vaccin-productieproces. De metabolische fluxen bij de verschillende groeisnelheden werden berekend met behulp van FBA. Varianties in de fluxen werden berekend met Monte Carlo simulatie en de betrouwbaarheid van de fluxdistributie kon worden aangegeven. De berekende opbrengst van biomassa op substraat (*yield*, $Y_{x/s}$) en de onderhoudscoëfficiënt (maintenance, m_s) zijn respectievelijk $0.44 (\pm 0.04) \text{ g.g}^{-1}$ en $0.04 (\pm 0.02) \text{ g.g}^{-1}.\text{h}^{-1}$. De groei- ($Y_{x/ATP}$) en niet-groei-geassocieerde energie behoefte voor onderhoud van de bacterie (m_{ATP}) werden geschat als respectievelijk $0.13 (\pm 0.04) \text{ mol.mol}^{-1}$ en $0.43 (\pm 0.14) \text{ mol.mol}^{-1}.\text{h}^{-1}$. Ratio analyse tussen de Entner-Doudoroff (ED) route en de pentose-fosfaat (PP) route, de enige aanwezige routes voor het metaboliseren van glucose, gaf aan dat, gegeven de gemeten omzettingssnelheden, een minimale flux door de ED-route nodig is in *N. meningitidis*. De ratio bleek een minimaal effect te hebben op de vormingssnelheid van ATP maar een groot effect op de fluxen door bijvoorbeeld de citroenzuurcyclus. Om deze reden werd het numerieke bereik van de onderbepaalde fluxen van het netwerk weergegeven in plaats van de fluxwaarden.

Volgens het *N. meningitidis* genoom is de Embden-Meyerhof-Parnas route (glycolyse) niet functioneel omdat het *pfkA* gen, dat codeert voor fosfofructokinase (PFK), niet aanwezig is. Uit de fylogenetische distributie van PFK in 312 bacteriën blijkt dat PFK afwezig is in de meeste strikt aerobe bacteriën, zoals beschreven staat in hoofdstuk 4. Het is aannemelijk dat dit komt door de geringe bijdrage van PFK aan de energievoor-

ziening in aerobe organismen, in vergelijking met de oxidatieve fosforylering. Onder anaerobe of micro-aerobe omstandigheden is de beschikbare energie limited en dat verklaart de aanwezigheid van PFK in veel facultatieve anaerobe organismen. *In silico* FBA voorspelt dat bij aanwezigheid van PFK de biomassa *yield* toeneemt. Hiertoe werd genetisch modificatie toegepast om *pfkA* uit *Escherichia coli*, tot expressie te brengen in *N. meningitidis*. Uit analyse van deze mutant bleek echter dat de *yield* van biomassa op substraat afnam in vergelijking met de controle mutant. Het feit dat er minder koolstof naar biomassa ging werd voornamelijk gecompenseerd door een toename van CO₂-productie, terwijl de productie van bijproducten vergelijkbaar was tussen beide mutanten. Er werd geconcludeerd dat de lagere biomassa *yield* mogelijk veroorzaakt wordt door actieve fosfatasen die futiele cycli creëren. Dit verklaart mogelijk waarom *N. meningitidis* dit gen niet zal verkrijgen middels horizontale gen-overdracht omdat het initieel ongunstig is voor biomassa *yield*.

De vergaarde kennis van het *N. meningitidis* serogroep B metabolisme heeft geleid tot de ontwikkeling van een kleinschalig kweekproces, inclusief de ontwikkeling van een chemisch gedefinieerd medium, dat geschikt is voor kweken tot hoge celdichtheid, en gedefinieerde kweekcondities. Daarnaast werd een reproduceerbare en robuuste celbank ontwikkeld voor de drie trivalente vaccin productiestammen (niet gepubliceerde resultaten). Om aan de verwachte vraag naar vaccin te kunnen voldoen, werd het kweekproces opgeschaald. Hoofdstuk 5 beschrijft de opschalingsbenadering voor het kweekproces, en het resulterend bioreactor-ontwerp en de besturingsstrategie, die samen hebben geleid tot een realiseerbare oplossing voor de bulk-productie van een vaccin tegen meningokokkenziekte. De combinatie van regime-analyse, zuurstof-opnamesnelheid als opschalingsparameter, gevolgd door een bioreactor ontwerp dat werd gebaseerd op empirische relaties en een gedefinieerde werkingsmodus, bleek een effectieve strategie te zijn, die overgenomen kan worden voor opschaling van aerobe kweekprocessen in het algemeen. De technisch gerealiseerde 1.2 m³ bioreactor werd uitgerust met een turbine impeller voor gasdispersie en werd aangevuld met een

opwaarts pompende impeller en een mechanische schuimbreker om het schuim, dat ontstaat tijdens het kweekproces, in de reactor te houden. Hierdoor werd het gebruik van anti-schuimmiddelen voorkomen met als gevolg dat complexe validatie studies konden uitblijven. Beluchting en ventilatie van de kweekvloeistof werden gecontroleerd door het toerental van de impeller en het gasdebiet simultaan te verhogen bij toename van de zuurstofvraag. De opschaling was succesvol en vergelijkbare groeicurven en substraat-consumptieprofielen werden bereikt op 0.06 m³ en 1.2 m³ schaal. Het kweekproces, inclusief de bioreactor-configuratie, is conform de richtlijnen voor productie van biofarmaceutische producten en levert op zijn minst voldoende biomassa voor de productie van *N. meningitidis* serogroup B vaccin voor de Nederlandse markt.

Het werk, dat beschreven staat in dit proefschrift, laat zien dat toepassen van systeem biologie voorziet in een nieuwe en effectieve manier voor de procesontwikkeling van vaccins tegen serogroup B meningokokken. Het toepassen van systeembioologie in vaccinontwikkeling en procesontwikkeling van vaccins zal leiden tot een significante reductie van de ontwikkelingstijd van vaccinkandidaat naar vaccin, een noodzaak in het huidige tijdperk van snel opkomende nieuwe infectieziektes.

Glossary

Acellular vaccine	A cell-free vaccine prepared from purified antigenic components of cell-free microorganisms, carrying less risk than whole-cell preparations.
Adjuvants	A substance that is used to enhance the immune response of antigens. Aluminium salts are regularly used as adjuvants.
Alleles	One member of a pair or series of different forms of a gene. In general, alleles are coding sequences.
Antibodies	Gamma globulin proteins (or immunoglobulins) that are found in blood or other bodily fluids, and are used by the immune system to identify and neutralize foreign objects, such as bacteria and viruses.
Antigen	A substance that prompts the generation of antibodies and can cause an immune response.
Attenuated vaccine	A vaccine prepared from live microorganisms or viruses cultured under adverse conditions leading to loss of their virulence but retention of their ability to induce protective immunity.
Bioreactor	A vessel or system in which is carried out a chemical process which involves organisms or biochemically active substances derived from such organisms. Bioreactors are commonly cylindrical, ranging in size from liters to cube meters, and are often made of glass or stainless steel.
Diplococcus	A round bacterium (a coccus) that typically occurs in pairs of two joined cells.
Efficacy	A measure of the ability of a drug to induce a biological response in its molecular target.
Epitope	The part of a macromolecule that is recognized by the immune system, specifically by antibodies, B cells, or T cells.

Eradication	The termination of all transmission of infection by extermination of an infectious agent through surveillance and containment. For instance, global eradication has been achieved for smallpox.
Filamentous	Having the form of fine threads (or filaments).
Genotype	The inherited instructions of an organism carried within its genetic code.
Gram-negative bacteria	Bacteria that do not retain crystal violet dye in the Gram staining protocol which is a method to differentiating bacterial species into two large groups (Gram-positive and Gram-negative) based on the chemical and physical properties of their cell walls.
Homology	Sequence similarity among proteins and DNA.
Immunoglobulins	See antibodies.
Immunotype	Lipopolysaccharide-serotype classification based on differences in lipopolysaccharide structure.
<i>In vitro</i>	Refers to the technique of performing a given experiment in a controlled environment outside of a living organism (Latin: within the glass).
<i>In vivo</i>	Refers to which takes place inside an organism. In science, <i>in vivo</i> refers to experimentation done in or on the living tissue of a whole, living organism (Latin: within the living).
Innate immune respons	The innate immune system comprises the cells and mechanisms that defend the host from infection by other organisms, in a non-specific manner. This means that the cells of the innate system recognize, and respond to, pathogens in a generic way, but unlike the adaptive immune system, it does not confer long-lasting or protective immunity to the host.

Lag phase	Adaption period of bacteria to growth conditions. It is the period where the individual bacteria are maturing and not yet able to divide. During the lag phase of the bacterial growth cycle, synthesis of RNA, enzymes and other molecules occurs.
Leukocytes	White blood cells, or leukocytes, are cells of the immune system defending the body against both infectious disease and foreign materials.
Macrophages	Cells within the tissues that originate from specific white blood cells called monocytes. Monocytes and macrophages are phagocytes, acting in both non-specific defense (or innate immunity) as well as specific defense (or cell-mediated immunity) of vertebrate animals. Their role is to phagocytose (engulf and then digest) cellular debris and pathogens either as stationary or mobile cells, and to stimulate lymphocytes and other immune cells to respond to the pathogen.
Meningitis	Inflammation of the protective membranes covering the brain and spinal cord, known collectively as the meninges.
Monocytes	Monocyte is a type of leukocyte, part of the human body's immune system. Monocytes have two main functions in the immune system: (1) replenish resident macrophages and dendritic cells under normal states, and (2) in response to inflammation signals, monocytes can move quickly (~ 8-12 hours) to sites of infection in the tissues and divide/differentiate into macrophages and dendritic cells to elicit an immune response.
Mucosa	Mucous membranes are linings of mostly endodermal origin, covered in epithelium, which are involved in

	absorption and secretion. They line various body cavities that are exposed to the external environment and internal organs.
Nasopharynx	Nasal part of the pharynx that lies behind the nose and above the level of the soft tissue constituting the back of the roof of the mouth.
Oropharynx	Oral part of the pharynx that reaches from the the soft tissue constituting the back of the roof of the mouth to the level of the hyoid bone (bone in the neck).
Orthology	Homologous sequences (e.g. a gene sequence) in different species that are similar to each other because they originated from a common ancestor.
Phagocytosis	Phagocytosis is involved in the immune system (and in the acquisition of nutrients for some cells) and is a major mechanism used to remove pathogens and cell debris. Bacteria, dead tissue cells, and small mineral particles are all examples of objects that may be phagocytosed.
Pharynx	The part of the neck and throat situated immediately (behind) the mouth and nasal cavity.
Phase variation	An immune evasion technique employed by various bacteria. It involves the switching of surface antigens, to evade specific adaptive immune system responses.
Phenotype	Any observable characteristic of an organism (e.g. its morphology, biochemical or physiological properties, or behaviour).
Pleiotropy	Occurs when a single gene influences multiple phenotypic characteristics of an organism that may be inherited, environmentally determined or somewhere in between.

Potency	A measure of the concentration of a drug at which it is effective.
Sepsis, septicaemia	Sepsis is a serious medical condition characterized by a whole-body inflammatory state caused by infection. Sepsis is broadly defined as the presence of various pus-forming and other pathogenic organisms, or their toxins, in the blood or tissues. The term sepsis is frequently used to refer to septicemia (blood poisoning).
Subunit vaccine	A vaccine produced from specific (protein) subunits of a pathogen and thus having less risk of adverse reactions than whole cell vaccines.
Virulence	The relative ability of a microbe to cause disease (the degree of pathogenicity).

Dankwoord

Het zit erop, dit is het dan. Dit proefschrift is het resultaat van ruim 6 jaar onderzoek bij het laboratorium voor product en procesontwikkeling van het Nederlands Vaccin Instituut in Bilthoven en nu, na ruim 7 jaar, is het eindelijk af. Het was een intensieve, interessante, leerzame en leuke tijd maar ik ben blij dat het erop zit. Het is tijd om verder te gaan. Dit proefschrift was nooit totstandgekomen zonder de hulp en/of steun van veel mensen die ik hiervoor graag wil bedanken.

Coen, jij kwam met het idee om mijn onderzoekswerk te combineren met een proefschrift en voorzag in de mogelijkheden om dit te kunnen doen binnen het MenB project. Jouw grenzeloze enthousiasme, oog voor noviteit, kennis van de literatuur en werklust zijn inspirerend en waren een belangrijke stimulans om door te gaan. In de moeilijke periode, na jouw vertrek op het NVI, bleef je mij, als mentor en als mens, steunen en dat zal ik nooit vergeten. *Dirk*, jij bent een hele goede docent, misschien wel de beste uit Wageningen. Jij hebt de rust en het geduld om complexe zaken uit te leggen en dat is een hele waardevolle eigenschap. Jij was de eerste die tegen mij zei “het is pas wetenschap als het is opgeschreven” en zette mij aan om te minderen met data verzamelen en meer tijd te stoppen in schrijven. Bij dit laatste liet je zien hoe belangrijk het is om structuur aan te brengen in een verhaal waardoor het altijd beter leesbaar werd. *Hans*, wat meer op de achtergrond volgde je mijn onderzoek maar zodra er een verhaal was, nam je er de tijd voor en kwam je altijd met opbouwende en oprechte opmerkingen, waarvan sommige memorabel zijn: “het is vlees noch vis”.

Elly, ik deelde met jou, bijna mijn gehele NVI-tijd, met veel plezier, een kamer. Je stond altijd voor me klaar, was altijd bereid om te luisteren en hebt veel werk verzet. Ik denk met heel veel plezier aan onze tijd terug. *Jan*, ook jij stond altijd voor me klaar en hebt mij het kweken in de praktijk geleerd. Jij bent de vrolijkste en liefste man die ik ken en ik hoop dat we nog vele jaren samen de piste en off-piste zullen nemen “hatsebats”. *Bert*, met NMR analyseerde jij voor mij heel veel supjes en je dacht altijd mee bij het interpreteren van de resultaten. Door jouw kennis en kunde was er altijd

wel iets te vinden om enthousiast over te zijn. Daarnaast was jij altijd bereid om raad te geven over wetenschappelijke en niet-wetenschappelijke zaken. *Alex*, bedankt voor alle HPLC en GC bepalingen en de vele vrolijke momenten... “windje”. *Govert*, *Dennis*, en *Wilfred*, door jullie hulp en flexibiliteit waren alle BIO5, BIO60, BIO440 en BIO1200 MenB kweken mogelijk. *Marvin*, jij zorgde ervoor dat BCSV deed wat ik graag wilde en loste problemen altijd razensnel op. *Colinda*, bedankt voor de DNA analyses en het soms vroegtijdig vrijgeven van resultaten en *Rudy* bedankt dat je toeliet dat er bij jou op de afdeling wel eens analyses voor mij gedaan werden. *Danny*, bedankt voor de SDS-pages die je voor mij hebt gedaan en voor het overdragen van veel handige spulletjes van vroeger. Geniet van je pensioen! *Luc*, helaas overleed jij aan de gevolgen van een slopende ziekte. Met name in de begintijd, toen we nog in gebouw U zaten, was jij er altijd. Jij bolde je sjekkies in je eigen lab en rookte die terplaatse op. Ook na werktijd en in het weekend analyseerde je voor mij heel veel monsters en zette vaak voor mij het MilliQ apparaat uit waardoor de hoeveelheid op te dweilen water op de mediumbereiding (en soms de gang) werd beperkt. *Theone*, *Aart* en *Arjen*, het MenB-DSP team, bedankt voor jullie begrip, steun en interesse voor mijn “nevenactiviteit” (het werk voor dit proefschrift). *Mathieu*, jij was de drijvende kracht van het andere belangrijke project maar vond toch altijd tijd om te discussiëren, mee te denken en plezier te maken. *Bas*, bedankt voor je enthousiasme en hulp bij het uitzoeken en uitvoeren van de microarrays. *Cor*, je vriesdroogde voor mij heel veel biomassa monsters en zorgde ervoor dat ik de glas-transitie-temperatuur van verschillende media kon meten bij SVM wat geresulteerd heeft in verbeterde condities voor de opslag van de verschillende MenB stammen. *Martin*, jij deed naast NMR analyses van vele supjes ook dunne laag chromatografie om de MenB phospholipiden te identificeren en kwantificeren. *Janny*, jouw kritische maar opbouwende opmerkingen voor en na besprekingen waren altijd waardevol en je leerde mij Elisa’s doen en werken op de Biacore. Het was een plezier om jou te zien genieten van schuine humor. *Bernard*, onze onderzoeken lagen wat ver uit elkaar maar we vonden altijd gesprekstof. Bedankt hiervoor en ook voor je hulp bij het gieten en

runnen van gelletjes. *Carmen*, het is weer al even geleden, bedankt voor het uitleggen van de immunologie. *Harry* en *Betsy*, bedankt voor de gesprekken en jullie hulp bij verschillende experimenten. *Betsy*, het was altijd een hele geruststelling om te weten dat ik niet de enige ben die het heerlijk vond om tot in de late uurtjes bezig te zijn. *Karin*, je was een ongekende toegevoegde waarde voor het lab en hebt een heel groot hart. Bedankt voor alle goede adviezen en de feestjes in je tuin. *Jan ten H*, en *Ad*, bedankt voor jullie hulp bij het bepalen van de lipid A samenstelling op de massaspectrometer. *Hendrik-Jan*, je begeleidde *Marc* bij het werk wat heeft geleid tot de fosfofructokinase mutant en was altijd bereid om te helpen met alles, bedankt hiervoor! *Marcel H.*, bedankt voor het aanleveren van het fosfofructokinase protocol. *Peter*, jij stond aan de basis van het multivalente vesicle vaccin en was altijd bereid om je kennis te delen en advies te geven. *Wilma*, bedankt voor je hulp bij o.a. het maken van posters. *Joost*, jij loste alle PC problemen razendsnel op en maakte geweldige foto's. *Paul*, bedankt voor je hulp bij het k_L werk. *Klaas*, jouw gevoel voor de orde grootte van getallen bleek uit je snelle kladpapier berekeningetjes die altijd heel dichtbij mijn uitgebreide opschalingsberekeningen lagen waar ik uren mee bezig was geweest. Dat je het wel eens niet kon volgen als het over metabolisme ging, stelde mij eerlijk gezegd gerust. *Loek* en *Otto*, bedankt voor jullie begrip en het geven van vertrouwen in de opschalingsstrategie, die voor NVI begrippen nogal onconventioneel was. Ook dank aan alle, soms tijdelijke, afdelingshoofden, in het bijzonder *Ron*, *Simone*, *Gideon* en *Leo*, voor het beschikbaar stellen van tijd om experimenten en berekeningen te doen voor dit proefschrift. *Ben*, bedankt voor de financiële ondersteuning. Verder wil ik alle mensen van de Unit O&O, de productie (U3), FTS en QC, die op het NVI rondlopen of liepen, bedanken voor de interesse in mijn werk en de leuke tijd.

Marieke, jij was mijn eerste student uit Wageningen en samen hebben we heel veel chemostaten gedaan die uiteindelijk hebben geleid tot een hoge impact publicatie in *Genome Biology*. *Marc*, jij kwam als tweede een afstudeervak bij mij doen en was in staat om op eigen kracht het genetisch werk te doen. Jou werklust en capaciteiten

waren ruim bovengemiddeld en ik hoop voor de Wetenschap dat je er nog in zit. *Dorinde*, jij kwam als derde student om de A- en D-stat methodiek toe te passen. Je was zelfstandig en hebt een groot deel van de experimenten zelf gedaan. Hoewel de resultaten uiteindelijk niet in dit proefschrift terecht gekomen zijn, sluit ik niet uit dat we er over een tijdje alsnog een mooie publicatie uitslepen! *Elnaz*, jij was mijn vierde student en kwam elke dag met de trein uit Leeuwarden. Jij was dagelijks meer dan drie uur onderweg om de gas-vloeistof overdracht in alle verschillende bioreactoren te karakteriseren. Je hebt enorm veel werk verzet, was ondanks de reistijd altijd vrolijk en hebt een belangrijke bijdrage geleverd aan het sluiten van de koolstofbalansen. *Tom*, jij was mijn laatste student uit Wageningen en jouw werk heeft ervoor gezorgd dat er geen twijfel meer bestaat over de homogeniteit van Lipid A, waarvan jij onder verschillende omstandigheden de samenstelling hebt bepaald. Bedankt allemaal!

Alle AIO's, inmiddels gepromoveerden en begeleiders van proceskunde en levensmiddelelentechnologie, bedankt voor het plezier tijdens de AIO-reizen naar Zuid-Afrika en Canada en de andere uitstapjes. Ook wil ik al mijn collega's en vrienden uit Gent bedanken voor de toffe sfeer en de waardevolle discussies. *Jo*, *Gaspard*, *Adi* en *Brecht* bedankt voor de (Matlab) tips, suggesties en discussies. *Joeri*, bedankt voor je hulp bij het zoeken op de vele internet databases. *Jo* en *Gaspard*, bedankt voor het lezen van mijn doctoraat. Laten we er nu maar eens een goeie lap op geven! *Pascal*, bedankt voor je hulp bij de layout en de vormgeving. Het ziet er fantastisch uit. *Woutine*, sinds Eindhoven waren we allerbeste maatjes en deelden lief en leed met elkaar. Door dik en dun, vrienden voor het leven, dachten we allebei, alleen hield dat van jou er veel te vroeg mee op. Bij deze postuum, bedankt voor je steun en voor wie je was voor mij, dikke kus. *Hans*, *Michiel*, *Bas*, *Marcel*, *Wim*, *Gino* en *Norman*, de mannen, jullie waren nooit te beroerd om uit interesse, medelijden of vriendschap te vragen hoe het met mijn proefschrift ging. Bedankt voor alle Rock Werchter edities. *Annie* en *Etiënne*, jullie staan altijd voor ons klaar, bedankt voor jullie steun en goede zorgen. *Guust*, bedankt voor alle kluswerk en dat je zo goed bent voor mijn ma. *Gert*, *Sieg* en

Ma, jullie hebben mij altijd onvoorwaardelijk gesteund. Het verleden bewijst dat we samen alles aankunnen. Bedankt voor alles!

Marjan, mijn lief, mijn vrouw, mijn allesie, you are the sunshine of my life. Zonder jou was het echt nooit gelukt. Bedankt voor je liefde, onvoorwaardelijke steun, zorg (in het bijzonder de koffie-met-koffiekoek ontbijtjes), je begrip voor de vele avonden en weekenden dat ik moest werken en de periode dat ik er wilde zijn voor *Woutine*, het creëren van mijn eigen werkkamer, de zondagochtenden met Frank Sinatra, de zondagavond dineetjes om bij te praten en nog zo veel meer. Pas geleden beviel jij van onze prachtige zoon *Valentijn* en dat bracht ons nog meer geluk. Het tijdperk proefschrift is afgesloten, ik beloof dat ik er nu echt meer zal zijn voor jou en jullie.

About the author

CURRICULUM VITAE

Gino J.E. Baart was born on 15 may 1973 and grew up in the south-west of the Netherlands. After high school (Westerschelde College, Terneuzen) he started to study Chemical Engineering at Eindhoven Polytechnic. During this study he did a 7 month traineeship at the Department of Chemical Engineering of the University of Adelaide in Australia and worked on a project entitled “Fine particle separation by electrical field flow fractionation”. He spent 2 months of this traineeship at the Center for Biopolymers at Interfaces of the University of Utah in the United States. During the last 6 months of his study he joined the Center for fiber reinforced plastics in Eindhoven for a research project that resulted in the thesis entitled “Development of vacuum-foil technique for large complex products”. In 1997 he obtained the B.Sc. degree in Chemical Engineering. Later that year he started to study Bioprocess Engineering at Wageningen University. During the last 8 months of this study he joined the Laboratory for Product and Process Development of the National Institute of Public Health and the Environment (RIVM) in Bilthoven, The Netherlands, for a research project that resulted in the thesis entitled “Quantification of the metabolic fluxes through the metabolic pathways of *Bordetella pertussis*”. In 1999 he obtained the M.Sc. degree in Biotechnology and started working as bioprocess engineer physiology at the Netherlands Vaccine Institute (NVI, formerly a division of the RIVM). In 2001 he started a Ph.D. (part-time), resulting in the thesis entitled “Towards a *Neisseria meningitidis* B vaccine – Introducing systems biology in process development”. This project was a collaboration between the Food and Bioprocess Engineering Group of Wageningen University and the Laboratory for Product and Process Development of the NVI. Since 2007, Gino is working as project manager metabolic modeling and metabolic engineering at the Faculty of Bioscience Engineering of Ghent University in Belgium.

BIBLIOGRAPHY

Baart GJE, Langenhof M, van de Waterbeemd B, Hamstra HJ, Zomer B, Beuvery EC, Tramper J, Martens DE. 2008. Heterologous expression of phosphofructokinase in *Neisseria meningitidis*. Submitted for publication

Baart GJE, Willemsen M, Khatami E, de Haan A, Zomer B, Beuvery EC, Tramper J, Martens DE. 2008. Modeling *Neisseria meningitidis* B metabolism at different specific growth rates. Biotechnology and Bioengineering, Accepted.

Baart GJ, Zomer B, de Haan A, van der Pol LA, Beuvery EC, Tramper J, Martens DE. 2007. Modeling *Neisseria meningitidis* metabolism: from genome to metabolic fluxes. Genome Biology 8:R136.

Baart GJE, de Jong G, Philippi M, Riet Kvt, van der Pol LA, Beuvery EC, Tramper J, Martens DE. 2007. Scale-up for bulk production of vaccine against meningococcal disease. Vaccine 25:6399-6408.

Meiring HD, Kuipers B, Van Gaans-Van Den Brink JAM, Poelen MCM, Timmermans H, Baart G, Brugghe H, Van Schie J, Boog CJP, De Jong AFJM et al. 2005. Mass tag-assisted identification of naturally processed HLA class II-presented meningococcal peptides recognized by CD4+ T lymphocytes. Journal of Immunology 174:5636-5643.

Metz B, Kersten GFA, Baart GJ, deJong A, Meiring H, tenHove J, vanSteenbergen MJ, Hennink WE, Crommelin DJA, Jiskoot W. 2006. Identification of Formaldehyde-Induced Modifications in Proteins: Reactions with Insulin. Bioconjugate Chemistry 17:815-822.

Layout

Pascal van den Bulck (www.ditisjulius.nl)

Cover

Scanning Electron Microscope image of *Neisseria meningitidis* (magnification: x3750).

Provided and copyright Dennis Kunkel Microscopy, Inc., USA (www.denniskunkel.com)

The research described in this thesis was done at the Unit Research and Development of The Netherlands Vaccine Institute in Bilthoven.